Arene Bridged Diuranium Compounds Supported by Amide and Ketimide Ligands

by

Paula L. Diaconescu

B.S. Chemistry
University of Bucharest, 1998

SUBMITTED TO THE DEPARTMENT OF CHEMISTRY IN PARTIAL
FULFILLMENT OF THE REQUIREMENTS FOR THE DEGREE OF

DOCTOR OF PHILOSOPHY IN CHEMISTRY
AT THE
MASSACHUSETTS INSTITUTE OF TECHNOLOGY

JUNE 2003

Signature of Author:..
Department of Chemistry
February 3, 2003

Certified by:..
Christopher C. Cummins
Professor of Chemistry
Thesis Supervisor

Accepted by:..
Robert W. Field
Chairman, Departmental Committee on Graduate Students
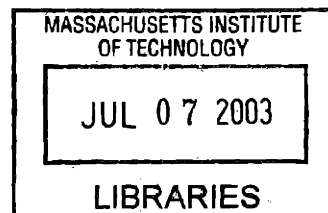
This doctoral thesis has been examined by a Committee of the Department of Chemistry as follows:

_____

Professor Richard R. Schrock
Chairman

_____

Professor Christopher C. Cummins
Thesis Supervisor

_____

Professor Alan Davison

Arene Bridged Diuranium Compounds Supported by Amide and Ketimide Ligands

By

Paula L. Diaconescu

Abstract

Chapter 1: The Intriguing Geometric and Electronic Structure of Arene-Bridged Diuranium Tetrakisamido Complexes

The focus of this chapter is to characterize and contextualize the bridged arene complex (μ-toluene)$U_2(N[t$-Bu]Ar)$_4$ (**1b$_2$-μ-toluene**, Ar = 3,5-$C_6H_3Me_2$). To do so, **1b$_2$-μ-toluene** is compared extensively with the mononuclear complexes (THF)U(N[^{1}Ad]Ar)$_3$ (**2a-THF**, THF = tetrahydrofuran), IU(N[t-Bu]Ar)$_3$ (**1a-I**), IU(N[^{1}Ad]Ar)$_3$ (**2a-I**), and Me$_3$SiNU(N[^{1}Ad]Ar)$_3$ (**2a-NSiMe$_3$**). In order to understand the properties of a unique compound such as **1b$_2$-μ-toluene**, the rest of the series is based on classical uranium amide compounds. The syntheses, structures (X-ray crystal structures and solution behavior based on variable temperature, VT, NMR data), spectroscopic (X-ray absorption near-edge structure, XANES, and electronic absorption – UV-vis-NIR) and magnetic properties are discussed and interpreted with reference to results of density functional theory (DFT) calculations performed on model compounds. Reactivity studies of **1b$_2$-μ-toluene** are then presented and analyzed.

Chapter 2: Arene Bridged Diuranium Complexes Supported by a Ketimide Ligand: Even and Odd Electron Redox Pairs

The ketimide ligand NC[t-Bu]Mes (Mes = 2,4,6-$C_6H_2Me_3$) employed in the present study allows for retention of three supporting ligands per uranium, giving rise to a three-legged piano stool geometry, and it also allows for incorporation of potassium ions as tight ion pairs. The generality of such a ligand is well supported by the existence of the two types of compounds M_2(μ-arene)U_2(NC[t-Bu]Mes)$_6$ (**M_2-3_2-μ-arene**, M = Na, K) and **K-3_2-μ-arene**, when the arene is naphthalene, biphenyl, *trans*-stilbene, or p-terphenyl. When toluene or benzene is the bridging arene, only odd electron species are formed including symmetrical complexes, **K_2I-3_2-μ-arene'**, and asymmetrical complexes, **K(DME)-3_2-μ-arene'** (arene' = benzene, toluene). The reactivity patterns observed for the bridging arene ketimide compounds are complicated by loss of an alkali metal ion (**K_2-3_2-μ-arene** with PhSSPh) or by additional redox processes (**K-3_2-μ-arene** with PhNNPh), but interesting products have been isolated. By contrast, the reaction of **K_2-3_2-μ-arene** with 1,3,5,7-cyclooctatetraene appears to be straightforward leading to **K-3-COT**. Compound **3_2-μ-COT** obtained from reaction of **K-3-COT** with **3-I-DME** is an interesting example of an inverted sandwich and can be referred to as "inverted uranocene".

Chapter 3: Uranium 2,2'-Bipyridyl Complexes Supported by Amide and Ketimide Ligands

The synthesis and characterization of (bipy)$_2$U(N[t-Bu]Ar)$_2$ (**1b-(bipy)$_2$**, bipy = 2,2'-bipyridyl, Ar = 3,5-$C_6H_3Me_2$), (bipy)U(N[^{1}Ad]Ar)$_3$ (**2a-bipy**), (bipy)$_2$U(NC[t-Bu]Mes)$_3$ (**3-(bipy)$_2$**, Mes = 2,4,6-$C_6H_2Me_3$), and IU(bipy)(NC[t-Bu]Mes)$_3$ (**3-I-bipy**) are reported. X-ray crystallography indicates that bipy coordinates as a radical anion in **1b-(bipy)$_2$** and **2a-bipy**, and as a neutral ligand in **3-I-bipy**. In **3-(bipy)$_2$**, one of the ligands is best viewed as a radical anion, while the other as a neutral ligand. These results are supported by NMR spectroscopy results of exchange experiments with 4,4'-dimethyl-2,2'-bipyridyl (dmb) and optical spectroscopy. In all complexes uranium is assigned a +4 formal oxidation state.

Table of Contents

7

List of Figures

9

List of Tables

List of Abbreviations

^{1}Ad	1-adamantyl
Anal.	elemental analysis
Ar	$3,5\text{-}C_6H_3Me_2$
br	broad
calcd.	calculated
CCD	Charge Coupled Device
d	doublet
equiv	equivalent(s)
F	structure factor
GOF	goodness of fit
HOMO	Highest Occupied Molecular Orbital
Hz	Hertz
IR	infrared
LUMO	Lowest Occupied Molecular Orbital
NMR	Nuclear Magnetic Resonance
SQUID	Superconducting Quantum Interference Device

Historical Aspects of Uranium Organometallic Chemistry

Uranium was the first f-element to be discovered.[1] In 1789, the German chemist Martin Klaproth analyzing pitchblende, a mineral thought to contain a mixture of zinc, iron, and tungsten oxides, showed that it also contained the oxide of a new element, which he called uranium, after the recently discovered planet Uranus. Thorium, protactinium, and uranium are the only naturally occurring actinide elements. About 100 years after its discovery, H. Becquerel observed the phenomenon of radioactivity in uranium. The discovery of radium in pitchblende at the beginning of the 20th century increased the interest in finding new deposits of this mineral.[2] The two most abundant isotopes found in natural uranium are ^{235}U (0.72%), which is fissionable by thermal, or slow, neutrons and ^{238}U (99.2%), which is not. At present, uranium is most commonly used as a fuel source in nuclear power generators.

The first well-defined organometallic complex of an f element is considered to be $U(\eta^5\text{-}C_5H_5)_3Cl$, which was synthesized in 1956.[3] The discovery of several other cyclopentadienyl uranium complexes followed, but reports were scarce[4,5] until the discovery of uranocene, $U(\eta^8\text{-}C_8H_8)_2$,[6] in 1968, which stimulated an increasing interest in f element organometallic chemistry. The two traditional focuses of uranium organometallic chemistry, cyclopentadienyl complexes[7] and uranocenes[8], still generate reports of new compounds[9,10] and theoretical and spectroscopic investigations.[11,12] Of theoretical interest is the fact that $U(\eta^5\text{-}C_5H_5)_4$ is the only type of organometallic compound which has four Cp groups, all bonded in η^5 fashion.[13] The analogous zirconium compound has the structure $Zr(\eta^5\text{-}C_5H_5)_3(\eta^1\text{-}C_5H_5)$.[14]

In 1989, the first neutral homoleptic tri-alkyl uranium complex, $U(CH(SiMe_3)_2)_3$, was reported by Van der Sluys, Burns, and Sattelberger.[15] It has a pyramidal structure, as expected because of the known structure for $Ln(CH(SiMe_3)_2)_3$ (Ln = La, Lu).[16] The f elements have a large

number of empty orbitals in various orientations and γ-agostic interactions are documented to occur for $U(CH(SiMe_3)_2)_3$.

An important report is the synthesis of $UI_3(THF)_4$ and analogous uranium triiodide complexes,[17] because of the possibility to access trivalent uranium compounds directly. The synthesis of $U(N[SiMe_3]_2)_3$, although initially synthesized from UCl_3 generated *in situ*, marks the beginning of uranium organometallic chemistry with complexes supported by non-cyclopentadienyl ligands.[18] Another example of uranium *tris*-amide complex is $(THF)U(N[t\text{-}Bu]Ar)_3$, which leads to a uranium-molybdenum dinitrogen dinuclear, $(Ar[t\text{-}Bu]U)_3\text{-}N=N\text{-}Mo(N[t\text{-}Bu]Ph)_3$.[19]

The first dinitrogen complex of an actinide, $[\{U(NN'_3)\}_2(\mu\text{-}\eta^2{:}\eta^2\text{-}N_2)]$ (NN'_3 = $N(CH_2CH_2NSiBu^tMe_2)_3$, was reported in 1998.[20] The dinitrogen ligand is side-on bonded to the two uranium centers, while the N-N bond length is similar to that of free dinitrogen. Theoretical investigations on model compounds concluded "back bonding without σ-bonding: a unique π-complex of dinitrogen with uranium".[21] The mixed cyclopentadienyl-pentalene complex $[U(\eta\text{-}Cp^*)(\eta\text{-}C_8H_4\{Si^iPr_3\text{-}1,4\}_2)]$ binds dinitrogen reversibly to afford $[\{U(\eta\text{-}Cp^*)(\eta\text{-}C_8H_4\{Si^iPr_3\text{-}1,4\}_2)\}_2(\mu\text{-}\eta^2{:}\eta^2\text{-}N_2)]$, whose X-ray crystal structure reveals a sideways-bound, bridging diazenido (N_2^{2-}) ligand.[22]

Of similar interest to the dinitrogen actinide compounds are carbonyl and isocyanide complexes. A detailed study of the isocyanide complexes $(Cp')_3U(CNR)$ (Cp'= C_5H_5, MeC_5H_4, $Me_3CC_5H_4$, and $Me_3SiC_5H_4$ and R = Et; Cp' = $1,3\text{-}(Me_3Si)_2C_5H_3$ and R = t-Bu; Cp' = Me_4C_5H and R = 4-(MeO)) and carbonyl complexes $(Cp')_3U(CO)$ (Cp' = $1,3\text{-}(Me_3Si)_2C_5H_3$, $Me_3SiC_5H_4$, $Me_3CC_5H_4$, C_5Me_4H) concluded that "the uranium metallocenes are better π donors than their cerium analogues, and the π-donating ability is dependent upon the ring substituents".[23]

The synthesis of ferrocene, $Fe(\eta^5-C_5H_5)_2$,[24] represents a landmark in organometallic chemistry. Analogous neutral arene transitional metal complexes have been the center of attention for a long time and numerous reports on their geometric and electronic structure have been published.[25] Because it was known that f element halides form intercalation compounds, it was predicted that complexes of these halides with benzene should be isolable. The first example to be crystallographically characterized, $U(\eta^2-AlCl_4)_3(\eta^6-C_6H_6)$, a formally uranium (III) compound, was reported by Cesari *et al.* in 1971.[26]

In 1994, Ephritikhine *et al.* reported an inverse cycloheptatrienyl diuranium sandwich complex, $[U(BH_4)_2(OC_4H_8)_5][(BH_4)_3U(\mu-\eta^7,\eta^7-C_7H_7)U(BH_4)_3]$, obtained by treatment of UX_4 (X= NEt$_2$, BH$_4$) with $K[C_7H_9]$.[27] Such complexes are of interest to the present study since similar bonding considerations apply to them and to the arene-bridged diuranium compounds reported here.[28] To date, the series of inverse sandwich diuranium complexes includes examples of benzene, toluene,[28] naphthalene,[29] cycloheptatrienyl,[27] and cyclooctatetrane dianion.[29] In most of these cases, as well as in actinocene complexes,[30] δ bonding between f orbitals of uranium and ligand LUMOs (lowest unoccupied molecular orbitals) with appropriate symmetry is thought to play a major role. Like π bonding in transition metal chemistry, study of δ bonding could be a key to understanding the properties and electronic structures of uranium complexes.

[1] Kaltsoyannis, N.; Scott, P. *The f Elements*; Oxford University Press Inc., New York, 1999.

[2] Aspinall, H. C. *Chemistry of the f-Block Elements*; Phillips, D.; O'Brien, P.; Roberts, S.; Eds., Gordon and Breach Science Publishers, Amsterdam, 2001.

[3] Reynolds, L. T.; Wilkinson, G. *J. Inorg. Nucl. Chem.* **1956**, *2*, 246.

[4] Mannerskantz, H. C. E.; Parshall, G. W.; Wilkinson, G. *J. Chem. Soc.* **1963**, 3163.

[5] Von Ammon, R.; Kanellakopulos, B.; Fischer, R. D. *Chemical Physics Letters* **1968**, *2*, 513.

[6] Streitwieser, A.; Müller-Westerhoff, U. *J. Am. Chem. Soc.* **1968**, *90*, 7364; Zalkin, A.; Raymond, K. N. *J. Am. Chem. Soc.* **1969**, *91*, 5667.

[7] Marks, T. J.; Fischer, R. D. *Organometallics of the f-Elements*, Reidel Publishing Co., Dordrecht, Holland, 1979.

[8] Streitwieser, A. in *Proc. Rare Earth Res. Conf., 11th*; Haschke, J. M.; Eick, H. A.; Eds., NTIS, Springfield, Va, 1974, 278.

[9] Kiplinger, J. L.; John, K. D.; Morris, D. E.; Scott, B. L.; Burns, C. J. *Organometallics* **2002**, *21*, 4306.

[10] Evans, W. J.; Nyce, G. W.; Ziller, J. W. *Angew. Chem. Int. Ed.* **2000**, *39*, 240.

[11] Bursten, B. E.; Strittmatter, R. J. *Angew. Chem. Int. Ed. Engl.* **1991**, *30*, 1069.

[12] DiBella, S.; Lanza, G.; Fragala, I. L.; Marks, T. J. *Organometallics* **1996**, *15*, 205; DiBella, S.; Gulino, A.; Lanza, G.; Fragala, I. L.; Stern, D. Marks, T. J. *Organometallics* **1994**, *13*, 3810.

[13] Burns, J. H. *J. Am. Chem. Soc.* **1973**, *95*, 3815.

[14] Rogers, R. D.; Bynum, R. V.; Atwood, J. L. *J. Am. Chem. Soc.* **1978**, *100*, 5238.

[15] Van der Sluys, W. G.; Burns, C. J.; Sattelberger, A. P. *Organometallics* **1989**, *8*, 855.

[16] Hitchcock, P. B.; Lappert, M. F.; Smith, R. G.; Bartlett, R. A.; Power, P. P. *J. Chem. Soc., Chem. Commun.* **1988**, 1007.

[17] Clark, D. L.; Sattelberger, A. P. *Inorg. Synth.* **1997**, *31*, 307.

[18] Andersen, R. A. *Inorg. Chem.* **1979**, *18*, 1507.

[19] Odom, A. L.; Arnold, P. L.; Cummins, C. C. *J. Am. Chem. Soc.* **1998**, *120*, 5836.

[20] Roussel, P.; Scott, P. *J. Am. Chem. Soc.* **1998**, *120*, 1070.

[21] Roussel, P.; Errington, W.; Kaltsoyannis, N.; Scott, P. *J. Organomet. Chem.* **2001**, *635*, 69.

[22] Cloke, F. Geoffrey N.; Hitchcock, P. B. *J. Am. Chem. Soc.* **2002**, *124*, 9352.

[23] Conejo, M. D.; Parry, J. S.; Carmona, E.; Schultz, M.; Brennann, J. G.; Beshouri, S. M.; Andersen, R. A.; Rogers, R. D.; Coles, S.; Hursthouse, M. *Chem.-Eur. J.* **1999**, *5*, 3000.

[24] Kealy, T. J.; Pauson, P. L. *Nature* **1951**, *168*, 1039; Miller, S. A.; Tebboth, J. A.; Tremaine, J. F. *J. Chem. Soc.* **1952**, 632; Wilkinson, G.; Rosenblum, M.; Whiting, M. C.; Woodward, R. B. *J. Am. Chem. Soc.* **1952**, *74*, 2125; Fischer, E. O.; Pfab, W. *Z. Naturforsch.* **1952**, *7B*, 377.

[25] Jellinek, F. *Nature* **1960**, *187*, 871; Fritz, H. P.; Fischer, E. O. *J. Organomet. Chem.* **1967**, *7*, 121; Herberich, G. E.; Mueller, J. *J. Organomet. Chem.* **1969**, *16*, 111; Foerster, E.; Albrecht, G.; Duerselen, W.; Kurras, E. *J. Organomet. Chem.* **1969**, *19*, 215; Cyvin, S. J.; Brunvoll, J.; Schaefer, L. *J. Chem. Phys.* **1971**, *54*, 1517; Anderson, S. E., Jr.; Drago, R. S. *Inorg. Chem.* **1972**, *11*, 1564; Connor, J. A.; Derrick, L. M. R.; Hillier, Ian H. *J. Chem. Soc., Faraday Trans.* **1974**, *70*, 941.

[26] Cesari, M.; Pedretti, U.; Zazzetta, A.; Lugli, G.; Marconi, W. *Inorg. Chim. Acta* **1971**, *5*, 439.

[27] Arliguie, T.; Lance, M.; Nierlich, M.; Vigner, J.; Ephritikhine, M. *J. Chem. Soc., Chem. Commun.* **1994**, 847; Arliguie, T.; Lance, M.; Nierlich, M.; Ephritikhine, M. *J. Chem. Soc., Chem. Commun.* **1997**, 2501.

[28] Diaconescu, P. L.; Arnold, P. L.; Baker, T. A.; Mindiola, D. J.; Cummins, C. C. *J. Am. Chem. Soc.* **2000**, *122*, 6108.

[29] Diaconescu, P. L.; Cummins, C. C. *J. Am. Chem. Soc.* **2002**, *124*, 7660.

[30] Elschenbroich, C.; Salzer, A. *Organometallics*, 2nd ed. VCH, Weinheim, 1992, 363.

The Intriguing Geometric and Electronic Structure of Arene-Bridged Diuranium Tetrakisamido Complexes

1.1. Introduction

Although the synthesis of the first well-defined organometallic complex of an f element, $U(\eta^5\text{-}C_5H_5)_3Cl$, (1956)[1] followed the discovery of ferrocene, $Fe(\eta^5\text{-}C_5H_5)_2$,[2] (1952) within only a few years,[3] it has only been in recent years that the organometallic chemistry of uranium has been intensely studied. Another landmark result, considered to be the true dawn of organouranium chemistry, was the synthesis of the cyclooctatetraene sandwich complex uranocene, $U(\eta^8\text{-}C_8H_8)_2$ (1968).[4] This discovery heralded striking differences that distinguish d and f element organometallic chemistries.

Amide ligands have become ubiquitous in transition metal chemistry[5] and they have also been successful in supporting interesting uranium complexes.[1,6,7,8] Their versatility is largely based on tunability of electronic and steric properties.[5,9] Compared to other ligands used in uranium chemistry, the amide ligands employed in the present study are both bulky and strong π donors.

Previous studies in the Cummins group by A. L. Odom showed that the readily available starting material *tris*-iodo-*tetrakis*-tetrahydrofuran uranium, $UI_3(THF)_4$,[10] can be transformed into a valuable precursor for this type of chemistry, $IU(N[t\text{-}Bu]Ar)_3$ (**1a-I**).[8] P. L. Arnold, following the same procedure but using the adamantyl analogue, $LiN[^1Ad]Ar$,[11] observed two major products: one, the corresponding iodo complex, $IU(N[^1Ad]Ar)_3$ (**2a-I**), the other, a very intriguing toluene bridged compound (μ-toluene)$U_2(N[^1Ad]Ar)_4$, **2b$_2$-μ-toluene**, for which the X-ray crystal structure was determined (Figure 1).

Known arene-bridged diuranium complexes incorporate benzene or toluene,[12] naphthalene,[13] cycloheptatrienyl,[14] and cyclooctatetraene,[13] as the bridging arene ligand. In most of these cases, as well as in actinocene complexes,[15] δ bonding between f orbitals of uranium and ligand LUMOs (lowest unoccupied molecular orbitals) with appropriate symmetry is thought to play a major role. Like π bonding in transition metal chemistry, study of δ bonding could be a key to understanding the properties and electronic structures of uranium complexes.
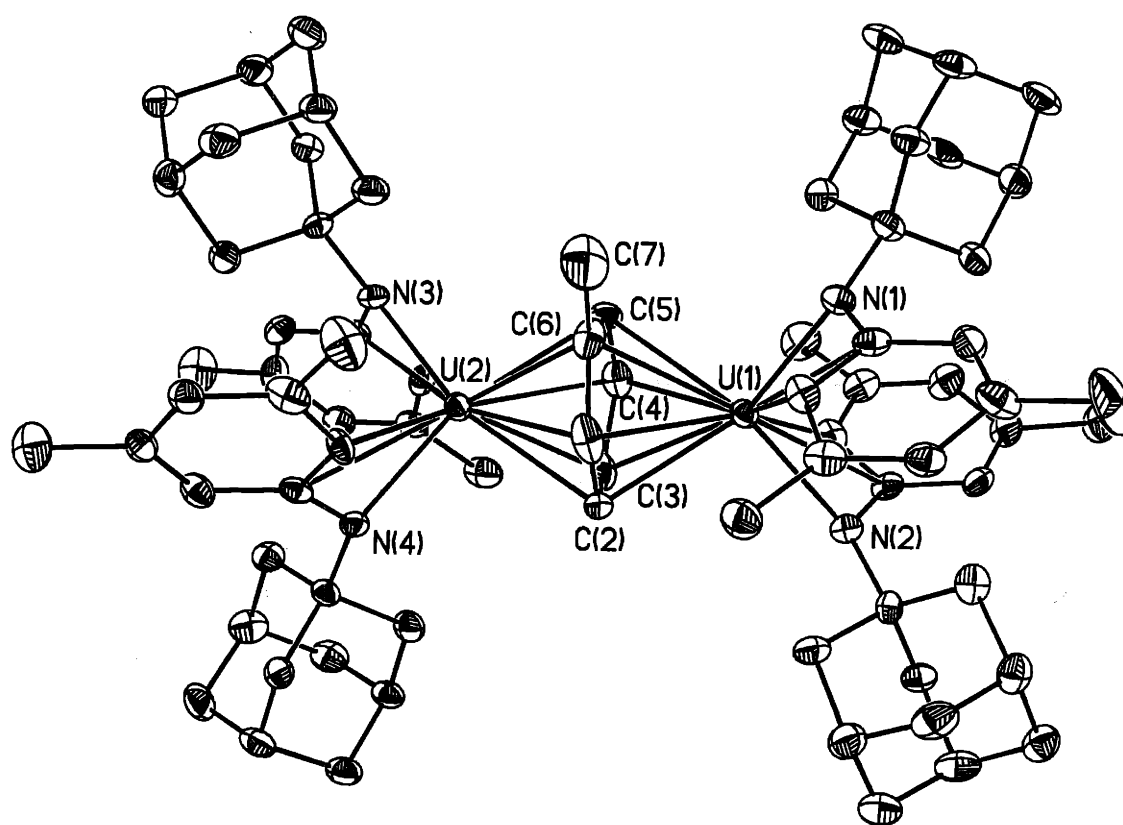
Figure 1. Structural drawing of complex **2b₂-μ-toluene** with thermal ellipsoids at the 35% probability level. Selected bond distances (Å): U-C (avg.), 2.594(30); U-N (avg.), 2.334(13); C-C (μ-toluene, avg.), 1.438(32).

The focus of this chapter is to characterize and contextualize the bridged arene complex (μ-toluene)$U_2(N[t$-Bu]Ar)$_4$ (**1b₂-μ-toluene**, Ar = 3,5-$C_6H_3Me_2$). To do so, **1b₂-μ-toluene** will be

compared extensively with the mononuclear complexes (THF)U(N[^{1}Ad]Ar)$_3$ (**2a-THF**, THF = tetrahydrofuran), IU(N[t-Bu]Ar)$_3$ (**1a-I**), IU(N[^{1}Ad]Ar)$_3$ (**2a-I**), and Me$_3$SiNU(N[^{1}Ad]Ar)$_3$ (**2a-NSiMe$_3$**). In order to understand the properties of a unique compound such as **1b$_2$-μ-toluene**, the rest of the series is based on classical uranium amide compounds. The syntheses, structures (X-ray crystal structures and solution behavior based on variable temperature, VT, NMR[16] data), spectroscopic (X-ray absorption near-edge structure, XANES,[17] and electronic absorption[18] – UV-vis-NIR), and magnetic properties[19] are discussed and interpreted with reference to results of density functional theory (DFT) calculations performed on model compounds. Reactivity studies of **1b$_2$-μ-toluene** are then presented and analyzed.

1.2. Results and discussion

1.2.1. Syntheses and X-ray crystal structures

Scheme 1 outlines the syntheses of all the complexes discussed. Compound UI$_3$(THF)$_4$[10] is a versatile starting material and can be employed to obtain *tris*-amidouranium iodide complexes **1a-I** and **2a-I** or can be used to generate **1b$_2$-μ-toluene** and **2a-THF** directly. In general, compounds based on the *N-tert*-butylanilide ligand are more lipophilic while compounds based on the *N*-adamantylanilide ligand are more crystalline, facilitating their characterization by X-ray crystallography.

Reduction of the *tris*-amidouranium iodide compounds affords either arene-bridged diuranium complexes when the arene is used as a solvent[12] or uranium *tris*-amide complexes with a molecule of THF coordinated to the uranium center when THF is used as a solvent.[8] Finally, **2a-NSiMe$_3$** is obtained from the reaction of Me$_3$SiN$_3$[20] with **2a-THF**, which can be generated *in situ* or isolated prior to the reaction (Scheme 1).
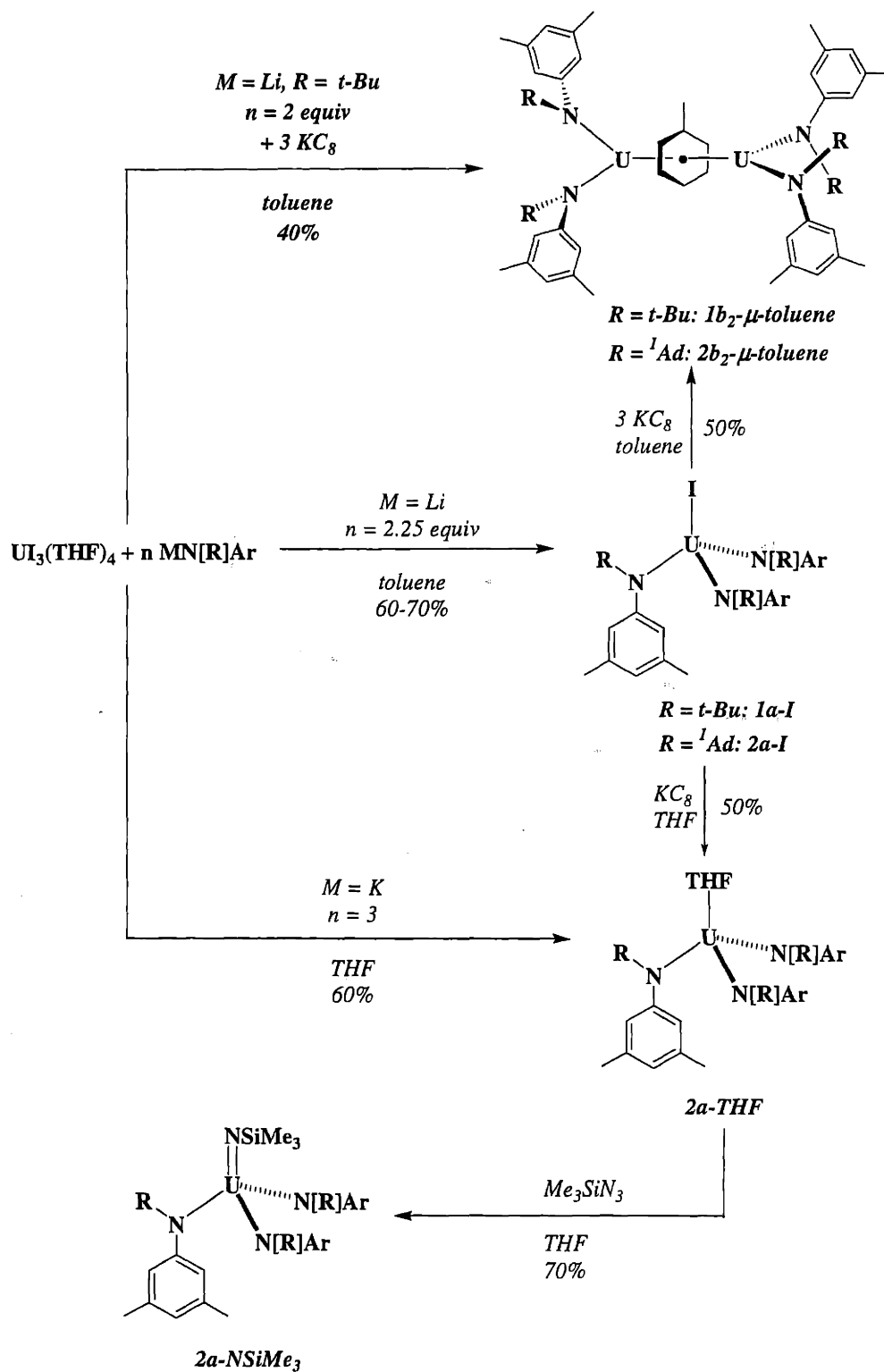
Scheme 1

Table 1. U-N$_{ligand}$ distances.

Compound	U-N$_{ligand}$ (avg., Å)
2b$_2$-μ-toluene	2.334(13)
2a-THF	2.346(9)
2a-I	2.204(9)
2a-NSiMe$_3$	2.245(7)
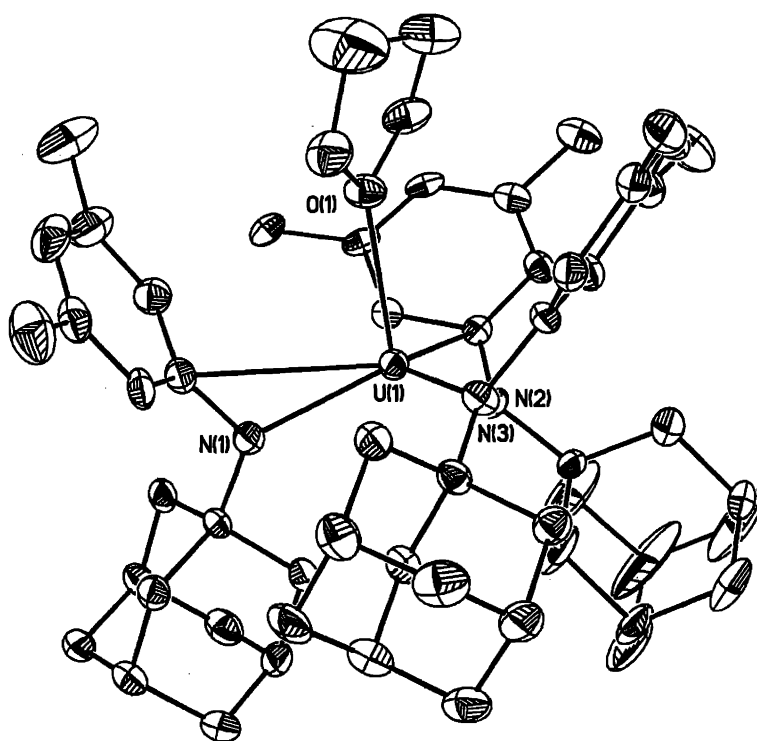
Figure 2. Structural drawing of **2a-THF** with thermal ellipsoids at the 35% probability level. Selected bond distances (Å): U-N (avg.), 2.346(9); U-O, 2.489(5).

The formulation of these compounds was verified by X-ray crystallography (Figures 1-4). A metrical parameter present throughout the entire series is the distance U-N$_{ligand}$ (avg.). This distance in compound **2b$_2$-μ-toluene**, 2.334(13) Å, compares well to the one in **2a-THF**,

2.346(9) Å and both are ca. 0.1 Å longer than those found in compounds **2a-I** and **2a-NSiMe₃**, 2.204(9) and 2.245(7) Å, respectively (Table 1). The trend observed here is in good agreement with the results of XANES experiments, which show that the effective charges on the uranium center are similar for **1b₂-μ-toluene** and uranium (III) compounds, on one hand, and for **2a-I** and **2a-NSiMe₃**, on the other hand.
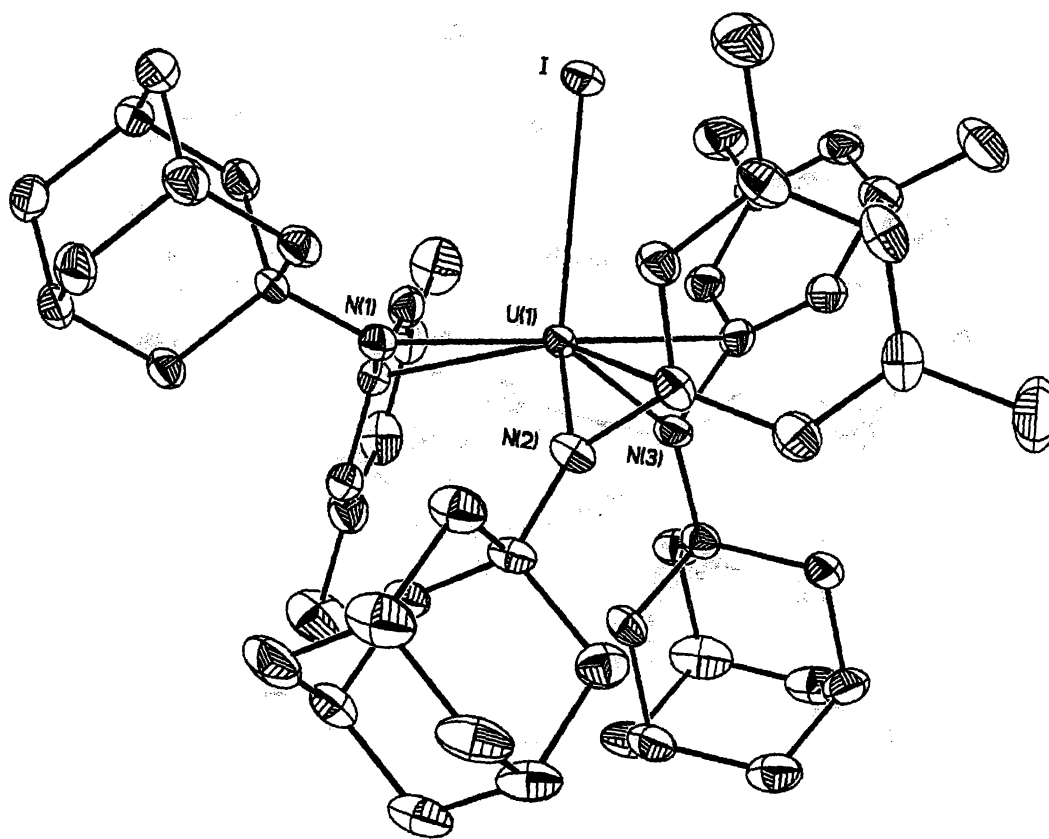
Figure 3. Structural drawing of **2a-I** with thermal ellipsoids at the 35% probability level. Selected bond distances (Å): U-N (avg.), 2.204(9); U-I, 3.0682(4).

Other interesting features evident from the structure of **2b₂-μ-toluene** are the distances from the uranium centers to the carbon atoms of the bridging toluene molecule and the distances between the arene carbon atoms. The average d$_{U-C}$ of 2.594(30) Å is among the shortest such distances

registered for carbon atoms of arene molecules coordinated to uranium centers. In benzene complexes such as $U(\eta^6\text{-}C_6Me_6)(BH_4)_3$[21] or $U(\eta^6\text{-}C_6H_5Me)(AlCl_4)_3$[22] the average $d_{U\text{-}C}$ is significantly longer, 2.93(2) and 2.94(1) Å, respectively, while for molecules in which the arene in its Hückel aromatic electronic configuration has a formal negative charge the average $d_{U\text{-}C}$ is shorter: 2.647(10) Å in uranocene, $U(\eta^8\text{-}C_8H_8)_2$,[23] and 2.807(18) Å in $U(\eta^5\text{-}C_5H_5)_4$.[24]
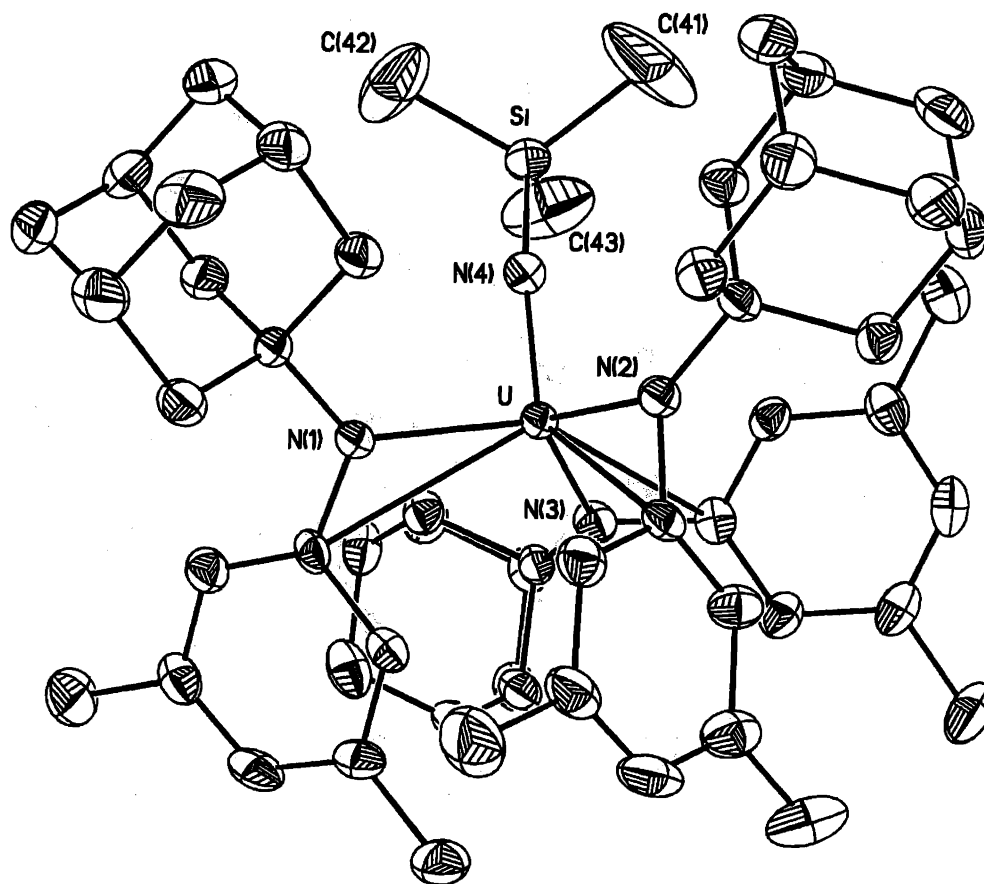
Figure 4. Structural drawing of **2a-NSiMe₃** with thermal ellipsoids at the 35% probability level. Selected bond distances (Å): U-N (avg.), 2.245(7); $U\text{-}N_{imide}$, 1.943(4).

Compared to the corresponding distances in free toluene, the average $d_{C\text{-}C}$ for the bridging toluene in **2b₂-μ-toluene** of 1.438(13) Å is ca. 0.04 Å longer.[25] In complexes of toluene such as K(18-crown-6)(toluene)[26] the C-C distances average 1.398(21) Å. The longer C-C distances in

complex **2b$_2$-μ-toluene** when compared to those in free toluene or toluene radical anion are consistent with substantial covalent overlap between filled f orbitals on uranium and LUMOs of the bridging toluene, as was found from DFT calculations on model compounds (see DFT calculations section).

Noteworthy from the structures of **2a-THF** and **2a-I** is the fact that the aryl groups form a protective pocket around THF and iodine, in contrast to analogous complexes of molybdenum in which such pockets are formed by the aliphatic groups.[9]

The structure of **2a-NSiMe$_3$** distinguishes itself by the U-N$_{imide}$ distance of 1.943(4) Å, which is ca. 0.3 Å shorter than the average U-N$_{ligand}$ in the same compound. Short U-N$_{imide}$ distances and angles close to 180° at N$_{imide}$ (170.1(13)° in **2a-NSiMe$_3$**) have been associated with multiple bond character between the uranium center and the imide nitrogen atom,[20] in accordance with our findings from DFT calculations on a model compound (see DFT calculations section).

As an example of the capability of uranium to access various oxidation states, reduction of **2a-NSiMe$_3$**, with lithium under argon or with KC$_8$ in THF results in the formation of Li(OEt$_2$)Me$_3$SiNU(N[^{1}Ad]Ar)$_3$ (Figure 8) or KMe$_3$SiNU(N[^{1}Ad]Ar)$_3$, formally uranium(IV) compounds. Although these complexes are not included in the classical uranium anilide series, the reduction reaction is presented as a means of obtaining complexes in which the formal oxidation state of the uranium center is intermediate between that of **2a-NSiMe$_3$** and that of its starting material, **2a-THF**. The longer distances U-N$_{anilide}$(avg.) of 2.357(5) Å and U-N$_{imide}$ of 2.050(3) Å in [Li(OEt$_2$)][Me$_3$SiNU(N[^{1}Ad]Ar)$_3$], compared to corresponding values in **2a-NSiMe$_3$**, are indicative of a more electron rich uranium center. DFT calculations on the model compound [H$_3$SiNU(NH$_2$)$_3$]$^-$ indicate that the two unpaired electrons reside in uranium f orbitals, consistent with the compound's formulation as a uranium(IV) species (see Appendix 2 for details).
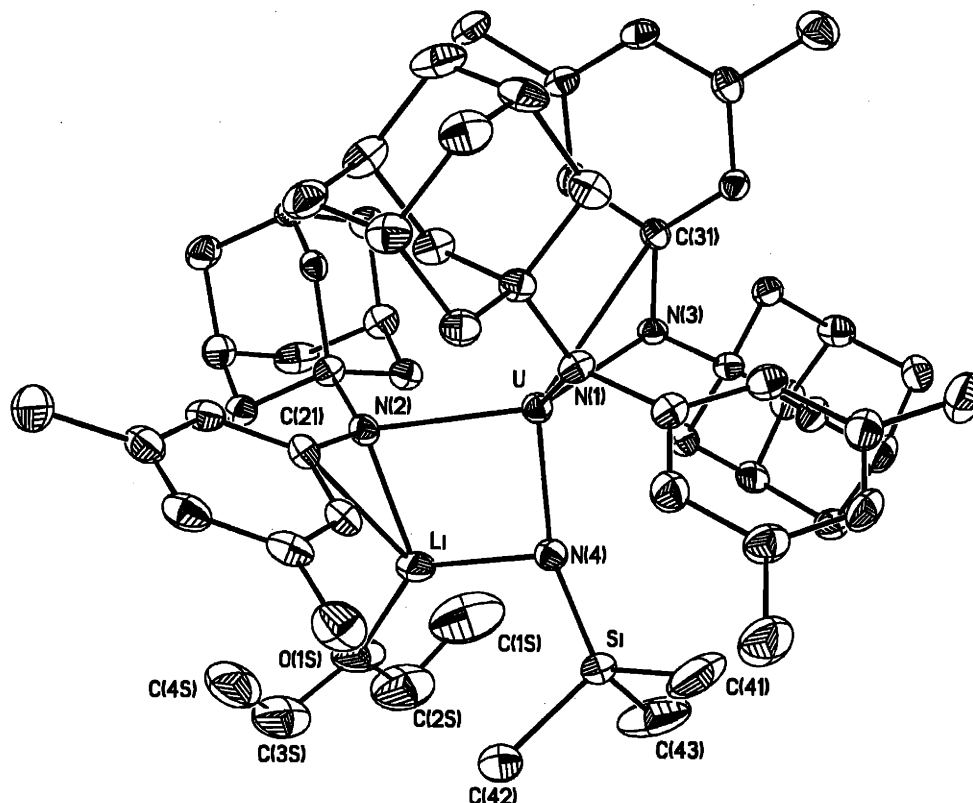
Figure 5. Structural representation of $Li(OEt_2)Me_3SiNU(N[^1Ad]Ar)_3$ with thermal ellipsoids at the 35% probability level. Selected bond distances (Å): $U\text{-}N_{ligand}$ (avg.), 2.357(5); $U\text{-}N_{imide}$, 2.050(3).

1.2.2. X-ray absorption near-edge structure (XANES) spectroscopy results*

The chemical shift of the absorption edge reflects the effective charge of the absorbing atom.[27,28] For uranium complexes, the U L_3 absorption edge, which corresponds to a $2p_{3/2}$ to $6d_{5/2}$ transition, has been shown to vary systematically with the uranium oxidation state.[29,30]
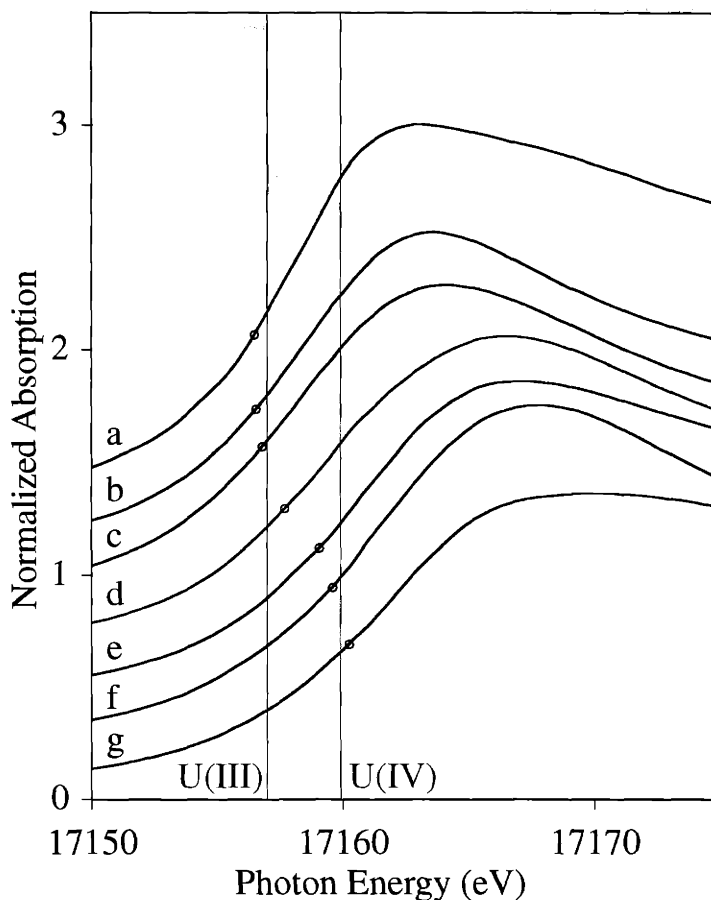
Figure 6. The U L$_3$ absorption edges of selected organouranium complexes. The edge height is normalized such that the absorption at the edge step is equal to one. The edge energies are referenced to the half height of a 0.1 M UO$_2$Cl$_2$ in 1M HCl solution set at 17163 eV. The compounds are: a) U[N(SiMe$_3$)$_2$]$_3$, b) [Cp''$_2$UCl]$_2$, c) [Cp$^{\ddagger}_2$UOH]$_2$, d) (μ-C$_7$H$_8$){U(N[t-Bu]Ar)$_2$}$_2$, e) IU(N[t-Bu]Ar)$_3$, f) IU(DME)(NC[t-Bu]Mes)$_3$, g) Me$_3$SiNU(N[^{1}Ad]Ar)$_3$. The point closest to the half-height is circled. The average edge shifts of U(III) and U(IV) complexes are indicated by the vertical lines.

Therefore, the chemical shifts of the U L$_3$ absorption edge are affected by changes in shielding of the 2p$_{3/2}$ electrons and can be used to compare the effective charges on the uranium centers in different complexes. The effective charge is most sensitive to the oxidation state of the absorbing atom, but other factors including coordination geometry and the degree of covalency in the ligand-metal interactions may also be significant.

References begin on page 75

Table 2. U L_3 chemical shifts of uranium complexes.

Compound	Edge Shift versus 0.1M UO_2Cl_2	Formal Oxidation State
1b$_2$-μ-toluene	-5.1	2
U[N(SiMe$_3$)$_2$]$_3$	-6.3	3
[Cp$^‡_2$UOH]$_2^i$	-6.4	3
[Cp$^‡_2$UF]$_2^i$	-5.0	3
[Cp$^‡_2$UCl]$_2^i$	-6.3	3
[Cp$^‡_2$UBr]$_2^i$	-5.7	3
[Cp''$_2$UF]$_2^i$	-5.9	3
[Cp''$_2$UCl]$_2^i$	-6.4	3
[Cp''$_2$UBr]$_2^i$	-5.6	3
IU(DME)(NC[t-Bu]Mes)$_3$	-3.3	4
1a-I	-3.8	4
[Cp$^‡_2$UO]$_2^i$	-2.0	4
Cp$^‡_2$UF$_2^i$	-2.4	4
Cp$^‡_2$UCl$_2^i$	-2.9	4
Cp$^‡_2$UBr$_2^i$	-3.5	4
Cp$^‡_2$UI$_2^i$	-3.6	4
Cp''$_2$UF$_2^i$	-2.6	4
Cp''$_2$UCl$_2^i$	-2.4	4
Cp''$_2$UBr$_2^i$	-3.7	4
Cp''$_2$UI$_2^i$	-3.6	4

Cp‡ = 1,3-(Me$_3$C)$_2$C$_5$H$_3$, Cp'' = 1,3-(Me$_3$Si)$_2$C$_5$H$_3$, DME = 1,2-dimethoxyethane; i: Lukens, W. W.; Allen, P. G.; Bucher, J. J.; Edelstein, N. N.; Hudson, E. A.; Shuh, D. K.; Reich, T.; Andersen, R. A. *Organometallics* **1999**, *18*, 1253.

References begin on page 75

For a series of formally trivalent organometallic and inorganic uranium compounds, the average chemical shift of the absorption edge relative to a UO_2Cl_2 sample is $-6.0(5)$ eV, and for a series of formally tetravalent uranium complexes, the average shift is $-3.1(6)$ eV as shown in Table 2 and Figure 6. Both sets of compounds include different coordination geometries and ligands with widely varying electronegativities. These chemical shifts can be used as standards to help understand the electronic structure of complexes in which the formal oxidation state is ambiguous.
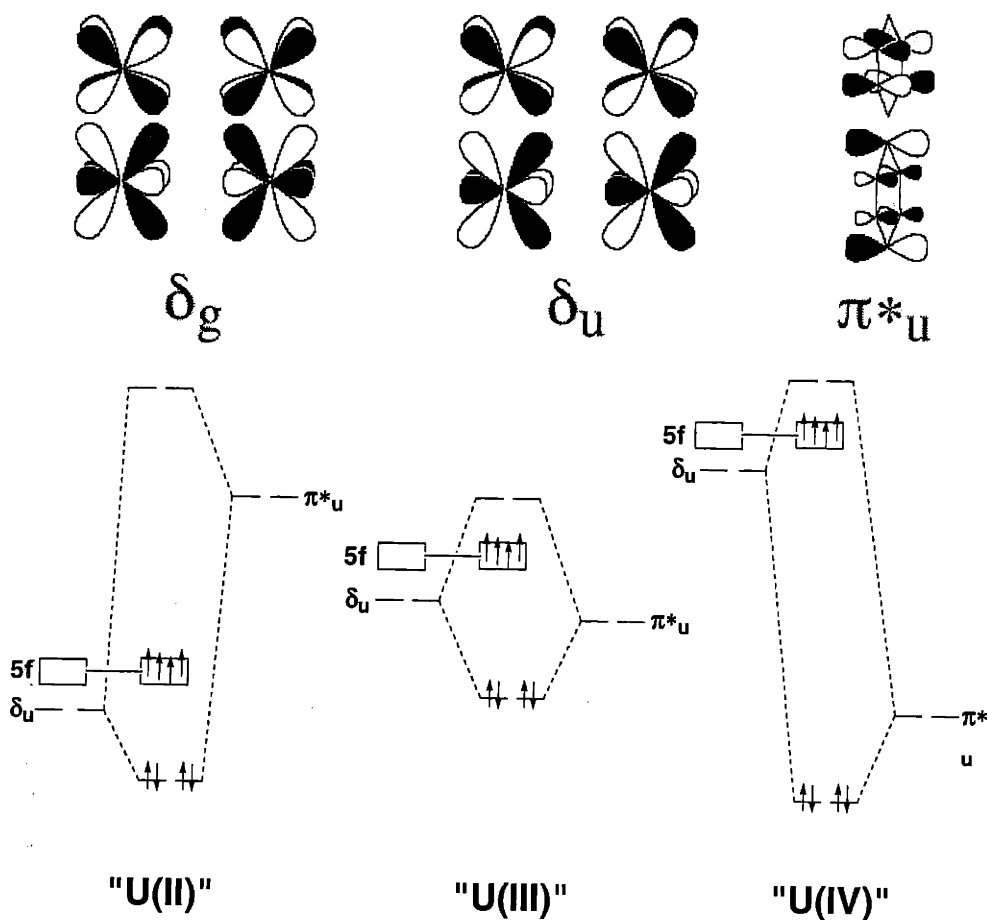
Figure 7

In the family of complexes $(\mu\text{-arene})[U(N[R]Ar)_2]_2$ the bonding evidently lies somewhere between two extremes: a neutral arene ligand and two uranium(II) centers, and an arene

tetraanion with two uranium(IV) centers (Figure 7). A series of the U L_3 absorption edges for selected uranium complexes is shown in Figure 6. Since the chemical shift of compound **1b$_2$-μ-toluene** is −5.1 eV, the effective charge of the U center in the complex is mostly similar to that of uranium(III) complexes.

A more precise description of the bonding requires information about the overlap between the ligand and metal orbitals, as well as their relative energies. Nonetheless, the observed chemical shift of the U L_3 edge is consistent with a strong, covalent interaction between the arene π^*_u orbitals and the δ_u orbitals of the two uranium centers.

1.2.3. DFT calculation results

In order to gain some insight into the bonding of the compounds discussed here, DFT calculations using the program ADF2002.01[31] were performed on model compounds. For each model, calculations were carried out using a variety of different density functionals, in order to assess their relative performance.

For the model compound $H_3SiNU(NH_2)_3$ the geometry optimizations were carried out with a single electron of spin α in excess of spin β. Because the value of the dihedral angles $HNUN_{imide}$ can be an important factor in determining the π bonds in which the nitrogen donors of the amide ligands participate, the initial geometry had these angles set to 0, 45, and 90° in accord with experimental values. Table 3 presents the agreement between the results of calculations and experimental parameters. All calculations that included gradient exchange correlations (i.e. all except LDA calculations) show reasonable agreement with the experimental values. Inspection of the orbitals revealed that HOMO-3 and HOMO-4 consist mainly of π $U-N_{imide}$ bonds (Figure 8), explaining both the short $U-N_{imide}$ distance and the angle of 170.1(3)° around the imide nitrogen atom.

Table 3. Optimized variables (distances in Å and angles in °) for $H_3SiNU(NH_2)_3$ and experimental values for **2a-NSiMe₃**.

Variable	PW91	BP86	BLYP	LDA[a]	Exp.
U-N$_{ligand}$	2.212	2.218	2.244	2.184	2.215(4)
	2.221	2.228	2.252	2.187	2.257(4)
	2.236	2.238	2.265	2.188	2.264(4)
U-N$_{imide}$	1.939	1.945	1.959	1.936	1.943(4)
N$_{ligand}$UN$_{imide}$	104.9	106.1	105.9	103.7	100.52(15)
	107.9	108.5	108.2	108.9	103.50(14)
	115.9	115.0	114.4	112.7	108.37(15)
Si-N$_{imide}$	1.724	1.729	1.733	1.709	1.722(4)
HSiN$_{imide}$	111.1	110.9	110.9	111.0	110.7(3)
	111.5	111.3	111.4	111.5	111.1(3)
	111.8	111.8	111.7	112.0	112.0(3)
HN$_{ligand}$UN$_{imide}$	5.0	5.0	4.5	2.2	2.02(52)
	41.9	43.2	42.4	41.5	41.20(40)
	86.6	87.0	86.8	88.1	92.91(32)

a: Non-Aufbau occupation
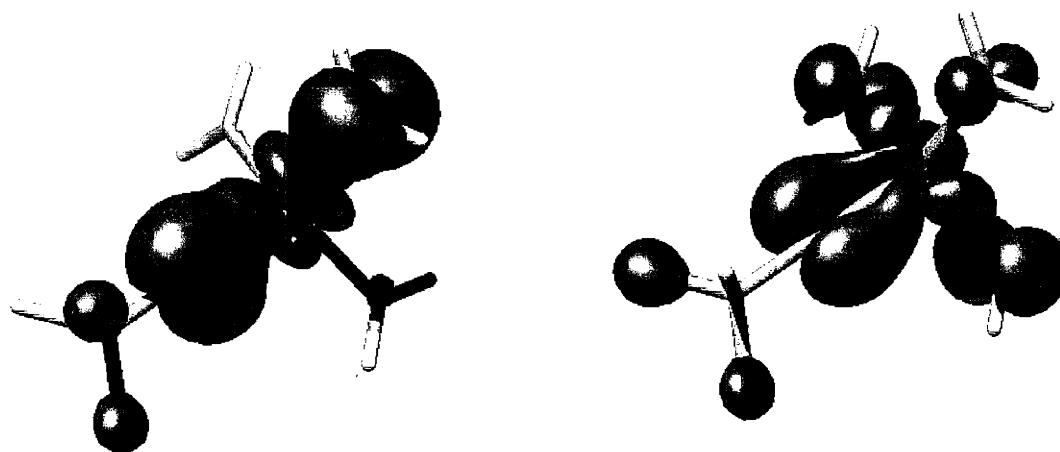
Figure 8. The U-N$_{imide}$ π bonds: SOMO-3 (left) and SOMO-4 (right). Orbitals are from the PW91 calculation and the α component is represented here.

A similar computational approach to the one presented for $H_3SiNU(NH_2)_3$ was used for the model compounds $IU(NH_2)_3$ and $(Me_2O)U(NH_2)_3$. Calculations were performed with different density functionals and the results of geometry optimizations are compared in Tables 4 and 5. The geometry optimizations were carried out with two electrons for $IU(NH_2)_3$ and three electrons for $(Me_2O)U(NH_2)_3$ of spin α in excess of spin β. The initial geometries had the dihedral angles IUNH were set to 8, 103 and 131° while the dihedral angles OUNH were set to -30 °, in accord with experimental values. All calculations that included gradient exchange correlations (i.e. all except LDA calculations) gave comparable and good results.

Table 4. Optimized variables (distances in Å and angles in °) for $IU(NH_2)_3$ and experimental values for **2a-I**.

Variable	PW91	BP86	BLYP	LDA[a]	Exp.
U-I	2.976	2.985	3.026	2.938	3.0682(4)
U-N	2.179	2.187	2.209	2.159	2.187(5)
	2.191	2.195	2.211	2.161	2.192(5)
	2.196	2.195	2.213	2.161	2.233(5)
IUN	110.3	110.0	112.6	111.6	94.29(13)
	110.5	111.1	113.0	113.9	113.38(12)
	112.6	112.6	114.3	116.1	126.22(12)
HNUI	2.39	3.0	6.1	-1.0	8.02(39)
	102.1	99.4	104.2	105.4	103.18(34)
	131.0	128.2	131.5	133.7	131.31(61)

a: Non-Aufbau occupation

In both cases the unpaired electrons reside in mainly uranium f-d hybrid orbitals and the LUMOs are also uranium f orbitals (three for $(Me_2O)U(NH_2)_3$, and four for $IU(NH_2)_3$). The double occupied molecular orbitals that follow immediately after the SOMOs consist of iodine p orbitals for $IU(NH_2)_3$, nitrogen p orbitals and U-N_{ligand} π bonds for $(Me_2O)U(NH_2)_3$.

Table 5. Optimized variables (distances in Å and angles in °) for $(Me_2O)U(NH_2)_3$ and experimental values for **2a-THF**.

Variable	PW91	BP86	BLYP	LDA[a]	Exp.
U-O	2.577	2.593	2.627	2.480	2.489(5)
U-N	2.223	2.217	2.242	2.179	2.308(5)
	2.224	2.219	2.245	2.179	2.339(5)
	2.225	2.219	2.252	2.181	2.392(5)
OUN	105.2	112.6	113.8	117.2	99.0(2)
	106.3	113.9	116.0	117.2	108.1(2)
	106.4	115.9	116.4	117.6	112.1(2)
C-O	1.433	1.437	1.450	1.410	1.441(9)
	1.434	1.438	1.450	1.410	1.448(9)
COU	123.5	122.9	122.6	123.7	116.9(4)
	123.8	124.6	124.7	123.9	128.4(4)
HNUO	89.0	130.7	143.2	145.7	124.77(51)
	90.9	131.1	145.7	145.8	133.34(57)
	92.4	133.7	149.4	146.6	152.66(57)

a: Non-Aufbau occupation

DFT calculations on the model $(\mu\text{-}C_6H_6)U_2(NH_2)_4$ have been reported already.[12] The calculations discussed here assume D_2 symmetry with two electrons of spin α in excess of spin β. The initial geometry had the dihedral angles set to 111° for HNUU, in accord with experimental data. The results of the geometry optimizations on Cartesian coordinates without imposing any restrictions on the system, using various functionals, are listed in Table 6. There is good agreement between optimized and experimental values. As noted previously,[12] the highest SOMOs are uranium f orbital combinations, while the next two double occupied orbitals represent two δ bonds (Figure 9) formed by appropriate symmetry uranium f orbitals and LUMOs of benzene. The existence of these bonds supports the XANES spectroscopy and X-ray crystallography results indicating that

the electronic density on the uranium center is similar to that for uranium(III) complexes. This similarity arises from the fact that the electrons in the δ bonds are equally shared by the uranium centers and the bridging toluene.

Table 6. Optimized variables (distances in Å and angles in °) for (μ-C_6H_6)U_2(NH_2)$_4$ and experimental values for **2b$_2$-μ-toluene**.

Variable	PW91	BP86	BLYP	LDA[a]	Exp. (avg.)
C-C	1.465	1.463	1.464	1.447	1.438(13)
U-C	2.567	2.570	2.626	2.529	2.594(30)
U-N	2.249	2.269	2.292	2.211	2.334(13)
NUN	99.8	106.7	104.9	104.2	103.4(3)
HNUU	94.1	108.4	108.4	108.2	111.1(7)

a: Non-Aufbau occupation
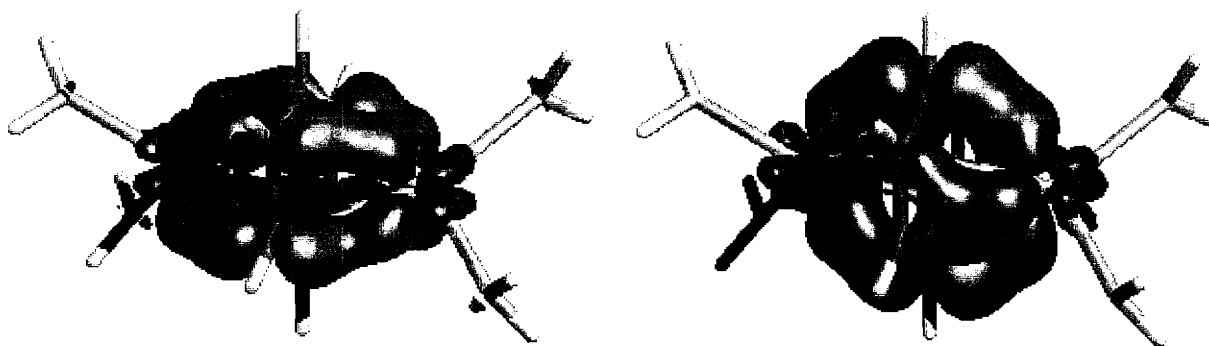
Figure 9. The δ bonds in (μ-C_6H_6)U_2(NH_2)$_4$: SOMO-4 (left) and SOMO-5 (right). Orbitals are from the PW91 calculation and the α component is represented here.

An intuitive way to assess the importance of δ backbonding in early actinide chemistry is outlined in Figure 10. The parallel between π backbonding in transition metal complexes and δ

backbonding in early actinide compounds is based on the fact that each bond involves one half of the total lobes in a specific orbital (two out of four in the case of d orbitals and four out of eight in the case of f orbitals) when interacting with LUMOs of the ligand in question.
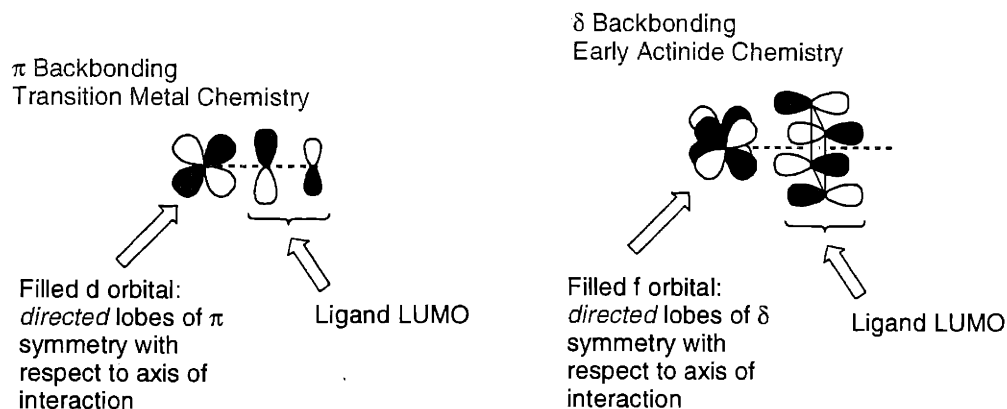
Figure 10. Comparison between π backbonding in transition metal chemistry and δ backbonding in early actinide chemistry.

1.2.4. NMR spectroscopy studies on compound 1b₂-μ-toluene: Probing stability and fluxionality

Almost all complexes of lanthanides and actinides are paramagnetic due to the presence of unpaired f electrons. When an NMR spectrum is recorded for a paramagnetic complex, the nucleus under investigation experiences the local magnetic field due to the paramagnetic metal ion in addition to the external magnetic field due to the NMR spectrometer. For most paramagnetic lanthanide and actinide complexes, strong spin-orbit coupling results in fast electron spin-lattice relaxation and so their NMR spectra show reasonably sharp lines.

The ^{1}H NMR spectra (22 °C, C_6D_6) of complexes **1b₂-μ-toluene**, **1b₂-μ-C_6H_6**, **2b₂-μ-toluene**, **2b₂-μ-C_6H_6** (Figure 11) are intriguing because the chemical shifts for the protons of the bridged

arene are spread over a broad range (+20 to -90 ppm). For example, the protons of the methyl group on the bridging toluene have a chemical shift around +20 ppm, while those bound to the aromatic carbons have chemical shifts in the range of -60 to -90 ppm. Bridging deuterated arene compounds helped in identifying the aromatic protons; also those belonging to the bridging benzene show a single chemical shift around -80 ppm.
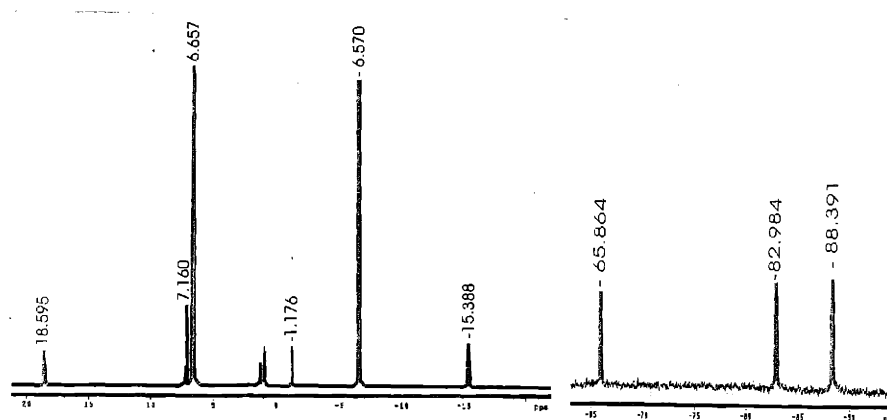
^{1}H NMR of $(\mu\text{-}C_7H_8)U_2(N[^tBu]Ar)_4$
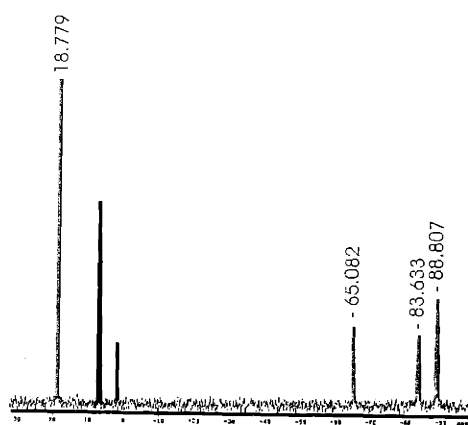
^{2}H NMR of $(\mu\text{-}C_7D_8)U_2(N[^tBu]Ar)_4$
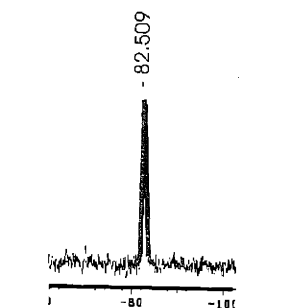
^{2}H NMR of $(\mu\text{-}C_6D_6)U_2(N[^tBu]Ar)_4$

Figure 11. ^{1}H NMR spectrum (22 °C, C_6D_6) of **1b$_2$-μ-toluene** and ^{2}H NMR spectra (22 °C, C_6H_6) of **1b$_2$-μ-toluene-d_8** and **1b$_2$-μ-C$_6$D$_6$**.

One interesting feature of this class of compounds is their remarkable thermal stability as probed by two types of experiments. First, variable temperature ^{1}H NMR studies in octane-d_{18} showed that compound **1b$_2$-μ-toluene** is stable up to 110 °C. In another experiment, **1b$_2$-μ-toluene** was heated in *n*-heptane at 90 °C for 48 h, after which time the compound's ^{1}H NMR spectrum indicated no decomposition.

The observed coordination geometry, μ-η^6,η^6, can be interpreted invoking the electronic structure of **1b$_2$-μ-toluene**, since having two uranium centers coordinated to the aromatic ring helps maintaining Hückel aromaticity (4n + 2, where n = 2), by forming two δ bonds with two LUMOs of the arene. In order to understand the extent for the preference of such a structure, arene exchange and VT NMR experiments were investigated.

^{1}H NMR analysis showed that the bridged toluene exchanges slowly with C$_6$D$_6$ (neat, 5% exchange in 24 h) at room temperature. Due to the thermal stability of **1b$_2$-μ-toluene**, arene exchange was then studied at higher temperatures. Preliminary results show that the bridged toluene molecule exchanges with C$_6$D$_6$ faster than the bridged benzene exchanges with toluene-d_8. Furthermore, the bridged toluene did not exchange with *p*-xylene over a 24 h period. The results from arene exchange experiments discussed here are the reverse of results from similar experiments for arene transition metal complexes.[22,32] For transition metal complexes, the π bond between HOMOs of the arene and empty metal d orbitals dictates such behavior, hence a less electron rich arene will exchange for a more electron rich one, like toluene or mesitylene versus benzene.[33] For the uranium bridged arene complexes the arene exchange reflects the existence of the backbond from filled uranium f orbitals to LUMOs of the arene and a less electron rich arene is preferred to a more electron rich one. Typical electron withdrawing groups are not compatible chemically with the reducing **1b$_2$-μ-toluene** complex, obviating the use of, e.g., PhCN, PhF, etc.

As implied by its formula and confirmed by X-ray crystallography, compound **1b$_2$-μ-toluene** is dinuclear in the solid state. In solution one could postulate an equilibrium between the dinuclear

structure and some mononuclear structures (either two uranium *bis*-amide fragments or a uranium *bis*-amide fragment and a coordinated benzene uranium *bis*-amide fragment, Figure 12). To rule out such a process, the variable temperature NMR behavior of **1b$_2$-μ-toluene** was examined between –70 °C and 120 °C. Investigation of solution structure for [Cp"$_2$UF$_2$]$_2$ (Cp" = 1,3-(Me$_3$Si)$_2$C$_5$H$_3$, a dimer in the solid state, by VT NMR spectroscopy revealed a dimer-monomer equilibrium exposed by nonlinear δ versus 1/T plots.[16]
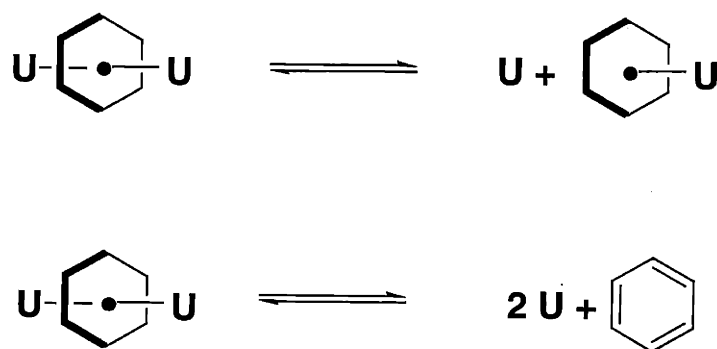
Figure 12. Possible equilibria between the dinuclear benzene-bridged structure and mononuclear structures (**U = 1b**).

Figure 13 presents the plot of δ versus 1/T for all the protons of the molecule. The plots representing the chemical shifts corresponding to amide protons are linear, indicating Curie-Weiss behavior for the complex **1b$_2$-μ-toluene**, therefore no temperature dependent processes take place in solution, suggesting that the dinuclear complex remains intact. The complex is the only species in solution detectable by NMR spectroscopy. The slight curvature observed in the plots for the chemical shifts of the bridging toluene protons might be due to errors caused by the broadness of these peaks. The Curie-Weiss behavior found for solutions of **1b$_2$-μ-toluene** (–70 to 25 °C) is consistent with similar behavior observed in the solid-state for the same temperature range (see below).
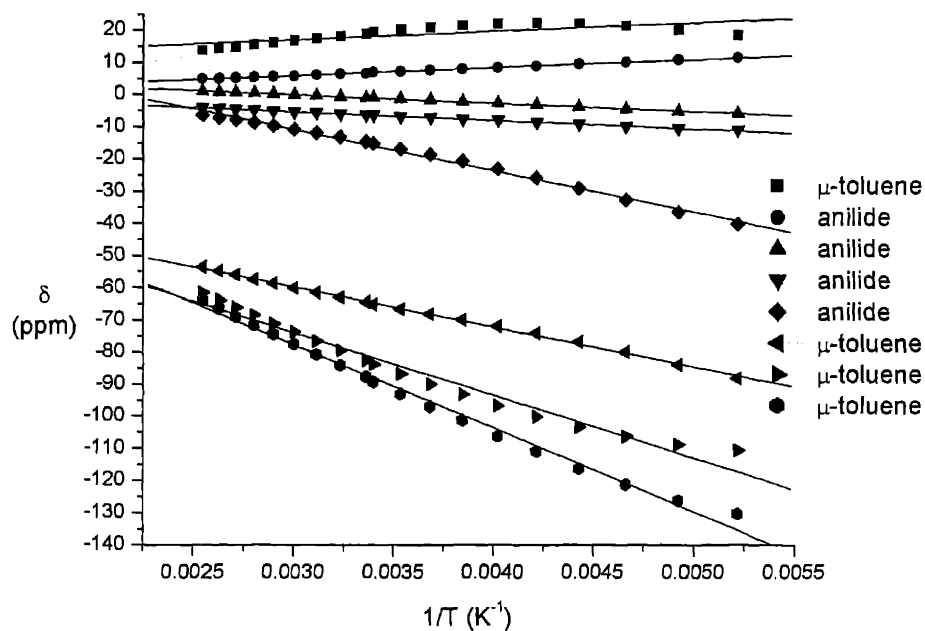
Figure 13. Plot of δ versus 1/T for compound **1b₂-μ-toluene**.
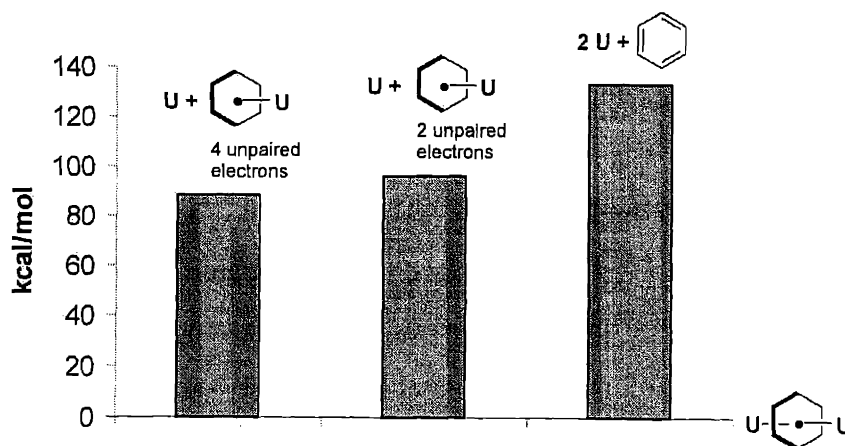
Figure 14. Energies for the dinuclear-mononuclear equilibria (U = U(NH₂)₂).

In order to further examine the possibility for the equilibria mentioned above, DFT calculations on the hypothetical fragments U(NH₂)₂ and (C₆H₆)U(NH₂)₂ were performed. Calculations on the fragment U(NH₂)₂ were carried out with four electrons of spin α in excess of spin β. As

indicated in Figure 13, for the fragment $(C_6H_6)U(NH_2)_2$ the calculations were carried out both with two and four electrons of spin α in excess of spin β. A comparison of the total bonding energies for the systems indicated in Figure 14 shows that $(\mu$-$C_6H_6)U_2(NH_2)_4$ has an energy lower by ca. 90 kcal/mol than that of any of the mononuclear systems considered.

1.2.5. Solid state magnetic susceptibility measurements

Magnetic properties of uranium compounds are more difficult to interpret than those of transition metal or even lanthanide compounds.[34] Because there is significant spin-orbit coupling in ions of lanthanides and actinides, the spin-only formula, which works well for many first row transition metal complexes, is not applicable to f-element complexes. The effective magnetic moment for these elements depends on J, where $J = L + S$.

$$\mu_{eff}{}^2 = g^2 J(J + 1),$$

where the Landé g value is given by $g = [3J(J + 1) + S(S + 1) - L(L + 1)]/[3J(J + 1)]$.[35]

SQUID measurements were carried out on the whole series in order to compare the behavior of the mononuclear compounds to that of the bridged toluene diuranium species **1b$_2$-μ-toluene**. The plots of $1/\chi$ and μ_{eff} versus T are shown in Figures 15-18. The solid-state magnetic properties of the mononuclear compounds follow some general trends. For example, at low temperatures the $1/\chi$ graphs of **1a-I** and **2a-I** show temperature independent paramagnetism (TIP, 5-25 K for **1a-I** and 5-15 K for **2a-I**). TIP behavior is specific to even electron species since at low temperatures the ground state can be an orbital singlet.[36] Odd electron species such as U(III) (**2a-THF**) and U(V) (**2a-NSiMe$_3$**) compounds would never present a singlet ground state, therefore their low temperature magnetic behavior is different than that of U(IV) compounds.
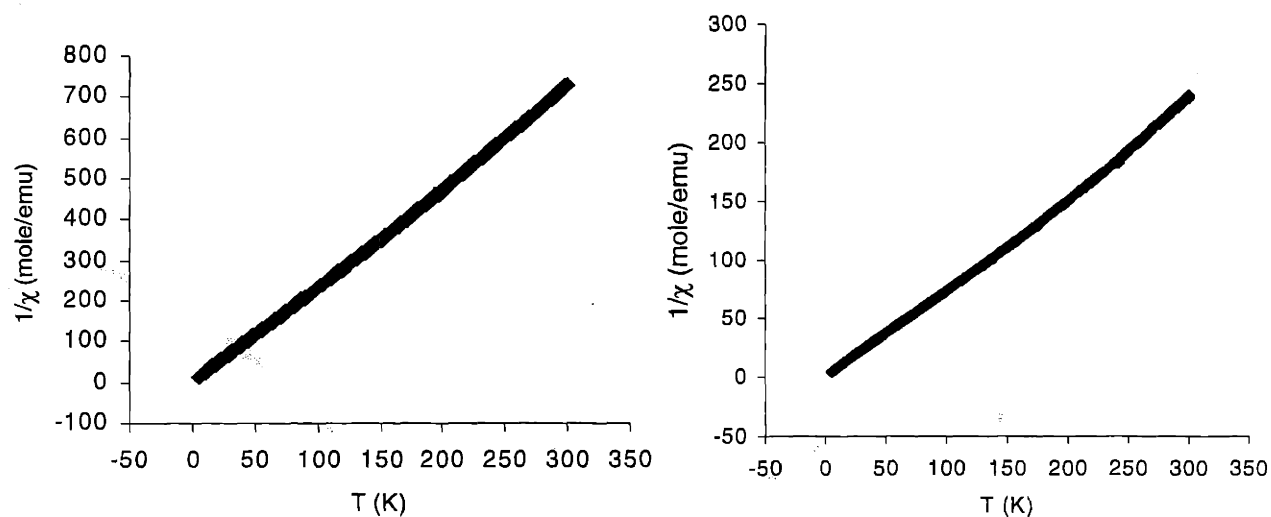
Figure 15. Plot of $1/\chi$ versus T for **2a-THF** (left) and **2a-NSiMe₃** (right).
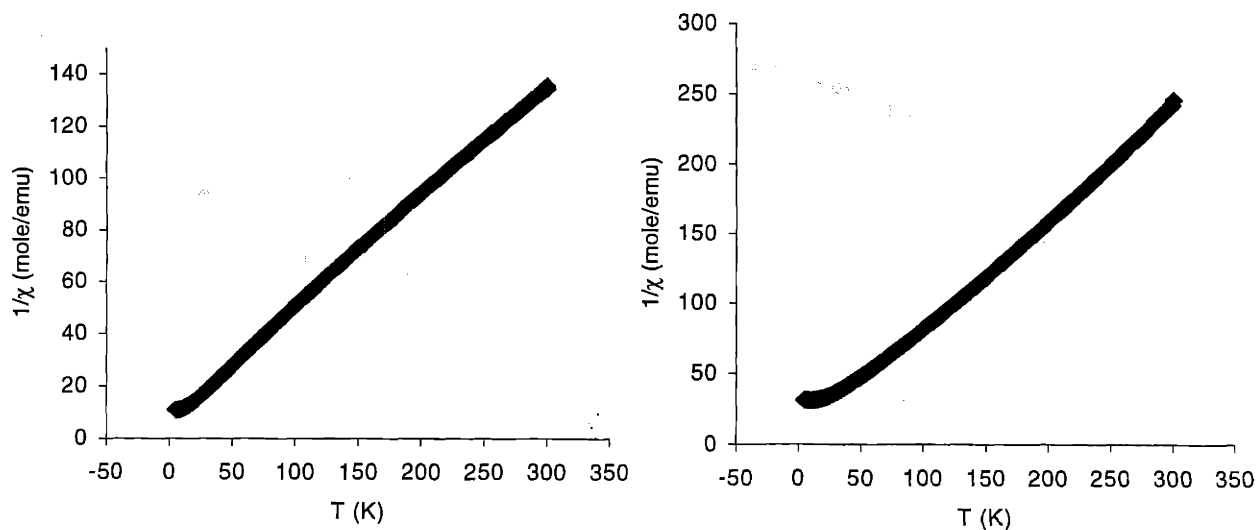
Figure 16. Plot of $1/\chi$ versus T for **1a-I** (left) and **2a-I** (right).

Although magnetic moments are difficult to interpret due to crystal field splitting of the ground state in the case of uranium compounds,[36] it is notable that the magnetic moment for compound **1b₂-μ-toluene** is temperature dependent (from 0.25 μ_B at 5 K to 1.50 μ_B at 300 K, values for one

References begin on page 75

uranium center), while the mononuclear compounds exhibit Curie-Weiss behavior on the 5-300 K temperature range (except for the TIP intervals for **1a-I** and **2a-I**).
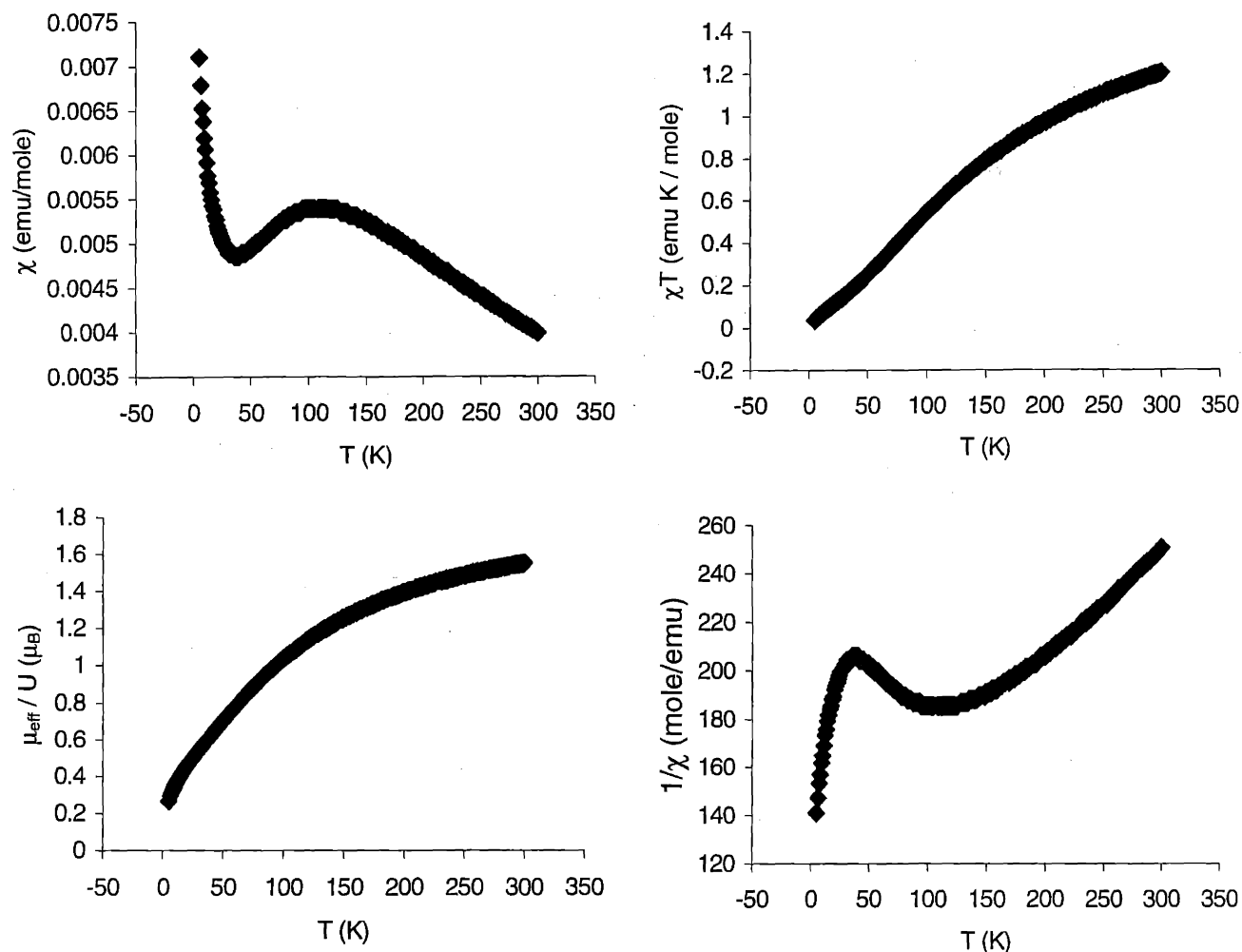
Figure 17. Plots of χ (top, left), χT (top, right), μ_{eff} (bttom, left) and $1/\chi$ (bottom, right) versus T for **1b$_2$-μ-toluene**.

The determined μ_{eff} for **2a-THF** (3.20 μ_B)[6] is lower than the magnetic moment of **2a-I** (3.52 μ_B, 30-300 K) and it has a similar value to μ_{eff} determined for **1a-I** (3.18 μ_B, 50-300 K). Overlap of magnetic moment values for uranium(III) and uranium(IV) compounds is normal since the calculated values for the free ions are very close: 3.62 μ_B for U(III) ($^4I_{9/2}$ ground state) and 3.58

μ_B for U(IV) ($^3H_4$ ground state). The magnetic moment obtained for **2a-NSiMe$_3$** is 1.81 μ_B, smaller than any of the other magnetic moments of the mononuclear compounds, but consistent with one unpaired electron and values for similar compounds.[37]

From the plot of χ versus T for **1b$_2$-μ-toluene** (Figure 17) we see that the magnetic susceptibility exhibits a broad maximum around 110 K and then decreases as the temperature is lowered, behavior consistent with an antiferromagnetic transition. On cooling below 30 K, χ increases again and below 20 K, the plot of $1/\chi$ versus T (Figure 17) is consistent with paramagnetic behavior. The interpretation of the magnetic behavior of **1b$_2$-μ-toluene** (30-300 K) in terms of an antiferromagnetic transition is supported by the fact that the product χT (Figure 17) continuously decreases as the temperature is lowered. A theoretical model that fits the experimental data has not been developed, but it is possible that antiferromagnetic coupling of the unpaired electrons in **1b$_2$-μ-toluene** occurs through the toluene bridge. The magnetic properties observed for **1b$_2$-μ-toluene** are not unusual for open-shell symmetrical dinuclear compounds.[38]

1.2.6. Electronic spectra

As is the case with magnetic properties, electronic spectra of uranium complexes are complicated due to the splitting by ligand-field and spin-orbit coupling of a multitude of states derived from f^n configurations.[39] The electronic spectra are comprised of $f \rightarrow f$, $f \rightarrow d$, and charge transfer bands. Usually, bands are assigned based on the magnitude of the molar absorption coefficient and the position of a band in a spectrum.[40] Therefore, as shown in Figures 18-22, bands present in the UV region (200-400 nm), because of their high intensity ($\varepsilon \approx 10^5$ M^{-1} cm^{-1}) can be assigned to $\pi \rightarrow \pi^*$ transitions of the arene rings or to ligand to metal charge transfer bands. Intense absorption bands present in the visible region (400-800 nm) that have $\varepsilon \approx 10^3$ M^{-1} cm^{-1} could be either $f \rightarrow d$ or charge transfer transitions.

The f → f transitions for lanthanides and actinides are, like d → d transitions of transition metal ions, electric-dipole forbidden by the Laporte selection rule. Interaction with the ligand field or with vibrational states mixes in electronic states with different parity and so f → f transitions become possible. However, because of the small radial extent of the f-orbitals, these interactions are weak and the intensity of f → f transitions is therefore much lower than that of d → d transitions, and the absorptions are much sharper.
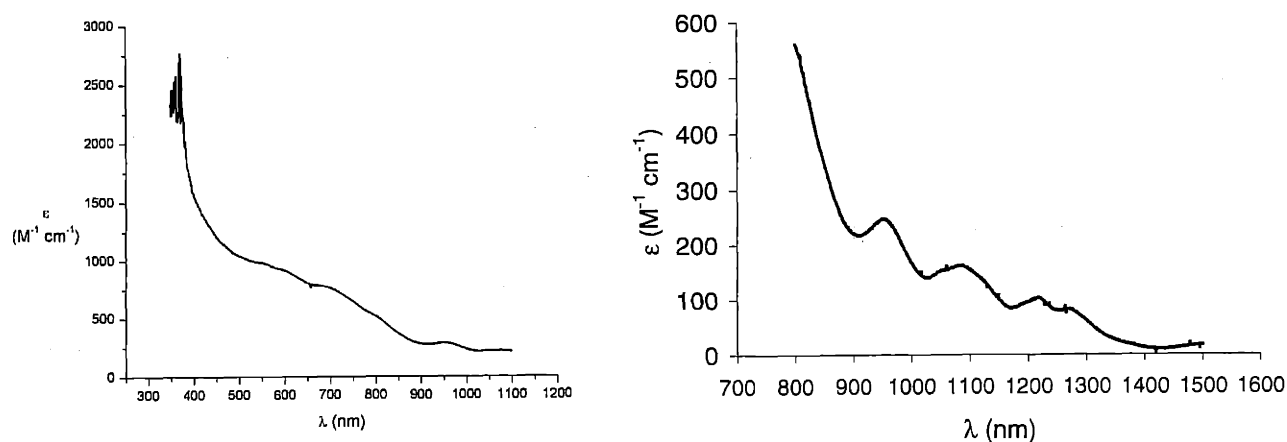
Figure 18. UV-vis (left) and NIR (right) absorption spectra of **2a-THF** in THF solution at 25 °C.
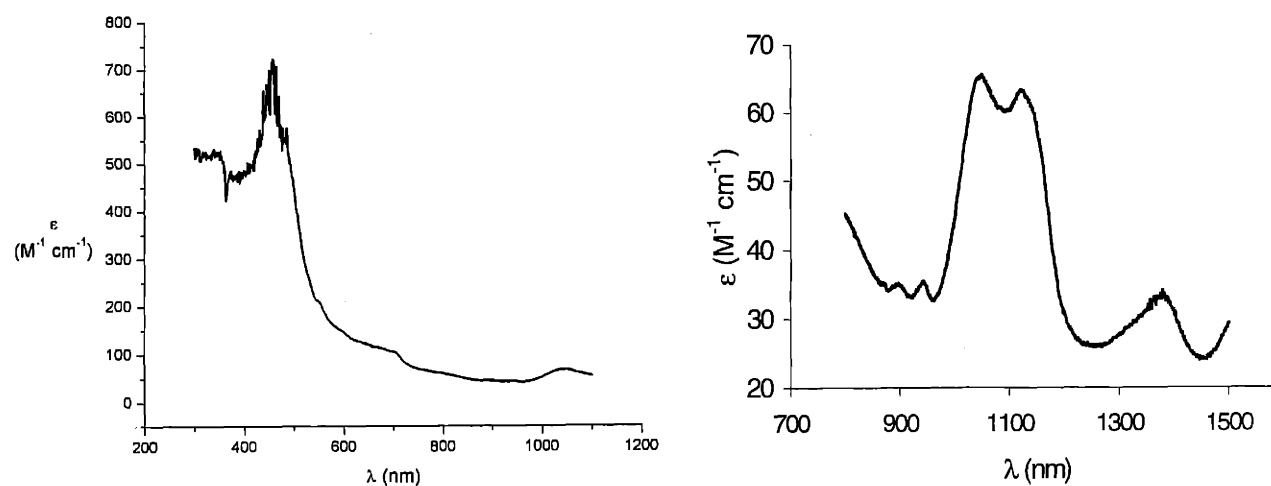
Figure 19. UV-vis (in benzene, left) and NIR (in toluene, right) absorption spectra of **2a-I** solutions at 25 °C.

Chapter 1

The most interesting region of the electronic spectra for uranium compounds is the NIR region (spectra reported here were recorded from 1500 to 800 nm) because most compounds show "fingerprint" features.[42] These characteristics are assigned to Laporte-forbidden f → f transitions and have molar absorption coefficients in the range $10\text{-}10^2$ M^{-1} cm^{-1}. With the exception of the U(III) compound **2a-THF** (ε = 100-260 M^{-1} cm^{-1}) the other mononuclear compounds show weak bands in the NIR region ($\varepsilon < 100$ M^{-1} cm^{-1}).
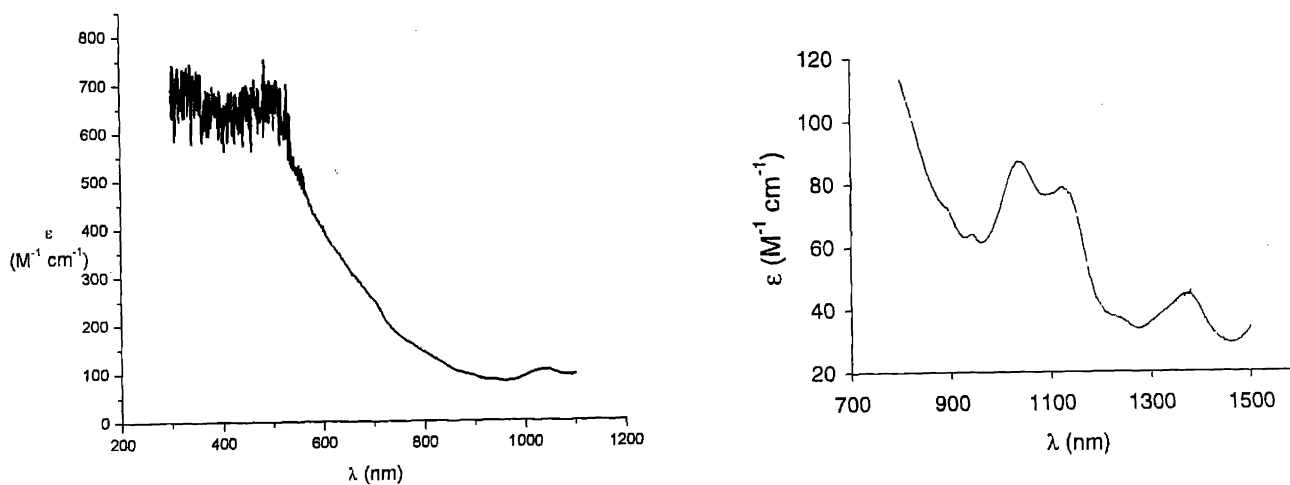
Figure 20. UV-vis (in benzene, left) and NIR (in toluene, right) absorption spectra of **1a-I** solutions at 25 °C.
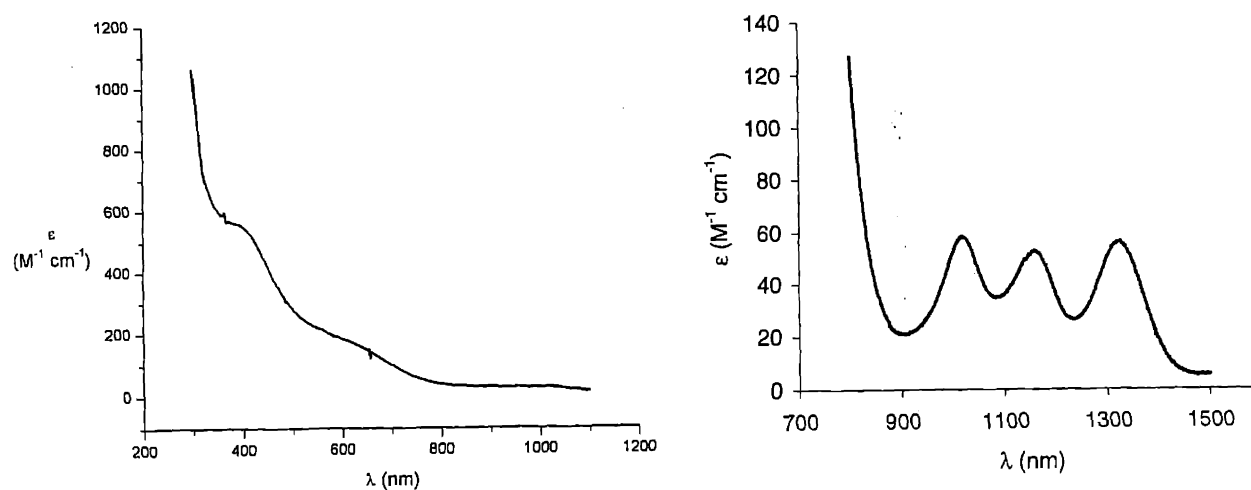
Figure 21. UV-vis (left) and NIR (right) absorption spectra of **2a-NSiMe3** in toluene solutions at 25 °C.

References begin on page 75

Interestingly, complex **1b$_2$-μ-toluene** has intense and sharp bands (ε = 200-600 M^{-1} cm^{-1}) in this region. One possible explanation is suggested by the results of the DFT calculations on the model compound (μ-C$_6$H$_6$)U$_2$(NH$_2$)$_4$. The combinations of f orbitals that are the highest single occupied molecular orbitals and the lowest unoccupied molecular orbitals are of different symmetry types, enhancing the probability of f → f transitions.
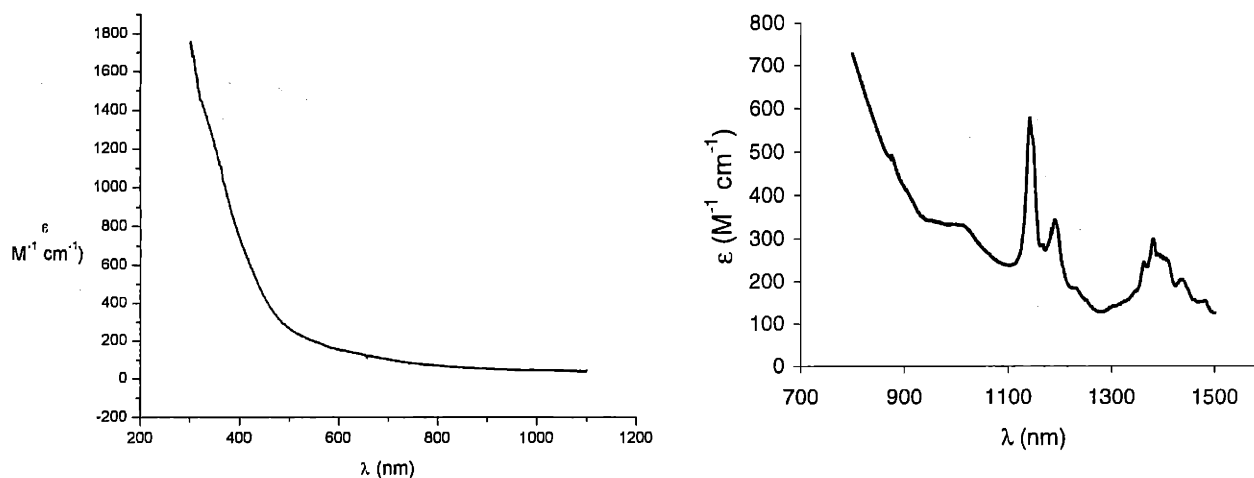
Figure 22. UV-vis (left) and NIR (right) absorption spectra of **1b$_2$-μ-toluene** in toluene solutions at 25 °C.

Intense bands in the NIR region have been associated with intervalence electron transfer (IT) from one redox site to another.[41,42] Intense and narrow bands are characteristic of IT that occurs between two metal centers of symmetrical complexes.[43] They have been noticed mostly for compounds in which the two metal centers are in different oxidation states and are an indication of a delocalized unpaired electron.[44] Since **1b$_2$-μ-toluene** contains unpaired electrons and uranium is known for the possibility of accessing multiple oxidation states, IT processes may be partially responsible for the intense, sharp, narrow bands observed in Figure 23.

1.2.7. Reactivity studies

Theoretical studies on $(\mu\text{-}C_6H_6)U_2(NH_2)_4$ highlighted the role of δ bonds. There are only scarce reports of early actinides with π-acceptor ligands (for example, two cases when N_2 acts as a ligand[7,8] and two cases when CO^{44} acts as a ligand. The paucity of such examples may arise from the high nodality of f orbitals,[45] which match poorly with π-ligand molecular orbitals. Prompted by this notion, experiments involving treatment of compound **1b₂-μ-toluene** with CO or ethylene were performed. Under stoichiometric conditions no reaction was observed.

Since the +4 oxidation state is pervasive in the organometallic chemistry of uranium,[46] reactivity studies of the bridged arene complexes were expected to reveal redox processes along with information on the number of electrons involved in such processes. Substrates including diphenyl disulfide and azobenzene were initially chosen to probe whether compound **1b₂-μ-toluene** can behave as a source of diamido uranium(II).[47]

2.0 S₂Ph₂
74%
─────────
─ toluene
R = C(CH₃)₃
Ar = 3,5-C₆H₃Me₂
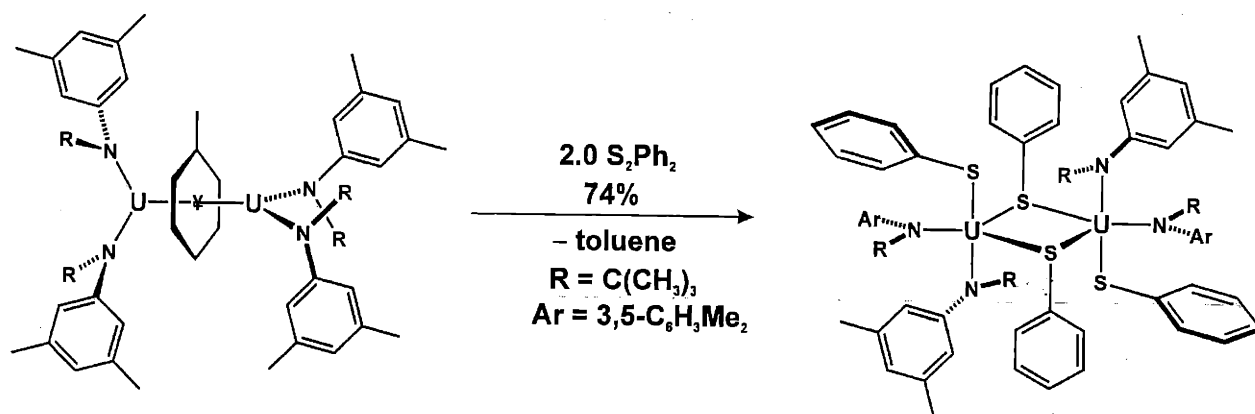
Scheme 2

Compound **1b₂-μ-toluene** reacts with diphenyl disulfide (2 equiv) to form a yellow compound isolated in 74% yield (Scheme 2). By X-ray crystallography, the product was determined to be a dimeric thiolate-bridged U(IV) derivative, $(\mu\text{-}SPh)_2U_2(N[t\text{-}Bu]Ar)_4(SPh)_2$ (**1b₂-(μ-SPh)₂(SPh)₂**)

(Figure 23). Due to the fact that X-ray crystallography is not optimal for ruling out the presence of hydride ligands, this reaction was also used in a Toepler pump experiment showing that H_2 is not produced, suggesting that compound **1b$_2$-μ-toluene** does not contain unobserved hydride ligands.
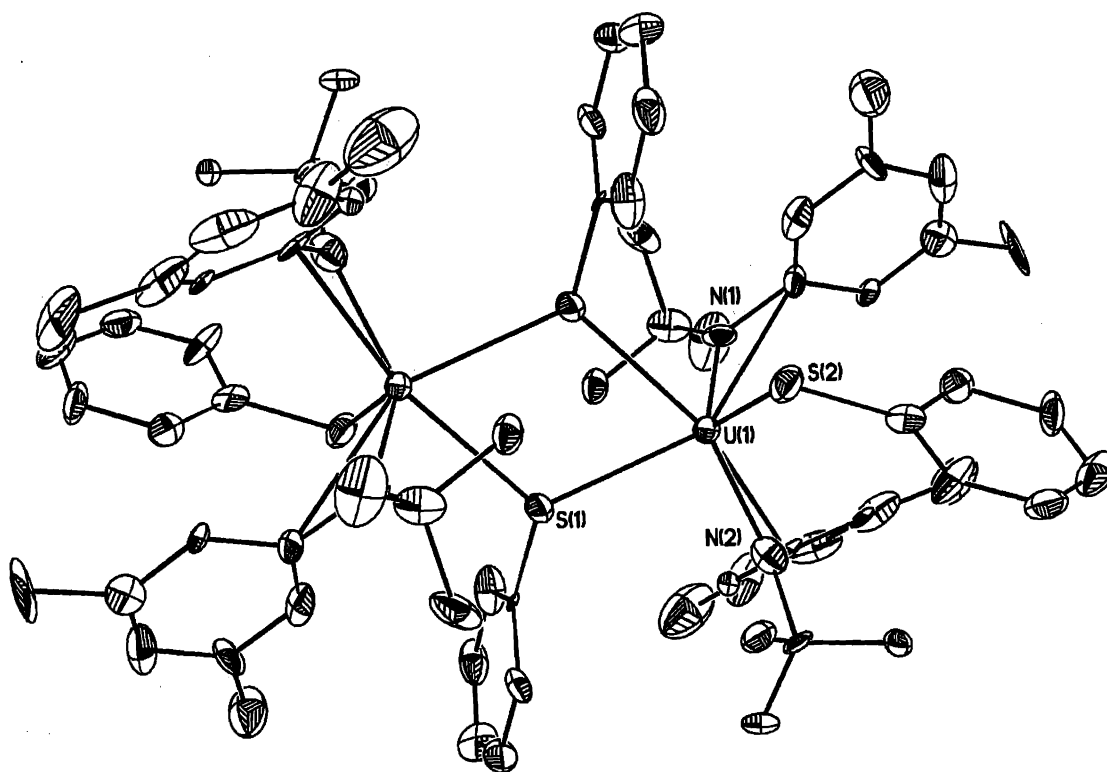
Figure 23. Structural drawing of complex **1b$_2$-(μ-SPh)$_2$(SPh)$_2$** with thermal ellipsoids at the 35% probability level. Selected bond distances (Å): U–S(1), 2.775(7); U–S(1A), 2.911(6); U–S(2), 2.674(7); U–N (avg.), 2.20(3); U–C(11), 3.00(3); U–C(21), 2.94(2).

Compound **1b$_2$-μ-toluene** also reacts with azobenzene (1 equiv) and forms a uranium(IV) phenylimido-bridged dimer, **(μ-NPh)$_2$U$_2$(N[*t*-Bu]Ar)$_4$** (**1b$_2$-(μ-NPh)$_2$**, Figure 24). Since the above reaction indicated that compound **1b$_2$-μ-toluene** indeed behaves as a uranium(II) source, oxidation by azobenzene is not surprising. However, there are few examples of 4 electron azobenzene reductive cleavage (Scheme 3) reported previously.[48,49]
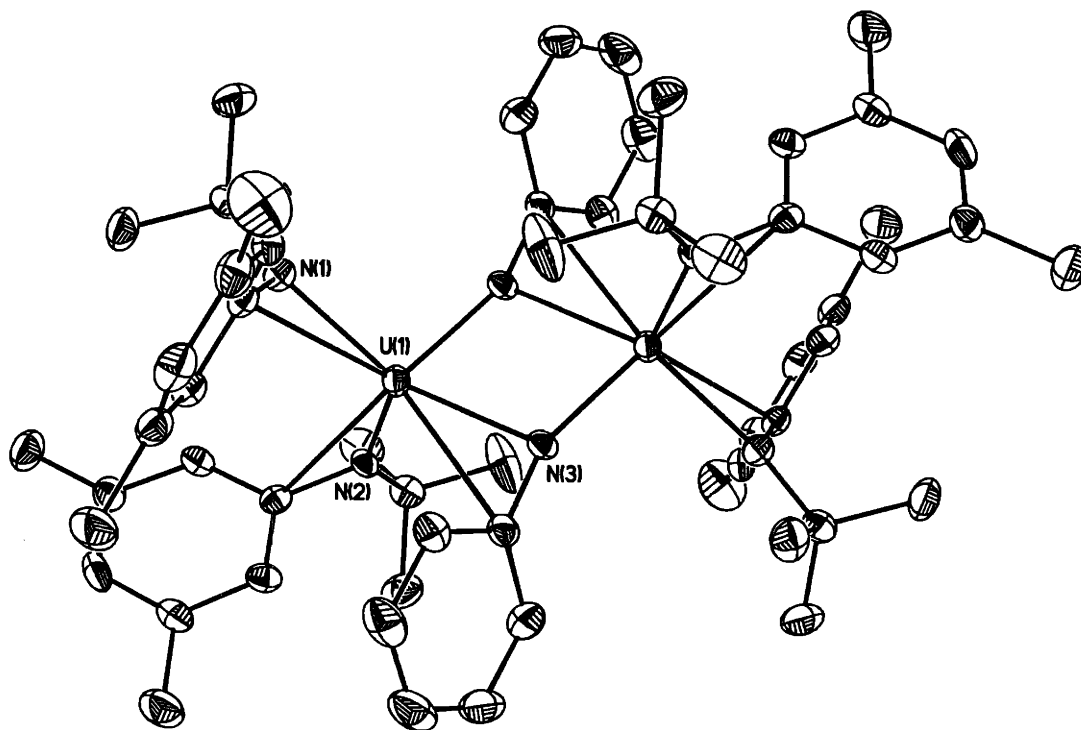
Figure 24. Structural drawing of complex **1b₂-(μ-NPh)₂** with thermal ellipsoids at the 35% probability level. Selected bond distances (Å): U(1)-N(3), 2.335(6); U(1)-N(3A), 2.153(6); U(1)-N(1), 2.236(6); U(1)-N(2), 2.249(5); U(1)-C(1), 2.835(7); U(1)-C(11), 2.913(7); U(1)-C(21), 2.914(7).
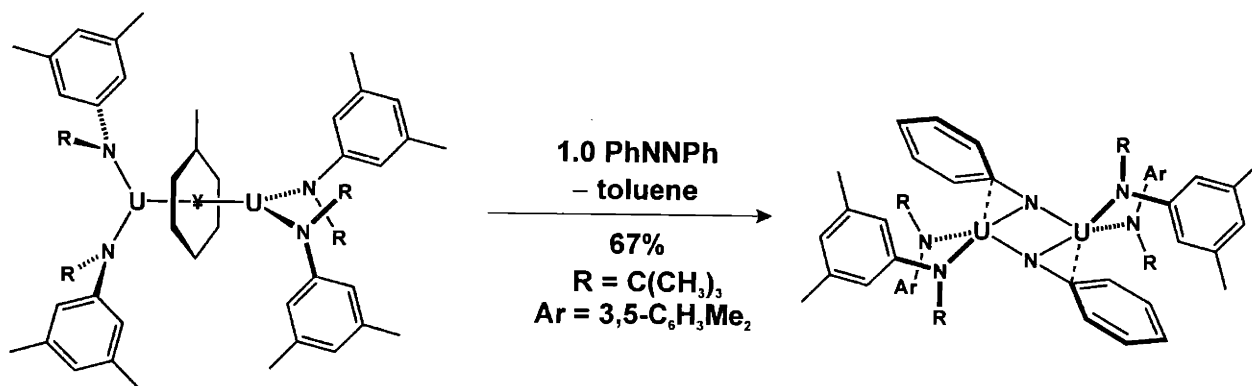
Scheme 3

The ^{1}H NMR spectrum of the crude mixture shows that the reaction was fairly clean and thus it could be monitored by ^{2}H NMR spectroscopy to determine whether toluene loss occurs from **1b₂-μ-toluene-*d*₈**. Integration of the ^{2}H NMR spectrum (based on the presence of an internal integration standard - octane-*d*₁₈) of the crude reaction mixture indicated that ca. 0.75 equiv of C_7D_8 was generated. The failure to observe the other 0.25 equiv is most likely due to experimental error rather than chemical transformations.
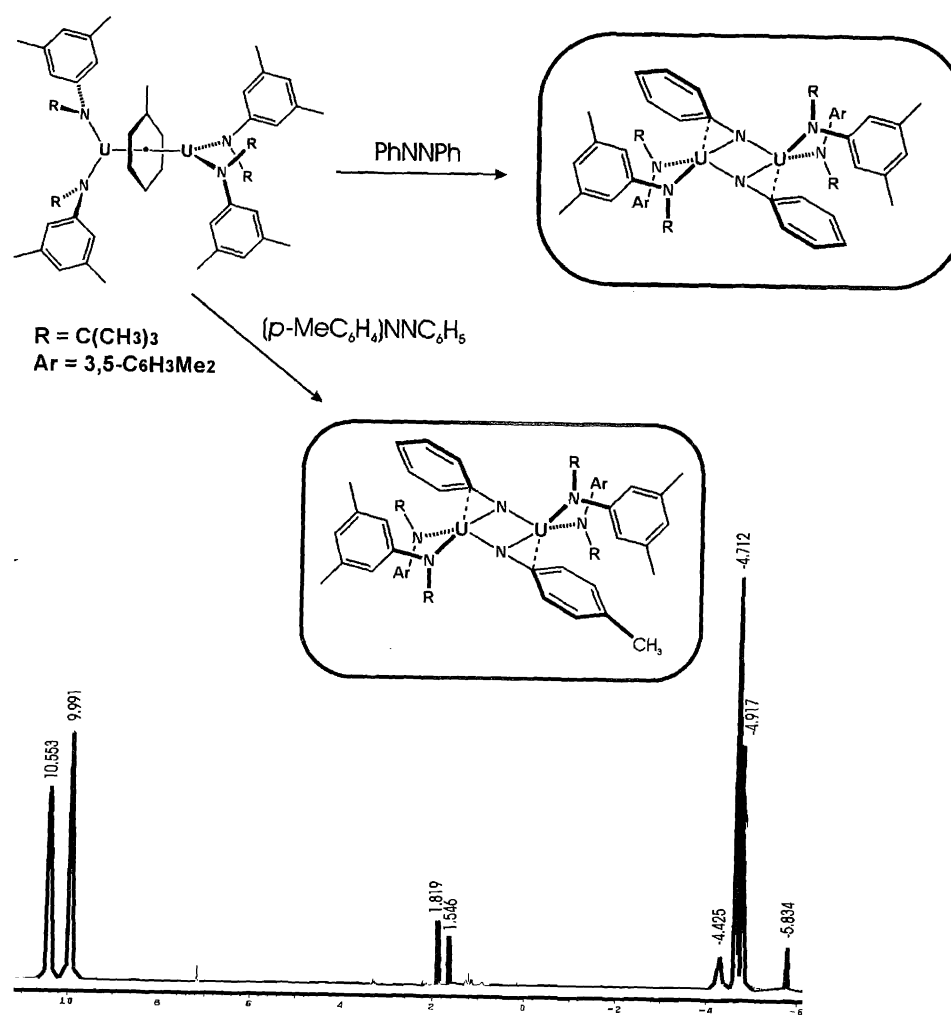
Figure 25. ^{1}H NMR spectrum of a mixture of **1b₂-(μ-NPh)₂** and **1b₂-(μ-NPh)(μ-NPh-*p*-Me)** after one week of mixing at room temperature.

The formation of the uranium(IV) phenylimido-bridged dinuclear compound, **1b$_2$-(μ-NPh)$_2$**, raises the possibility of a monomeric reaction intermediate, (PhN)U(N[t-Bu]Ar)$_2$. To verify if this is the case, a similar reaction was carried out using an asymmetric azobenzene substrate, 4-methyl-azobenzene.[50] The observation of only one major product, which was different than the one isolated in the reaction with azobenzene (by ^{1}H NMR analysis), demonstrated that the above monomeric intermediate is unlikely to form in the course of the reaction. If the monomeric (PhN)U(N[t-Bu]Ar)$_2$ is in equilibrium with **1b$_2$-(μ-NPh)$_2$**, then a mixture of **1b$_2$-(μ-NPh)$_2$** and **1b$_2$-(μ-NPh)(μ-NPh-p-Me)** should lead to a statistical mixture of **1b$_2$-(μ-NPh)$_2$**, **1b$_2$-(μ-NPh)(μ-NPh-p-Me)**, and **1b$_2$-(μ-NPh)$_2$** after reaching equilibrium. The ^{1}H NMR spectrum of such a mixture (**1b$_2$-(μ-NPh)$_2$** and **1b$_2$-(μ-NPh)(μ-NPh-p-Me)**) shows a superposition of the ^{1}H NMR spectra of the two compounds even after one week at room temperature (Figure 25). A plausible mechanism involves the formation of a mononuclear η^2-azoarene complex or of a *bis*-imido-*bis*-amidouranium compound (PhN)$_2$U(N[t-Bu]Ar)$_2$, which then reacts with another uranium center to produce the bridged phenylimido dimer. This proposed mechanism would also be in agreement with the general assumption that the formation of either an η^2-intermediate (or a diazametallocyclopropane complex)[51] or a *bis*-imido intermediate alters the N=N bond by reducing its order.[50]

In light of the redox reactions presented above, reactions with elemental chalcogens were expected to lead to *bis*-amide uranium structures, either mononuclear or dinuclear. Surprisingly, the reaction between **1b$_2$-μ-toluene** and excess selenium led to (μ-Se)U$_2$(N[t-Bu]Ar)$_6$ **1a$_2$-μ-Se** (Figure 26). Similar reactions with elemental sulfur or elemental tellurium produce known dinuclear compounds based on tris-amide fragments: (μ-S$_2$)U$_2$(N[t-Bu]Ar)$_6$ **1a$_2$-μ-S$_2$** and (μ-Te)U$_2$(N[t-Bu]Ar)$_6$ **1a$_2$-μ-Te**.[52] Also, the reaction between **1b$_2$-μ-toluene** and oxygen sources such as OPPh$_3$ gave (μ-O)U$_2$(N[t-Bu]Ar)$_6$ **1a$_2$-μ-O**. The series of uranium chalcogenides was initially prepared by P. L. Arnold from **1a-THF** and X-ray crystal structures for **1a$_2$-μ-O** and **1a$_2$-μ-S$_2$** were determined.[51]
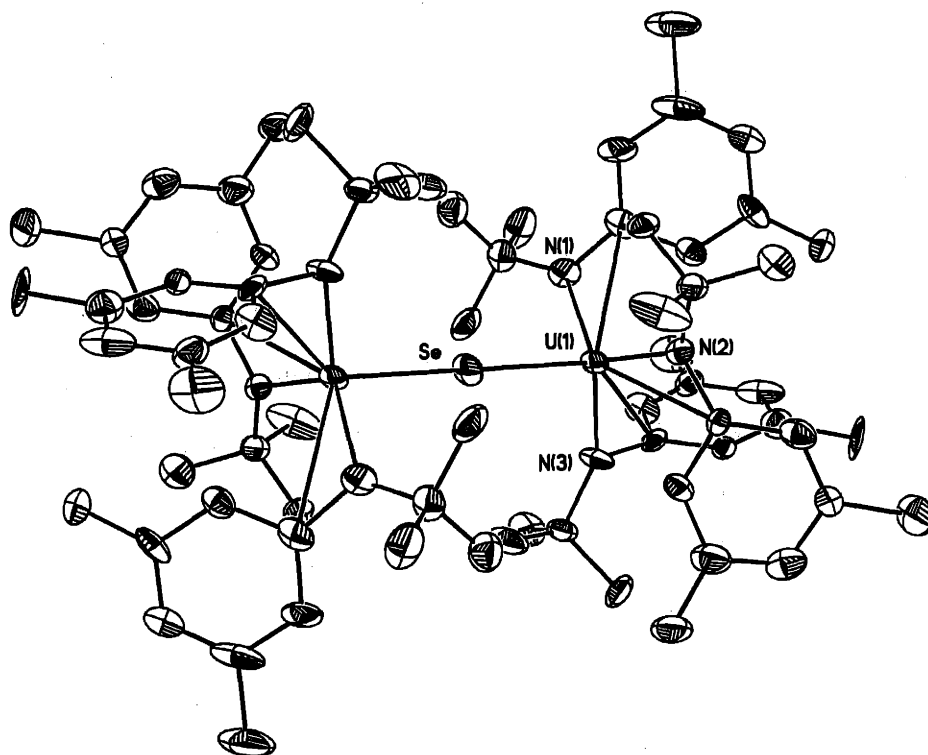
Figure 26. Structural drawing of complex **1a₂-µ-Se** with thermal ellipsoids at the 35% probability level. Selected bond distances (Å): U-N (avg.), 2.235(27); U-Se, 2.7560(7).
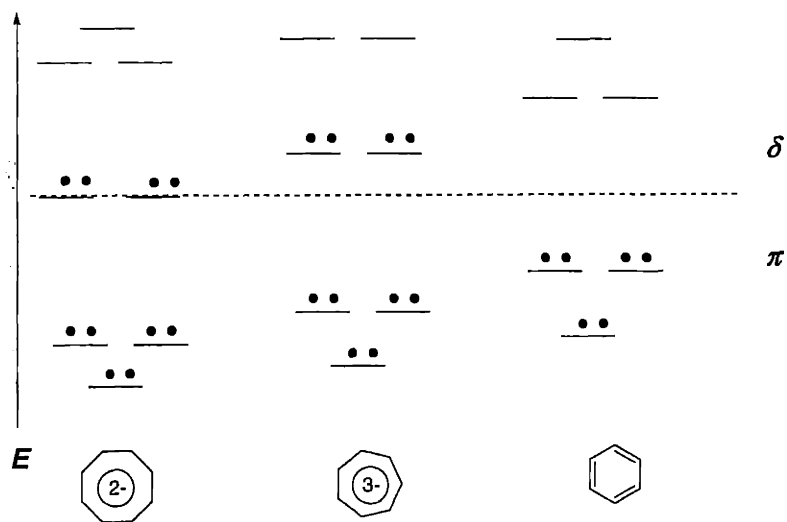
Scheme 4
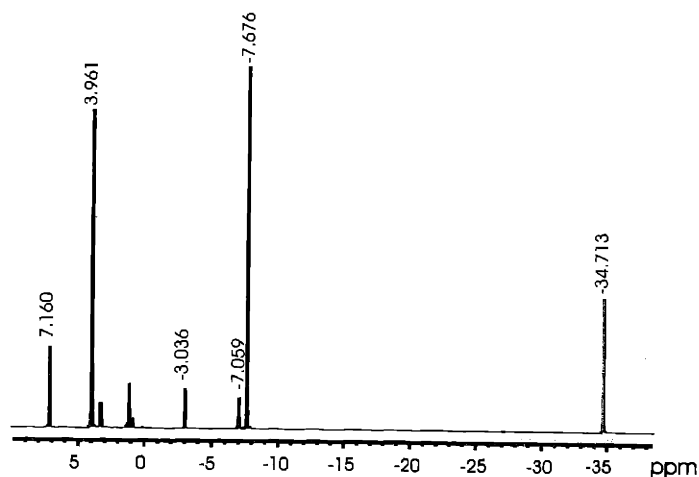
Figure 27. ^{1}H NMR (300 MHz, C_6D_6, 22°C) spectrum of (COT)U(N[*t*-Bu]Ar)$_2$.
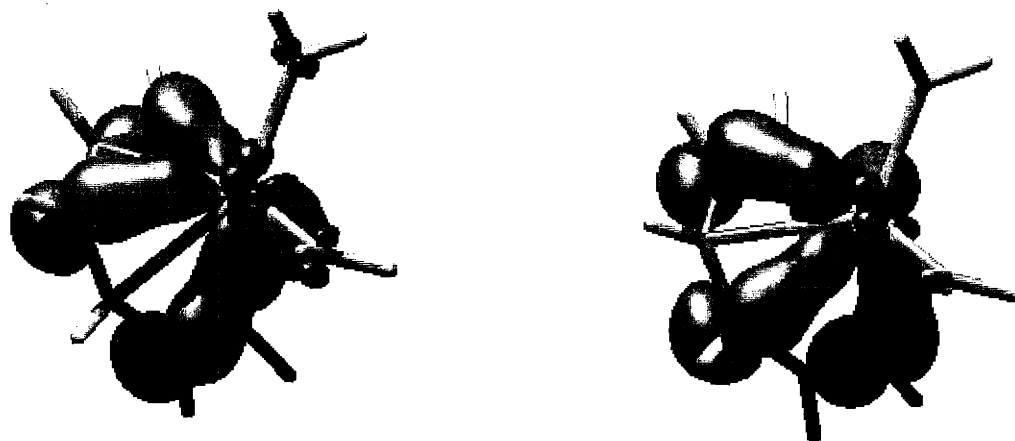
Figure 28. The δ bonds in (COT)U(NH$_2$)$_2$: SOMO-2 (left) and SOMO-3 (right). Orbitals are from a PW91 calculation and the α component is represented here.

Cyclooctatetraene is an interesting choice for a reaction with **1b$_2$-μ-toluene** since the δ-symmetry orbitals are now occupied (Scheme 4). Reaction of **1b$_2$-μ-toluene** with 2 equiv of 1,3,5,7-cyclooctatetraene leads to a single product (95% yield), presumably (COT)U(N[*t*-Bu]Ar)$_2$ based on its ^{1}H NMR spectrum (Figure 27) and elemental analysis. The protons belonging to the COT ring are equivalent and give rise to a single peak in ^{1}H NMR spectrum at ca. –35 ppm. This chemical shift compares well to the corresponding one for K(COT)U(NC[*t*-

Bu]Mes)$_3$. Although it was not possible to characterize the compound by X-ray crystallography, a DFT calculation on the model $(COT)U(NH_2)_2$ indicates that there is good overlap between the f orbitals of δ symmetry and the HOMOs of COT (Figure 28). The two unpaired electrons reside in uranium f orbitals and the double occupied orbitals following these SOMOs are the δ bonds.

1.3. Conclusions

The fascinating compound **1b$_2$-μ-toluene** has been studied extensively using a variety of methods and its properties compared to the properties of a series of mononuclear uranium amide complexes. While the mononuclear compounds display expected electronic and magnetic properties for uranium complexes, **1b$_2$-μ-toluene** shows complicated properties by contrast. Optical and magnetic characteristics of **1b$_2$-μ-toluene** are difficult to relate to reported examples of classical uranium organometallic complexes. This difficulty arises from the peculiarities of the electronic structure of the arene-bridged diuranium core. XANES spectroscopy, X-ray crystallography, and DFT calculation results corroborate the bonding interpretation: the unpaired electrons reside in mainly f orbitals (some optical and magnetic features could be identified as due to these electrons) and between the uranium centers and toluene there is a pair of δ bonds formed by filled uranium f orbitals and LUMOs of toluene. An effective electronic charge comparable to that encountered in classical uranium (III) compounds is consistent with the covalent bond between uranium and toluene and reflected in the metrical parameters from the X-ray crystal structure of **2b$_2$-μ-toluene**.

Reactivity studies demonstrate that the powerful reductant U(II) can be accessed from **1b$_2$-μ-toluene** in the presence of adequate substrates. Reactions with azobenzene and diphenyl disulfide lead to bridged dinuclear uranium *tetrakis*-amide complexes. Rather surprisingly, bridged dinuclear uranium *hexakis*-amide complexes are formed in the presence of chalcogens. This ligand disproportionation reaction and the fact that one ligand is lost during the reduction of

References begin on page 75

the *tris*-amidouranium iodide complexes prompted the investigation of a more generally applicable set of ligands (see Chapter 2). Mononuclear uranium compounds can be formed from reactions of **1b$_2$-μ-toluene** with certain substrates as shown for 1,3,5,7-cyclooctatetraene and will be presented for 2,2'-bipyridyl (see Chapter 3).

1.4. Experimental

1.4.1. General considerations

Unless stated otherwise, all operations were performed in a Vacuum Atmospheres drybox under an atmosphere of purified nitrogen or using Schlenk techniques under an argon atmosphere. Anhydrous diethyl ether was purchased from Mallinckrodt; pentane, *n*-hexane and tetrahydrofuran were purchased from EM Science. Diethyl ether, toluene, benzene, pentane and *n*-hexane were dried and deoxygenated by the method of Grubbs.[53] THF was distilled under nitrogen from purple sodium benzophenone ketyl. Distilled solvents were transferred under vacuum into bombs before being pumped into a Vacuum Atmospheres dry box. (Me$_3$Si)$_2$O was degassed and dried over 4 Å sieves. C$_6$D$_6$, toluene-d_8 and octane-d_{18} were purchased from Cambridge Isotopes and were degassed and dried over 4 Å sieves. 4 Å sieves, alumina and Celite were dried *in vacuo* overnight at a temperature just above 200 °C. UI$_3$(THF)$_4$,[10] IU(N[*t*-Bu]Ar)$_3$ (**1a-I**),[8] LiN[^{1}Ad]Ar,[11] KC$_8$,[54] PhNNPh-d_{10},[55] and *p*-MePhNNPh[45] were prepared acoording to literature methods. Other chemicals were used as received. ^{1}H and ^{2}H NMR spectra were recorded on Varian XL-300 or Varian INOVA-501 spectrometers at room temperature unless otherwise specified. Chemical shifts are reported with respect to C$_6$D$_6$ (7.16 ppm) as an internal or external standard. UV-vis spectra were recorded on a HP spectrophotometer from 200 to 1100 nm using matched 1 cm quartz cells. Spectra were recorded on 5 different samples and errors determined. NIR spectra were recorded on an Aviv 14DS spectrophotometer from 800 to 1500

nm using matched 1 cm quartz cells; all spectra were obtained using a solvent reference blank.[*]
Numerical modeling of all data was done using the program Origin 6.0. CHN analyses were
performed by H. Kolbe Mikroanalytisches Laboratorium (Mülheim an der Ruhr, Germany).

1.4.2.1. Synthesis of compound (μ-toluene)U₂(N[*t*-Bu]Ar)₄ 1b₂-μ-toluene

Method A. 1a-I (0.554 g, 0.620 mmol) was dissolved in 60 mL of toluene. Separately, a slurry
of KC_8 (0.251 g, 1.86 mmol, 3 equiv) in 40 mL of toluene was prepared and both solutions were
cooled to near freezing. The thawing KC_8 slurry was added slowly over 5 min to the thawing
solution of **1a-I**. The reaction mixture was stirred for 40 min after which was filtered through
Celite and washed with pentane (25 mL). The volatiles were removed under reduced pressure,
the product extracted with pentane (100 mL) and the extract filtered through Celite. The
operations in the last statement were repeated twice (three extractions with pentane total), the
new extract was concentrated to about 15 mL and cooled to -35 °C. After 2-3 days, compound
1b₂-μ-toluene was obtained in 38% yield (0.150 g, 0.118 mmol) as dark-brown crystals.

Method B. A mixture of UI₃(THF)₄ (0.620 g, 0.684 mmol), Li(OEt₂)(N[*t*-Bu]Ar) (0.351 g, 1.366
mmol, 2 equiv), and KC_8 (0.277 g, 2.051 mmol, 3 equiv) was cooled to -100 °C for 30 min.
Thawing toluene (125 mL) was added to the stirring mixture and the reaction allowed to go for
135 min. The slurry was filtered through Celite and washed with 25 mL of pentane. The volatiles
were removed under reduced pressure, the product extracted with pentane (100 mL), and the
extract filtered through Celite. The operations in the last statement were repeated twice (three
extractions with pentane total), the new extract was concentrated to about 15 mL and cooled to -
35 °C. Compound **1b₂-μ-toluene** was obtained after 2-3 days in 32% yield (0.140 g, 0.110
mmol).

---

[*] The NIR spectra were obtained in the laboratories of Prof. Daniel G. Nocera with the help of Aetna Wun.

Note: Attempts to scale up the above procedures for the synthesis of **1b$_2$-μ-toluene** were not successful.

^{1}H NMR (300 MHz, C$_6$D$_6$, 22°C): δ = 18.68 (s, 3H, *CH$_3$*-toluene); 6.68 (s, 36H, *t-Bu*); -1.22 (s, 4H, *p*-Ar); -6.64 (s, 24H, *Me*-Ar); -15.54 (s, 8H, *o*-Ar); -65.86 (s, 1H, *p*-toluene); -82.98 (s, 2H, *m*-toluene); -88.39 (s, 2H, *o*-toluene).

UV-vis-NIR (toluene, 22 °C): λ$_{max}$ (nm, ε × 10^{-2} M^{-1}, cm^{-1}) = 288 (240.2 ± 21.9); 300 (190.6 ± 18.9); 496 (21.2 ± 2.1); 962 (3.4); 1010 (3.3); 1142 (5.8); 1195 (3.3); 1230 (1.8); 1363 (2.4); 1380 (3.0); 1407 (2.5); 1438 (2.0); 1480 (1.5).

Anal. calcd. for C$_{55}$H$_{84}$N$_4$U$_2$: C, 51.88; H, 6.33; N, 4.40. Found: C, 51.74; H, 6.22; N, 4.41.

1.4.2.2. Thermal stability of 1b$_2$-μ-toluene

In one experiment, variable temperature ^{1}H NMR studies in octane-d_{18} showed that **1b$_2$-μ-toluene** is stable up to 110 °C. The spectra were acquired from 20 °C to 110 °C at 10 °C intervals, and after reaching 110 °C, another spectrum was obtained on the same sample back to 20 °C. In another experiment, 40 mg of **1b$_2$-μ-toluene** in 20 mL of heptane was heated at 80 °C for 24 h. ^{1}H NMR spectrum of a sample taken from that solution indicated that the compound did not decompose.

1.4.2.3. Synthesis of compound 1b$_2$-μ-toluene-d_8

The procedure is similar to that reported for **1b$_2$-μ-toluene**, except for using toluene-d_8 instead of toluene.

^{1}H NMR (300 MHz, C$_6$D$_6$, 22 °C): δ = 6.68 (s, 36H, *t-Bu*); -1.22 (s, 4H, *p*-Ar); -6.64 (s, 24H, *Me*-Ar); -15.54 (s, 8H, *o*-Ar). ^{2}H NMR (76 MHz, pentane, 22 °C): δ = 18.68 (s, 3D, *CD$_3$*-toluene); -65.08 (s, 1D, *p*-toluene); -83.63 (s, 2D, *m*-toluene); -88.81 (s, 2D, *o*-toluene).

1.4.2.4. Synthesis of compound 1b$_2$-μ-C$_6$D$_6$

Two solutions of **1a-I** (0.100 g, 0.089 mmol) in 8 mL and KC$_8$ (0.045 g, 0.333 mmol, 3 equiv) in 4 mL of C$_6$D$_6$, respectively, were frozen. To the thawing **1a-I** solution was added dropwise the thawing KC$_8$ slurry. The reaction mixture was stirred for 15 min after which it was filtered through Celite and volatiles removed under reduced pressure. After extraction with pentane the solution (20 mL) was concentrated to 3 mL and cooled to -35 °C. The crystals (0.015 g, 0.012 mmol, 13% yield) obtained were used to prepare the NMR sample.

^{1}H NMR (300 MHz, C$_6$D$_6$, 22 °C): δ = 6.68 (s, 36H, *t-Bu*); -1.75 (s, 4H, *p*-Ar); -7.17 (s, 24H, *Me*-Ar); -16.70 (s, 8H, *o*-Ar). ^{2}H NMR (76 MHz, pentane, 22 °C): δ = -81.50 (s, μ-C$_6$*D$_6$*).

1.4.2.5. Synthesis of compound 2a-I

A slurry of UI$_3$(THF)$_4$ (2.291 g, 2.52 mmol) in 50 mL of toluene and a slurry of 1.780 g LiN[^{1}Ad]Ar (6.82 mmol, 2.7 equiv) in 30 mL of toluene were cooled to near freezing. The thawing LiN[^{1}Ad]Ar slurry was added with a pipette to the UI$_3$(THF)$_4$ slurry, after which the removal of volatiles under reduced pressure was initiated. After 12 h, 20 mL of heptane was added, the mixture stirred for 2-3 h, and then dried for another 12 h. The desired product was extracted in *n*-hexane, filtered through Celite, then the solvent removed and 30 mL of hexamethyldisiloxane were used to precipitate 1.440 g (1.28 mmol, 51% yield) of the desired product. The hexamethyldisiloxane filtrate was concentrated to 10 mL, cooled to -35 °C for 2-3 days and a second crop of 0.3 g (0.266 mmol, 61% total yield) was obtained.

^{1}H NMR (300 MHz, C$_6$D$_6$, 22 °C): δ = 10.70 (s, 2H, *o*-Ar); 9.13 (s, 6H, Ad distal C*H$_2$*); 6.13 (s, 3H, Ad C*H*); 4.54 (app doublets, 6H, Ad proximal C*H$_2$*); 0.50 (s, 1H, *p*-Ar); -3.74 (s, 6H, *Me*-Ar).

UV-vis (C$_6$H$_6$, 22 °C) and NIR (toluene, 22 °C): λ$_{max}$ (nm, ε × 10^{-2} M^{-1}, cm^{-1}) = 290 (135.2 ± 9.4); 412 (28.2 ± 0.8); 704 (1.10 ± 0.01); 897 (0.3); 943 (0.3); 1045 (0.6); 1121 (0.6); 1379 (0.3).

Anal. calcd. for $C_{54}H_{72}N_3IU$: C, 57.49; H, 6.43; N, 3.72. Found: C, 57.44; H, 6.51; N, 3.65.

1.4.2.6. Synthesis of compound 2b₂-μ-toluene

Solutions of **2a-I** (0.100 g, 0.089 mmol) in 8 mL and of KC_8 (0.045 g, 0.333 mmol, 3 equiv) in 4 mL of toluene, respectively, were cooled to near freezing. The thawing KC_8 slurry was added to the thawing **2a-I** solution and the reaction was allowed to proceed for 10 min after which the mixture was filtered through Celite and volatiles removed under vacuum. A pentane extract (20 mL) was filtered through Celite, then concentrated to 3 mL and cooled to -35 °C. The product was isolated as dark-brown crystals (0.020 g, 0.012 mmol, 28% yield).

^{1}H NMR (300 MHz, C_6D_6, 22 °C): δ = 19.90 (s, 3H, C*H₃*-toluene); 6.76 (s, 24H, Ad distal C*H₂*); 4.40 (s, 12H, Ad C*H*); 3.15 (app doublets, 24H, Ad proximal C*H₂*); -1.96 (s, 4H, *p*-Ar); -7.20 (s, 24H, *Me*-Ar); -15.90 (s, 8H, *o*-Ar); -61.04 (s, 1H, *p*-toluene); -84.94 (s, 2H, *m*-toluene); -92.20 (s, 2H, *o*-toluene).

Anal. calcd. for $C_{79}H_{104}N_4U_2$: C, 59.83; H, 6.61; N, 3.53. Found: C, 60.07; H, 6.76; N, 3.64.

1.4.2.7. Synthesis of compound 2a-THF

A 100 mL round bottom flask was charged with $UI_3(THF)_4$ (0.526 g, 0.56 mmol), KN[^{1}Ad]Ar (0.510 g, 1.74 mmol, 3 equiv), and a stirring bar, then placed in the cold well. Thawing THF (50 mL) was added to the solid mixture as quickly as possible and the reaction mixture stirred for 45 min. Filtration of the reaction mixture through Celite afforded a solution from which the solvent was removed. The solid obtained was collected on a frit, and washed with small portions of diethyl ether (2 × 15 mL). The solid obtained on the frit was dried, redissolved in diethyl ether, the solution concentrated in placed in a freezer at −35 °C. After several days, the solution was

decanted and the black microcrystalline solid (**2a-THF**, 0.304 g, 0.29 mmol, 51% yield) dried under reduced pressure.

^{1}H NMR (300 MHz, C$_6$D$_6$, 22 °C): δ = 37.55 (s, 4H, THF-C*H*$_2$); 0.65 (bs, 9H, *o*- and *p*-Ar); 0.23 (s, 9H, Ad-C*H*); 0.13 (d, 18H, Ad-C*H*$_2$); -0.13 (d, 18H, Ad-C*H*$_2$); -6.64 (s, 18H, Ar-*Me*); -15.80 (s, 4H, THF-C*H*$_2$).

UV-vis-NIR (THF, 22 °C): λ$_{max}$ (nm, ε × 10^{-2} M^{-1}, cm^{-1}) = 296 (95.0 ± 4.0); 540 (10.1 ± 0.1); 597 (sh, 9.4 ± 0.2); 695 (7.8 ± 0.1); 807 (5.0 ± 0.1); 956 (2.7 ± 0.1); 1053 (1.5); 1084 (1.6); 1217 (1.0); 1270 (0.8).

Anal. calcd. for C$_{58}$H$_{83}$N$_3$OU: C, 64.72; H, 7.77; N, 3.90. Found: C, 64.79; H, 7.93; N, 3.72.

1.4.2.8. Synthesis of Me$_3$SiNU(N[^{1}Ad]Ar)$_3$ (2a-NSiMe$_3$)

a) **From 2a-THF.** Solutions in THF of **2a-THF** (1.169 g, 1.14 mmol, 80 mL) and Me$_3$SiN$_3$ (0.144 g, 1.25 mmol, 1.1 equiv, 20 mL) were frozen. To the thawing solution of **2a-THF** was added dropwise the solution of Me$_3$SiN$_3$, the reaction mixture allowed to warm to room temperature and stirred for 1 h. After the reaction was finished, the solvent was removed under reduced pressure, the obtained solid was dissolved in pentane, the new solution was concentrated and stored at −35 °C for several days. **2a-NSiMe$_3$** was obtained as a black, crystalline solid in two crops amounting to 0.586 g (0.56 mmol, 49% yield).

b) **From UI$_3$(THF)$_4$ directly.** UI$_3$(THF)$_4$ (1.193 g, 1.31 mmol) and KN[^{1}Ad]Ar (1.156 g, 3.94 mmol, 3 equiv) were mixed as solids in a 250 mL round bottom flask and placed in the cold well. To the stirring mixture was added thawing THF (100 mL). The reaction mixture was let to warm to room temperature and stirred for a total of 35 min after which it was filtered through Celite, and the resulted solution frozen again. To this thawing solution it was added dropwise a thawing solution of Me$_3$SiN$_3$ (0.136 g, 1.18 mmol, 0.9 equiv) in THF (20 mL). After the addition was finished, the removal of solvent was started immediately. The obtained solid was extracted with pentane, and the solution

filtered through Celite. The solvent was removed and the last two operations repeated. The new solution was concentrated to ca. 20 mL and placed in a –35 °C freezer. **2a-NSiMe₃** was obtained as a black, crystalline solid in two crops amounting to 0.521 g (0.50 mmol, 38% yield).

^{1}H NMR (300 MHz, C₆D₆, 22 °C): δ = 11.95 (bs, 2H, *o*-Ar); 8.28 (s, 3H, Si-C*H₃*); 6.24 (s, 1H, *p*-Ar); 2.03 (s, 6H, Ar-*Me*); 1.09 (s, 3H, Ad-C*H*); -0.06 (d of d, 6H, Ad-C*H₂*); -5.59 (bs, 6H, Ad-C*H₂*).

UV-vis-NIR (toluene, 22 °C): λ$_{max}$ (nm, ε × 10^{-2} M^{-1}, cm^{-1}) = 284 (124.9 ± 2.6); 400 (49.8 ± 4.8); 592 (16.5 ± 1.4); 1018 (0.6); 1160 (0.5); 1325 (0.6).

Anal. calcd. for C₅₇H₈₁N₄SiU: C, 62.90; H, 7.50; N, 5.15. Found: C, 62.80; H, 7.52; N, 5.11.

1.4.2.9. Synthesis of Li(OEt₂)Me₃SiNU(N[¹Ad]Ar)₃

Small cubes of lithium (2-3) were washed with hexanes and transferred to a round bottom flask under argon charged with a magnetic stirring bar. To this flask was transferred via canula a THF solution (25 mL) of **2a-NSiMe₃** (0.699 g, 0.67 mmol) prepared in the glove box. The reaction mixture was stirred for 2 h at room temperature after which the solvent was removed under reduced pressure. The flask was taken into the box, the solid obtained was extracted with pentane and the new solution filtered through Celite. After the solvent was removed from the filtrate, the extraction with pentane and the filtration were repeated and the new solution was concentrated and placed in a –35 °C freezer. Li(OEt₂)Me₃SiNU(N[¹Ad]Ar)₃ was obtained as orange crystals in two crops amounting to 0.502 g (0.43 mmol, 64% yield).

^{1}H NMR (300 MHz, C₆D₆, 22 °C): δ = 11.49 (bs, 6H, Et₂O-C*H₃*); 10.61 (bs, 6H, *o*-Ar); 9.12 (s, 9H, Si-C*H₃*); 8.10 (s, 3H, *o*-Ar); 7.13 (d, 4H, Et₂O-C*H₂*); 2.06 (s, 18H, Ar-*Me*); -1.99 (d of d, 18H, Ad-C*H₂*); -3.34 (s, 9H, Ad-C*H*); -15.16 (bs, 18H, Ad-C*H₂*).

Anal. calcd. for C₆₁H₉₁N₄SiOLiU: C, 62.59; H, 7.78; N, 4.79. Found: C, 62.60; H, 8.35; N, 4.71.

1.4.2.10. Synthesis of KMe₃SiNU(N[¹Ad]Ar)₃

A thawing slurry of KC_8 (0.188 g, 1.39 mmol, 2.8 equiv) in THF (15 mL) was added dropwise to a thawing THF solution (20 mL) of **2a-NSiMe₃** (0.518 g, 0.50 mmol). The reaction mixture was allowed to reach room temperature and stirred for 1.5 h, after which the solvent was removed under reduced pressure. The solid obtained was extracted with diethyl ether and the new solution filtered through Celite. After the solvent was removed from the filtrate, the extraction with diethyl ether and the filtration were repeated and the new solution was concentrated and placed in a −35 °C freezer. KMe₃SiNU(N[¹Ad]Ar)₃ was obtained as dark orange crystals in one crop amounting to 0.415 g (0.38 mmol, 77% yield).

¹H NMR (300 MHz, C₆D₆, 22 °C): δ = 20.67 (s, 3H, Si-C*H₃*); 4.75 (s, 1H, *p*-Ar); 1.99 (s, 3H, Ad-C*H*); 0.82 (d of d, 6H, Ad-C*H₂*); 0.09 (s, 6H, Ar-*Me*); -1.05 (bs, 2H, *o*-Ar); -2.58 (bs, 6H, Ad-C*H₂*).

1.4.11. Arene exchange experiments

Compound **1b₂-μ-toluene** was dissolved in C₆D₆, the solution transferred to an NMR tube, the NMR tube sealed, and then placed in a heated oil bath. After 24 h at 90 °C, analysis of the ¹H NMR spectrum indicated 3% exchange based on the integration of the peaks at ca. −7 ppm (*Me*-Ar). Integration of the same peak indicated 14% exchange after additional 24 h at 100 °C and 18% exchange after another 48 h. A similar experiment conducted with compound **1b₂-μ-C₆H₆** dissolved in toluene-*d₈* showed 6% exchange after 48 h at 100 °C and 11% exchange based on integration of the *t-Bu* peaks (ca. 7ppm) after a total of 96 h. For the exchange experiment with *p*-xylene, **1b₂-μ-toluene** was dissolved in *p*-xylene, the solution transferred to a tube, the tube sealed, and heated in an oil bath at 90 °C. After 24 h, the tube was taken into the box, broken, and its content transferred to a vial. Volatiles were removed. Analysis of the compound's ¹H NMR spectrum (C₆D₆, 300 MHz, 22 °C) indicated no transformation of **1b₂-μ-toluene**.

1.4.2.12. UV-vis (C₆H₆, 22 °C) and NIR (toluene, 22 °C) of 1a-I

λ_{max} (nm, $\varepsilon \times 10^{-2}$ M⁻¹, cm⁻¹) = 284 (131.9 ± 4.7); 400 (41.9 ± 1.2); 706 (2.2 ± 0.1); 895 (0.7); 943 (0.6); 1036 (0.9); 1128 (0.8); 1210 (0.4); 1372 (0.4).

1.4.2.13. Reaction of compound 1b₂-μ-toluene with PhSSPh

1b₂-μ-toluene (0.150 g, 0.117 mmol) and PhSSPh (0.051 g, 0.234 mmol, 2 equiv) were mixed and cooled to -100 °C. Thawing pentane (10 mL) was added to the stirring mixture of solids. After 30 min, volatiles were removed under vacuum, the product mixture washed with 3 mL of pentane and the remaining solid dissolved in diethyl ether (25 mL). After filtration through Celite and concentration to 10 mL, 0.140 g (0.09 mmol) of the desired product, **1b₂-(μ-SPh)₂(SPh)₂**, (74% yield) was obtained as yellow crystals from cooling the above solution layered with pentane to -35 °C (several crops over a period of ca. 1 month).

Anal. calcd. for $C_{72}H_{92}N_4S_2U_2$: C, 53.45; H, 5.73; N, 3.46. Found: C, 52.40; H, 5.30; N, 3.44.

1.4.2.14. Toepler pump experiment*

1b₂-μ-toluene (0.150 g, 0.117 mmol) and PhSSPh (0.051 g, 0.234 mmol) were mixed in a Schlenk flask and the pressure inside the flask was reduced to 10⁻³ mmHg. 10 mL of pentane was degassed by repeating the freezing-evacuating-thawing cycle on a HiVac line (until the pressure was 10⁻⁵ mmHg) 5 times. The pentane was vacuum transferred to the frozen mixture of the solids until the pressure returned to 10⁻³ mmHg. After the pentane was added to the solids, the reaction mixture was allowed to reach room temperature and the reaction to proceed for 35 min. After that time, the reaction mixture was frozen, the Toepler pump was verified to not indicate any

---

* This experiment was carried out in the laboratories of Prof. Daniel G. Nocera with the help of Alan F. Heyduk.

References begin on page 75

residual gas and then the connections between the reaction flask and the pump were opened. For 1.5 h the pump did not indicate any gas collection.

1.4.2.15.a. Reaction of compound 1b$_2$-μ-toluene with PhNNPh

1b$_2$-μ-toluene (0.144 g, 0.113 mmol) in 15 mL of n-hexane and PhNNPh (0.0206 g, 0.113 mmol) in 5 mL of n-hexane were frozen. The thawing PhNNPh solution was added to the thawing solution of **1b$_2$-μ-toluene** dropwise. The reaction mixture was stirred for 15 min, and then volatiles were removed under vacuum. The remaining brown solid was washed with 2 mL of pentane and then dissolved in diethyl ether (15 mL). The diethyl ether solution was filtered through Celite and then concentrated to 5 mL. Dark-red crystals of **1b$_2$-(μ-NPh)$_2$** (0.1035 g, 0.076 mmol, 67% yield) were obtained from the diethyl ether solution layered with pentane at -35 °C (several crops over a period of ca. 1 month).

^{1}H NMR (300 MHz, C$_6$D$_6$, 22 °C): δ = 10.48 (s, 18H, t-Bu); 1.53 (s, 2H, p-Ar); -4.92 (s, 12H, Me-Ar); -5.06 (s, 4H, o-Ar); -6.75 (t, 1H, p-NPh); -8.10 (s, 2H, m-NPh); -43.07 (s, 2H, o-NPh). Anal. calcd. for C$_{60}$H$_{82}$N$_6$U$_2$: C, 52.86; H, 6.06; N, 6.16. Found: C, 52.82; H, 6.18; N, 5.28.

1.4.2.15.b. Synthesis of 1b$_2$-(μ-NPh)$_2$-d_{10}

Similar synthesis as for the non-deuterated compound **1b$_2$-(μ-NPh)$_2$**, using PhNNPh-d_{10} instead of PhNNPh.

^{1}H NMR (300 MHz, C$_6$D$_6$, 22 °C): δ = 10.43 (s, 18H, t-Bu); 1.63 (s, 2H, p-Ar); -4.78 (s, 12H, Me-Ar); -4.87 (s, 4H, o-Ar). ^{2}H NMR (76 MHz, pentane, 22 °C): -6.20, -6.71 (d, 1H, p-NPh); -7.86 (s, 2H, m-NPh); -43.06 (s, 2H, o-NPh).

1.4.2.15.c. Reaction of compound 1b$_2$-μ-toluene with *p*-MePhNNPh

Similar synthesis to that for compound **1b$_2$-(μ-NPh)$_2$**, using *p*-MePhNNPh instead of PhNNPh. ^{1}H NMR (500 MHz, C$_6$D$_6$, 22 °C): δ = 9.99 (s, 36H, *t-Bu*); 1.82 (s, 4H, *p*-Ar); -4.42 (s, 3H, *p-* *Me*-NPh); -4.71 (s, 24H, *Me*-Ar); -5.83 (s, 8H, *o*-Ar); -6.31 (t, 1H, *p*-NPh); -7.82 (s, 2H, *m*-NPh); -7.97 (s, 2H, *m*-NPh); -43.32 (s, 2H, *o*-NPh); -43.46 (s, 2H, *o*-NPh).

1.4.2.16. Experiment to evidence the toluene-d_8 eliminated in the reaction of 1b$_2$-μ-toluene-d_8 with PhNNPh

Before proceeding with the reaction, stock solutions of 0.0173 M octane-d_{18} in hexamethyldisiloxane (to be used as an internal standard) and of 0.0186 M PhNNPh in hexamethyldisiloxane were made. A 20 mL scintillation vial was charged with 0.0085 g (0.0066 mmol) of **1b$_2$-μ-toluene-d_8** and a stirring bar and then frozen. A mixture of 0.357 mL of the PhNNPh solution and 0.2 mL of the octane-d_{18} solution was frozen and while thawing was added to the solid. The reaction went for 15 min and then the mixture was transferred to an NMR tube, and the vial washed with 0.3 mL (3 × 0.1 mL) of hexamethyldisiloxane, which was added subsequently to the NMR sample. The ^{2}H NMR spectrum after integration indicated 68% yield based on the CD$_3$ and 83% yield based on the C$_6$D$_5$ deuterons of the free toluene-d_8 liberated in the reaction.

1.4.2.17. Reaction of compound 1b$_2$-μ-toluene with selenium

A solution of **1b$_2$-μ-toluene** (0.075 g, 0.06 mmol) in 15 mL of *n*-hexane was added to a slurry of selenium (0.028 g, 0.35 mmol, 6 equiv) in 5 mL of toluene. The reaction mixture was stirred for 4.5 h at room temperature and then filtered to remove excess selenium. The volatiles were

removed and the brown solid obtained was dissolved in pentane (15 mL). The pentane solution was filtered through Celite and then concentrated to 5 mL. Dark brown crystals of **1a₂-μ-Se** (0.029 g, 0.02 mmol, 46% calculated yield based on formation of uranium as a by-product) were obtained from the pentane solution at -35 °C.

^{1}H NMR (300 MHz, C₆D₆, 22 °C): δ = 11.82 (s, 9H, *t-Bu*); -0.37 (s, 1H, *p*-Ar); -2.35 (s, 2H, *o*-Ar); -6.88 (s, 6H, *Me*-Ar). The elemental analysis of the compound has been accomplished by P. L. Arnold.

1.4.2.18. Reaction of compound 1b₂-μ-toluene with 1,3,5,7-cyclooctatetraene

1b₂-μ-toluene (0.410 g, 0.32 mmol) in 15 mL of *n*-hexane and 1,3,5,7-cyclooctatetraene (0.0738 g, 0.71 mmol, 2.2 equiv) in 5 mL of *n*-hexane were frozen. The thawing 1,3,5,7-cyclooctatetraene solution was added dropwise to the thawing solution of **1b₂-μ-toluene**. The reaction mixture was stirred for 30 min, and then volatiles were removed under vacuum. The dark yellow solid obtained was dissolved in pentane (15 mL). The pentane solution was filtered through Celite and then concentrated to 5 mL. Dark yellow crystals of **1b-COT** (0.309 g, 0.44 mmol, 69% yield) were obtained from the pentane solution at -35 °C. An additional crop of 0.065 g (0.09 mmol, total yield of 84%) was obtained over a period of ca. 1 month.

^{1}H NMR (300 MHz, C₆D₆, 22 °C): δ = 3.96 (s, 9H, *t-Bu*); -3.04 (s, 1H, *p*-Ar); -7.06 (s, 2H, *o*-Ar); -7.68 (s, 6H, *Me*-Ar); -34.72 (s, 4H, *COT*). Anal. calcd. for C₃₂H₄₄N₂U: C, 55.33; H, 6.34; N, 4.03. Found: C, 55.15; H, 6.38; N, 4.03.

1.4.3. X-ray crystal structures

1.4.3.1. General considerations

The X-ray data collections were carried out on a Siemens Platform three-circle goniometer with a CCD detector using Mo-K_α radiation (λ = 0.71073 Å). The data were processed utilizing the program SAINT supplied by Siemens Industrial Automation, Inc. The structures were solved by direct methods (SHELXTL v5.03, Sheldrick, G. M., and Siemens Industrial Automation, Inc., 1995) in conjunction with standard difference Fourier techniques. Tables with atomic coordinates and equivalent isotropic displacement parameters, with all the bond lengths and angles, and with anisotropic displacement parameters are listed in Appendix 1.

1.4.3.2. X-ray crystal structure of 2a-THF

Inside the glove box, crystals of **2a-THF,** obtained from a saturated diethyl ether solution at –35 °C were coated with Paratone N oil (an Exxon product) on a microscope slide. A black block of approximate dimensions 0.58 x 0.20 x 0.08 mm^3 was selected and mounted with wax on a glass fiber. A total of 23522 reflections (-53 $\leq$ h $\leq$ 52, -12 $\leq$ k $\leq$ 12, -17 $\leq$ 1 $\leq$ 26) were collected at 201(2) K in the θ range of 1.82 to 23.25 °, of which 8404 were unique (R_{int} = 0.0646). The structure was solved by direct methods (SHELXTL V5.10, G. M. Sheldrick and Siemens Industrial Automation, Inc., 1997) in conjunction with standard difference Fourier techniques. All non-hydrogen atoms were refined anisotropically and hydrogen atoms were placed in calculated (d_{C-H} = 0.96 Å) positions. The unit cell contains 1.5 molecules of diethyl ether as crystallization solvent. The residual peak and hole electron density were 0.685 and –1.184 e·Å^{-3}, respectively and these values are in the normal range due to the large scattering effect of uranium centers. A semi-empirical absorption correction was applied based on pseudo-psi-scans with maximum and minimum transmission equal to 0.8067 and 0.2929, respectively. The least

squares refinement converged normally with residuals of $R_1 = 0.0490$, $wR_2 = 0.1003$ based upon $I > 2\sigma(I)$, and GOF = 1.221 (based on F^2). An extinction coefficient of 0.00003(2) was applied to the refinement.

Crystal and refinement data: formula $C_{64}H_{95}N_3O_{2.5}U$, space group C2/c, $a = 48.3194(7)$ Å, $b = 11.5899(2)$ Å, $c = 24.0370(3)$ Å, $\alpha = 90.0$ °, $\beta = 119.1480(10)$ °, $\gamma = 90.0$ °, $V = 11756.5(3)$ Å^3, $Z = 8$, $\mu = 2.806$ mm^{-1}, $D_{calc} = 1.338$ g·cm^{-3}, $F(000) = 4896$, R_1 (based on F) = 0.0608, and wR_2 (based on F^2) = 0.1054.

1.4.3.3. X-ray crystal structure of 2a-I

Inside the glove box, crystals of **2a-I,** obtained from a saturated pentane solution at –35 °C were coated with Paratone N oil (an Exxon product) on a microscope slide. A yellow block of approximate dimensions 0.38 x 0.23 x 0.10 mm^3 was selected and mounted with wax on a glass fiber. A total of 11449 reflections (-11 $\leq$ h $\leq$ 12, -8 $\leq$ k $\leq$ 13, -24 $\leq$ l $\leq$ 25) were collected at 293(2) K in the θ range of 1.81 to 23.26 °, of which 7771 were unique ($R_{int} = 0.0325$). The structure was solved by direct methods (SHELXTL V5.10, G. M. Sheldrick and Siemens Industrial Automation, Inc., 1997) in conjunction with standard difference Fourier techniques. The unit cell contains one molecule of pentane as crystallization solvent. All non-hydrogen atoms were refined anisotropically, except the solvent atoms that were refined only isotropically. Hydrogen atoms were placed in calculated ($d_{C-H} = 0.96$ Å) positions, except for the solvent atoms for which no hydrogen atoms were added. The residual peak and hole electron density were 0.993 and -0.913 e·Å^{-3}, respectively and these values are in the normal range due to the large scattering effect of uranium centers. A semi-empirical absorption correction was applied based on pseudo-psi-scans with maximum and minimum transmission equal to 0.5278 and 0.3764, respectively. The least squares refinement converged normally with residuals of $R_1 = 0.0345$, $wR_2 = 0.0885$ based upon $I > 2\sigma(I)$, and GOF = 1.252 (based on F^2). An extinction coefficient of 0.00140(17) was applied to the refinement.

Crystal and refinement data: formula $C_{59}H_{72}N_3IU$, space group P-1, a = 11.0165(2) Å, b = 12.4826(3) Å, c = 22.6984(6) Å, α = 79.2150(10) °, β = 78.35 °, γ = 64.9070(10) °, V = 2750.34(11) Å^3, Z = 2, μ = 3.550 mm^{-1}, D_{calc} = 1.435 g·cm^{-3}, $F(000)$ = 1184, R_1 (based on F) = 0.0378, and wR_2 (based on F^2) = 0.0926.

1.4.3.4. X-ray crystal structure of 2a-NSiMe₃

Inside the glove box, crystals of **2a-NSiMe₃**, obtained from a saturated pentane solution at –35 °C were coated with Paratone N oil (an Exxon product) on a microscope slide. A dark brown block of approximate dimensions 0.27 x 0.15 x 0.11 mm^3 was selected and mounted with wax on a glass fiber. A total of 12119 reflections (-11 ≤ h ≤ 10, -12 ≤ k ≤ 12, -25 ≤ l ≤ 28) were collected at 183(2) K in the θ range of 2.41 to 23.28 °, of which 8389 were unique (R_{int} = 0.0375). The structure was solved using the Patterson method (SHELXTL V5.10, G. M. Sheldrick and Siemens Industrial Automation, Inc., 1997) in conjunction with standard difference Fourier techniques. The unit cell contains 1.5 molecules of pentane as crystallization solvent. All non-hydrogen atoms were refined anisotropically. Two carbon atoms, C41 and C42, belonging to the trimethylsilyl group, are slightly disordered, but no attempts have been made to model this disorder. C6S, the carbon atom that sits on an inversion center, is disordered and the disorder has been modeled to ½ occupancy. Most hydrogen atoms were found in the electronic density map; the remaining ones were placed in calculated (d_{C-H} = 0.96 Å) positions, except for C6S for which no hydrogen atoms were added. The residual peak and hole electron density were 1.021 and -0.624 e·Å^{-3}, respectively and these values are in the normal range due to the large scattering effect of uranium centers. A semi-empirical absorption correction was applied based on pseudo-psi-scans with maximum and minimum transmission equal to 0.7505 and 0.5220, respectively. The least squares refinement converged normally with residuals of R_1 = 0.0328, wR_2 = 0.0768 based upon I > 2σ(I), and GOF = 1.125 (based on F^2). No extinction coefficient was applied to the refinement.

Crystal and refinement data: formula $C_{64.5}H_{98}N_4SiU$, space group P-1, a = 10.7784(14) Å, b = 11.3375(15) Å, c = 25.600(3) Å, α = 82.255(2) °, β = 89.666(2) °, γ = 75.380(2) °, V = 2998.1(7) Å^3, Z = 2, μ = 2.768 mm^{-1}, D_{calc} = 1.324 g·cm^{-3}, $F(000)$ = 1238, R_1 (based on F) = 0.0358, and wR_2 (based on F^2) = 0.0780.

1.4.3.5. X-ray crystal structure of Li(OEt₂)Me₃SiNU(N[¹Ad]Ar)₃

Inside the glove box, crystals of Li(OEt₂)Me₃SiNU(N[¹Ad]Ar)₃, obtained from a saturated diethyl ether solution at –35 °C were coated with Paratone N oil (an Exxon product) on a microscope slide. A light orange block of approximate dimensions 0.17 x 0.14 x 0.11 mm^3 was selected and mounted with wax on a glass fiber. A total of 22460 reflections (-24 $\leq$ h $\leq$ 24, -12 $\leq$ k $\leq$ 14, -24 $\leq$ l $\leq$ 24) were collected at 183(2) K in the θ range of 2.14 to 23.27 °, of which 8141 were unique (R_{int} = 0.0391). The structure was solved using the Patterson method (SHELXTL V5.10, G. M. Sheldrick and Siemens Industrial Automation, Inc., 1997) in conjunction with standard difference Fourier techniques. All non-hydrogen atoms were refined anisotropically. All hydrogen atoms were found in the electronic density map, except for H13C, H43A, H43B, H43C, which were placed in calculated (d_{C-H} = 0.96 Å) positions. The residual peak and hole electron density were 0.585 and -0.997 e·Å^{-3}, respectively and these values are in the normal range due to the large scattering effect of uranium centers. A semi-empirical absorption correction was applied based on pseudo-psi-scans with maximum and minimum transmission equal to 0.7390 and 0.6361, respectively. The least squares refinement converged normally with residuals of R_1 = 0.0339, wR_2 = 0.0591 based upon I > 2σ(I), and GOF = 1.112 (based on F^2). No extinction coefficient was applied to the refinement.

Crystal and refinement data: formula $C_{61}H_{91}N_4SiOLiU$, space group P2(1)/c, a = 22.2766(14) Å, b = 12.6684(8) Å, c = 22.4330(15) Å, α = 90 °, β = 116.4060(10) °, γ = 90 °, V = 5670.3(6) Å^3, Z = 4, μ = 2.926 mm^{-1}, D_{calc} = 1.370 g·cm^{-3}, $F(000)$ = 2408, R_1 (based on F) = 0.0448, and wR_2 (based on F^2) = 0.0618.

1.4.3.6. X-ray crystal structure of $1b_2$-(μ-SPh)$_2$(SPh)$_2$

Crystals of $1b_2$-(μ-SPh)$_2$(SPh)$_2$ grown from a concentrated diethyl ether solution layered with pentane at -35 °C were quickly moved from a scintillation vial to a microscope slide containing Paratone N (an Exxon product) oil. A yellow plate of approximate dimensions 0.30 x 0.08 x 0.02 mm^3 was selected and mounted with wax on a glass fiber. A total of 11316 reflections ($-17 \leq h \leq$ 15, $-13 \leq k \leq 11$, $-21 \leq l \leq 21$) were collected at 183(2) K in the θ range of 1.35 to 21.25 °, of which 3864 were unique ($R_{int} = 0.1463$). The structure was solved by direct methods (SHELXTL V5.10, G. M. Sheldrick and Siemens Industrial Automation, Inc., 1997) in conjunction with standard difference Fourier techniques. All non-hydrogen atoms were refined anisotropically with the exception of C15 and hydrogen atoms were placed in calculated ($d_{C-H} = 0.96$ Å) positions. The residual peak and hole electron density were 4.012 and -2.122 e·Å^{-3}, respectively and these values are in the normal range due to the large scattering effect of uranium centers. A semi-empirical absorption correction was applied based on pseudo-psi-scans with maximum and minimum transmission equal to 1.0000 and 0.5818, respectively. The least squares refinement converged normally with residuals of $R_1 = 0.0930$, $wR_2 = 0.2212$ based upon I > 2σ(I), and GOF = 1.285 (based on F^2). No extinction coefficient was applied to the refinement.

Crystal and refinement data: formula $C_{36}H_{46}N_2S_2U$, space group P2(1)/c, $a = 15.2217(3)$ Å, $b =$ 12.2381(2) Å, $c = 18.8867(3)$ Å, $\alpha = 90$ °, $\beta = 98.5570(10)$ °, $\gamma = 90$ °, $V = 3479.14(19)$ Å^3, $Z = 4$, $\mu = 2.926$ mm^{-1}, $D_{calc} = 1.544$ g·cm^{-3}, $F(000) = 1600$, R_1 (based on F) = 0. 1309, and wR_2 (based on F^2) = 0.2539.

1.4.3.7. X-ray crystal structure of $1b_2$-(μ-NPh)$_2$

Crystals of $1b_2$-(μ-NPh)$_2$ grown from a concentrated diethyl ether solution layered with pentane at -35 °C were quickly moved from a scintillation vial to a microscope slide containing Paratone N (an Exxon product) oil. A red plate was selected and mounted with wax on a glass fiber. A

total of 11573 reflections (-13 $\leq$ h $\leq$ 13, -15 $\leq$ k $\leq$ 13, -18 $\leq$ l $\leq$ 17) were collected at 183(2) K in the θ range of 1.91 to 23.27 °, of which 4119 were unique (R_{int} = 0.0664). The structure was solved by direct methods (SHELXTL V5.10, G. M. Sheldrick and Siemens Industrial Automation, Inc., 1997) in conjunction with standard difference Fourier techniques. All non-hydrogen atoms were refined anisotropically and hydrogen atoms were placed in calculated (d_{C-H} = 0.96 Å) positions. The residual peak and hole electron density were 0.618 and -1.288 e·Å^{-3}, respectively and these values are in the normal range due to the large scattering effect of uranium centers. A semi-empirical absorption correction was applied based on pseudo-psi-scans with maximum and minimum transmission equal to 0.8500 and 0.2753, respectively. The least squares refinement converged normally with residuals of R_1 = 0.0398, wR_2 = 0.0854 based upon I > 2σ(I), and GOF = 1.307 (based on F^2). No extinction coefficient was applied to the refinement.

Crystal and refinement data: formula $C_{30}H_{41}N_3U$, space group P2(1)/n, a = 12.56740(10) Å, b = 14.1378(2) Å, c = 16.3176(3) Å, α = 90 °, β = 97.2990(10) °, γ = 90 °, V = 2875.74(7) Å^3, Z = 4, μ = 5.665 mm^{-1}, D_{calc} = 1.575 g·cm^{-3}, F(000) = 1336, R_1 (based on F) = 0. 0479, and wR_2 (based on F^2) = 0.0931.

1.4.3.8. X-ray crystal structure of 1a$_2$-μ-Se

Crystals of **1a$_2$-μ-Se** grown from a concentrated diethyl ether solution at -35 °C were quickly moved from a scintillation vial to a microscope slide containing Paratone N (an Exxon product) oil. An orange plate of approximate dimensions 0.55 x 0.14 x 0.09 mm^3 was selected and mounted with wax on a glass fiber. A total of 8411 reflections (-12 $\leq$ h $\leq$ 11, -15 $\leq$ k $\leq$ 14, -17 $\leq$ l $\leq$ 16) were collected at 183(2) K in the θ range of 2.64 to 23.29 °, of which 5893 were unique (R_{int} = 0.1534). The structure was solved by direct methods (SHELXTL V5.10, G. M. Sheldrick and Siemens Industrial Automation, Inc., 1997) in conjunction with standard difference Fourier techniques. All non-hydrogen atoms were refined anisotropically and hydrogen atoms were

placed in calculated (d_{C-H} = 0.96 Å) positions. The residual peak and hole electron density were 6.025 and -5.338 e·Å^{-3}, respectively and these values are in the normal range due to the large scattering effect of uranium centers. A semi-empirical absorption correction was applied based on pseudo-psi-scans with maximum and minimum transmission equal to 1.0000 and 0.3461, respectively. The least squares refinement converged normally with residuals of R_1 = 0.1095, wR_2 = 0.3009 based upon I > 2σ(I), and GOF = 1.050 (based on F^2). No extinction coefficient was applied to the refinement.

Crystal and refinement data: formula $C_{36}H_{54}N_3Se_{0.5}U$, space group P-1, a = 11.679(2) Å, b = 13.579(2) Å, c = 15.432(3) Å, α = 100.675(3) °, β = 107.691(3) °, γ = 108.680(3) °, V = 2097.8(6) Å^3, Z = 2, μ = 4.325 mm^{-1}, D_{calc} = 1.277 g·cm^{-3}, F(000) = 800, R_1 (based on F) = 0.1179, and wR_2 (based on F^2) = 0.3218.

1.4.4. XANES measurements

Everything, except for the Teflon tape and the uranium samples, was baked out at 110 °C for several days. In an Ar-filled glove box, approximately 10 mg of uranium complex was powdered and mixed with dry boron nitride. The samples were packaged in aluminum holders with kapton tape. The samples were sealed with Teflon tape inside the dry box. The samples showed no signs of decomposition either before or immediately after the XANES experiment. After several hours in the air, the samples began to discolor around the edges.

X-ray absorption spectra were acquired at the Stanford Synchrotron Radiation Laboratory (SSRL) at beamline 11-2 or 4-1 using a Si(220) double crystal monochromator detuned 50% to reduce the higher order harmonic content of the beam. X-ray absorption spectra were obtained in the transmission mode at room temperature using argon filled ionization chambers. The data analysis was performed by standard procedures using the EXAFSPAK suite of programs developed by G. George of SSRL. The background was removed by fitting a polynomial to the

pre-edge data. Edge shifts are determined from the half-height of the U L_3 absorption edge at 17166 eV and are referenced to the half-height of a 0.1 M solution of UO_2Cl_2 in hydrochloric acid.

1.4.5. Susceptibility measurements

Measurements for the same compound were carried out on batches obtained independently. Samples used were multiply times recrystallized. Magnetic susceptibility measurements were recorded using a SQUID magnetometer at 5000 G. The samples were prepared in the glove box (50 – 100 mg) loaded in a gelatin capsule that was positioned inside a plastic straw and carried to the magnetometer in a tube under N_2. The sample was quickly inserted into the instrument, centered and data obtained from 5 to 300 K. The contribution from the sample holders was not accounted for. The diamagnetic contributions were calculated using Pascal constants and subtracted from χ_{mol}. Effective magnetic moments were calculated either by linear regression from plots of $1/\chi_{mol}$ versus T (K) for Curie-Weiss behavior or by using the formula $2.828*\sqrt{(T* \chi_{mol})}$ for non-Curie-Weiss behavior.

1.4.6. Computational details

The Amsterdam Density Functional package (version *ADF2002.01*)[31] was used to do a full geometry optimization on Cartesian coordinates of the model compounds specified in the text. Full electronic configuration was used for all atoms, except for uranium and silicon for which the frozen core approach was used. Basis set TZ2P ZORA(V) was used as implemented in the ADF suite. The local density approximation (LDA) by Vosko, Wilk and Nusair (VWN) was used together with the exchange and correlation corrections specified in each input file. The calculations were carried out with relativistic corrections,[56] using the spin-unrestricted

References begin on page 75

formalism,[57] with the number of spin-α electrons in excess of spin-β electrons specified in the input files. Input files are given in Appendix 2.

[1] Reynolds, L. T.; Wilkinson, G. *J. Inorg. Nucl. Chem.* **1956**, *2*, 246.

[2] Kealy, T. J.; Pauson, P. L. *Nature* **1951**, *168*, 1039; Miller, S. A.; Tebboth, J. A.; Tremaine, J. F. *J. Chem. Soc.* **1952**, 632; Wilkinson, G.; Rosenblum, M.; Whiting, M. C.; Woodward, R. B. *J. Am. Chem. Soc.* **1952**, *74*, 2125; Fischer, E. O.; Pfab, W. *Z. Naturforsch.* **1952**, *7B*, 377.

[3] Bursten, B. E.; Strittmatter, R. J. *Angew. Chem. Int. Ed. Engl.* **1991**, *30*, 1069.

[4] Streitwieser, A.; Müller-Westerhoff, U. *J. Am. Chem. Soc.* **1968**, *90*, 7364; Zalkin, A.; Raymond, K. N. *J. Am. Chem. Soc.* **1969**, *91*, 5667.

[5] Kempe, R. *Angew. Chem. Int. Ed.* **2000**, *39*, 468.

[6] Andersen, R. A. *Inorg. Chem.* **1979**, *18*, 1507; Stewart, J. L.; Andersen, R. A. *Polyhedron* **1998**, *17*, 953.

[7] Roussel, P.; Scott, P. *J. Am. Chem. Soc.* **1998**, *120*, 1070; Roussel, P.; Errington, W.; Kaltsoyannis, N.; Scott, P. *J. Organomet. Chem.* **2001**, *635*, 69.

[8] Odom, A. L.; Arnold, P. L.; Cummins, C. C. *J. Am. Chem. Soc.* **1998**, *120*, 5836.

[9] Cummins, C. C. *Chem. Commun.* **1998**, 1777.

[10] Clark, D. L.; Sattelberger, A. P. *Inorg. Synth.* **1997**, *31*, 307.

[11] Ruppa, K. B. P.; Desmangles, N.; Gambarotta, S.; Yap, G.; Rheingold, A. *Inorg. Chem.* **1997**, *36*, 1194.

[12] Diaconescu, P. L.; Arnold, P. L.; Baker, T. A.; Mindiola, D. J.; Cummins, C. C. *J. Am. Chem. Soc.* **2000**, *122*, 6108.

[13] Diaconescu, P. L.; Cummins, C. C. *J. Am. Chem. Soc.* **2002**, *124*, 7660.

[14] Arliguie, T.; Lance, M.; Nierlich, M.; Vigner, J.; Ephritikhine, M. *J. Chem. Soc., Chem. Commun.* **1994**, 847; Arliguie, T.; Lance, M.; Nierlich, M.; Ephritikhine, M. *J. Chem. Soc., Chem. Commun.* **1997**, 2501.

[15] Elschenbroich, C.; Salzer, A. *Organometallics*, 2nd ed. VCH, Weinheim, 1992, 363.

[16] Lukens, W. W.; Beshouri, S. M.; Blosch, L. L.; Stuart, A. L.; Andersen, R. A. *Organometallics* **1999**, *18*, 1235.

[17] DenAuwer, C.; Madic, C.; Berthet, J. C.; Ephritikhine, M.; Rehr, J. J.; Guillaumont, R. *Radiochim. Acta* **1997**, *76*, 211; Hu, Z. W.; Kaindl, G.; Meyer, G. *J. Alloy Compd.* **1998**, *274*, 38.

[18] Nelson, J. E.; Clark, D. L.; Burns, C. J.; Sattelberger, A. P. *Inorg. Chem.* **1992**, *31*, 1973.

[19] Siddall, T. H. in *Theory and applications of molecular paramagnetism*; Bondreau, E. A. and Mulay, L. N., Eds.; Wiley, New York, 1976, chaps. 4 and 6.

[20] Brennan, J. G.; Andersen, R. A. *J. Am. Chem. Soc.* **1985**, *107*, 514.

[21] Baudry, D.; Bulot, E.; Charpin, P.; Ephritikhine, M.; Lance, M.; Nierlich, M.; Vigner, J. *J. Organomet. Chem.* **1989**, *371*, 155.

[22] Garbar, A. V.; Leonov, M. R.; Zakharov, L. N.; Struchkov, Y. T. *Russ. Chem. Bull.* **1996**, *45*, 451.

[23] Avdeef, A.; Raymond, K. N.; Hodgson, K. O.; Zalkin, A. *Inorg. Chem.* **1972**, *11*, 1083.

[24] Burns, J. H. *J. Organomet. Chem.* **1974**, *69*, 225.

[25] Madelung, O., Ed. *Landolt-Börnstein: Numerical data and functional relationships in science and technology*; Springer: Berlin, 1987; *15*.

[26] Hitchcock, P. B.; Lappert, M. F.; Protchenko, A. V. *J. Am. Chem. Soc.* **2001**, *123*, 189.

[27] Brown, F. C. in *Synchrotron radiation research*; Winick, H., Doniach, S., Eds.; Plenum Press: New York, 1980, 61.

[28] Koningsberger, D. C.; Prins, R. *X-ray absorption: Principles, applications, techniques of exafs, sexafs, and xanes*; John Wiley & Sons: New York, 1988.

[29] Kalkowski, G.; Kaindl, G.; Brewer, W. D.; Krone, W. *J. Physique* **1986**, *C8*, 943.

[30] Bertsch, P. M.; Hunter, D. B.; Sutton, S. R.; Bajt, S.; Rivers, M. L. *Environ. Sci. Technol.* **1994**, *28*, 980.

[31] te Velde, G.; Bickelhaupt, F. M.; Gisbergen, S. J. A. van; Fonseca Guerra, C.; Baerends, E. J.; Snijders, J. G.; Ziegler, T. *J. Comput. Chem.* **2001**, *22*, 931; Fonseca Guerra, C.; Snijders, J. G.; te Velde, G.; Baerends, E. J. *Theor. Chem. Acc.* **1998**, *99*, 391; ADF2002.01, SCM, Theoretical Chemistry, Vrije Universiteit, Amsterdam, The Netherlands, http://www.scm.com.

[32] Duff, A. W.; Jonas, K.; Goddard, R.; Kraus, H.-J.; Krüger, C. *J. Am. Chem. Soc.* **1983**, *105*, 5479.

[33] Goryunov, L. I.; Litvak, V. V. *Organomet. Chem. USSR* **1989**, *2*, 967.

[34] Kanellakopulos, B. in *Organometallics of the f-Elements*, Marks, T. J.; Fischer, R. D. Eds., Reidel, Dordrecht, 1979,1.

[35] Carlin, R. L.; van Duyneveldt, A. J. *Magnetic properties of transition metal compounds*; Springer Verlag: New York, 1977.

[36] Stewart, J. L.; Andersen, R. A. *New J. Chem.* **1995**, *19*, 587.

[37] Rosen, R. K.; Andersen, R. A.; Edelstein, N. M. *J. Am. Chem. Soc.* **1990**, *112*, 4588.

[38] Kahn, O. *Molecular magnetism*; VCH Publishers: New York, 1993.

[39] Li, J.; Bursten, B. E. *J. Am. Chem. Soc.* **1998**, *120*, 11456.

[40] Avens, L. R.; Bott, S. G.; Clark, D. L.; Sattelberger, A. P.; Watkin, J. G.; Zwick, B. D. *Inorg. Chem.* **1994**, *33*, 2248.

[41] Macatangay, A. V.; Endicott, J. F. *Inorg. Chem.* **2000**, *39*, 437.

[42] Sutton, J. E.; Sutton, P. M.; Taube, H. *Inorg. Chem.* **1979**, *18*, 1017.

[43] Piepho, S. B.; Krausz, E. R., Schatz, P. N. *J. Am. Chem. Soc.* **1978**, *100*, 2996.

[44] Brennan, J. G.; Andersen, R. A.; Robbins, J. L. *J. Am. Chem. Soc.* **1986**, *108*, 335; Parry, J.; Carmona, E.; Coles, S.; Hursthouse, M. *J. Am. Chem. Soc.* **1995**, *117*, 2649; Conejo, M. D.; Parry, J. S.; Carmona, E.; Schultz, M.; Brennan, J. G.; Beshouri, S. M.; Andersen, R. A.; Rogers, R. D.; Coles, S.; Hursthouse, M. *Chem. Eur. J.* **1999**, *5*, 3000.

[45] King, R. B. *Inorg. Chem.* **1992**, *31*, 1978.

[46] Edelmann, F. T.; Lorenz V. *Coordin. Chem. Rev.* **2000**, *209*, 99.

[47] Warner, B. P.; Scott, B. L.; Burns, C. J. *Angew. Chem. Int. Ed. Engl.* **1998**, *37*, 959; Fagan, P. J.; Manriquez, J. M.; Marks, T. J.; Day, C. S.; Vollmer, S. H.; Day, V. W. *Organometallics* **1982**, *1*, 170.

[48] Lockwood, M. A.; Fanwick, P. E.; Eisenstein, O.; Rothwell, I. P. *J. Am. Chem. Soc.* **1996**, *118*, 2762; Peters, R. G.; Warner, B. P.; Burns, C. J. *J. Am. Chem. Soc.* **1999**, *121*, 5585.

[49] Aubart, M. A.; Bergman, R. G. *Organometallics* **1999**, *18*, 811.

[50] Brown, E. V.; Kipp, W. H. *J. Org. Chem.* **1971**, *36*, 170.

[51] Schrock, R. R.; Glassman, T. E.; Vale, M. G.; Kol, M. J. *J. Am. Chem. Soc.* **1993**, *115*, 1760; Kisch, H.; Holzmeier, P. *Adv. Organomet. Chem.* **1992**, *34*, 67; Fochi, G.; Floriani, C.; Bart, J. C. J.; Giunchi, R. *J. Chem. Soc., Dalton Trans.* **1983**, *8*, 1515; Sutton, D. *Chem. Rev.* **1993**, *93*, 995.

[52] Arnold, P. L.; Odom, A. L.; Cummins, C. C. *unpublished results*.

[53] Pangborn, A. B.; Giardello, M. A.; Grubbs, R. H.; Rosen, R. K.; Timmers, F. J. *Organometallics* **1996**, *15*, 1518.

[54] Schwindt, M.; Lejon, T.; Hegedus, L. *Organometallics* **1990**, *9*, 2814.

[55] Stern, M. K.; Cheng, B. K.; Hileman, F. D.; Allman, J. M. *J. Org. Chem.* **1994**, *59*, 5627.

[56] Lethe, E. van; Baerends, E. J.; Snijders, J. G. *J. Chem. Phys.* **1993**, *99*, 4597; Lethe, E. van; Baerends, E. J.; Snijders, J. G. *J. Chem. Phys.* **1994**, *101*, 9783; Lethe, E. van; Baerends, E. J.; Snijders, J. G. *J. Chem. Phys.* **1999**, *110*, 8943.

[57] Snijders, J. G.; Baerends, E. J.; Ros, P. *Mol. Phys.* **1979**, *38*, 1909; Boerrigter, P. M.; Baerends, E. J.; Snijders, J. G. *Chem. Phys.* **1988**, *122*, 357; Ziegler, T.; Tschinke, V.; Baerends, E. J.; Snijders, J. G.; Ravenek, W. *J. Chem. Phys.* **1989**, *93*, 3050.

Arene Bridged Diuranium Complexes Supported by a Ketimide Ligand: Even and Odd Electron Redox Pairs

2.1. Introduction

The diuranium complex $(\mu\text{-}C_7H_8)U_2(N[^tBu]Ar)_4$ (**1b$_2$-μ-toluene**),[1] described in Chapter 1, exhibits a two-legged piano stool coordination environment at uranium, one *N-tert*-butyl anilide ligand having been stripped from each uranium center during conversion from the uranium *tris*-amide precursor, IU(N[^tBu]Ar)$_3$.[2] Since the synthesis involved treatment with excess KC$_8$[3] in the neat arene solvent, it is presumed that the stripped ligand was lost as its potassium salt. The ketimide ligand (NC[^tBu]Mes, Mes = 2,4,6-C$_6$H$_2$Me$_3$) employed in the present study allows for retention of three supporting ligands per uranium, giving rise to a three-legged piano stool geometry, and it also allows for incorporation of potassium ions as tight ion pairs. A further advantage accorded by the implementation of ketimide ligands[4] is the ability to use dimethoxyethane (DME) as a solvent and stoichiometric amounts of an arene ligand such as toluene, naphthalene, biphenyl, or *trans*-stilbene, in the present study.

An ancillary ligand capable of supporting a broad range of arene-bridged compounds was targeted in order to facilitate structural and spectroscopic comparisons as a function of the bridging arene ligand. In comparing ketimide and amide ligands, two differences are important. First, the ketimide ligand has the steric bulk moved one atom further from the coordination center and secondly, the nitrogen donor of the ketimide ligands can function as a π donor as well as a π acceptor. This chapter reports on the chemistry of a uranium *tris*-ketimide fragment that permitted the isolation of unique arene bridged diuranium complexes.

References begin on page 155

2.2. Results and discussion

2.2.1.1. Synthesis of iodo-uranium *tris*-ketimide complex

Reaction of readily available $UI_3(DME)_2$[5] with $KNC[^tBu]Mes$ in DME (Scheme 1) led to the isolation of the uranium(IV) complex $IU(DME)(NC[^tBu]Mes)_3$ (**3-I-DME**),[6] in 30% yield calculated with respect to the starting material, $UI_3(DME)_2$. The low yield is attributed to disproportionation of uranium (III) and to the high lipophilicity of the desired material.
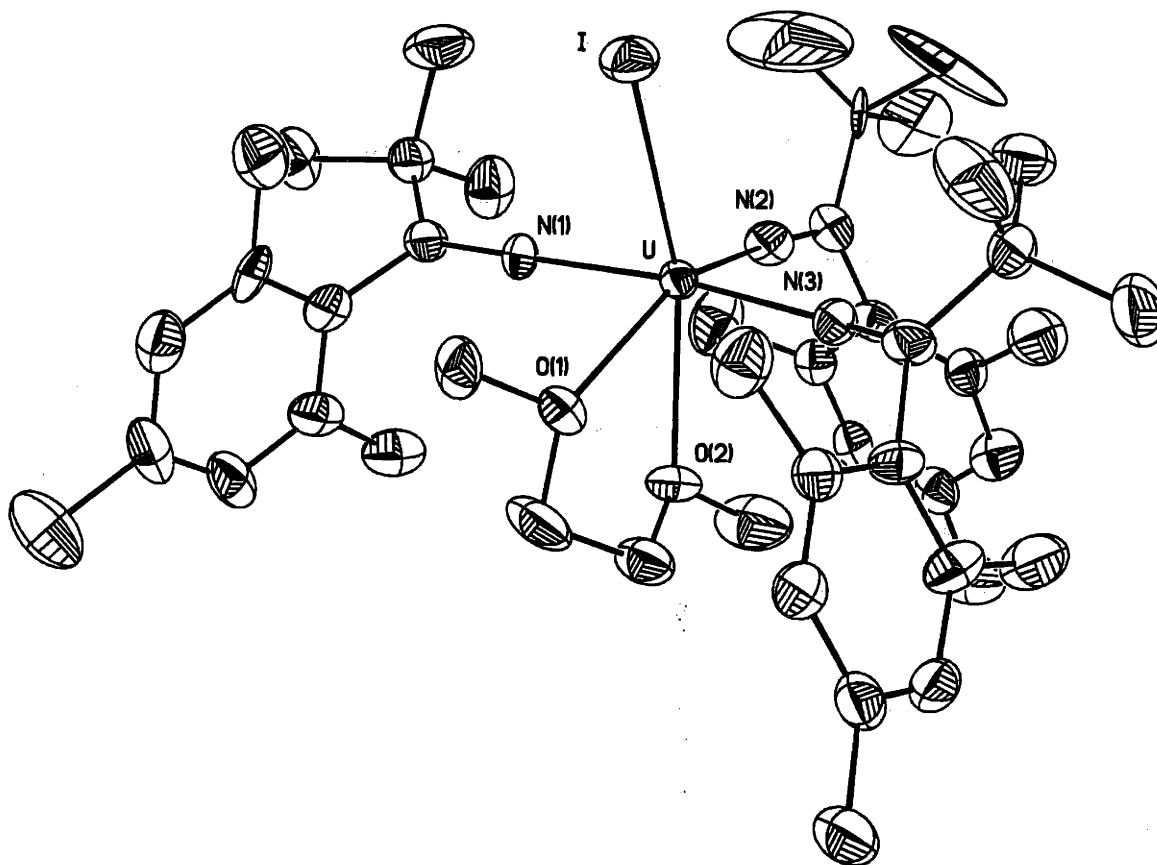
Figure 1. Structural drawing of complex **3-I-DME** with thermal ellipsoids at the 35% probability level. Selected bond distances (Å): U-I, 3.0602(13); U-N(avg.), 2.189(21); U-O (avg.), 2.552(13), and angles (°): UNC (avg.), 168.5(2.7).
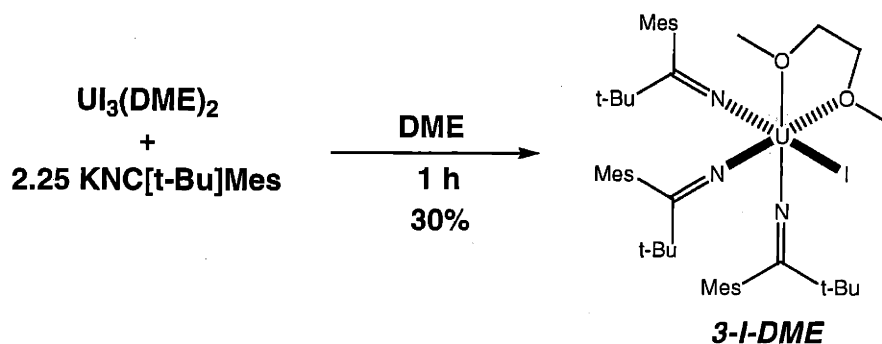
Scheme 1

A single-crystal X-ray diffraction study of **3-I-DME** (Figure 1) revealed that a molecule of DME coordinates to the uranium center in the pocket formed by the mesityl groups. The observed near-linear UNC angles (avg. 168.5(2.7) °) are suggestive of significant π bonding between nitrogen and uranium. This stable uranium iodide species serves as a useful precursor for a number of arene-bridged complexes.

2.2.1.2. Synthesis of even-electron arene-bridged diuranium complexes

Treatment of **3-I-DME** with 4 equiv of KC_8 and 0.5 equiv of naphthalene in DME allowed the isolation of a naphthalene-bridged compound, $K_2(\mu\text{-}\eta^6,\eta^6\text{-}C_{10}H_8)[U(NC[^tBu]Mes)_3]_2$ **K_2-3_2-μ-$C_{10}H_8$**, (Scheme 2) in 60% yield as a dark brown powder. The most interesting structural feature of this dinuclear compound is the coordination mode, $\mu\text{-}\eta^6,\eta^6$, of the bridging naphthalene to the uranium centers[1] (Figure 2), reminiscent of the coordination mode of the toluene ligand in compound **$1b_2$-μ-toluene**. Transition metal complexes of bridging naphthalene or biphenyl, contrastingly, always have the two metal centers coordinated to different rings. Such compounds are known as "slipped triple-decker" complexes.[7]
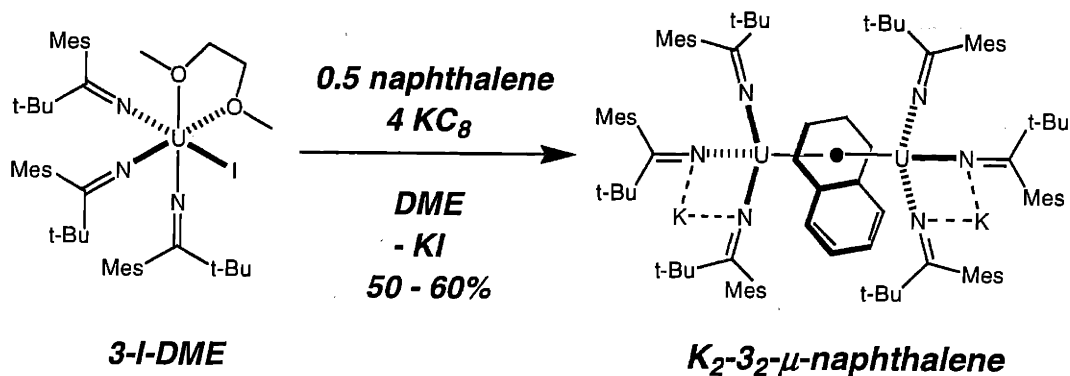
Scheme 2
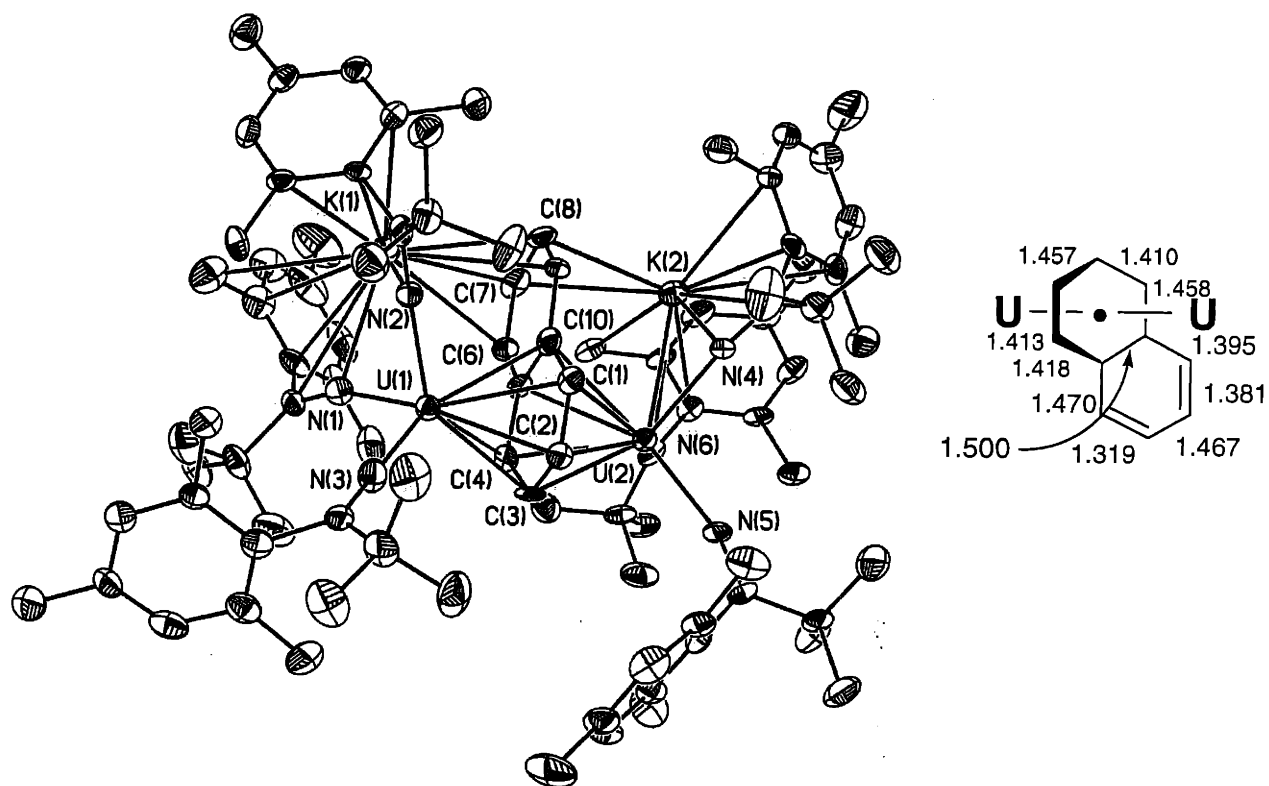
Figure 2. Left: Structural drawing of complex **K₂-3₂-μ-naphthalene** with thermal ellipsoids at the 35% probability level. Selected bond distances (Å): U-N (avg.), 2.261(20); U-C$_{naph}$ (avg.), 2.649(34), C-C$_{naph}$ (avg.), 1.443(35); C5-C6, 1.470(16); C6-C7, 1.319(17); C7-C8, 1.467(18); C8-C9, 1.381(15), C9-C10, 1.395(15). Right: C-C bond distances (Å) in bridging naphthalene.

The twelve U-C distances are rather short, varying from 2.565(11) Å to 2.749(10) Å, but the average U-C distance of 2.649(34) Å is similar to the average U-C distance of 2.594(30) Å found for **1b$_2$-μ-toluene**. The longer bonds are registered to the two carbon atoms fusing the two six membered rings, a fact understandable inasmuch as the LUMO of naphthalene lacks any orbital contributions from these atoms.[8] The C-C distances (Figure 2) in the bound ring are not alternating (avg. of 1.443(35) Å), consistent with the aromatic character expected for that ring, while in the pendant ring a diene-like character is suggested by bond alternation (1.470(16), 1.319(17), 1.467(18), 1.381(15), and 1.395(15) Å). Each potassium ion is clasped by a complement of two mesityl rings, the pendant portion of the naphthalene ligand, and two ketimide nitrogen atoms in a side-on fashion. Complexation of the potassium ions in this way provides them with a near-spherical shroud of electron density, revealing $[3_2\text{-}\mu\text{-}C_{10}H_8]^{2-}$ to be an excellent alkali-metal cation receptor. Furthermore, internalizing the positive ions permits the system to present to its exterior solely lipophilic residues, accounting for the observed solubility in hydrocarbon solvents.[9]

It is worth mentioning that neither the uranium nor the potassium centers retain DME as a coordinated solvent molecule. The U-N distances are elongated by ca. 0.1 Å with respect to those in precursor **3-I-DME**, consistent with an increase in formal negative charge (decrease in oxidation state) at uranium.

The corresponding sodium derivative, $Na_2(\mu\text{-}\eta^6,\eta^6\text{-}C_{10}H_8)[U(NC[^tBu]Mes)_3]_2$ **Na$_2$-3$_2$-μ-naphthalene**, was obtained as dark green-brown crystals in 40% yield by reducing **3-I-DME** over a sodium mirror in tetrahydrofuran (THF) in the presence of 0.6 equiv of naphthalene. A preliminary X-ray crystal structure indicated that **Na$_2$-3$_2$-μ-naphthalene** crystallizes with two THF molecules coordinated to each sodium center, while ^{1}H NMR spectroscopic data are consistent with desolvation after vacuum drying for several hours.

The synthetic strategy that allowed the isolation of **K$_2$-3$_2$-μ-naphthalene** can be applied for other arenes as well (Scheme 3). Thus, reduction of **3-I-DME** with 4 equiv of KC$_8$ in the presence of stoichiometric amounts of the desired arene proved to be a general synthetic route for obtaining the dipotassium salts. The pentane solubility was seen qualitatively to increase in the order: naphthalene < biphenyl < *trans*-stilbene ≈ *p*-terphenyl (i.e. **K$_2$-3$_2$-μ-naphthalene** is slightly soluble in pentane, but **K$_2$-3$_2$-μ-*p*-terphenyl** is fairly soluble in pentane). In order to obtain disodium salts, reduction of **3-I-DME** in THF over a mirror of sodium and stoichiometric amounts of the arene can be employed for naphthalene[6] or reduction of **1-I-DME** in THF with 3 equiv Na/biphenyl can be used for biphenyl. The disodium salts are highly lipophilic, accounting for the low isolated yields for these compounds.

3-I-DME

0.5 R-C$_6$H$_5$
4 KC$_8$

DME
- KI
50 - 60%

K$_2$-3$_2$-μ-biphenyl (R = C$_6$H$_5$)
K$_2$-3$_2$-μ-trans-stilbene (R = trans-CH=CH-C$_6$H$_5$)
K$_2$-3$_2$-μ-p-terphenyl (R = p-C$_6$H$_4$-C$_6$H$_5$)
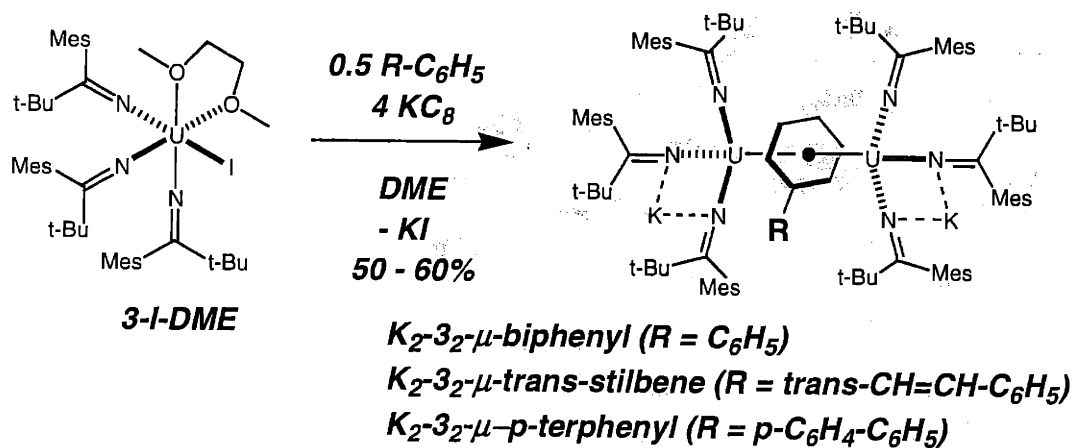
Scheme 3

Obtaining the biphenyl and the *trans*-stilbene bridged compounds is important since it makes it possible to compare C-C distances in a phenyl ring sandwiched between the two uranium centers to C-C distances in an unbound ring within the same molecule. Figures 3 and 4 display the structural representations of **Na$_2$(Et$_2$O)-3$_2$-μ-biphenyl** and **K$_2$-3$_2$-μ-*trans*-stilbene**, and the C-C distances of the coordinating arene. The C-C distances in the bound rings of ca. 1.44 Å are very similar in all three complexes **K$_2$-3$_2$-μ-naphthalene**, **Na$_2$(Et$_2$O)-3$_2$-μ-biphenyl**, and **K$_2$-3$_2$-μ-**

trans-stilbene as well as in **2b₂-μ-toluene**. The difference between the average C-C distance in a bound versus in an unbound ring is ca. 0.06 Å for **Na₂(Et₂O)-3₂-μ-biphenyl** and ca. 0.07 Å for **K₂-3₂-μ-*trans*-stilbene**, and they match closely the difference between the average C-C distance in the bridging toluene of **2b₂-μ-toluene** and in free toluene (ca. 0.04 Å, see Chapter 1).
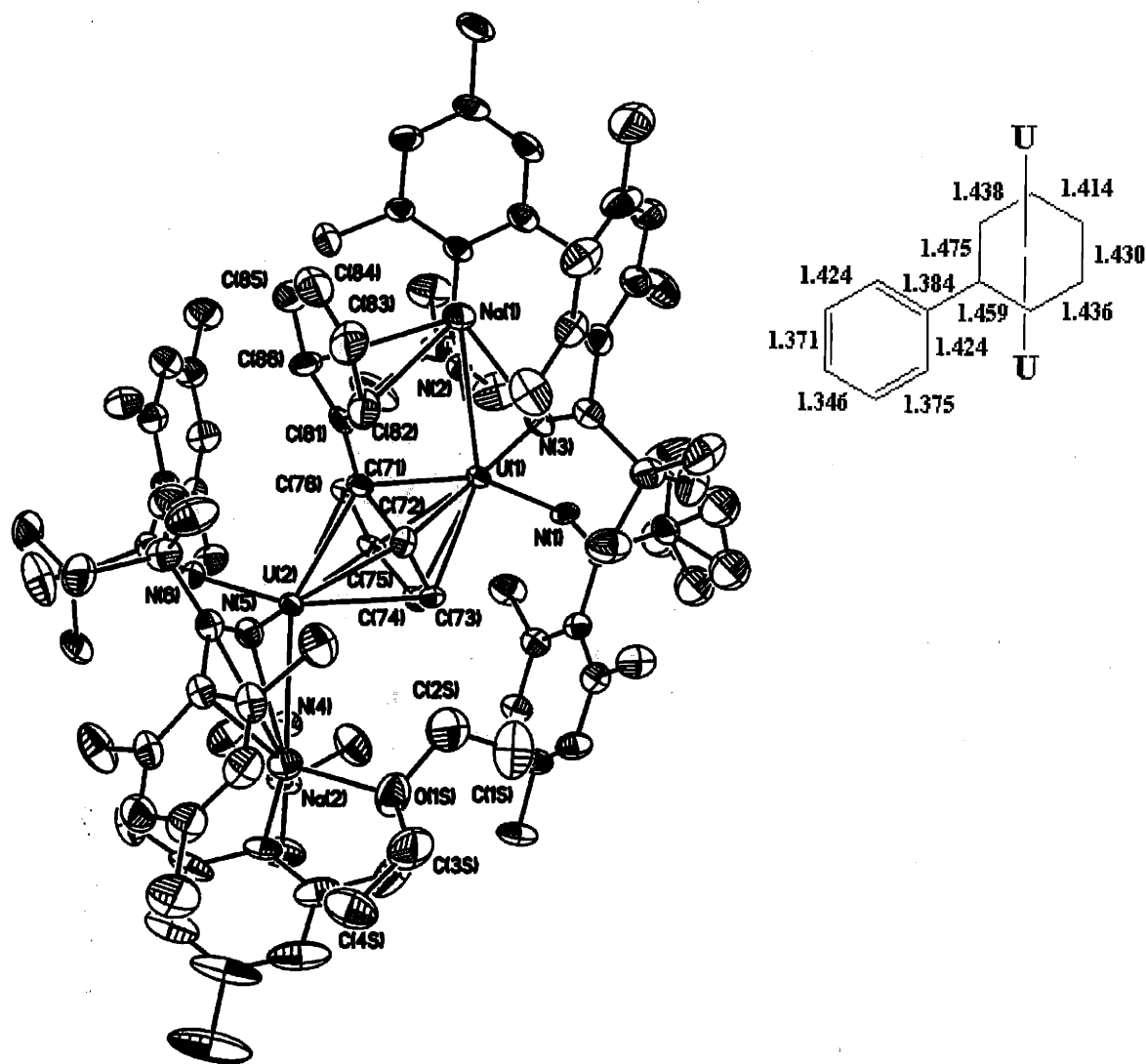
Figure 3. Left: structural drawing of complex **Na₂(Et₂O)-3₂-μ-biphenyl** with thermal ellipsoids at the 35% probability level. Selected bond distances (Å): U-N (avg.), 2.295(15); U-C$_{biph}$ (avg.), 2.627(25); C-C$_{biph-bound}$ (avg.), 1.442(25); C-C$_{biph-unbound}$ (avg.), 1.387(34). Right: C-C bond distances (Å) in bridging biphenyl.

The U-N$_{\text{ketimide}}$ distances are ca. 0.1 Å longer in the arene-bridged compounds than in **3-I-DME** and they vary from 2.248(19) Å in **K$_2$-3$_2$-μ-*trans*-stilbene**, to 2.261(20) Å in **K$_2$-3$_2$-μ-naphthalene**, and to 2.295(15) Å in **Na$_2$(Et$_2$O)-3$_2$-μ-biphenyl**. The distances between the uranium center and the carbon atoms of the bridging arene follow an inverse trend: 2.627(25) Å in **Na$_2$(Et$_2$O)-3$_2$-μ-biphenyl**, 2.649(34) Å in **K$_2$-3$_2$-μ-naphthalene**, and 2.658(30) Å in **K$_2$-3$_2$-μ-*trans*-stilbene**, but they are not statistically different.
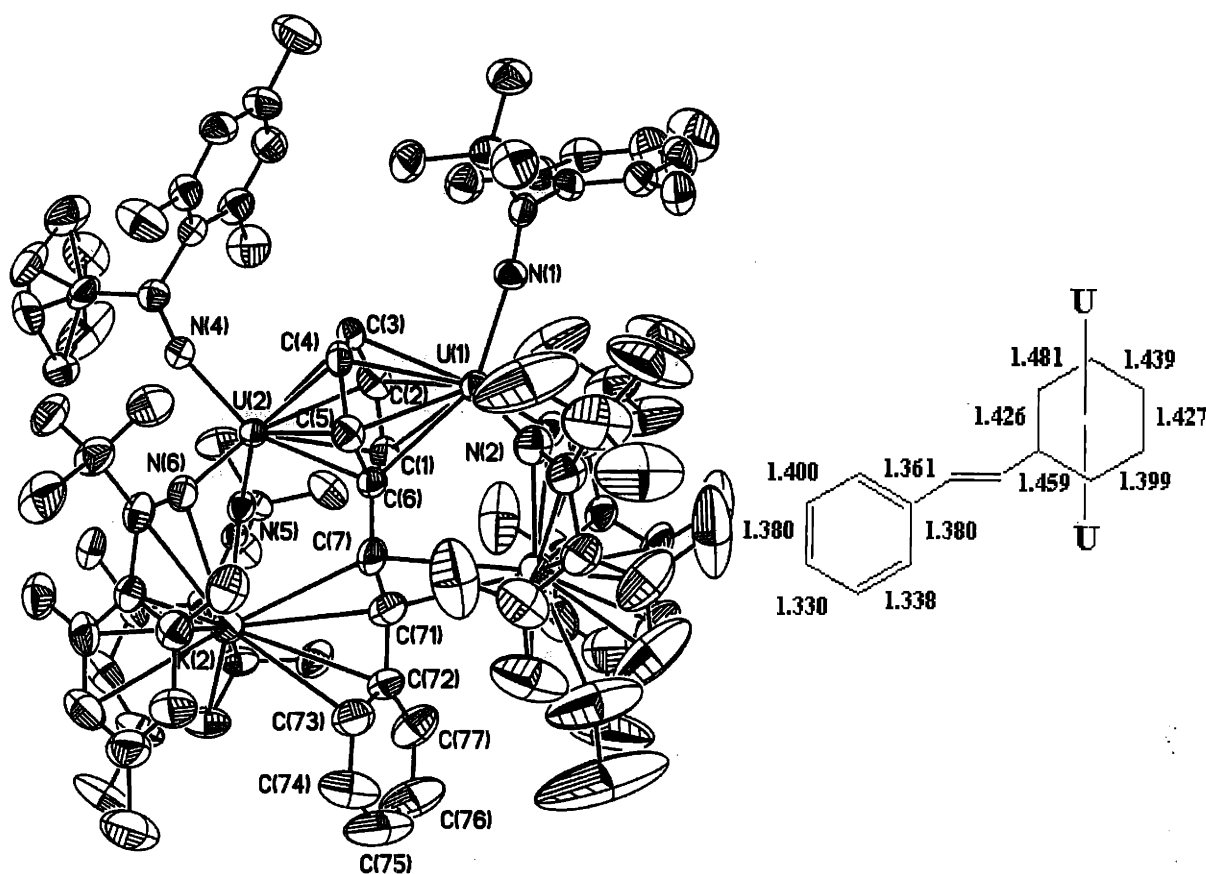
Figure 4. Left: structural drawing of complex **K$_2$-3$_2$-μ-*trans*-stilbene** with thermal ellipsoids at the 35% probability level. Selected bond distances (Å): U-N (avg.), 2.248(19); U-C$_{\text{stilbene}}$ (avg.), 2.658(30); C-C$_{\text{stilbene-bound}}$ (avg.), 1.438(34); C-C$_{\text{stilbene-unbound}}$ (avg.), 1.365(55). Right: C-C bond distances (Å) in bridging *trans*-stilbene.

The bridging arene ketimide complexes described in the present section feature three ligands around each uranium center and retain two alkali metal ions. A general synthesis can be applied for the isolation of dipotassium salts, which are the preferred compounds to employ in further studies due to their solubility properties. Crystallographic characterization of naphthalene, biphenyl, and *trans*-stilbene bridging dinuclear complexes permitted bond length comparison of C-C distances in a bound versus an unbound arene ring.

2.2.1.3. Synthesis of odd-electron arene-bridged diuranium complexes

If in the general synthesis of ketimide arene-bridged complexes the amount of KC_8 is changed from 4 equiv to 2 equiv, a different arene-bridged compound is obtained. As illustrated in Scheme 4, instead of the dipotassium salt, a monopotassium salt is obtained; this strategy applies to biphenyl, *trans*-stilbene, *p*-terphenyl, and naphthalene. Unfortunately, all attempts to obtain a good quality X-ray crystal structure of a **K-3₂-μ-arene** compound have failed so far (with the exception of toluene, see below). A poor quality X-ray crystal structure was obtained for **K-3₂-μ-trans-stilbene** and Figure 5 shows atom connectivities in this complex.

3-I-DME

0.5 R-C₆H₅
2 KC₈

DME
- KI
70 - 80%

K-3₂-μ-biphenyl (R = C₆H₅)
K-3₂-μ-trans-stilbene (R = trans-CH=CH-C₆H₅)
K-3₂-μ-p-terphenyl (R = p-C₆H₄-C₆H₅)
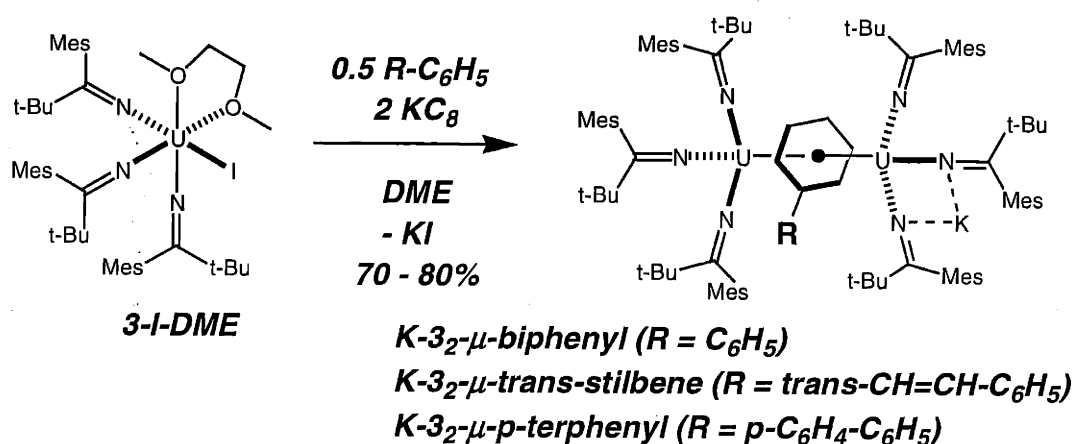
Scheme 4

The drawing in Figure 5 shows that the coordination of the bridging arene is similar to the one encountered for the even electron species. The potassium ion is bound to two ketimide ligands of the same uranium center and also to the pendant styrenyl substituent. It is apparent that in the solid state the ketimide ligands of one uranium fragment are not involved in sequestering the countercation.
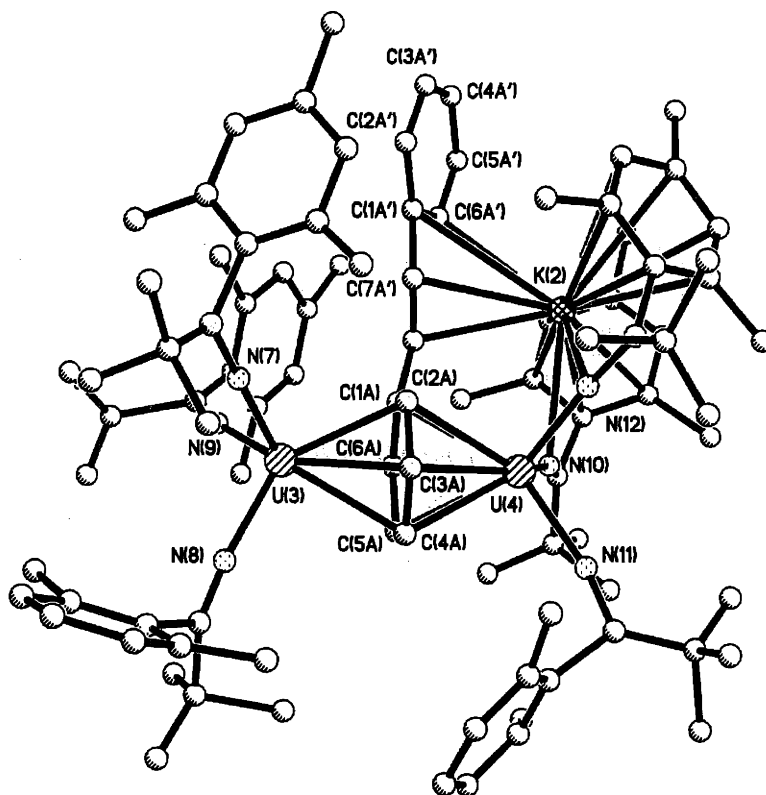
Figure 5. Atom connectivities in **K-3₂-μ-*trans*-stilbene**.

In addition to elemental analysis, chemical means have been employed to support the formulation of the odd electron species **K-3₂-μ-arene** (arene = biphenyl, *trans*-stilbene, *p*-terphenyl, Scheme 5, naphthalene, not shown). On one hand, complexes **K₂-3₂-μ-arene** can be oxidized to **K-3₂-μ-arene** with one equiv of P_4 or Fc[OTf] (ferrocenium triflate) in diethyl ether. The initial use of P_4 as an oxidant was not intentional. Presumably, the potassium ion is eliminated as $(K_2P_4)_n$[10] or K[OTf], but the identity of these salts has not been established. On the

other hand, the odd electron species **K-3₂-μ-arene** can be reduced with one equiv of K/anthracene in THF to give **K₂-3₂-μ-arene**. The redox reactions presented in Scheme 5 can also be used preparatively; general yields of 80% for the reduction and of 70% for the oxidation reactions were obtained. The preferred methods to synthesize the arene-bridged species remain the ones that start with **3-I-DME**, fewer steps being involved in achieving the final products.

+ K / anthracene

THF

+ FcOTf or P₄

Et₂O

$R = C_6H_5$
$trans\text{-}CH=CH\text{-}C_6H_5$
$p\text{-}terphenyl$
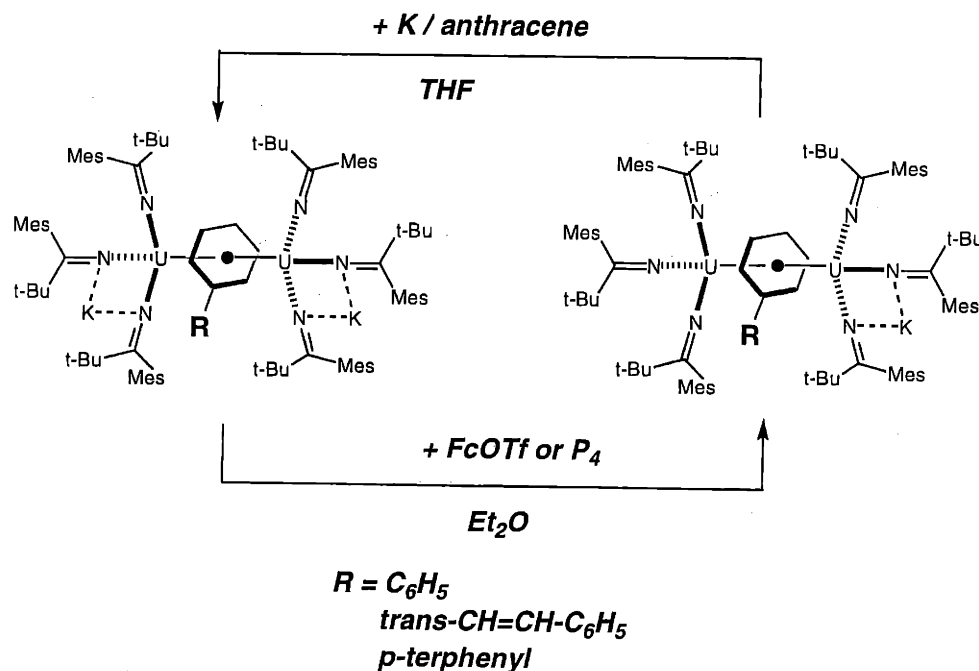
Scheme 5

Indirect support for the formulation of the **K-3₂-μ-arene** species is provided by the isolation and characterization of odd electron toluene-bridged species (Scheme 6). Following the general strategy of synthesizing bridging arene ketimide complexes, reduction of **3-I-DME** with KC_8 in DME in the presence of a slight excess of toluene leads to **K(DME)-3₂-μ-toluene** (Figure 6). However, if toluene is used as a solvent, an equivalent of KI is incorporated into the molecule and **K₂I-3₂-μ-toluene** is formed. The structure of **K₂I-3₂-μ-toluene** (Figure 7) reveals that the

iodide anion is symmetrically bound between two potassium cations, which are internally solvated.

The X-ray crystal structures of the two toluene compounds are interesting to analyze in detail, because they reflect the symmetry or lack thereof suggested by the two molecular formulae (Table 1). For example, in the case of **K₂I-3₂-μ-toluene** the values indicated in Figure 7 arise from rather similar average values calculated for each side of the molecule: U-N from U_1-N (avg.) of 2.227(19) Å and U_2-N (avg.) 2.229(19) Å; U-C from U_1-C (avg.) of 2.663(33) Å and U_2-C (avg.) of 2.631(35) Å.
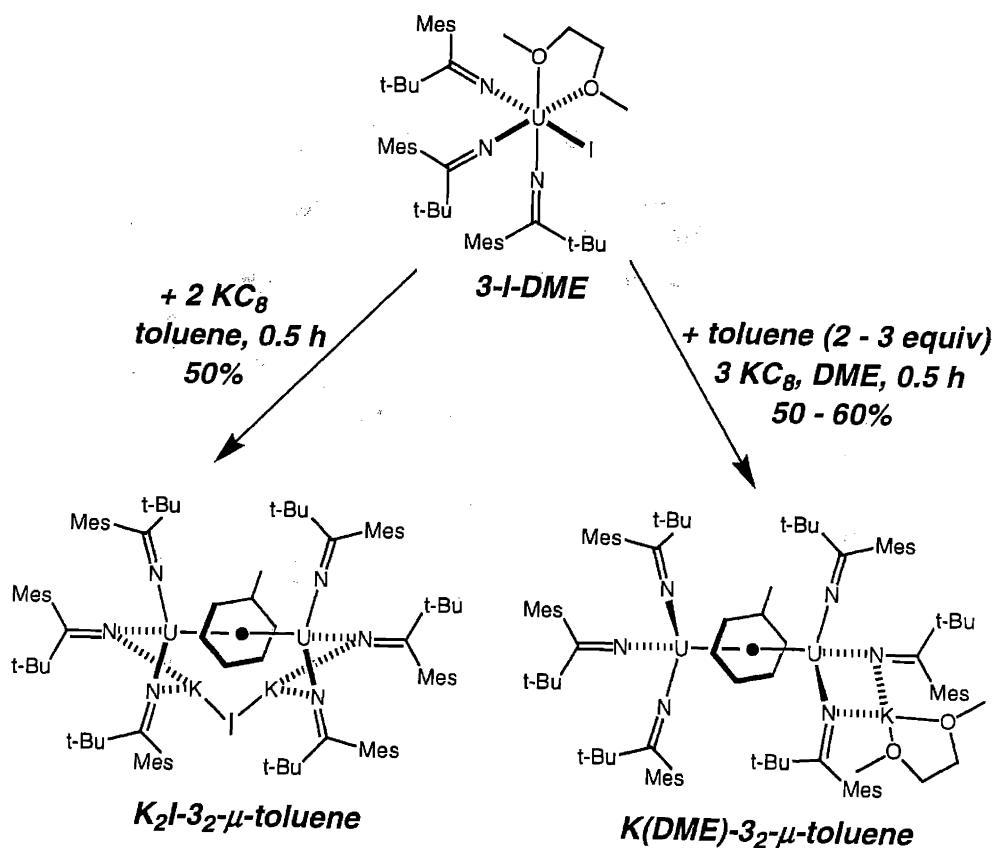
Scheme 6

Table 1. Comparison of average bond lengths in **K$_2$I-3$_2$-μ-toluene** and **K(DME)-3$_2$-μ-toluene**.

Bond	K$_2$I-3$_2$-μ-toluene		K(DME)-3$_2$-μ-toluene	
	U$_1$ side	U$_2$ side	U$_1$ / U$_3$ side	U$_2$ / U$_4$ side
U-N (avg.)	2.227(19)	2.229(19)	2.243	2.211
			2.263	2.209
U-C (avg.)	2.663(33)	2.631(35)	2.594	2.640
			2.626	2.631
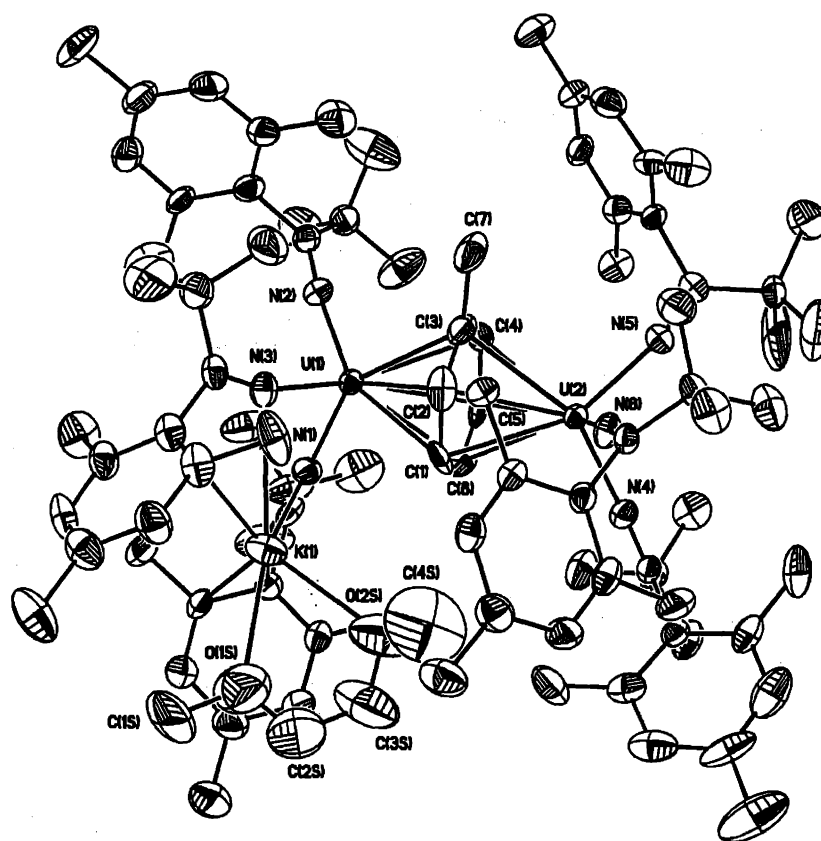
Figure 6. Structural drawing of complex **K(DME)-3$_2$-μ-toluene** with thermal ellipsoids at the 35% probability level. Selected bond distances (Å):[11] U-N (avg.), 2.232; U-C$_{toluene}$ (avg.), 2.623; C-C$_{toluene}$ (avg.), 1.405. Only one of the two independent molecules in the unit cell is shown.

For **K(DME)-3₂-μ-toluene** the asymmetry is obvious: U-N is calculated from U_1-N (avg.) of 2.243 Å and U_3-N (avg.) of 2.263 Å for the side that coordinates the potassium ion and U_2-N (avg.) of 2.211 Å and U_4-N (avg.) of 2.209 Å for the other side of the molecule; U-C is calculated from U_1-C (avg.) of 2.594 Å and U_3-C (avg.) of 2.626 Å for one side of the molecule and U_2-C (avg.) of 2.640 Å and U_4-C (avg.) of 2.631 Å for the other side of the molecule.
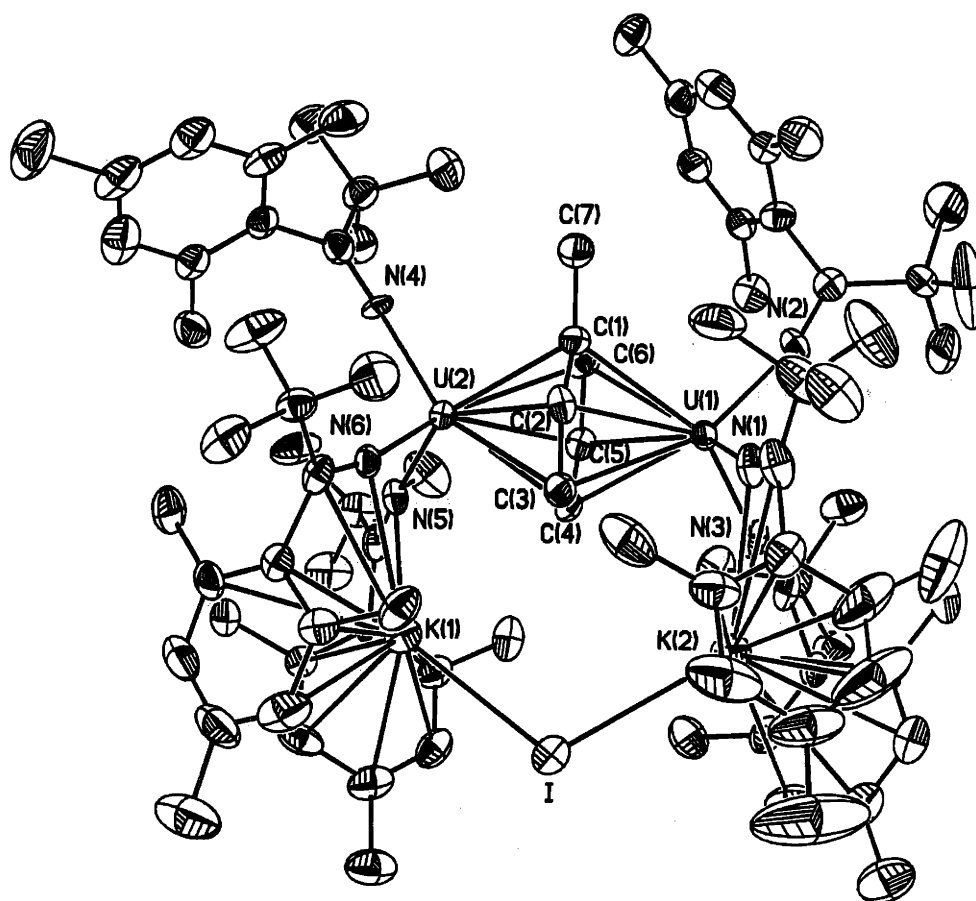
Figure 7. Structural drawing of complex **K₂I-3₂-μ-toluene** with thermal ellipsoids at the 35% probability level. Selected bond distances (Å): U-N (avg.), 2.228(27); U-$C_{toluene}$ (avg.), 2.647(48); C-$C_{toluene}$ (avg.), 1.447(49).

Since in the case of the other arenes (naphthalene, biphenyl, *trans*-stilbene, *p*-terphenyl), both even *and* odd electron species were isolated, several (unsuccessful) attempts to reduce the

toluene bridged compounds **K(DME)-3$_2$-μ-arene** and **K$_2$I-3$_2$-μ-arene** (arene = benzene, toluene) were made. An intuitive explanation for the lack of a dianionic toluene derivative stems from the fact that toluene is harder to reduce than the other arenes employed.[12] Stated alternatively, toluene is a relatively poor δ acid ligand.

Unlike in the case of **1b$_2$-μ-toluene**, which is an even electron species, the bridging toluene diuranium complexes supported by ketimide ligands are odd electron species. Such odd electron species have been isolated for the other arenes (naphthalene, biphenyl, *trans*-stilbene, *p*-terphenyl), for which even electron species can be obtained as well. Computational studies can provide insight into the bonding properties of these compounds, as explored in the next section.

2.2.2. DFT calculation results

As for **1b$_2$-μ-toluene** (see Section 1.2.3), DFT calculations were carried out on model systems for the even electron naphthalene bridged[*] and for the symmetrical toluene bridged species,[**] respectively on $[(\mu\text{-}C_{10}H_8)U_2(NCH_2)_6]^{2-}$ and $[(\mu\text{-}C_6H_6)U_2(NCH_2)_6]^-$. The ketimide systems are more complex than the amide ones from a computational point of view; therefore an extensive DFT study was not undertaken. However, useful information could be obtained from a less detailed study. The geometry optimizations were carried out with relativistic corrections,[13] using the spin-unrestricted formalism,[14] and with four and three electrons of spin α in excess of spin β, respectively; comparisons between the optimized and experimental values are shown in Tables 2 and 3.

---

[*] Calculations presented here for $[(\mu\text{-}\eta^6,\eta^6\text{-}C_{10}H_8)U_2(NCH_2)_6]^{2-}$ were carried out by Víctor Durà-Vilà.
[**] Calculations presented here for $[(\mu\text{-}C_6H_6)U_2(NCH_2)_6]^-$ were carried out by Theodor Agapie.

Table 2. Calculated structural parameters for $[(\mu\text{-}\eta^6,\eta^6\text{-}C_{10}H_8)U_2(NCH_2)_6]^{2-}$ and experimental parameters for $K_2\text{-}3_2\text{-}\mu\text{-naphthalene}$.

Structural parameter	Calculated (Å)	Experimental (avg., Å)
U-N	2.196	2.261(20)
N-C	1.288	1.272(29)
C-C$_{bridging}$	1.448	1.410(16); 1.458(15); 1.457(15); 1.413(15); 1.418(15); 1.500(14)
C-C$_{non\text{-}bridging}$	1.412, 1.397	1.470(16); 1.319(17); 1.467(18); 1.381(15); 1.395(15)

Figure 8. The two δ-bonds (α component, β component not shown) between the uranium centers and the naphthalene fragment: SOMO-4 (left) and SOMO-5 (right).

The good agreement between calculated and experimental values in the case of $[(\mu\text{-}\eta^6,\eta^6\text{-}C_{10}H_8)U_2(NCH_2)_6]^{2-}$ is especially reflected in the fact that for the non-bridging ring of naphthalene the C-C distances alternate, similarly to what was observed for the crystal structure. As expected, the DFT calculations confirm the presence of δ bonds between the uranium centers

References begin on page 155

and LUMOs of naphthalene (Figure 8). The δ bonds follow immediately in energy below the orbitals containing the four unpaired electrons.

Table 3. Calculated structural parameters for $[(\mu\text{-}\eta^6,\eta^6\text{-}C_6H_6)U_2(NCH_2)_6]^-$ and experimental parameters for $K_2I\text{-}3_2\text{-}\mu\text{-toluene}$.

Structural parameter	Calculated (Å)	Experimental (avg., Å)
U-N	2.238	2.228(27)
U-C	2.703	2.647(48)
N-C	1.268	1.272(29)
C-C	1.439	1.447(49)
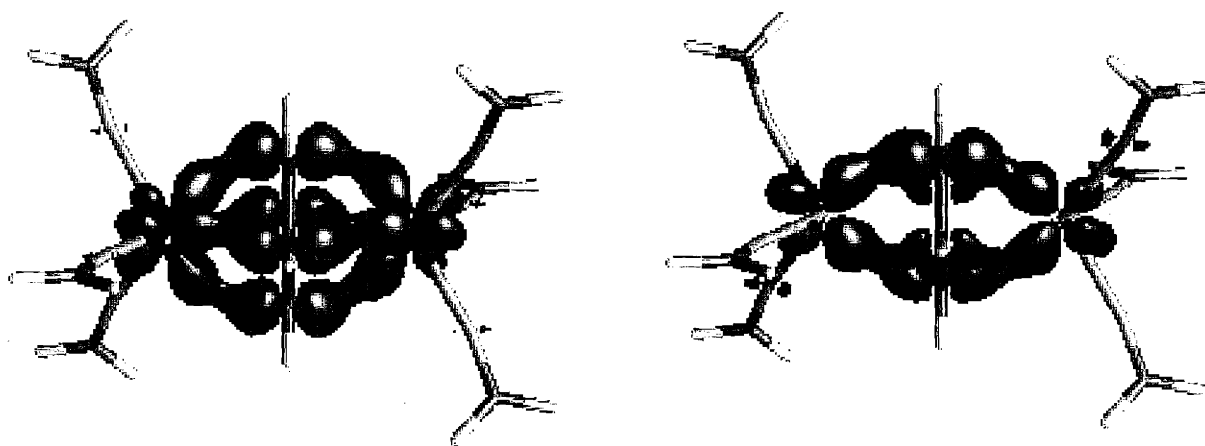
Figure 9. The two δ-bonds (α component, β component not shown) between the uranium centers and the benzene fragment: SOMO-3 (left) and SOMO-4 (right).

DFT calculations on the model compound $[(\mu\text{-}\eta^6,\eta^6\text{-}C_6H_6)U_2(NCH_2)_6]^-$ were carried out for the symmetrical version, the alkali metal ion not being included. Similar to what was found for the model of the naphthalene-bridged compound, the δ bonds are located energetically immediately below the three nonbonding f electrons.

References begin on page 155

2.2.3. Magnetic susceptibility measurements

Solid-state magnetic properties are used in complete analyses of electronic structures. Due to the difficulty of deriving detailed interpretations of these properties for uranium compounds (see Chapter 1), the magnetic susceptibility measurements presented in this section are used as a means for finding signatures for either odd or even electron structures.

From all the ketimide compounds presented in this chapter, **3-I-DME** can be used as a standard, because it is a mononuclear uranium compound with two unpaired electrons. Its magnetic properties are similar to those of the uranium iodide tris-amide compounds: it presents TIP (temperature independent paramagnetism) at low temperatures (10-40 K) and Curie-Weiss behavior from 50 to 300 K. The magnetic moment (50-300 K) of 3.62 μ_B is in the expected range for this type of compound (see Chapter 1) and has a value very close to that of the U^{4+} free ion (3.58 μ_B for a $^3H_4$ ground state).[15]
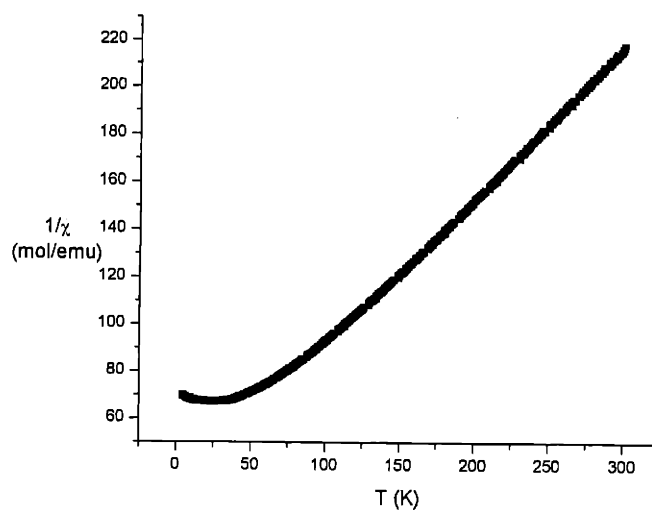
Figure 10. Plot of $1/\chi$ versus T for **3-I-DME**.

For the arene-bridged complexes, the magnetic properties are more complicated, as expected for dinuclear uranium compounds. Figures 11 and 12 display the plots of $1/\chi$ and μ_{eff} versus T for

References begin on page 155

the bridging *trans*-stilbene compounds. These are representative for the series of arene-bridged compounds when the arene is *trans*-stilbene, naphthalene, biphenyl, or *p*-terphenyl. Both types of species (even and odd electron) present nearly linear graphs of $1/\chi$ versus T on the entire temperature range studied, but the plots of μ_{eff} versus T do not agree with Curie-Weiss behavior. Inspection of χT versus T graphs also shows a continuous decrease in χT as the temperature is lowered. Such behavior is not unusual for uranium compounds,[16] and it is due to mixing of different spin states. The change in the value of the effective magnetic moment is more pronounced for the even electron species.
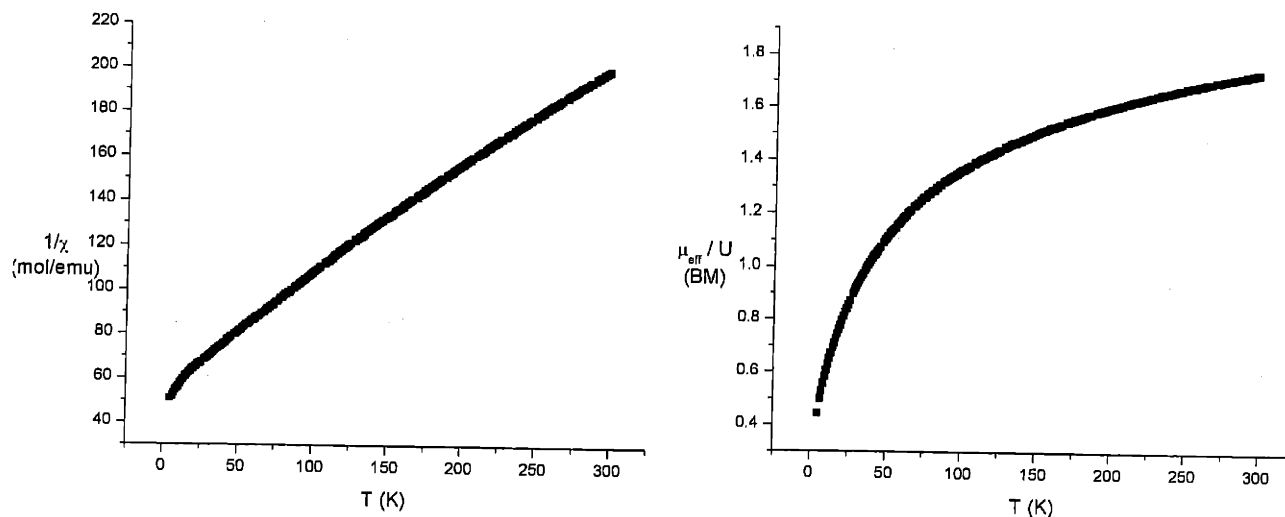
Figure 11. Plots of $1/\chi$ (left) and μ_{eff} (right) versus T for K_2-3_2-μ-*trans*-stilbene.

The value of μ_{eff} for the odd electron species at low temperatures supports the notion of an odd number of unpaired electrons, even in the event of antiferromagnetic coupling. At higher temperatures, the values of the magnetic moments for the odd and even electron species (ca. 2.4 μ_B at 300 K) are closer in magnitude, but μ_{eff} for the odd electron species is always higher than that for the even electron species (ca. 1.7 μ_B at 300 K).
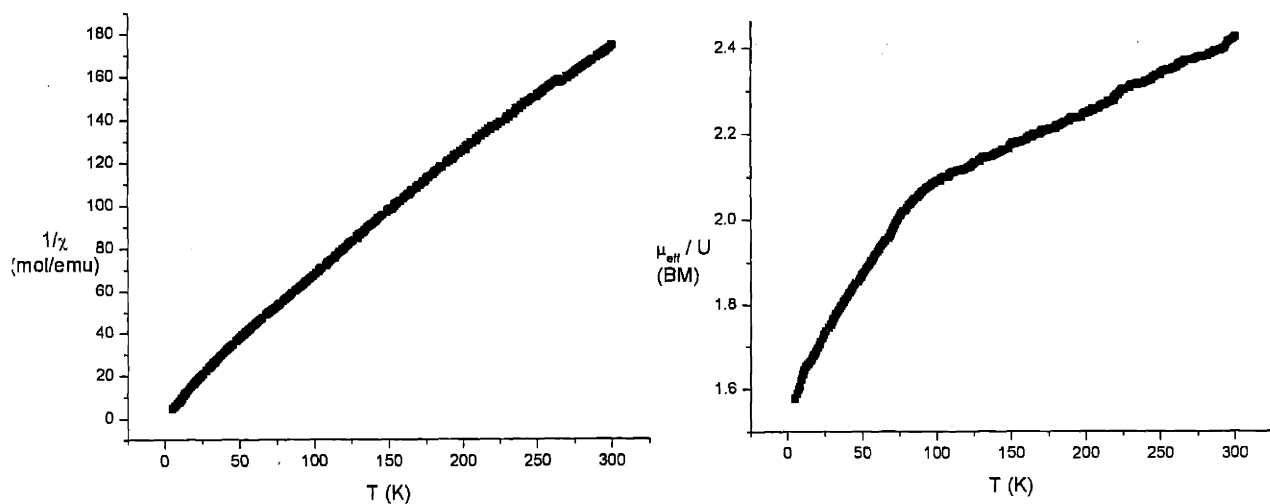
Figure 12. Plots of $1/\chi$ (left) and μ_{eff} (right) versus T for **K-3_2-μ-*trans*-stilbene**.
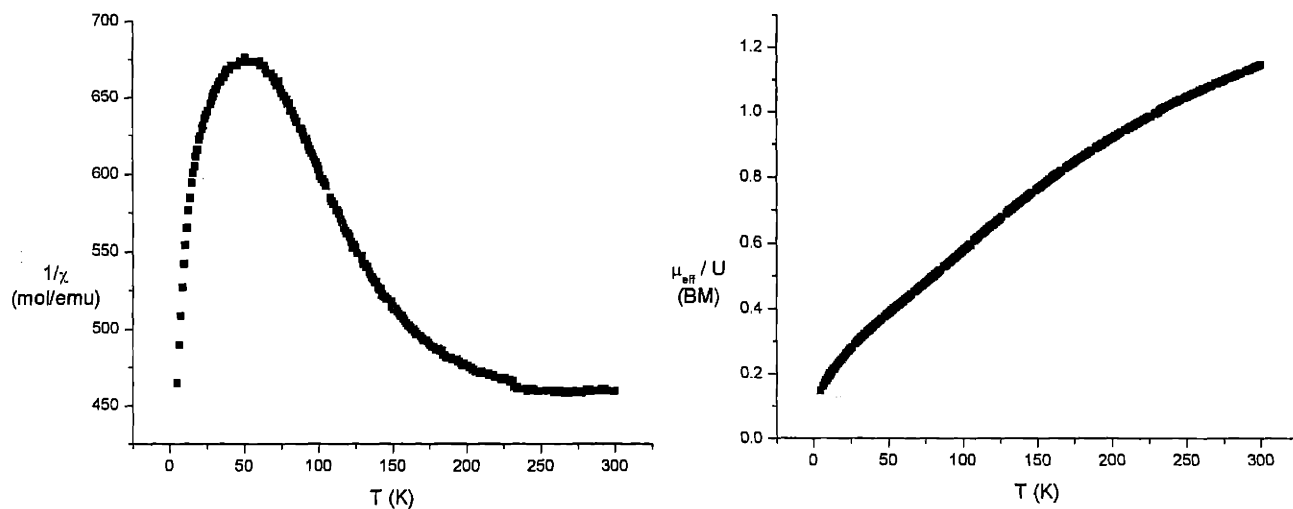
Figure 13. Plots of $1/\chi$ (left) and μ_{eff} (right) versus T for **K_2I-3_2-μ-toluene**.

Interestingly, the magnetic behavior of **K_2I-3_2-μ-toluene** is comparable to that of the toluene-bridged amide compound **$1b_2$-μ-toluene** (see Section 1.2.5) and not to that of odd electron, arene-bridged ketimide compounds. Even more peculiar is the fact that the values of the magnetic moment vary from ca. 0.1 μ_B at 5 K to ca. 1.1 μ_B at 300 K, being lower than those for the even electron arene-bridged ketimide compounds. From the plot of $1/\chi$ versus T for **K_2I-3_2-μ-toluene** (Figure 13) paramagnetic behavior is observed from 5 to 50 K. As the temperature

References begin on page 155

increases, the magnetic susceptibility of the sample passes through a maximum around room temperature. The minimum values in the $1/\chi$ versus T graph observed between 250 and 300 K are characteristic of an antiferromagnetic transition. Supposedly, at temperatures higher than 300 K, the magnetic behavior of **K_2I-3_2-μ-toluene** would be similar to that of **$1b_2$-μ-toluene** from 150 to 300 K. Interestingly, the antiferromagnetic transitions occur for the two compounds on intervals separated by 200 K. This very broad antiferromagnetic transition explains the almost constant and low values of the magnetic moment observed for **K_2I-3_2-μ-toluene**.

Magnetic properties of arene-bridged, ketimide complexes could be used in differentiating even from odd electron species if values of the effective magnetic moment at low temperatures are compared. For the symmetrical **K_2I-3_2-μ-toluene** compound, although an odd electron species, its magnetic behavior is similar to that of **$1b_2$-μ-toluene** and rather different from that of **K-3_2-μ-arene** (arene = naphthalene, biphenyl, *trans*-stilbene, *p*-terphenyl). Theoretical fitting of the experimental data, although difficult to develop, would provide more insight into the electronic structures. Collaborative studies to this end are ongoing.

2.2.4. NMR spectroscopy studies

NMR spectroscopy was used to study the behavior of the arene-bridged species in solution. The issues addressed in this section include the manifestation of fluxional behavior and the assignment of chemical shifts for the protons/deuterons belonging to the bridging arene.

The strategy used to assign chemical shifts for the protons/deuterons of the bridging arene in some of the complexes is described in detail for **K_2-3_2-μ-biphenyl**. ^{2}H NMR spectroscopy (46 MHz, toluene, 22 °C) on **K_2-3_2-μ-biphenyl-d_{10}** (Table 4) revealed the following six peaks: 33.98, -5.72, -21.45, -46.85, -79.75, -126.24 ppm. Use of biphenyl-2-d_1 and biphenyl-4-d_1 led to the synthesis of complexes each with two positions deuterated: one in the bridging ring and one in

the pendant ring. Based on the ^{2}H NMR spectra of the biphenyl-d_1 complexes the peaks at 33.98 and −5.72 ppm could be assigned to *para* deuterons, while the peaks at −21.45 and −126.24 ppm could be assigned to *ortho* deuterons. By inference, the peaks at −46.85 and −79.75 ppm were assigned to *meta* deuterons. After assigning the chemical shifts belonging to the deuterons of the bridging biphenyl, ^{1}H NMR spectroscopy was used to differentiate between protons of the bridging and of the pendant ring: the broader peak of the two was considered to correspond to a proton of the bridging ring. Thus, the chemical shifts (500 MHz, toluene-d_8, 20 °C) of the protons pertaining to the bound ring are 34.04, -73.53, and -126.56 ppm. Since only one ketimide ligand environment is evident in the ^{1}H NMR spectrum of **K$_2$-3$_2$-μ-biphenyl**, it is clear that the potassium ions are mobile within the NC[*t*-Bu]Mes ligand array.
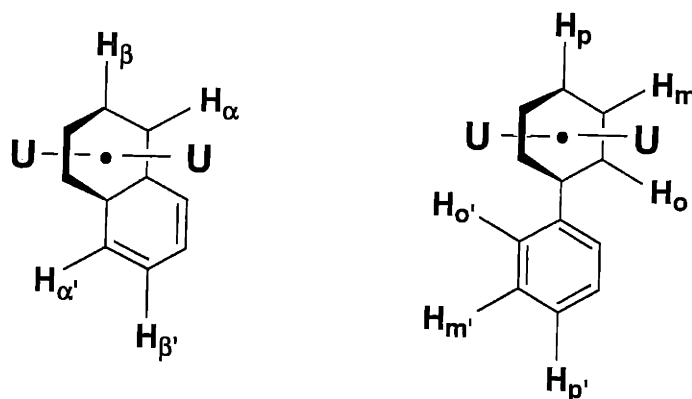
Figure 14. Labeling of the bridging arene protons used in the NMR chemical shift assignment.

Investigation of the even electron naphthalene-bridged systems by ^{1}H NMR spectroscopy revealed fluxional behavior, a single ketimide ligand environment being observed. For both **M$_2$-3$_2$-μ-C$_{10}$H$_8$** (M = Na, K) the corresponding mono and fully deuterated naphthalene-bridged compounds were prepared by using α-naphthalene-d_1 and naphthalene-d_8. The solution structure is consistent with that observed in the solid state with respect to the naphthalene coordination, since four ^{2}H NMR signals are observed for the d_8 derivative. Combining the results of 2D NMR correlation experiments with the line width of the signals in the ^{1}H NMR spectrum, and with the

References begin on page 155

Chapter 2

signals found in the ^{2}H NMR spectrum of **Na$_2$-3$_2$-μ-C$_{10}$H$_7$D(α)** the peaks at 79.2 (β-*H*) and -128.9 (α-*H*) ppm were assigned to the deuterons of the ring bridging the two uranium centers, while the peaks at -28.9 (α-*H*) and -36.5 (β-*H*) ppm were assigned to the deuterons of the dangling ring (see Table 5 for assignments for the potassium salt).

Table 4. Chemical shift (ppm) assignments for the protons (500 MHz, toluene-d_8, 20 °C) of the bridged biphenyl in **K$_2$-3$_2$-μ-biphenyl** and **K-3$_2$-μ-biphenyl**.

Proton (see Figure 14)	K$_2$-3$_2$-μ-biphenyl	K-3$_2$-μ-biphenyl
H$_o$	-126.56	-164.92
H$_m$	-73.53	-141.20
H$_p$	34.04	-83.62
H$_{o'}$	-21.40	-9.19
H$_{m'}$	-47.13	16.86
H$_{p'}$	-5.78	-14.18

Table 5. Chemical shift (ppm) assignments for the protons (500 MHz, 20 °C) of the bridged naphthalene in **K$_2$-3$_2$-μ-naphthalene** and **K-3$_2$-μ-naphthalene**.

Proton (see Figure 14)	K$_2$-3$_2$-μ-naphthalene (in C$_6$D$_6$)	K-3$_2$-μ-naphthalene (in toluene-d_8)
H$_α$	-141.55	-121.98
H$_β$	110.14	-125.23
H$_{α'}$	-32.88	-0.62
H$_{β'}$	-43.56	-38.15

Partially and fully deuterated naphthalene and biphenyl were used similarly to assign the peaks corresponding to the deuterons of the bridging arene for the odd electron species. Results are

References begin on page 155

presented in Tables 4 and 5. For bridging *trans*-stilbene, compounds the peaks belonging to the arene were identified, but not fully assigned (see Experimental section).

In the case of the bridging *p*-terphenyl compounds we may consider two structural alternatives; one where the uranium centers are bound to the central ring and another where they are bound to a terminal ring. Statistically, the latter structure should be favored. Structures in which the uranium rings are bound to different rings are not considered based on the X-ray crystal structures discussed above and also Hückel aromaticity (see above), along with the symmetry dictated by NMR spectra. Investigation of the ^{2}H NMR (77 MHz, Et$_2$O, 22 °C) spectrum of **K$_2$-3$_2$-μ-*p*-terphenyl** revealed eight peaks at 22.27, 8.16, 6.00, 3.84, 2.89, -15.66, -51.72, and – 117.58 ppm, while the ^{2}H NMR (77 MHz, Et$_2$O, 22 °C) spectrum of **K-3$_2$-μ-*p*-terphenyl** displayed eight peaks at 18.94, 12.17, 8.45, 6.83, -5.84, -87.88, -145.83, -162.46 ppm. These results are consistent with a structure in which the uranium centers are bound to the terminal ring for both **K$_2$-3$_2$-μ-*p*-terphenyl** and **K-3$_2$-μ-*p*-terphenyl**.

Interestingly, for the odd electron arene-bridged species, the solution structures are asymmetrical. ^{1}H NMR spectra of **K-3$_2$-μ-arene** compounds display two ancillary ketimide ligand environments, in a 2:1 ratio, meaning that some fluxional behavior is manifest. Although it is impossible to be absolutely certain of the assignments for the peaks corresponding to the ketimide ligand protons,* the observed pattern can be most rationally associated with two ligands that coordinate the potassium ion and one ligand that does not. It is interesting that in solution both uranium centers are equivalent.

For all **K-3$_2$-μ-arene**, on one hand, and **K$_2$-3$_2$-μ-arene**, on the other hand, compounds discussed here, the chemical shifts that can be associated with ancillary ketimide ligand protons are very

---

* Although the peaks in ^{1}H NMR spectra of uranium paramagnetic compounds are reasonably sharp in most cases, unless specific experiments are designed, their assignment is made based on relative values of the integrated areas. In the present cases, the numbers of protons of a specific kind are the same and also some broad peaks may be composed of more than one peak.

Chapter 2

similar, such that ^{1}H NMR spectroscopy constitutes an important means of characterizing and identifying these compounds.

Of note, the only odd electron, arene-bridged compounds that do not present a C_{2v} solution structure are **K$_2$I-3$_2$-μ-toluene** and **K(DME)-3$_2$-μ-toluene**, only one ketimide ligand environment being observed. This fact is not surprising for **K$_2$I-3$_2$-μ-toluene** since the solid-state structure suggests a pattern (Figure 7) similar to the one observed for **K$_2$-3$_2$-μ-arene** complexes.

For assignments of protons of the bridging toluene (Table 6), the method outlined in Chapter 1 for **1b$_2$-μ-toluene** was employed. Compound **K$_2$I-3$_2$-μ-benzene** was synthesized and its ^{1}H NMR spectrum (500 MHz, C$_6$D$_6$, 22 °C) recorded. Therefore, based on the chemical shift of – 44.91 ppm for the protons of the bridging benzene in **K$_2$I-3$_2$-μ-benzene** and the relative intensities of peaks (500 MHz, toluene-d_8, 20 °C), the chemical shifts at 34.62, -38.23, -43.18, and –44.70 could be assigned to the protons of the bridging toluene in **K$_2$I-3$_2$-μ-toluene** as follows: *Me*-C$_7$H$_8$, *o*-C$_7$H$_8$, *p*-C$_7$H$_8$, and *m*-C$_7$H$_8$, respectively.

Table 6. Chemical shift (ppm) assignments for the protons (500 MHz, 20 °C) of the bridged arene (toluene, benzene) in **K$_2$I-3$_2$-μ-arene** and **K(DME)-3$_2$-μ-arene**.

Proton	K$_2$I-3$_2$-μ-C$_7$H$_8$	K$_2$I-3$_2$-μ-C$_6$H$_6$	K(DME)-3$_2$-μ-C$_7$H$_8$	K(DME)-3$_2$-μ-C$_6$H$_6$
C$_6$H$_6$		-44.91		-112.83
Me-C$_7$H$_8$	34.62		64.48	
o-C$_7$H$_8$	-38.23		-109.52	
m-C$_7$H$_8$	-44.70		-113.84	
p-C$_7$H$_8$	-43.18		-126.52	

If it is reasonable for **K$_2$I-3$_2$-μ-toluene** to display a single ketimide ligand environment in its ^{1}H NMR spectrum, the same finding for **K(DME)-3$_2$-μ-toluene** is more surprising since the odd

electron, arene-bridged complexes **K-3₂-µ-arene** (arene = naphthalene, biphenyl, *trans*-stilbene, and *p*-terphneyl) show two ketimide ligand environments (2:1). For benzene or toluene the U(NC[*t*-Bu]Mes)₃ moiety rotates relative to the arene ring, while for the other arenes rotation of the same moiety is slow. The assignment of the chemical shifts for the protons of the bridging toluene is presented in Table 6.

A graph of δ versus 1/T (Figure 15) for **K₂I-3₂-µ-toluene** displays non-linear plots for all the protons. This observation is in agreement with the observed magnetic properties for polycrystalline samples (see Section 2.2.3 and Section 1.2.4 about similar plot and interpretation for **1b₂-µ-toluene**). Preliminary thermal stability studies conducted with **K₂-3₂-µ-arene** and **K-3₂-µ-arene** (arene = naphthalene, biphenyl, *trans*-stilbene, and *p*-terphenyl) in toluene-*d*₈ showed that while the former, even electron, compounds are stable for at least a week at 80 °C, the latter, odd electron, compounds are transformed quantitatively to **K-3₂-µ-toluene-*d*₈** at 60 °C within an hour.
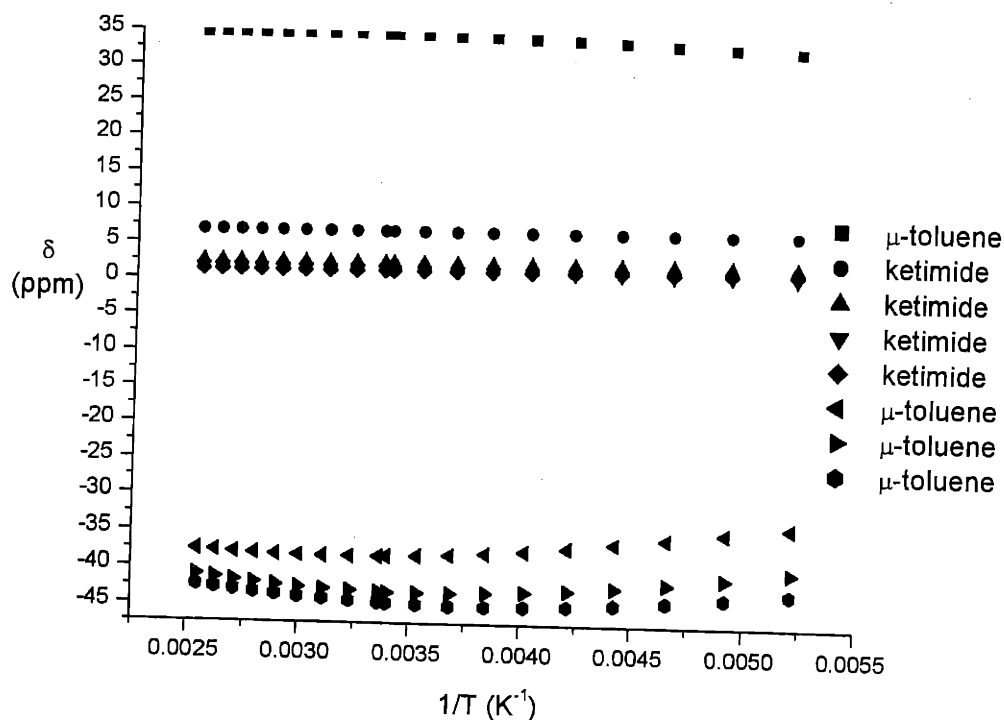
Figure 15. Plot of δ versus 1/T for compound **K₂I-3₂-µ-toluene**.

NMR spectroscopy proved to be a powerful technique for characterizing the arene-bridged complexes supported by ketimide ligands. Similar complexes, such as **K₂-3₂-µ-arene**, on one hand, and **K-3₂-µ-arene**, on the other hand (arene = naphthalene, biphenyl, *trans*-stilbene, and *p*-terphneyl) present similar chemical shifts for the ketimide protons. Using compounds which have the bridging arene partially or fully deuterated allowed for assignment of the chemical shifts for the protons of the arene. A special case is presented by the toluene complexes, **K₂I-3₂-µ-toluene** and **K(DME)-3₂-µ-toluene**, that show only a single ketimide ligand environment in their ¹H NMR spectra (22 °C) unlike the other odd electron, arene-bridged complexes, which show two ligand environments.

2.2.5. Electronic spectra

The general comments made for the compounds discussed in Chapter 1 are also valid for those discussed in the present chapter. Therefore, from the spectra shown in Figures 16-18, the following assignments are based on the value of the molar absorption coefficient and the position of a band in the spectrum.[17] Bands present in the UV region (200-400 nm), because of their high intensity ($\varepsilon \approx 10^5$ M⁻¹ cm⁻¹) can be assigned to $\pi \rightarrow \pi^*$ transitions of the arene rings and to ligand to metal charge transfer transitions. Intense absorption bands present in the visible region (400-800 nm) that have $\varepsilon \approx 10^3$ M⁻¹ cm⁻¹ could be either f → d or charge transfer transitions.

Although not identical, the UV-vis spectra of the various ketimide arene-bridged complexes are rather similar to one another. Besides the bands from the UV region, they all have one or two prominent, very broad bands in the visible region. For compounds based on the same bridging arene, the bands in the visible region are very similar in their intensity and position, with a more pronounced difference in the case of the *trans*-stilbene pair; this dissimilarity correlates well with the distinctive colors observed visually for the two compounds: **K₂-3₂-µ-*trans*-stilbene** gives

dark blue solutions, while **K-3₂-μ-*trans*-stilbene** leads to dark orange solutions. The colors of the corresponding naphthalene or biphenyl compounds are brown and orange brown, respectively.
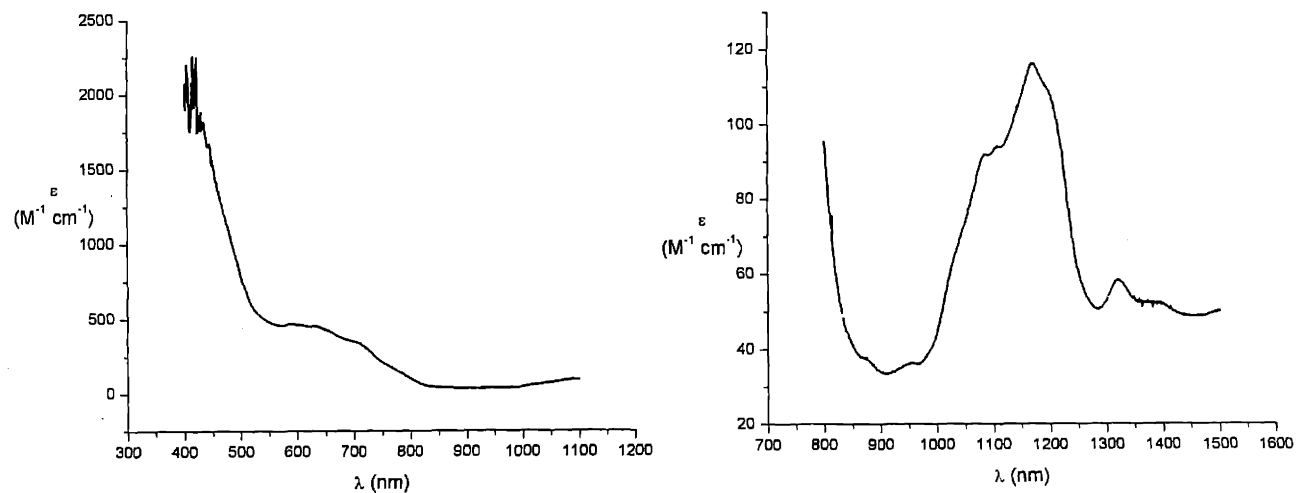
Figure 16. UV-vis (left) and NIR (right) absorption spectra of **3-I-DME** in toluene solutions at 25 °C.
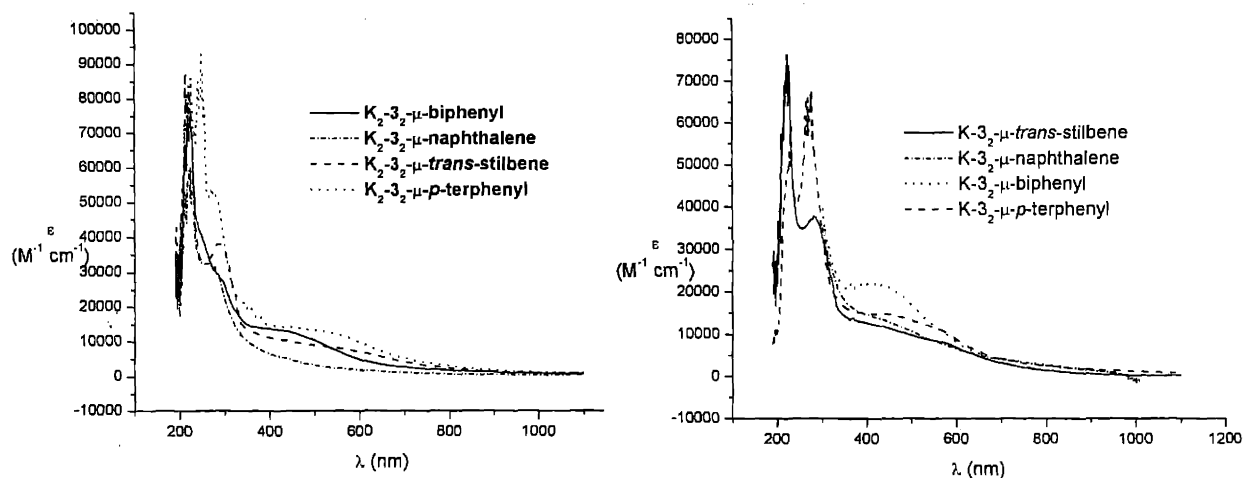
Figure 17. UV-vis absorption spectra of the even electron species (left) and the odd electron species (right) solutions at 25 °C.

References begin on page 155
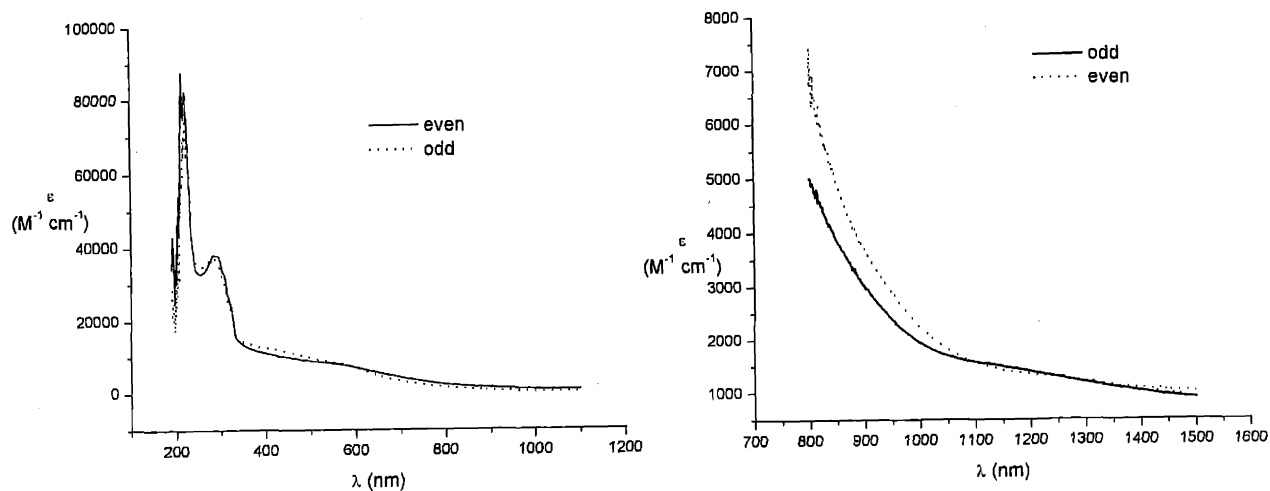
Figure 18. UV-vis (left, in diethyl ether) and NIR (right, in toluene) absorption spectra of K_2-3_2-µ-*trans*-stilbene and K-3_2-µ-*trans*-stilbene solutions at 25 °C.

The NIR absorption spectra have been recorded for the compounds discussed here, but they are not very informative. Unlike the cases presented in Chapter 1, there are no sharp bands in the region from 800 to 1500 nm. Even for **3-I-DME**, although its NIR spectrum is rather similar to those of the iodide uranium amide complexes, the bands tend to overlap.
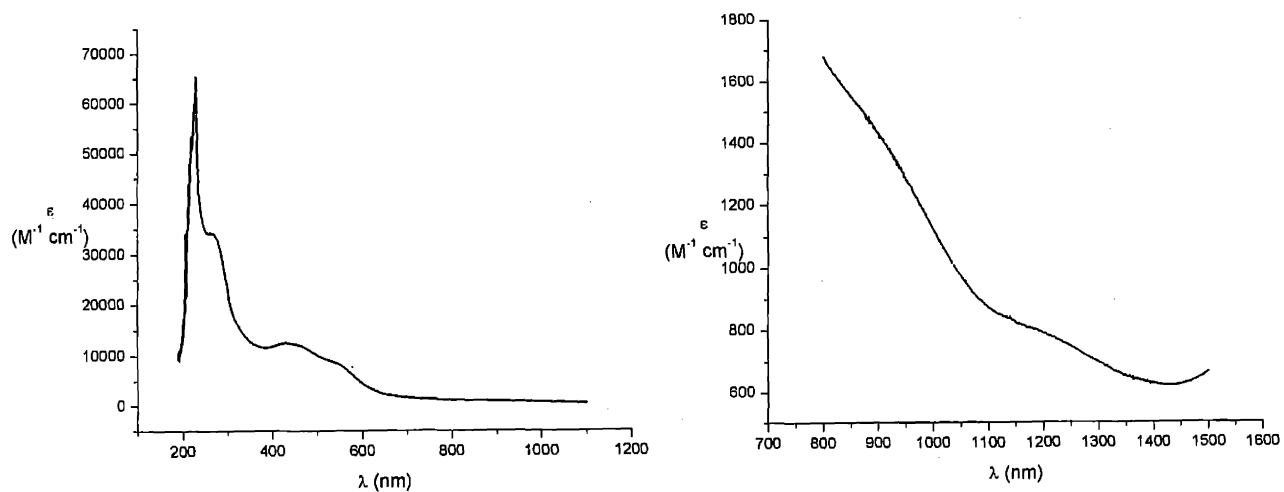
Figure 19. UV-vis (left, in diethyl ether) and NIR (right, in toluene) absorption spectra of K_2I-3_2-µ-**toluene** solutions at 25 °C.

It is seen that the broad band centered around 1100 nm has a molar extinction coefficient of ca. 800 M^{-1} cm^{-1} for **K_2I-3_2-μ-toluene** (comparable to ε ≈ 600 M^{-1} cm^{-1} of **$1b_2$-μ-toluene**) and of ca. 1500 M^{-1} cm^{-1} for the bridging *trans*-stilbene compounds. For **$1b_2$-μ-toluene**, even though the bands in the NIR region were more intense than expected for uranium compounds, they were rather sharp (see Section 1.2.6). As mentioned in Chapter 1, the high intensity of these bands may be associated with transitions between combinations of f orbitals that are of different symmetries or to intervalence transfer transitions. The broadness and intensity of the bands makes them a distinctive mark for the ketimide arene-bridged complexes, especially since **3-I-DME** displays a regular NIR spectrum (Figure 16).

2.2.6. Reactivity studies

It has been shown in Chapter 1 that compound **$1b_2$-μ-toluene** behaves as a powerful 4 electron reducing agent. It is interesting to examine the behavior of arene-bridged ketimide complexes towards the same substrates investigated with **$1b_2$-μ-toluene**. A new question arises also: do the even and odd electron species that include the same bridging arene lead to the same products in reaction with the same substrate? The results presented in this section reveal that the reaction chemistry of arene-bridged ketimide compounds is more complicated than that of **$1b_2$-μ-toluene**.

2.2.6.1. Inverting uranocene

Treatment of **M_2-3_2-μ-naphthalene** (M = Na, K) with 2 equiv of 1,3,5,7-cyclooctatetraene afforded a mixture of two products (Scheme 7). Compounds $K[(COT)U(NC[^tBu]Mes)_3]$ (**K-3-COT**) and $[Na(S)][(COT)U(NC[^tBu]Mes)_3]$ (**Na-3-COT**, S = Et_2O, Figure 20) are insoluble in pentane, facilitating their separation from the neutral co-product (μ-$η^8$,$η^8$-

COT)U$_2$(NC[^{t}Bu]Mes)$_6$ (**3$_2$-μ-COT**, Figure 21). The latter compound is remarkable in possessing a COT ligand sandwiched between two *tris*-ketimidouranium fragments.

Structurally related systems (with presumably far greater ionic character) exist for samarium, europium and ytterbium.[18] In **Na-3-COT** the sodium ion is coordinated to two nitrogen centers; its coordination sphere is completed by a molecule of diethyl ether and some carbon atoms of the ketimide ligands. The U-C$_{arene}$ distance in compound **3$_2$-μ-COT** is longer on average than in its naphthalene counterpart **K$_2$-3$_2$-μ-naphthalene** (2.822 *vs.* 2.634 Å), in accord with bonding considerations (Figure 22) that indicate poorer covalent overlap in the former.

M$_2$-3$_2$-μ-C$_{10}$H$_8$
M = Na, K

2 C$_8$H$_8$
- M$_2$COT

M-3-COT + *3$_2$-μ-COT*

+ 3-I-DME
- MI, -DME
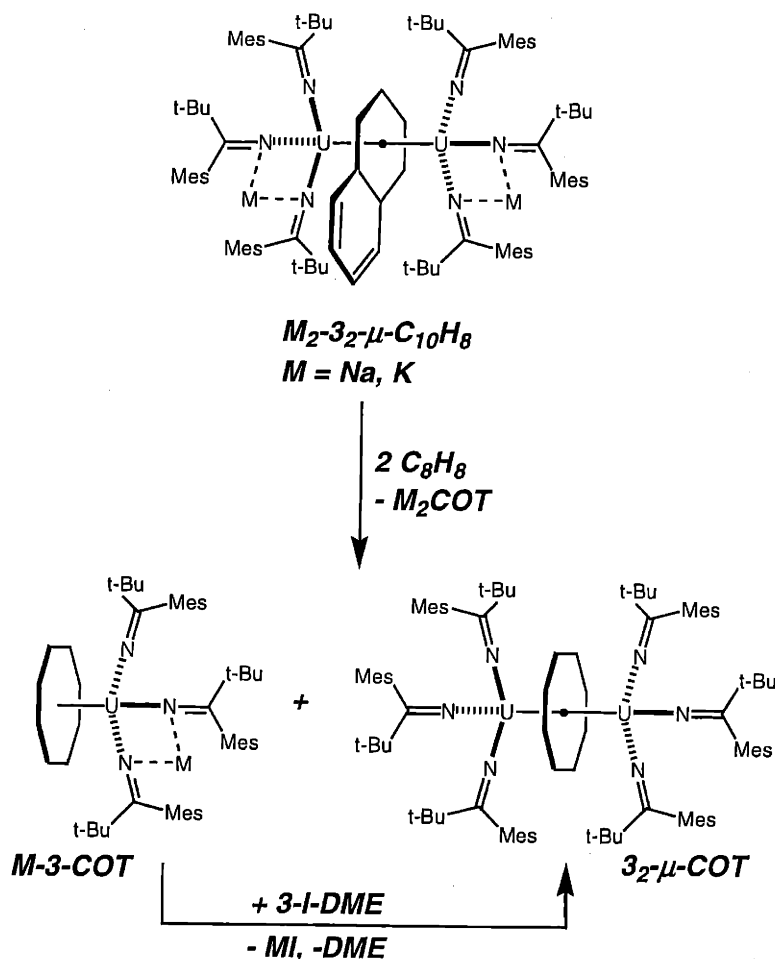
Scheme 7

The ratio in which the two compounds are formed seems independent of the solvent employed. If Na_2-3_2-μ-naphthalene is used the two compounds form in a 1:1 ratio and 3_2-μ-COT may be isolated in 35% yield. When K_2-3_2-μ-$C_{10}H_8$ is used as a starting material for the reaction with 1,3,5,7-cyclooctatetraene, K-3-COT is formed in great preference. Thus, the [3-COT]⁻ anion is easiest to isolate as its potassium salt (diethyl ether, 60% yield). Interestingly, compound 3_2-μ-COT can be assembled independently in 90% yield by salt elimination upon reaction of M-3-COT with iodide 3-I-DME (Scheme 7).
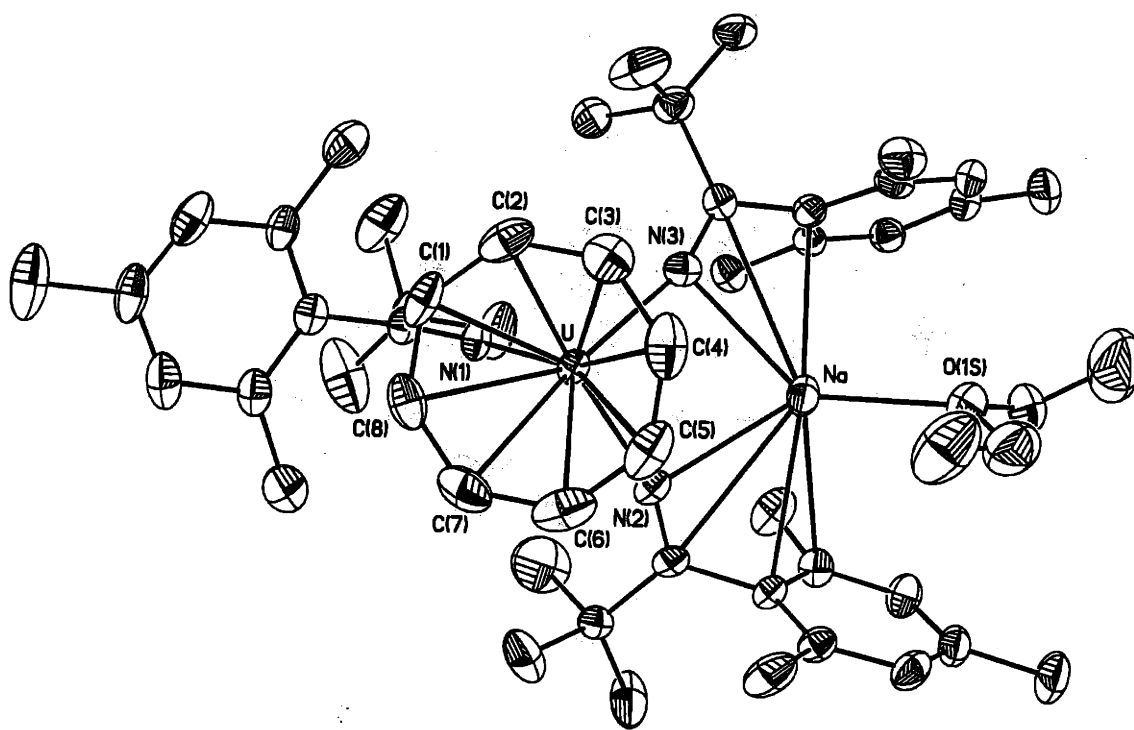
Figure 20. Structural drawing of complex **Na-3-COT** with thermal ellipsoids at the 35% probability level. Selected bond distances (Å): U-N (avg.), 2.269(8); U-C (avg.), 2.736(19); C-C (avg.), 1.392(31); Na-O, 2.349(5); Na-N (avg.), 2.524(7).

The reactions forming 3_2-μ-COT are referred to as "inverting uranocene" because they result in a C_8H_8 ring being sandwiched symmetrically between two uranium atoms instead of the reverse (Figure 23). Uranocene, $U(\eta^8\text{-}C_8H_8)_2$, was first synthesized in 1968[19] and its X-ray crystal structure determined shortly after that.[20] Bonding studies on uranocene indicated that the two

unpaired electrons are located in e_{3u} orbitals and there are two δ bonds (e_{2u} orbitals) between f orbitals on uranium and HOMOs of COT[21] (Figure 23). The interaction that constitutes the e_{2u} orbitals can take place only through f orbitals.[22]
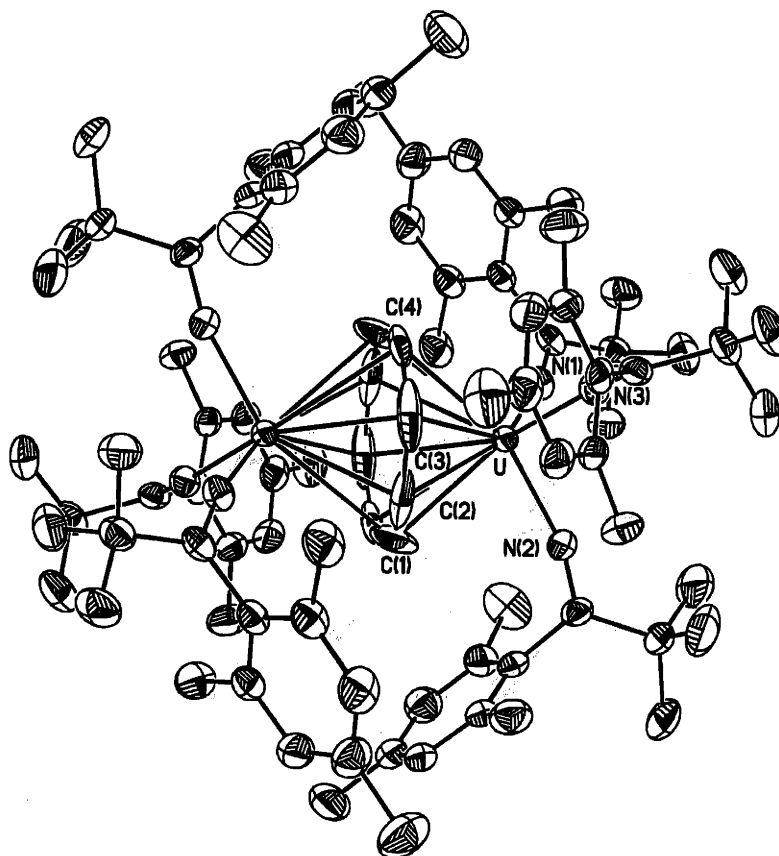
Figure 21. Structural drawing of complex 3_2-μ-COT with thermal ellipsoids at the 35% probability level. Selected bond distances (Å): U-N (avg.), 2.174(6); U-C (avg.), 2.822(15); C-C (avg.), 1.380(22).

DFT calculations on the model compound (μ-η^8,η^8-COT)U$_2$(NCH$_2$)$_6$* also indicate the existence of δ bonds between uranium f orbitals and HOMOs of COT (Figure 22). These orbitals (SOMO-10 and SOMO-11) do not follow immediately below the orbitals that contain the unpaired electrons, indicating a strong interaction between COT and the *tris*-ketimidouranium fragments.

---

* Calculations presented here for (μ-η^8,η^8-COT)U$_2$(NCH$_2$)$_6$ were carried out by Theodor Agapie.
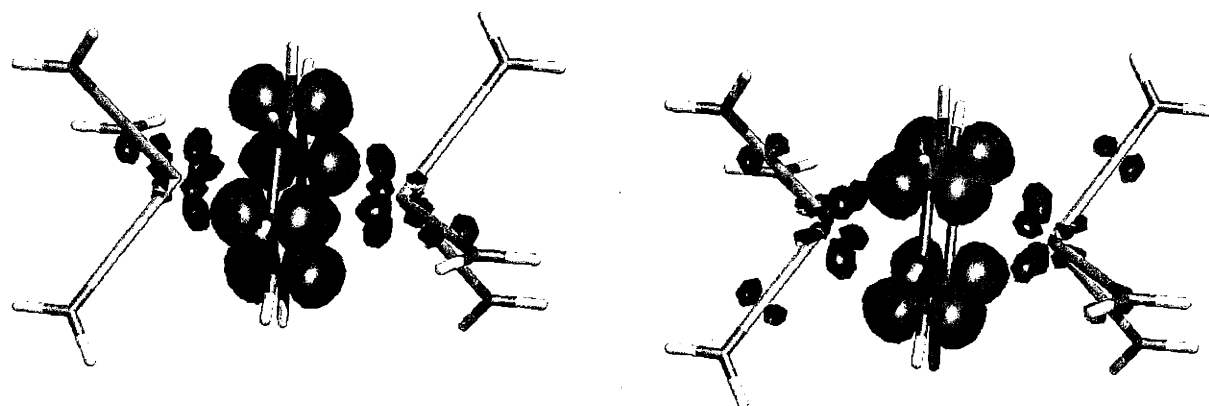
Figure 22. The two δ-bonds (α component, β component is not shown) between the uranium centers and the COT fragment: SOMO-10 (left) and SOMO-11 (right).
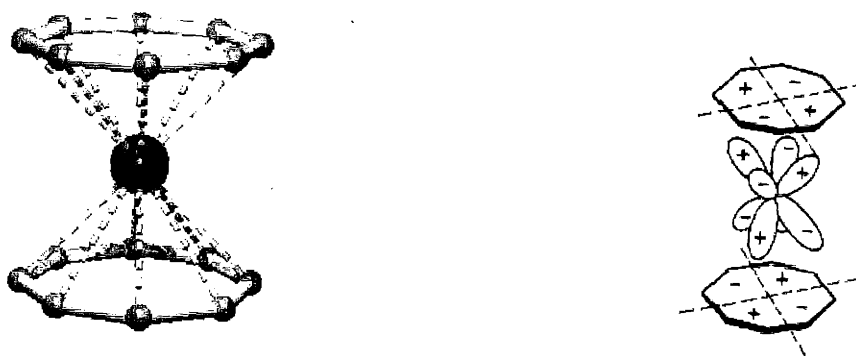
Figure 23. Left: ball and stick representation of uranocene. Right: one of the e_{2u} orbitals in uranocene.

When looking at the reaction of even electron species with 1,3,5,7-cyclooctatetraene it was found that all dipotassium salts provide **K-3-COT**. As mentioned previously, **Na_2-3_2-μ-naphthalene** forms **Na-3-COT** and **3_2-μ-COT** in a 1:1 ratio. At the other extreme, **Na_2-3_2-μ-biphenyl** forms only **3_2-μ-COT**. It is important to note that while all the COT reactions discussed take place within two hours, the last mentioned reaction requires 20 h for completion. Monitoring a diethyl ether solution of pure **K-3-COT** at room temperature, no formation of **3_2-μ-COT** was observed even after 23 h. In the case of odd electron species, a mixture of **K-3-COT** and **3_2-μ-COT** in different ratios always was formed. Therefore, **K-3-COT** can be synthesized from any even

electron species, **Na-3-COT** from **Na$_2$-3$_2$-μ-naphthalene**, and **3$_2$-μ-COT** from the reaction of **3-I-DME** with either salt **M-3-COT** (M = Na, K).
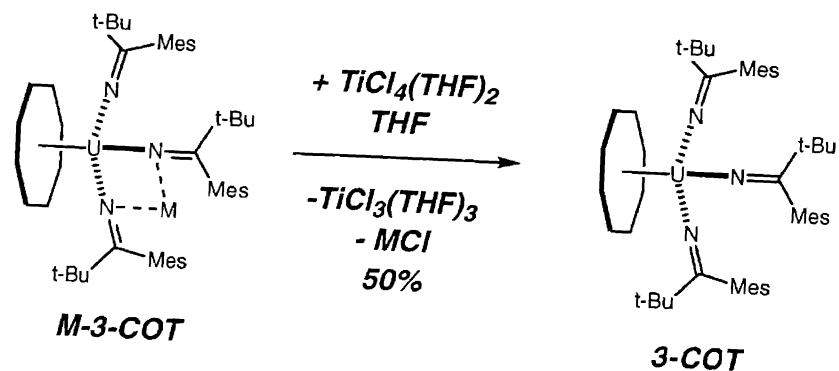
Scheme 8

Compounds **M-3-COT** can be oxidized to **3-COT** (Figure 24) by reaction with TiCl$_4$(THF)$_2$ (Scheme 8). As expected for a formally U(V) compound, the U-C (avg.) distance is shorter (2.715(30) Å) than in **3$_2$-μ-COT** (2.822(15) Å). Similar uranium (V) COT complexes have been reported: COTU(NR$_2$)$_3$ (R = Me, Et) obtained also by oxidation of the corresponding anion.[23]

Starting from μ-η^6,η^6-arene bridged complexes, mononuclear **M-3-COT** and "inverted uranocene" **3$_2$-μ-COT** were synthesized. As shown in Section 1.2.7 and above, the main difference between μ-η^6,η^6-arene bridged compounds and **3$_2$-μ-COT** is that the δ symmetry orbitals are LUMOs of the arene for the first case and HOMOs of COT for the latter. This difference is reflected in structural parameters such as U-C$_{arene}$ and C-C distances, although longer U-C$_{COT}$ distances are expected also on the basis of a larger ring size.
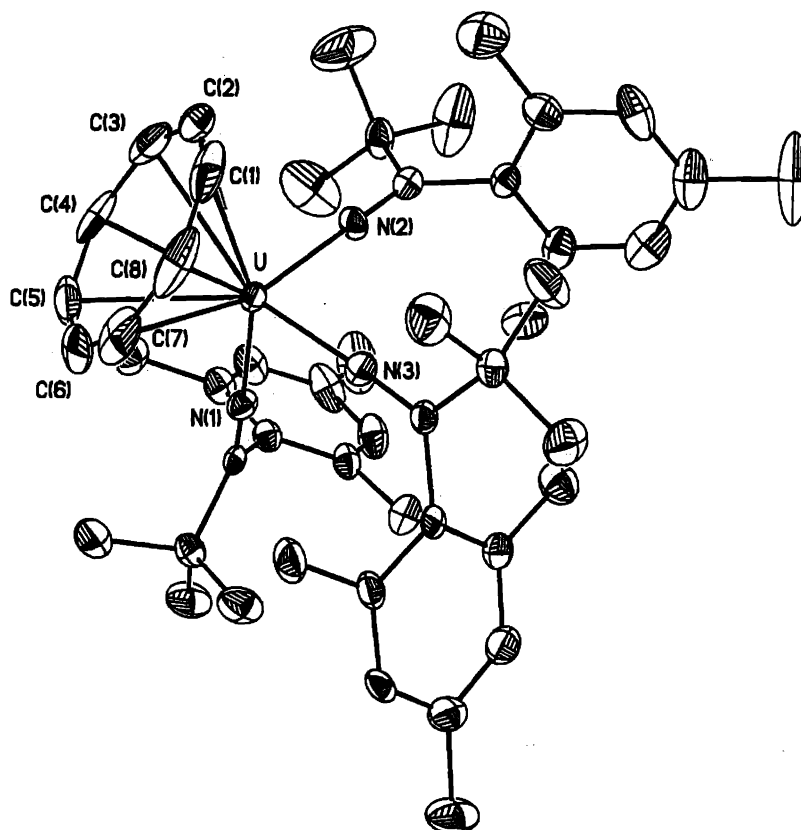
Figure 24. Structural drawing of complex **3-COT** with thermal ellipsoids at the 35% probability level. Selected bond distances (Å): U-N (avg.), 2.171(13); U-C (avg.), 2.715(30); C-C (avg.), 1.38(6).

2.2.6.2. Reaction of arene-bridged complexes with PhSSPh and PhNNPh

Compound **Na$_2$-3$_2$-μ-naphthalene** reacts with diphenyl disulfide (2 equiv) to form a dark yellow compound isolated in 60% yield (Scheme 9). By X-ray crystallography, the product was determined to be a dinuclear *tris*-thiolate-bridged uranium(IV) derivative, **Na[(μ-SPh)$_3$U$_2$(NC[*t*-Bu]Mes)$_6$]** (**Na-3$_2$-(μ-SPh)$_3$**) (Figure 25). Although the redox reaction involved the transfer of four electrons, as expected, it was surprising to find that the structure of the product is organized such that one sodium ion is retained.

References begin on page 155

Scheme 9
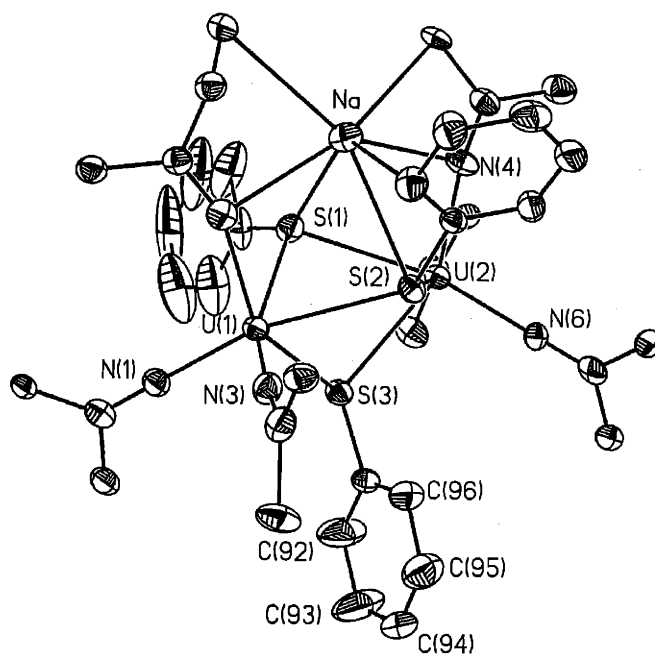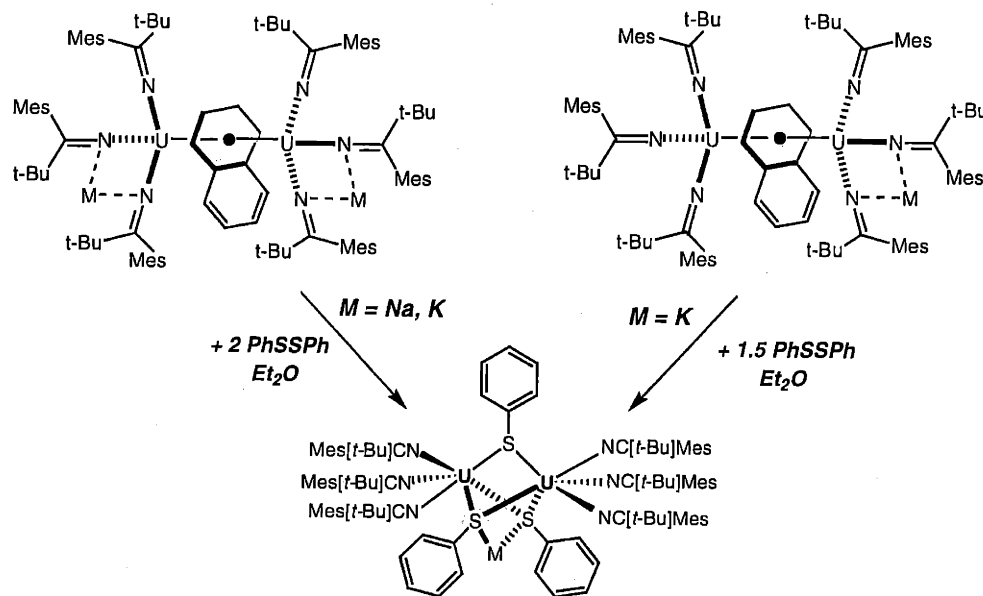
Figure 25. Structural drawing of complex **Na-3₂-(μ-SPh)₃** with thermal ellipsoids at the 35% probability level. The substituents of the ligands have been left out for clarity. Selected bond distances (Å): U-N (avg.), 2.215(22); U-S (avg.), 2.928(7); Na-N (avg.), 2.805(14); Na-S (avg.), 2.904(7).

Even more surprising is the fact that if **K$_2$-3$_2$-μ-arene** (arene = naphthalene, biphenyl, *trans*-stilbene, *p*-terphenyl) compounds form **K-3$_2$-(μ-SPh)$_3$**, the corresponding odd electron, arene-bridged species form the same compound in similar reactions. It is probable that in the reactions of **M$_2$-3$_2$-μ-arene** (M = Na, K), the other alkali metal cation is eliminated as MSPh, although the identity of the byproducts has not been established. In the case of **K-3$_2$-μ-arene** (arene = naphthalene, biphenyl, *trans*-stilbene, *p*-terphenyl) reactions the stoichiometry can be adjusted and these reactions involve the transfer of three electrons.

Reaction with azobenzene proceeded cleanly to a single major product in the case of the bridging toluene compounds (Scheme 10). Even so, the reaction is not a straightforward one since the isolated product is **(μ-NPh)$_2$U$_2$(NC[*t*-Bu]Mes)$_6$** (**3$_2$-(μ-NPh)$_2$**, Figure 26). K[PhNNPh], a known compound,[24] is proposed to be the byproduct. This supposition would be in accord with the fact that the reaction with 2 equiv of PhNNPh is cleaner than is the reaction with only one equivalent of azobenzene. Five electrons are transferred during this reaction.
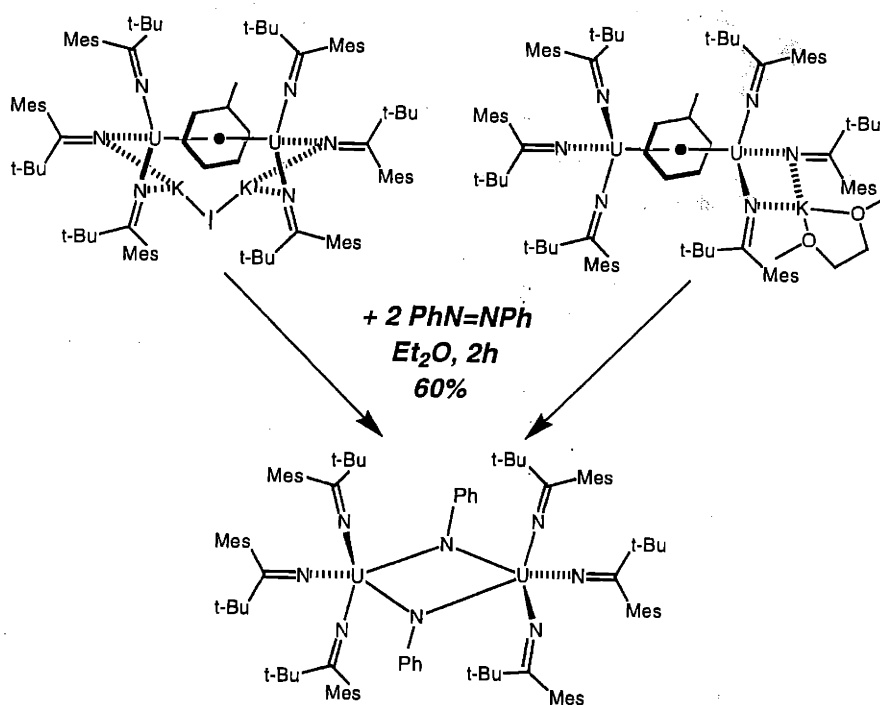
Scheme 10

Other **K-3₂-μ-arene** (arene = naphthalene, biphenyl, *trans*-stilbene, *p*-terphenyl) compounds also give **3₂-(μ-NPh)₂** as a major product upon azobenzene treatment, but the reactions are somewhat messier than in the case of the toluene-bridged complexes. The reactions of **K₂-3₂-μ-arene** with PhNNPh have also been tried, but they are not as straightforward as for **K-3₂-μ-arene**, even when the stoichiometry was adjusted to 3 equiv PhNNPh.
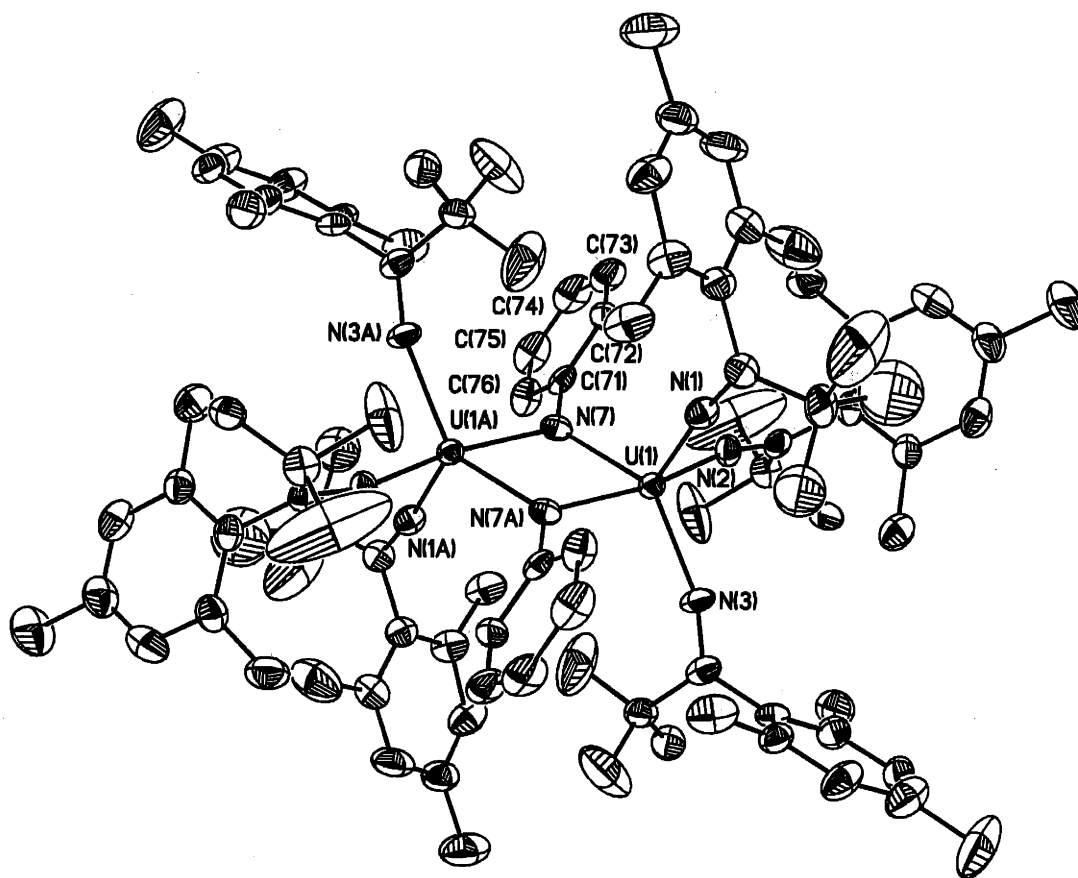
Figure 26. Structural drawing of complex **3₂-(μ-NPh)₂** with thermal ellipsoids at the 35% probability level. Selected bond distances (Å): $U-N_{ketimide}$ (avg.), 2.180(14); U(1)-N(7), 2.279(8); U(1)-N(7A), 2.177(8).

Because the NIR absorption spectra of the arene-bridged diuranium ketimide complexes did not present distinct bands, the absorption spectra of **Na-3₂-(μ-SPh)₃** and **3₂-(μ-NPh)₂** were recorded

and are shown in Figure 27 for comparison (NIR spectra only, UV-vis spectra not shown). Although the molar extinction coefficients are slightly high (200-300 M^{-1} cm^{-1}), the NIR spectra resemble very closely those of mononuclear compounds: that of **Na-3$_2$-(μ-SPh)$_3$** is similar to the spectrum of **3-I-DME** (see Absorption spectra section) and that of **3$_2$-(μ-NPh)$_2$** is not very different than the spectrum of **2a-NSiMe$_3$** (see Chapter 1). It is reasonable to assume that the uranium centers in these dinuclear complexes behave as isolated centers and do not communicate electronically at room temperature.

The magnetic susceptibility of polycrystalline samples of **3$_2$-(μ-NPh)$_2$** was measured and the results presented in Figure 28. The maximum at ca. 25 K in the plot of χ versus T is consistent with an antiferromagnetic transition, an observation supported by the fact that the value of χT decreases as the temperature is lowered. A similar antiferromagnetic transition at low temperatures (ca. 20 K) has been observed for $[(MeC_5H_4)_3U]_2[μ-1,4-N_2C_6H_4]$,[25] a related *bis*-imido diuranium(V) complex.
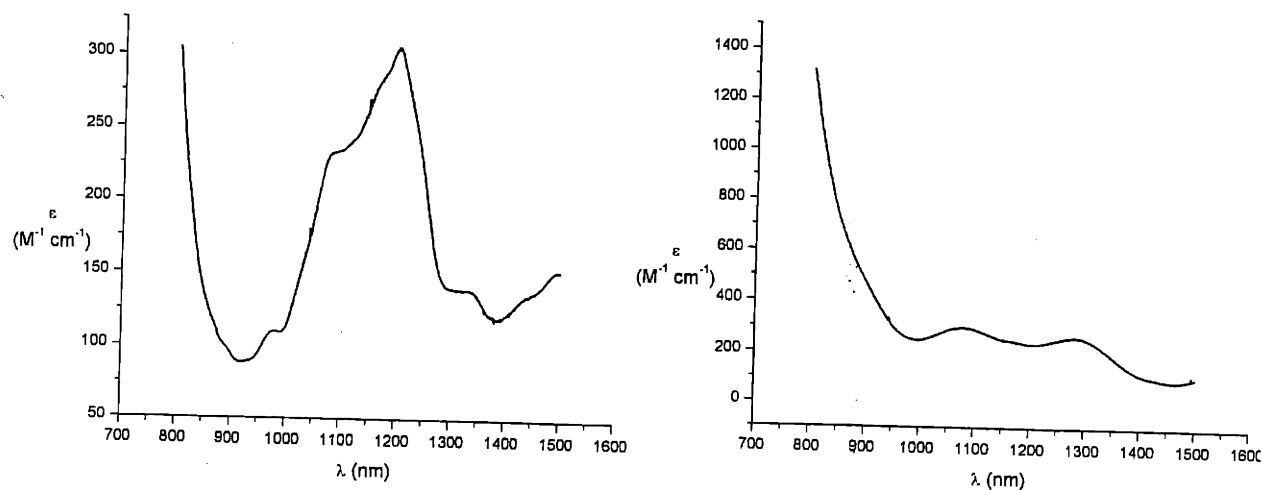
Figure 27. NIR absorption spectra of **Na-3$_2$-(μ-SPh)$_3$** (left) and **3$_2$-(μ-NPh)$_2$** (right) toluene solutions at 25 °C.
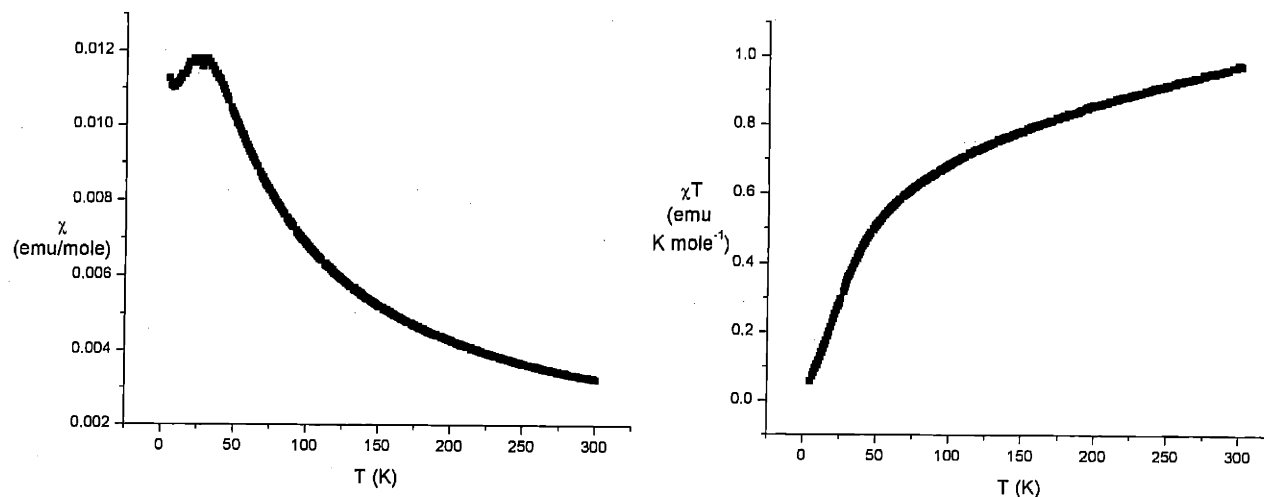
Figure 28. Plots of χ (left) and χT (right) versus T for 3_2-$(\mu$-NPh$)_2$.

2.3. Conclusions and further studies

Attempts to synthesize arene-bridged compounds supported by amide ligands where the arene is other than benzene or toluene led to disproportionation reactions, the identifiable species in the mixture of products being $U(N[t\text{-}Bu]Ar)_4$. Unlike the amide ligands, the ketimide ligand $NC[t\text{-}Bu]Mes$ has however proven more robust toward disproportionation reactions, making possible the isolation of a variety of arene-bridged complexes, which all retain three ketimide ligands around a uranium center. The generality of such a ligand was demonstrated further by the existence of the two types of compounds M_2-3_2-μ-**arene** (M = Na, K) and K-3_2-μ-**arene**, when the arene is naphthalene, biphenyl, or *trans*-stilbene.

Although these arenes present two 6-membered rings, in all cases the coordination geometry observed is μ-η^6,η^6, unlike reported cases of transition metal compounds where such arenes coordinate μ-η^6,$\eta^{6'}$.[6] A yttrium complex, $(\mu$-η^6,η^6-biphenyl)$Y_2[P_2N_2]_2$ (P_2N_2 = $PhP(CH_2SiMe_2NSiMe_2CH_2)_2PPh$) has been crystallographically characterized, but VT ^{1}H NMR spectroscopy studies showed that this is a low temperature structure.[26] At higher temperatures the

two yttrium centers coordinate to different rings of the bridging biphenyl ligand. In the uranium case, having both centers coordinated to one ring helps maintaining Hückel aromaticity (4n + 2, where n = 2), by forming two δ bonds with two LUMOs of the arene (4 electrons can be considered to occupy the LUMOs, instead of 2 + 2 electrons if the uranium centers coordinate to different rings). Understanding the preference for the exhibited coordination mode in the uranium examples requires detailed computational studies on model compounds that show the alternate coordination mode.

When toluene or benzene is the bridging arene, only odd electron species are formed including symmetrical complexes, **K_2I-3_2-μ-arene**, and assymetrical complexes, **K(DME)-3_2-μ-arene** (arene = benzene, toluene). The physical characteristics of the symmetrical species are different than those of **K-3_2-μ-arene** compounds, rather resembling those of **$1b_2$-μ-toluene**.

The reactivity patterns observed for the bridging arene ketimide compounds are complicated by loss of an alkali metal ion (**K_2-3_2-μ-arene** with PhSSPh) or by additional redox processes (**K-3_2-μ-arene** with PhNNPh), but interesting products have been isolated. By contrast, the reaction of **K_2-3_2-μ-arene** with 1,3,5,7-cyclooctatetraene appears to be straightforward leading to **K-3-COT**. Compound **3_2-μ-COT** obtained from reaction of **K-3-COT** with **3-I-DME** is an interesting example of an inverted sandwich and can be referred to as "inverted uranocene".

Being in possession of general synthetic strategies to isolate a multitude of arene-bridged diuranium complexes, further studies are necessary in order to extend this class of compounds. Reaction of **3-I-DME** with (2.2)-*p*-cyclophane in the presence of KC_8 could lead to the isolation of complexes that have only one uranium center coordinated to one aromatic ring. The existence or non-existence of such complexes could offer some information about the preference for a specific coordination mode.

Investigation of xylenes, tri-, tetra-, penta-, and hexamethylbenzene would offer information if complexes of such arenes can be formed. An important problem is the exchange of the bridging arene with a different one. Preliminary studies on **K-3$_2$-μ-arene** indicate that conditions for determining equilibrium constants might be met.

Although difficult to achieve, the development of theoretical models that fit the characterization data, especially the magnetic and optical properties, would offer detailed insight into the electronic structure of the bridging arene complexes.

The fact that most of the reactions of arene-bridged ketimide complexes are complicated could be turned to advantage since these compounds are powerful reducing agents. Screening of various substrates could lead to new products and to understanding patterns in the reactivity of these compounds.

2.4. Experimental

2.4.1. General considerations

Unless stated otherwise, all operations were performed in a Vacuum Atmospheres dry box under purified nitrogen or using Schlenk techniques under an argon atmosphere. Anhydrous diethyl ether was purchased from Mallinckrodt; dimethoxyethane (DME) sealed under nitrogen was purchased from Aldrich; n-pentane, n-hexane and tetrahydrofuran (THF) were purchased from EM Science. Diethyl ether, toluene, benzene, n-pentane and n-hexane were dried and deoxygenated by the method of Grubbs.[27] THF and DME were distilled under nitrogen from purple sodium benzophenone ketyl. Distilled solvents were transferred under nitrogen into glass vessels before being pumped into the dry box. Hexamethyldisiloxane (($Me_3Si)_2O$) was degassed and dried over 4 Å sieves. C_6D_6, toluene-d_8, and octane-d_{18} were purchased from Cambridge

Isotopes and were degassed and dried over 4 Å sieves. Biphenyl-d_{10} and p-terphenyl-d_{14} were purchased from Cambridge Isotopes. 4 Å sieves, alumina and Celite were dried *in vacuo* overnight at a temperature just above 200 °C. $UI_3(DME)_2$,[5] KC_8,[3] and $KCH_2C_6H_5$[28] were prepared according to literature methods. MesBr was degassed by stirring it under vacuum for 0.5-1 h. *t*-BuCN was degassed and stored over 4 Å sieves. Naphthalene, α-naphthalene-d_1,[29] naphthalene-d_8, biphenyl, biphenyl-d_{10}, o-biphenyl-d_1,[29] p-biphenyl-d_1,[29] p-terphenyl, and p-terphenyl-d_{14} were dissolved in THF, their solutions passed through alumina, concentrated and placed in a −35 °C refrigerator. The crystals obtained were dried extensively under vacuum (at least 3 h) before use. 1,3,5,7-Cyclooctatetraene was passed through alumina and stored in a refrigerator at −35 °C. Other chemicals were used as received. ^{1}H, ^{13}C and ^{2}H NMR spectra were recorded on Varian XL-300 or Varian INOVA-501 spectrometers at room temperature unless specified otherwise. Chemical shifts are reported with respect to internal or external solvent, 7.16 ppm and 128.39 ppm (C_6D_6). UV-vis spectra were recorded on a HP spectrophotometer from 200 to 1100 nm using matched 1 cm quartz cells. Spectra were recorded on 5 different samples and errors determined. NIR spectra were recorded on an Aviv 14DS spectrophotometer from 800 to 1500 nm using matched 1 cm quartz cells; all spectra were obtained using a solvent reference blank. Numerical modeling of all data was done using the program Origin 6.0. CHN analyses were performed by H. Kolbe Mikroanalytisches Laboratorium (Mülheim an der Ruhr, Germany).

2.4.2.1. Synthesis of HNC[^{t}Bu]Mes

A 1000 mL round bottom flask was charged with MesBr (41.94 g, 0.211 mol) and diethyl ether (500 mL), and the solution was frozen. A 1.7 M solution of ^{t}BuLi in pentane (0.425 mol, 250 mL) was also frozen. The thawing ^{t}BuLi solution was added to the thawing MesBr solution by pipette over a period of 30 min. The resulting solution was warmed to room temperature and stirred for 24 h. After this period of time a solution of ^{t}BuCN (17.50 g) in diethyl ether (35 mL)

was added dropwise over 30 min such that the mixture did not warm too fast and did not reach the boiling point of diethyl ether. To the slurry obtained THF (30 mL) was added in order to produce a homogeneous solution and the reaction mixture was stirred for another 12 h. The resulting reaction mixture was then removed from the dry box and poured into 500 mL of water. The organic phase was separated and the aqueous phase extracted twice with 200 mL of Et$_2$O. The combined organics were dried over MgSO$_4$ and the solvent removed under reduced pressure. The yellow oil obtained was fractionally distilled under vacuum (0.25 mm Hg) affording pure HNC[^{t}Bu]Mes (42.80 g, 0.186 mol, 88%) by ^{1}H NMR spectroscopy.

^{1}H NMR (300 MHz, C$_6$D$_6$, 22 °C): δ = 9.29 (s, 1H, N*H*); 6.65 (s, 2H, *m*-Ar); 2.11 (s, 3H, *p-Me*); 2.06 (s, 6H, *o-Me*); 1.28 (s, 9H, ^{t}*Bu*).

^{13}C{^{1}H} NMR (75 MHz, C$_6$D$_6$, 22 °C): δ = 191.34 (N*C*); 141.43 (aryl ipso); 136.67 (aryl meta); 133.24 (aryl ortho); 129.11 (vb, aryl para); 40.67 (*C*Me$_3$); 30.82 (C*Me*$_3$); 21.55 (ortho-*Me*); 21.51 (para-*Me*).

2.4.2.2. Synthesis of KNC[^{t}Bu]Mes

A 500 mL round bottom flask was charged with HNC[^{t}Bu]Mes (19.69 g, 97 mmol) and diethyl ether (300 mL), and the solution was frozen. Solid KCH$_2$C$_6$H$_5$ (12.62 g, 97 mmol) was added to the thawing solution, the reaction mixture was allowed to warm up to room temperature, and was stirred for 2-3 h. Filtration of the resulting solution afforded a first crop of solid that was washed with pentane. The solvent of the remaining filtrate was removed under reduced pressure. To the solid obtained pentane (*ca.* 25 mL) was added and the solid was collected by filtration and washed with additional pentane (*ca.* 15 mL). The two crops of solids were dried under reduced pressure and amounted to 19.42 g of KNC[^{t}Bu]Mes (80 mmol, 83%).

^{1}H NMR (300 MHz, C$_6$D$_6$, 22 °C): δ = 6.69 (s, 2H, *m*-Ar); 2.17 (s, 3H, *p-Me*); 2.06 (s, 6H, *o-Me*); 1.15 (s, 9H, ^{t}*Bu*).

2.4.2.3. Synthesis of IU(DME)(NC[^{t}Bu]Mes)$_3$ (3-I-DME)

Compound UI$_3$(DME)$_2$ (3.83 g, 4.8 mmol) and compound KNC[^{t}Bu]Mes (2.61 g, 10.8 mmol, 2.25 equiv) were slurried independently in DME (75 and 100 mL, respectively) and then the mixtures frozen. The thawing KNC[^{t}Bu]Mes slurry was added to the UI$_3$(DME)$_2$ slurry dropwise, over a period of 15 min. After the addition was completed, the reaction mixture was stirred for ca. 1 h and then filtered through Celite. Removal of solvent was followed by extraction with pentane (ca. 200 mL) and filtration of the extract through Celite. Pentane was removed from the filtrate under reduced pressure and the resulting solid was dried for at least 2 h, extracted in 10 mL of diethyl ether and the solution filtered through Celite again. From the diethyl ether solution, dark green crystals were obtained after 2 to 3 days at –35 °C (1.50 g, 1.5 mmol, 30% yield).

^{1}H NMR (500 MHz, C$_6$D$_6$): at room temperature only very broad peaks can be observed between 0-12 ppm. These peaks sharpen significantly with increasing the temperature and at 100 °C they can be partially assigned: δ = 7.92 (s, 2H, *m*-Ar); 3.28 (s, 3H, *p-Me*); 2.91 and 2.60 (s, broad and overlapping, 15H, *o-Me* and ^{t}*Bu*). The chemical shifts for the protons of the coordinated DME could not be conclusively assigned.

UV-vis-NIR (toluene, 22 °C): λ_{max} (nm, $\varepsilon \times 10^{-2}$ M^{-1}, cm^{-1}) = 288 (117.2 ± 8.0); 311 (48.8 ± 6.1); 412 (21.6 ± 1.1); 590 (4.6 ± 0.1); 632 (4.5 ± 0.1); 660 (4.2 ± 0.1); 706 (3.5 ± 0.1); 875 (0.4); 950 (0.4); 1084 (0.9); 1107 (0.9); 1168 (1.2); 1195 (1.1); 1320 (0.6); 1387 (0.5).

Anal. calcd. for C$_{46}$H$_{70}$N$_3$O$_2$IU: C, 52.02; H, 6.64; N, 3.96. Found: C, 51.99; H, 6.63; N, 3.86.

2.4.2.4.a. Synthesis of K$_2$(μ-η^6,η^6-C$_{10}$H$_8$)[U(NC[^{t}Bu]Mes)$_3$]$_2$ (K$_2$-3$_2$-μ-naphthalene)

Note: The following synthesis was used for all **K$_2$-3$_2$-μ-arene** (arene = naphthalene, biphenyl, *trans*-stilbene, *p*-terphenyl) compounds. Only isolated yields and characterization data are presented separately.

Compounds **3-I-DME** (0.560 g, 0.53 mmol) and naphthalene (0.034 g, 0.26 mmol, 0.5 equiv) were dissolved in DME (15 mL) and the solution frozen. Separately, KC_8 (0.285 g, 2.11 mmol, 4 equiv) was slurried in DME (10 mL) and the slurry was also frozen. The thawing KC_8 slurry was added dropwise to the thawing solution mentioned above. After the addition was completed, the reaction mixture was stirred for 25 min and then filtered through Celite. After the solvent was removed, the dark brown solid was extracted with pentane (*ca.* 100 mL), the new solution filtered through Celite and the solvent removed completely. The solid obtained was slurried in a 1:1 mixture of pentane and diethyl ether (total of 10 mL), transferred to a vial and stored in a –35 °C refrigerator for several days. After decanting the solution and drying the solid obtained, a first crop of 0.222 g (0.24 mmol, 44.4% yield) was obtained. A second crop (*ca.* 0.080 g) was obtained giving a total yield of 60% (0.32 mmol).

^{1}H NMR (500 MHz, C_6D_6, 22 °C): δ = 110.14 (s, v. broad, 2H, *naphthalene*); 9.33 (s, 12H, *m-Ar*); 4.50 (s, 18H, *p-Me*); 3.72 (s, 36H, *o-Me*); -4.68 (s, 54H, *^{t}Bu*); -32.88 (s, broad, 2H, *naphthalene*); -43.56 (s, broad, 2H, *naphthalene*); -141.55 (s, v. broad, 2H, *naphthalene*).

UV-vis (Et_2O, 22 °C): λ_{max} (nm, $\varepsilon \times 10^{-2}$ M^{-1}, cm^{-1}) = 214 (2810.2 ± 308.4); 279 (684.7 ± 127.1); 375 (119.1 ± 17.2).

Anal. calcd. for $C_{94}H_{128}N_6K_2U_2$: C, 59.54; H, 6.80; N, 4.43. Found: C, 59.86; H, 6.95; N, 4.46.

2.4.2.4.b. Synthesis of $K_2(\mu\text{-}\eta^6,\eta^6\text{-}C_{10}D_8)[U(NC[^tBu]Mes)_3]_2$ ($K_2\text{-}3_2\text{-}\mu\text{-}C_{10}D_8$)

The experimental procedure is similar to the one that leads to $K_2\text{-}3_2\text{-}\mu\text{-}C_{10}H_8$, naphthalene-$d_8$ being used instead of non-deuterated naphthalene.

^{1}H NMR (500 MHz, C_6D_6, 22 °C): δ = 9.33 (s, 2H, *m-Ar*); 4.50 (s, 3H, *p-Me*); 3.75 (s, 6H, *o-Me*); -4.66 (s, 9H, *^{t}Bu*).

^{2}H NMR (46 MHz, Et_2O, 22 °C): δ = 111.68 (s, 1D); -32.50 (s, 1D); -43.44 (s, 1D); -142.29 (s, 1D).

2.4.2.4.c. Synthesis of $K_2(\mu\text{-}\eta^6,\eta^6\text{-}C_{10}H_7D)[U(NC[^tBu]Mes)_3]_2$ $(K_2\text{-}3_2\text{-}\mu\text{-}C_{10}H_7D)$

The experimental procedure is similar to the one that leads to $K_2\text{-}3_2\text{-}\mu\text{-}C_{10}H_8$, α-naphthalene-$d_1$ being used instead of non-deuterated naphthalene.

^1H NMR (300 MHz, C_6D_6, 22 °C): very similar to the chemical shifts reported for the non-deuterated compound.

^2H NMR (46 MHz, Et_2O, 22 °C): δ = -43.44 (s, 1D); -141.71 (s, 1D).

Based on the chemical shifts obtained for the three species ($K_2\text{-}3_2\text{-}\mu\text{-}C_{10}H_8$, $K_2\text{-}3_2\text{-}\mu\text{-}C_{10}H_7D$, $K_2\text{-}3_2\text{-}\mu\text{-}C_{10}D_8$) and on the line widths, the peaks for the naphthalene protons are assigned as follows (values taken from the ^1H chemical shifts): δ = 110.14 (s, β-H-bound ring); -32.88 (s, α-H-non-bound ring); -43.56 (s, β-H-non-bound ring); -141.55 (s, α-H-bound ring).

2.4.2.5.a. Synthesis of $Na_2(\mu\text{-}\eta^6,\eta^6\text{-}C_{10}H_8)[U(NC[^tBu]Mes)_3]_2$ $(Na_2\text{-}3_2\text{-}\mu\text{-}C_{10}H_8)$

A solution of **3-I-DME** (0.651 g, 0.60 mmol) and naphthalene (0.047 g, 0.37 mmol) in THF (20 mL) was added to a 20 mL scintillation vial containing a sodium mirror (the sodium was layered to at least half of the surface of the vial) and stirred vigorously for 45 min. After that time, the solution was decanted and the solvent removed. The resulting solid was extracted with pentane and the solution filtered through Celite. The solvent was removed again, the solid extracted with pentane, and after filtration of the extract through Celite the volume of the filtrate was reduced to *ca.* 10 mL. The compound is very soluble in pentane and although its solution is shown to be rather pure by ^1H NMR spectroscopy, the yield of the crystallized compound is low (0.234 g, 41%). A preliminary X-ray study indicated that $Na_2\text{-}3_2\text{-}\mu\text{-}C_{10}H_8$ crystallizes with two molecules of THF, but extensive drying of the crystals leads to a solvent free compound.

^1H NMR (500 MHz, C_6D_6, 22°C): δ = 84.30 (s, $v_{1/2}$ = 68Hz, 2H, *naphthalene*); 8.20 (s, 12H, *m-Ar*); 3.75 (s, 18H, *p-Me*); 3.46 (s, 36H, *o-Me*); -3.23 (s, 54H, *^tBu*); -29.85 (s, $v_{1/2}$ = 11Hz, 2H,

naphthalene); -38.37 (s, $\nu_{1/2} = 15$Hz, 2H, *naphthalene*); -133.28 (s, $\nu_{1/2} = 56$Hz, 2H, *naphthalene*). A g-COSY experiment indicated that the peak at 84.30 ppm is coupled with the one at -133.28 ppm and the peak at -29.85 ppm is coupled with the one at -38.37 ppm. Based on the values of $\nu_{1/2}$ it can be proposed that the first couple corresponds to the protons of the ring bridging the uranium centers while the latter corresponds to the other ring of the naphthalene. A variable temperature NMR experiment showed that the compound is stable up to at least 80 °C. The experiment was performed in C_6D_6 and spectra were recorded at room temperature, every 10 °C from 30 °C to 80 °C and then back to room temperature.

Anal. calcd. for $C_{94}H_{128}N_6Na_2U_2$: C, 61.02; H, 6.92; N, 4.54. Found: C, 61.19; H, 6.78; N, 4.35.

2.4.2.5.b. Synthesis of $Na_2(\mu\text{-}\eta^6,\eta^6\text{-}C_{10}D_8)[U(NC[^tBu]Mes)_3]_2$ (Na_2-3_2-μ-$C_{10}D_8$)

The experimental procedure is similar to the one that leads to Na_2-3_2-μ-$C_{10}H_8$, naphthalene-d_8 being used instead of non-deuterated naphthalene.

^{1}H NMR (500 MHz, C_6D_6, 22 °C): δ = 8.23 (s, 2H, *m-Ar*); 3.76 (s, 3H, *p-Me*); 3.50 (s, 6H, *o-Me*); -3.35 (s, 9H, *^tBu*).

^{2}H NMR (76 MHz, Et_2O, 22 °C): δ = 79.19 (s, 1D), -28.90 (s, 1D), -36.45 (s, 1D), -128.90 (s, 1D).

^{2}H NMR (46 MHz, Et_2O, 22 °C): δ = 48.99 (s, 1D), -27.63 (s, 1D), -29.78 (s, 1D), -111.68 (s, 1D).

2.4.2.5.c. Synthesis of $Na_2(\mu\text{-}\eta^6,\eta^6\text{-}C_{10}H_7D)[U(NC[^tBu]Mes)_3]_2$ (Na_2-3_2-μ-$C_{10}H_7D$)

The experimental procedure is similar to the one that leads to Na_2-3_2-μ-$C_{10}H_8$, α-naphthalene-d_1 being used instead of non-deuterated naphthalene.

^{1}H NMR (300 MHz, C_6D_6, 22 °C): very similar to the chemical shifts reported for the non-deuterated compound.

^{2}H NMR (46 MHz, Et_2O, 22 °C): δ = -29.39 (s, 1D), -110.50 (s, 1D).

Based on the chemical shifts obtained for the three species (Na_2-3_2-μ-$C_{10}H_8$, Na_2-3_2-μ-$C_{10}H_7D$, Na_2-3_2-μ-$C_{10}D_8$) and on the line widths, the peaks for the bridged naphthalene protons are assigned as follows (values taken from the ^{1}H chemical shifts): δ = 84.30 (s, $v_{1/2}$ = 68Hz, β-*H*-bound ring); -29.85 (s, $v_{1/2}$ = 11Hz, α-*H*-non-bound ring); -38.37 (s, $v_{1/2}$ = 15Hz, β-*H*-non-bound ring); -133.28 (s, $v_{1/2}$ = 56Hz, α-*H*-bound ring).

2.4.2.6.a. Synthesis of $K_2(\mu$-η^6,η^6-biphenyl)[U(NC[^{t}Bu]Mes)$_3$]$_2$ (K_2-3_2-μ-biphenyl)

Yield: 46% for the first crop (after 5 days, from Et_2O); 56% total yield.

^{1}H NMR (500 MHz, toluene-d_8, 20 °C): δ = 34.04 (s, $v_{1/2}$ = 22 Hz, 1H, *bound p-biphenyl*); 8.30 (s, 12H, *m-Ar*); 3.74 (s, 18H, *p-Me*); 3.03 (s, 36H, *o-Me*); -3.09 (s, 54H, ^{t}Bu); -5.78 (s, $v_{1/2}$ = 6 Hz, 1H, *unbound p-biphenyl*); -21.40 (s, $v_{1/2}$ = 17 Hz, 2H, *unbound o-biphenyl*); -47.13 (s, $v_{1/2}$ = 48 Hz, 2H, *unbound m-biphenyl*); -73.53 (s, very broad, 2H, *bound m-biphenyl*); -126.56 (s, $v_{1/2}$ = 64 Hz, 2H, *bound o-biphenyl*).

UV-vis (Et_2O, 22 °C): λ_{max} (nm, ε × 10^{-2} M^{-1}, cm^{-1}) = 212 (2555.7 ± 110.1); 244 (808.6 ± 38.5); 282 (476.4 ± 24.8); 395 (152.2 ± 8.6).

Anal. calcd. for $C_{96}H_{130}N_6K_2U_2$: C, 59.98; H, 6.82; N, 4.37. Found: C, 60.06; H, 6.48; N, 4.11.

2.4.2.6.b. Synthesis of $K_2(\mu$-η^6,η^6-biphenyl-d_{10})[U(NC[^{t}Bu]Mes)$_3$]$_2$ (K_2-3_2-μ-biphenyl-d_{10})

The experimental procedure is similar to the one that leads to K_2-3_2-μ-biphenyl, biphenyl-d_{10} being used instead of non-deuterated biphenyl.

References begin on page 155

^{2}H NMR (46 MHz, Et$_2$O, 22 °C): δ = -33.98 (s, 1D), -5.72 (s, 1D); -21.45 (s, 2D); -46.85 (s, 2D); -79.75 (s, 2D); -126.24 (s, 2D).

2.4.2.6.c. Synthesis of K$_2$(μ-η^6,η^6-biphenyl-2-d_1)[U(NC[^{t}Bu]Mes)$_3$]$_2$ (K$_2$-3$_2$-μ-biphenyl-2-d_1)

The experimental procedure is similar to the one that leads to **K$_2$-3$_2$-μ-biphenyl**, 2-biphenyl-d_1 being used instead of non-deuterated biphenyl.

^{2}H NMR (46 MHz, Et$_2$O, 22 °C): δ = -21.05 (s, 1D), -125.43 (s, 1D).

2.4.2.6.d. Synthesis of K$_2$(μ-η^6,η^6-biphenyl-4-d_1)[U(NC[^{t}Bu]Mes)$_3$]$_2$ (K$_2$-3$_2$-μ-biphenyl-4-d_1)

The experimental procedure is similar to the one that leads to **K$_2$-3$_2$-μ-biphenyl**, 4-biphenyl-d_1 being used instead of non-deuterated biphenyl.

^{2}H NMR (46 MHz, Et$_2$O, 22 °C): δ = 34.31 (s, 1D), -5.53 (s, 1D).

2.4.2.7. Synthesis of Na$_2$(μ-η^6,η^6-biphenyl)[U(NC[^{t}Bu]Mes)$_3$]$_2$ (Na$_2$-3$_2$-μ-biphenyl)

Sodium (0.030 g, 1.30 mmol, 3.5 equiv) was added to a THF solution (6 mL) of biphenyl (0.172 g, 1.12 mmol, 3 equiv) in a vial protected from light (with electrical tape) and the resulting mixture was stirred at room temperature for 1 h, after which time the vial was placed in a cold well. Separately, a solution of **1-I-DME** (0.400 g, 0.38 mmol) in THF (10 mL) was frozen. The thawing Na / biphenyl mixture was added dropwise to the **1-I-DME** solution, including the piece of sodium. The new mixture was allowed to reach room temperature and stirred for 2 h, after which time the solution was decanted from sodium and was transferred to a filter flask. After removal of volatiles under reduced pressure, the solid obtained was extracted in pentane, the

extract filtered through Celite, and pentane removed. A new extraction in pentane and filtration through Celite led to a new filtrate (5 mL), which was placed in a refrigerator overnight. The next day, the solution was decanted from the solid obtained (biphenyl with traces of **Na$_2$-3$_2$-μ-biphenyl**) and the volatiles removed under reduced pressure. The solid obtained was extracted with pentane (3 mL) followed by diethyl ether, but the two filtrates were not combined at this stage. From the second filtrate, diethyl ether was removed and the solid obtained was extracted with pentane. At this point the two pentane fractions were combined, the solution concentrated and placed in a refrigerator. Compound **Na$_2$-3$_2$-μ-biphenyl** is obtained as a microcrystalline powder in 57% yield (0.204 g, 0.11 mmol) after one day. ^{1}H NMR (300 MHz, C$_6$D$_6$, 22 °C): δ = 15.07 (s, 1H, *bound p-biphenyl*); 8.28 (s, 12H, *m-Ar*); 3.68 (s, 18H, *p-Me*); 2.71 (s, 36H, *o-Me*); -2.97 (s, 54H, *^{t}Bu*); -3.67 (s, 1H, *unbound p-biphenyl*); -14.61 (s, 2H, *unbound o-biphenyl*); -53.94 (s, 2H, *unbound m-biphenyl*); -76.03 (s, 2H, *bound m-biphenyl*); -108.42 (s, 2H, *bound o-biphenyl*). Anal. calcd. for C$_{96}$H$_{130}$N$_6$U$_2$Na$_2$: C, 61.00; H, 6.93; N, 4.45. Found: C, 60.90; H, 7.56; N, 4.34.

2.4.2.8. Synthesis of K$_2$(μ-η^6,η^6-*trans*-stilbene)[U(NC[^{t}Bu]Mes)$_3$]$_2$ (K$_2$-3$_2$-μ-*trans*-stilbene)

Yield: 63% for the first crop (after 10 days, from pentane).

^{1}H NMR (500 MHz, C$_6$D$_6$, 22 °C): δ = 71.48 (s, *trans-stilbene*); 8.76 (s, 12H, *m-Ar*); 8.58 (s, 18H, *p-Me*); 4.12 (s, 36H, *o-Me*); -3.04 (s, 54H, *^{t}Bu*); -3.81 (s, *trans-stilbene*); -24.25 (s, *trans-stilbene*); -33.30 (s, *trans-stilbene*); -35.04 (s, *trans-stilbene*); -48.58 (s, *trans-stilbene*); -144.18 (s, *trans-stilbene*); -153.84 (s, *trans-stilbene*).

UV-vis (Et$_2$O, 22 °C): λ$_{max}$ (nm, ε × 10^{-2} M^{-1}, cm^{-1}) = 210 (2554.0 ± 305.6); 280 (648.4 ± 99.1); 290 (350.7 ± 14.8); 353 (153.0 ± 8.5); 610 (93.0 ± 10.0).

Anal. calcd. for C$_{98}$H$_{132}$N$_6$K$_2$U$_2$: C, 60.41; H, 6.83; N, 4.31. Found: C, 60.21; H, 6.56; N, 4.30.

2.4.2.9.a. Synthesis of K$_2$(μ-η^6,η^6-p-terphenyl)[U(NC[^{t}Bu]Mes)$_3$]$_2$ (K$_2$-3$_2$-μ-p-terphenyl)

Yield: 67% for the first crop (after 7 days, from pentane).

^{1}H NMR (500 MHz, toluene-d_8, 22 °C): δ = 31.74 (s, $\nu_{1/2}$ = 93 MHz, 1H, *p-bound-p-terphenyl*); 8.22 (s, 12H, *m-Ar*); 7.56 (m, 2H, *unbound-p-terphenyl*); 5.43 (m, 1H, *p-unbound-p-terphenyl*); 3.76 (s, 18H, *p-Me*); 3.38 (m, 2H, *unbound-p-terphenyl*); 2.88 (s, 36H, *o-Me*); 2.23 (m, 2H, *unbound-p-terphenyl*); -2.36 (s, 54H, *^{t}Bu*); -17.71 (s, $\nu_{1/2}$ = 20 MHz, 2H, *unbound-p-terphenyl*); -49.79 (s, $\nu_{1/2}$ = 61 MHz, 2H, *bound-p-terphenyl*); -123.53 (s, $\nu_{1/2}$ = 76 MHz, 2H, *bound-p-terphenyl*).

UV-vis (Et$_2$O, 22 °C): λ_{max} (nm, ε × 10^{-2} M^{-1}, cm^{-1}) = 214 (2646.8 ± 136.0); 246 (1032.0 ± 142.1); 273 (820.9 ± 76.7); 494 (103.9 ± 10.0).

Anal. calcd. for C$_{102}$H$_{134}$N$_6$K$_2$U$_2$: C, 61.30; H, 6.76; N, 4.21. Found: C, 61.51; H, 6.48; N, 4.12.

2.4.2.9.b. Synthesis of K$_2$(μ-η^6,η^6-p-terphenyl-d_{14})[U(NC[^{t}Bu]Mes)$_3$]$_2$ (K$_2$-3$_2$-μ-p-terphenyl-d_{14})

The experimental procedure is similar to the one that leads to **K$_2$-3$_2$-μ-p-terphenyl**, *p*-terphenyl-d_{14} being used instead of non-deuterated *p*-terphenyl.

^{2}H NMR (76 MHz, toluene, 22 °C): δ = 22.28 (s, 1D); 8.16 (s, 2D); 6.00 (s, 1D); 3.84 (s, 2D); 2.89 (s, 2D); -17.84 (s, 2D); -49.76 (s, 2D); -123.71 (s, 2D).

2.4.2.10.a. Synthesis of K(μ-η^6,η^6-C$_{10}$H$_8$)[U(NC[^{t}Bu]Mes)$_3$]$_2$ (K-3$_2$-μ-naphthalene)

Note: The following synthesis was used for all **K-3$_2$-μ-arene** (arene = naphthalene, biphenyl, *trans*-stilbene, *p*-terphenyl) compounds. Only isolated yields and characterization data are presented separately.

References begin on page 155

Compounds **3-I-DME** (0.492 g, 0.46 mmol) and naphthalene (0.030 g, 0.23 mmol, 0.5 equiv) were dissolved in DME (15 mL) and the solution frozen. Separately, KC_8 (0.125 g, 0.92 mmol, 2 equiv) was slurried in DME (12 mL) and the slurry was also frozen. The thawing KC_8 slurry was added dropwise to the thawing solution mentioned above. After the addition was completed, the reaction mixture was stirred for 20 min and then filtered through Celite. After the solvent was removed, the dark brown solid was extracted with pentane (ca. 100 mL), the new solution filtered through Celite and the solvent removed completely. The solid obtained was slurried in a 2:1 mixture of pentane and diethyl ether (total of 10 mL), transferred to a vial and stored in a −35 °C refrigerator for one day. After decanting the solution and drying the solid obtained, a first crop of 0.251 g (0.13 mmol, 56% yield) was obtained.

^{1}H NMR (300 MHz, C_6D_6, 22 °C): δ = 20.22 (s, 6H, *m'-Ar*); 9.34 (s, 6H, *p'-Me*); 8.93 (s, 8H, *m-Ar*); 4.49 (s, 12H, *o'-Me* or *p-Me*); 3.65 (s, 12H, *o'-Me* or *p-Me*); 1.29 (s, 36H, *t-Bu*); -0.14 (s, 18H, *t-Bu'*); -1.19 (s, 2H, *unbound α-naphthalene*); -2.19 (s, 24H, *o-Me*); -37.96 (s, 2H, *unbound β-naphthalene*); -121.17 (s, 2H, *bound α-naphthalene*); -124.53 (s, 2H, *bound β-naphthalene*). (*Note:* Because of the two ligand environments (2:1), with " ' " is designated the latter ligand.)

UV-vis (toluene, 22 °C): λ_{max} (nm, $\varepsilon \times 10^{-2}$ M^{-1}, cm^{-1}) = 282 (376.7 ± 28.4); 388 (134.9 ± 12.1); 632 (47.5 ± 7.4).

Anal. calcd. for $C_{94}H_{128}N_6KU_2$: C, 60.79; H, 6.95; N, 4.53. Found: C, 60.70; H, 6.86; N, 4.70.

2.4.2.10.b. Synthesis of $K(\mu\text{-}\eta^6,\eta^6\text{-}C_{10}D_8)[U(NC[^tBu]Mes)_3]_2$ ($K\text{-}3_2\text{-}\mu\text{-}C_{10}D_8$)

The experimental procedure is similar to the one that leads to **K-3$_2$-μ-C$_{10}$H$_8$**, naphthalene-d_8 being used instead of non-deuterated naphthalene.

^{2}H NMR (46 MHz, Et_2O, 22 °C): δ = -0.46 (s, 1D); -38.97 (s, 1D); -117.73 (s, 1D); -126.53 (s, 1D).

2.4.2.10.c. Synthesis of K(μ-η^6,η^6-C$_{10}$H$_7$D)[U(NC['Bu]Mes)$_3$]$_2$ (K-3$_2$-μ-C$_{10}$H$_7$D)

The experimental procedure is similar to the one that leads to **K-3$_2$-μ-C$_{10}$H$_8$**, α-naphthalene-d_1 being used instead of non-deuterated naphthalene.

^{2}H NMR (46 MHz, Et$_2$O, 22 °C): δ = -0.42 (s, 1D); -117.49 (s, 1D).

2.4.2.11.a. Synthesis of K(μ-η^6,η^6-biphenyl)[U(NC['Bu]Mes)$_3$]$_2$ (K-3$_2$-μ-biphenyl)

Yield: 42% for the first crop (after 3 days, from pentane/Et$_2$O).

^{1}H NMR (300 MHz, C$_6$D$_6$, 22 °C): δ = 16.86 (s, 6H, *unbound m-biphenyl* and *m'-Ar*); 8.96 (s, 8H, *m-Ar*); 7.95 (s, 6H, *p'-Me*); 4.50 (s, 12H, *o'-Me* or *p-Me*); 3.91 (s, 12H, *o'-Me* or *p-Me*); 1.02 (s, 36H, *t-Bu*); 0.02 (s, 18H, *t-Bu'*); -2.17 (s, 24H, *o-Me*); -9.19 (s, 2H, *unbound o-biphenyl*); -14.18 (s, 1H, *unbound p-biphenyl*); -83.57 (s, 1H, *bound p-biphenyl*); -140.72 (s, 2H, *bound m-biphenyl*); -163.87 (s, 2H, *bound o-biphenyl*).

UV-vis (toluene, 22 °C): λ$_{max}$ (nm, ε × 10^{-2} M^{-1}, cm^{-1}) = 285 (354.8 ± 23.3); 431 (188.4 ± 17.9); 647 (45.2 ± 4.1).

Anal. calcd. for C$_{96}$H$_{130}$N$_6$KU$_2$: C, 61.22; H, 6.96; N, 4.46. Found: C, 60.74; H, 6.48; N, 3.94.

2.4.2.11.b. Synthesis of K(μ-η^6,η^6-biphenyl-d_{10})[U(NC['Bu]Mes)$_3$]$_2$ (K-3$_2$-μ-biphenyl-d_{10})

The experimental procedure is similar to the one that leads to **K-3$_2$-μ-biphenyl**, biphenyl-d_{10} being used instead of non-deuterated biphenyl.

^{2}H NMR (46 MHz, Et$_2$O, 22 °C): δ = 17.02 (s, 2D), -9.14 (s, 2D); -13.87 (s, 1D); -83.62 (s, 1D); -141.20 (s, 2D); -164.92 (s, 2D).

2.4.2.11.c. Synthesis of K(μ-η^6,η^6-biphenyl-2-d_1)[U(NC[^{t}Bu]Mes)$_3$]$_2$ (K-3$_2$-μ-biphenyl-2-d_1)

The experimental procedure is similar to the one that leads to **K-3$_2$-μ-biphenyl**, 2-biphenyl-d_1 being used instead of non-deuterated biphenyl.

^{2}H NMR (46 MHz, Et$_2$O, 22 °C): δ = -9.20 (s, 1D), -164.46 (s, 1D).

2.4.2.11.d. Synthesis of K(μ-η^6,η^6-biphenyl-4-d_1)[U(NC[^{t}Bu]Mes)$_3$]$_2$ (K-3$_2$-μ-biphenyl-4-d_1)

The experimental procedure is similar to the one that leads to **K-3$_2$-μ-biphenyl**, 4-biphenyl-d_1 being used instead of non-deuterated biphenyl.

^{2}H NMR (46 MHz, Et$_2$O, 22 °C): δ = -14.02 (s, 1D), -82.99 (s, 1D).

2.4.2.12. Synthesis of K(μ-η^6,η^6-*trans*-stilbene)[U(NC[^{t}Bu]Mes)$_3$]$_2$ (K-3$_2$-μ-*trans*-stilbene)

Yield: 83% for the first crop (after one day, from pentane).

^{1}H NMR (500 MHz, C$_6$D$_6$, 22 °C): δ = 16.64 (s, 4H, *m'-Ar*); 16.08 (s, *trans-stilbene*); 9.47 (s, 6H, *p'-Me*); 8.01 (s, 8H, *m-Ar*); 4.81 (s, 12H, *o'-Me* or *p-Me*); 4.10 (s, 12H, *o'-Me* or *p-Me*); 0.63 (s, 36H, *t-Bu*); -0.44 (s, 18H, *t-Bu'*); -2.11 (s, 24H, *o-Me*); -46.02 (s, *trans-stilbene*); -71.89 (s, *trans-stilbene*).

UV-vis (Et$_2$O, 22 °C): λ_{max} (nm, $\varepsilon \times 10^{-2}$ M^{-1}, cm^{-1}) = 215 (2118.9 $\pm$ 103.3); 282 (532.9 $\pm$ 56.2); 382 (150.3 $\pm$ 5.4); 568 (97.3 $\pm$ 4.7).

Anal. calcd. for C$_{98}$H$_{132}$N$_6$KU$_2$: C, 61.65; H, 6.97; N, 4.40. Found: C, 61.68; H, 6.81; N, 4.40.

2.4.2.13.a. Synthesis of K(μ-η^6,η^6-p-terphenyl)[U(NC[^{t}Bu]Mes)$_3$]$_2$ (K-3$_2$-μ-p-terphenyl)

Yield: 69% for the first crop (after 1 day, from pentane).

^{1}H NMR (500 MHz, toluene-d_8, 22 °C): δ = 18.11 (s, 2H, *unbound p*-terphenyl); 11.32 (m, 2H, *unbound p*-terphenyl); 8.88 (s, 8H, *m-Ar*); 7.97 (s, 6H, *p'-Me*); 7.51 (m, 1H, *p-unbound p-*terphenyl); 4.39 (s, 12H, *o'-Me* or *p-Me*); 3.95 (s, 12H, *o'-Me* or *p-Me*); 0.89 (s, 36H, *t-Bu*); -0.12 (s, 18H, *t-Bu'*); -1.75 (s, 24H, *o-Me*); -7.35 (s, 2H, *unbound p*-terphenyl); -81.17 (s, $v_{1/2}$ = 106 Hz, 1H, *p-bound p*-terphenyl); -142.44 (s, $v_{1/2}$ = 78 Hz, 2H, *m* or *o-bound p*-terphenyl); -163.31 (s, $v_{1/2}$ = 156 Hz, 2H, *m* or *o-bound p*-terphenyl).

UV-vis (toluene, 22 °C): λ_{max} (nm, $\varepsilon \times 10^{-2}$ M^{-1}, cm^{-1}) = 285 (552.9 ± 27.2); 447 (199.1 ± 7.8); 517 (174.2 ± 7.8).

Anal. calcd. for $C_{102}H_{134}N_6KU_2$: C, 62.52; H, 6.89; N, 4.29. Found: C, 62.57; H, 6.90; N, 4.06.

2.4.2.13.b. Synthesis of K(μ-η^6,η^6-p-terphenyl-d_{14})[U(NC[^{t}Bu]Mes)$_3$]$_2$ (K-3$_2$-μ-p-terphenyl-d_{14})

The experimental procedure is similar to the one that leads to **K-3$_2$-μ-p-terphenyl**, *p*-terphenyl-d_{14} being used instead of non-deuterated *p*-terphenyl.

^{2}H NMR (76 MHz, toluene, 22 °C): δ = 18.87 (s, 2D), 12.17 (s, 2D), 8.45 (s, 1D), 6.83(s, 2D), -5.84 (s, 2D), -88.13 (s, 1D); -145.85 (s, 2D); -162.39 (s, 2D).

2.4.2.14.a. Oxidation of K$_2$-1$_2$-μ-arene to K-1$_2$-μ-arene using Fc[OTf]

Note: Only the oxidation of K$_2$-**1$_2$**-μ-*trans*-stilbene to K-**1$_2$**-μ-*trans*-stilbene is described in detail, the reactions for the other three K$_2$-**1$_2$**-μ-arene (arene = naphthalene, biphenyl, *p*-terphenyl) compounds being similar.

References begin on page 155

Solutions of K_2-1_2-μ-*trans*-stilbene (0.253 g, 0.13 mmol) and Fc[OTf] (0.044 g, 0.13 mmol, 1 equiv) in diethyl ether were frozen. The thawing K_2-1_2-μ-*trans*-stilbene solution was added dropwise to the thawing Fc[OTf] solution, the reaction mixture was allowed to reach room temperature, and stirred for 1 h. After that time, the mixture was filtered through Celite and volatiles were removed. The solid obtained was extracted in pentane, the solution obtained was filtered through Celite again, concentrated and placed in a –35 °C refrigerator. After 8 days, K-1_2-μ-*trans*-stilbene was obtained as a microcrystalline solid (0.200 g, 0.10 mmol) in 81% yield.

2.4.2.14.b. Oxidation of K_2-1_2-μ-arene to K-1_2-μ-arene using P_4

Note: Only the oxidation of K_2-1_2-μ-*trans*-stilbene to K-1_2-μ-*trans*-stilbene is described in detail, the reactions for the other three K_2-1_2-μ-arene (arene = naphthalene, biphenyl, *p*-terphenyl) compounds being similar.

Solutions of K_2-1_2-μ-*trans*-stilbene (0.109 g, 0.06 mmol) and P_4 (0.009 g, 0.07 mmol, 1.3 equiv) in diethyl ether were frozen. The thawing K_2-1_2-μ-*trans*-stilbene solution was added dropwise to the thawing P_4 slurry, the reaction mixture was allowed to reach room temperature, and stirred for 0.5 h. After that time, the mixture was filtered through Celite and volatiles were removed. The solid obtained was extracted in pentane, the solution obtained was filtered through Celite again, concentrated and placed in a –35 °C refrigerator. After 5 days, K-1_2-μ-*trans*-stilbene was obtained as a microcrystalline solid (0.074 g, 0.10 mmol) in 69% yield.

2.4.2.15. Reduction of K-1_2-μ-arene to K_2-1_2-μ-arene using K/anthracene

Note: Only the reduction of K-1_2-μ-*trans*-stilbene to K_2-1_2-μ-*trans*-stilbene is described in detail, the reactions for the other three K-1_2-μ-arene (arene = naphthalene, biphenyl, *p*-terphenyl) compounds being similar.

Potassium (0.100 g, 2.6 mmol, 5.2 equiv) was added to a THF solution (3 mL) of anthracene (0.010 g, 0.05 mmol, 1 equiv) in a vial protected from light (with electrical tape) and the resulting mixture was stirred at room temperature for 1 h, after which time the vial was placed in a cold well. Separately, a solution of K-1_2-μ-*trans*-stilbene (0.091 g, 0.05 mmol) in THF (2 mL) was frozen. The thawing K/anthracene mixture was added dropwise to the K-1_2-μ-*trans*-stilbene solution, the excess of potassium being left behind. The new mixture was allowed to reach room temperature and stirred for 1 h, after which time the solution was transferred to a filter flask. After removal of volatiles under reduced pressure, the solid obtained was extracted in pentane, the extract filtered through Celite, and pentane removed. A new extraction in pentane and filtration through Celite led to a new filtrate (5 mL), which was concentrated and placed in a refrigerator overnight. Compound K_2-1_2-μ-*trans*-stilbene is obtained as a microcrystalline powder in 78% yield (0.073 g, 0.04 mmol) after several days.

2.4.2.16.a. Synthesis of $K_2I(\mu-\eta^6,\eta^6$-toluene)$[U(NC[^tBu]Mes)_3]_2$ (K_2I-3_2-μ-toluene)

A solution of **3-I-DME** (2.075 g, 1.95 mmol, 60 mL) and a slurry of KC_8 (0.527 g, 3.90 mmol, 2 equiv, 100 mL) in toluene were frozen. To the thawing **3-I-DME** solution was added dropwise the KC_8 slurry, the reaction mixture was stirred for 2 h at room temperature, and then filtered through Celite. The solvent from the filtrate was removed and the solid extracted in diethyl ether (100 mL).The last operations were repeated and the solution was concentrated (10 mL) and then placed in a refrigerator for several days. **K_2I-3_2-μ-toluene** was obtained as a dark orange brown microcrystalline solid (0.852 g, 0.43 mmol, 44% yield).

^{1}H NMR (300 MHz, C_6D_6, 22 °C): δ = 34.70 (s, 3H, toluene-CH_3); 6.98 (s, 12H, *m-Ar*); 2.53 (s, 18H, *p-Me*); 1.63 (s, 54H, ^tBu); 1.50 (s, 36H, *o-Me*); -38.01 (s, 2H, *o* or *m*-toluene); 43.05 (s, 1H, *p*-toluene); -44.63 (s, 2H, *o* or *m*-toluene).

UV-vis (Et_2O, 22 °C): λ_{max} (nm, ε × 10^{-2} M^{-1}, cm^{-1}) = 214 (2099.2 ± 255.7); 267 (593.3 ± 108.6); 432 (120.5 ± 10.5); 541 (80.7 ± 8.1).

Anal. calcd. for $C_{84}H_{120}N_6U_2K_2I$: C, 55.03; H, 6.45; N, 4.23. Found: C, 54.45; H, 5.85; N, 3.92.

2.4.2.16.b. Synthesis of $K_2I(\mu\text{-}\eta^6,\eta^6\text{-toluene-}d_8)[U(NC[^tBu]Mes)_3]_2$ ($K_2I\text{-}3_2\text{-}\mu\text{-toluene-}d_8$)

A solution of **3-I-DME** (0.090 g, 0.08 mmol, 8 mL) and a slurry of KC_8 (0.023 g, 0.17 mmol, 2 equiv) in 4 mL of C_7D_8, respectively, were frozen. To the thawing **3-I-DME** solution was added dropwise the thawing KC_8 slurry. The reaction mixture was stirred for 20 min after which it was filtered through Celite and volatiles removed under reduced pressure. After extraction with pentane the solution (20 mL) was concentrated to 3 mL and cooled to -35 °C. The crystals (0.018 g, 0.009 mmol, 11% yield) obtained were used to prepare the NMR sample.

^{2}H NMR (76 MHz, pentane, 22 °C): δ = 34.42 (s, 3D, CD_3-toluene); -37.76 (s, 2D, o or m-toluene); -42.73 (s, 1D, p-toluene); -44.43 (s, 2D, o or m-toluene).

2.4.2.16.c. Synthesis of $K_2I(\mu\text{-}\eta^6,\eta^6\text{-benzene})[U(NC[^tBu]Mes)_3]_2$ ($K_2I\text{-}3_2\text{-}\mu\text{-benzene}$)

A solution of **3-I-DME** (0.090 g, 0.08 mmol, 8 mL) and a slurry of KC_8 (0.023 g, 0.17 mmol, 2 equiv) in 4 mL of C_6H_6, respectively, were frozen. To the thawing **3-I-DME** solution was added dropwise the thawing KC_8 slurry. The reaction mixture was stirred for 20 min after which it was filtered through Celite and volatiles removed under reduced pressure. After extraction with pentane the solution (20 mL) was concentrated to 3 mL and cooled to -35 °C. The crystals (0.018 g, 0.009 mmol, 11% yield) obtained were used to prepare the NMR sample.

^{1}H NMR (300 MHz, C_6D_6, 22 °C): δ = 6.97 (s, 2H, m-Ar); 2.57 (s, 3H, p-Me); 1.87 (s, 9H, ^tBu); 1.36 (s, 6H, o-Me); -44.91 (s, 1H, C_6H_6).

2.4.2.17.a. Synthesis of K(DME)(μ-η^6,η^6-toluene)[U(NC[^{t}Bu]Mes)$_3$]$_2$ (K(DME)-3$_2$-μ-toluene)

Complex **3-I-DME** (0.163 g, 0.15 mmol) and toluene (3 drops, ca. 0.030 g, 0.33 mmol, 2.2 equiv) were dissolved in DME (5 mL) and the solution frozen. Separately, KC$_8$ (0.062 g, 0.46 mmol, 3 equiv) was slurried in DME (3 mL) and the slurry was also frozen. The thawing KC$_8$ slurry was added dropwise to the thawing solution mentioned above. After the addition was completed, the reaction mixture was stirred for 20 min and then filtered through Celite. After the solvent was removed, the dark brown solid was extracted with pentane (ca. 15 mL), the new solution filtered through Celite and the solvent removed completely. The solid obtained was extracted in pentane (10 mL), the solution filtered through Celite, concentrated to 3 mL, and stored in a –35 °C refrigerator for several days. After decanting the solution and drying the solid obtained, a first crop of 0.061 g (0.03 mmol, 41% yield) was obtained.

^{1}H NMR (500 MHz, toluene-d_8, 22 °C): δ = 8.61 (s, 12H, *m-Ar*); 4.15 (s, 18H, *p-Me*); 3.36 (s, 4H, C*H$_2$*-DME); 3.15 (s, 6H, C*H$_3$*-DME); 1.22 (s, 36H, *o-Me*); -1.20 (s, 54H, ^{t}*Bu*).

UV-vis (Et$_2$O, 22 °C): λ_{max} (nm, $\varepsilon \times 10^{-2}$ M^{-1}, cm^{-1}) = 214 (2099.2 ± 255.7); 267 (593.3 ± 108.6); 432 (120.5 ± 10.5); 541 (80.7 ± 8.1).

Anal. calcd. for C$_{95}$H$_{138}$N$_6$U$_2$O$_2$K: C, 59.70; H, 7.28; N, 4.40. Found: C, 60.10; H, 7.17; N, 4.59.

2.4.2.17.b. Synthesis of K(DME)(μ-η^6,η^6-toluene-d_8)[U(NC[^{t}Bu]Mes)$_3$]$_2$ (K(DME)-3$_2$-μ-toluene-d_8)

A solution of **3-I-DME** (0.090 g, 0.08 mmol, 8 mL) and a slurry of KC$_8$ (0.023 g, 0.17 mmol, 2 equiv) in 4 mL of C$_7$D$_8$, respectively, were frozen. To the thawing **3-I-DME** solution was added dropwise the thawing KC$_8$ slurry. The reaction mixture was stirred for 20 min after which it was filtered through Celite and volatiles removed under reduced pressure. After extraction with

pentane the solution (20 mL) was concentrated to 3 mL and cooled to -35 °C. The crystals (0.018 g, 0.009 mmol, 11% yield) obtained were used to prepare the NMR sample.

^{2}H NMR (76 MHz, pentane, 22 °C): δ = 34.42 (s, 3D, CD_3-toluene); -37.76 (s, 2D, *o* or *m*-toluene); -42.73 (s, 1D, *p*-toluene); -44.43 (s, 2D, *o* or *m*-toluene).

2.4.2.17.c. Synthesis of K(DME)(μ-η^6,η^6-benzene)[U(NC['Bu]Mes)$_3$]$_2$ (K(DME)-3$_2$-μ-benzene)

A solution of **3-I-DME** (0.090 g, 0.08 mmol, 8 mL) and a slurry of KC$_8$ (0.023 g, 0.17 mmol, 2 equiv) in 4 mL of C$_6$H$_6$, respectively, were frozen. To the thawing **3-I-DME** solution was added dropwise the thawing KC$_8$ slurry. The reaction mixture was stirred for 20 min after which it was filtered through Celite and volatiles removed under reduced pressure. After extraction with pentane the solution (20 mL) was concentrated to 3 mL and cooled to -35 °C. The crystals (0.018 g, 0.009 mmol, 11% yield) obtained were used to prepare the NMR sample.

^{1}H NMR (300 MHz, C$_6$D$_6$, 22 °C): δ = 6.97 (s, 2H, *m-Ar*); 2.57 (s, 3H, *p-Me*); 1.87 (s, 9H, *'Bu*); 1.36 (s, 6H, *o-Me*); -44.91 (s, 1H, C$_6$$H_6$).

2.4.2.18.a. Reaction of K$_2$(μ-η^6,η^6-C$_{10}$H$_8$)[U(NC['Bu]Mes)$_3$]$_2$ (K$_2$-3$_2$-μ-C$_{10}$H$_8$) with 1,3,5,7-cyclooctatetraene*

Compound **K$_2$-3$_2$-μ-C$_{10}$H$_8$** (0.222 g, 0.12 mmol) was dissolved in diethyl ether (10 mL) and the solution frozen. To this thawing solution was added dropwise a thawing solution of 1,3,5,7-cyclooctatetraene (0.025 g, 0.24 mmol, 2 equiv) in Et$_2$O (10 mL). The reaction mixture was stirred for 1h and then the solvent was removed. The solid obtained was extracted in Et$_2$O (10

---

* Similar procedures were followed for the reactions between the other **K$_2$-3$_2$-μ-arene** and **K-3$_2$-μ-arene** (arene = naphthalene, biphenyl, *trans*-stilbene, and *p*-terphenyl).

mL) and the solution was filtered through Celite. From the filtrate the solvent was removed, the solid obtained was extracted again in Et_2O (10 mL) and the solution was filtered through Celite. The volume of the filtrate was reduced to *ca.* 3 mL and the solution was stored at -35 °C for a couple of days. The solid obtained amounted to 0.140 g (0.07 mmol, 62% yield) in two crops. Compound 3_2-μ-COT forms in negligible quantity as indicated by ^1H NMR spectroscopy.

^1H NMR (500 MHz, C_6D_6, 22 °C): The spectrum indicates that the three ligands are not equivalent in these conditions. From the number of peaks (9, 8 for the ligand protons and 1 for COT protons) it can be suggested that there are two ligand environments, but the complete assignment of the peaks could not be conclusively established. δ = 27.68 (s, 6H, *p-Me* or *o-Me'*); 20.50 (s), 16.02 (s), 11.62 (s): the values of the integrals are similar (2-4H) - *p-Me'*, *m-Ar'* or *m-Ar*; -3.92 (s, 12H, *o-Me*); -9.56 (s, 9H, *$^tBu'$*); -11.12 (s, 6H, *p-Me* or *o-Me'*); -11.62 (s, 18H, *^tBu*); -30.15 (s, 8H, *COT*). The peak at -30.15 ppm was assigned to the COT protons because of a similar peak displayed by **Na-3-COT** (*vide infra*).

Anal. calcd. for $C_{50}H_{68}N_3KU$: C, 62.16; H, 7.04; N, 4.44. Found: C, 61.86; H, 7.10; N, 4.39.

2.4.2.18.b. Reaction of $Na_2(μ-η^6,η^6-C_{10}H_8)[U(NC[^tBu]Mes)_3]_2$ (Na_2-3_2-μ-$C_{10}H_8$) with 1,3,5,7-cyclooctatetraene

The reaction is similar to the one reported in section 2.3.2.14.a., but the yield for the isolated **Na-3-COT** is never higher than 40%. The X-ray crystal structure shows that there is a molecule of diethyl ether coordinated to the sodium center, but extensive drying of the crystals leads to a solvent free compound.

^1H NMR (500 MHz, C_6D_6, 22 °C): δ = 8.42 (s, 6H, *m-Ar*); 4.31 (s, 9H, *p-Me*); -0.83 (s, 18H, *o-Me*); -7.60 (s, 27H, *^tBu*); -24.78 (s, 4H, *COT*).

Anal. calcd. for $C_{50}H_{68}N_3NaU$: C, 63.21; H, 7.21; N, 4.42. Found: C, 62.82; H, 7.33; N, 4.06.

2.4.2.19. Synthesis of (μ-η^8,η^8-C$_8$H$_8$)[U(NC[^{t}Bu]Mes)$_3$]$_2$ (3$_2$-μ-COT)

Solutions of **K-3-COT** (0.067 g, 0.07 mmol) and **3-I-DME** (0.073 g, 0.07 mmol, 1 equiv) in diethyl ether (3 mL each) were frozen. To the thawing **3-I-DME** solution was added dropwise the **K-3-COT** solution and the reaction mixture was stirred for 1 h at room temperature. After that time, the solvent was removed and the solid extracted in pentane (10 mL). The solution was concentrated and then placed in a refrigerator for several days. **3$_2$-μ-COT** was obtained as a dark brown microcrystalline solid (0.057 g, 92% yield). Similarly, **3$_2$-μ-COT** was obtained from **Na-3-COT**.

^{1}H NMR (500 MHz, C$_6$D$_6$, 22 °C): δ = 6.61 (s, 6H, *m-Ar*); 2.96 (s, 9H, *p-Me*); 1.82 (s, 27H, *^{t}Bu*); -1.05 (s, 18H, *o-Me*); -39.19 (s, 4H, *COT*).

Anal. calcd. for C$_{92}$H$_{128}$N$_6$U$_2$: C, 61.59; H, 7.19; N, 4.68. Found: C, 61.65; H, 6.75; N, 4.88.

2.4.2.20. Synthesis of (η^8-C$_8$H$_8$)U(NC[^{t}Bu]Mes)$_3$ (3-COT)

Solutions of **K-3-COT** (0.063 g, 0.06 mmol) and TiCl$_4$(THF)$_2$ (0.022 g, 0.06 mmol, 1 equiv) in diethyl ether (3 mL each) were frozen. To the thawing TiCl$_4$(THF)$_2$ solution was added dropwise the **K-3-COT** solution, the reaction mixture was stirred for 3 h at room temperature, and then filtered through Celite. The solvent from the filtrate was removed and the solid extracted in pentane (5 mL) and the rest in diethyl ether. The solution was concentrated and then placed in a refrigerator for several days. **3-μ-COT** was obtained as an orange brown microcrystalline solid (0.035 g, 58% yield, 0.03 mmol).

^{1}H NMR (500 MHz, C$_6$D$_6$, 22 °C): δ = 7.35 (s, 6H, *m-Ar*); 3.13 (s, 27H, *^{t}Bu*); 2.70 (s, 9H, *p-Me*); 1.53 (s, 18H, *o-Me*); -14.84 (s, 4H, *COT*).

Anal. calcd. for C$_{50}$H$_{68}$N$_3$U: C, 63.28; H, 7.22; N, 4.43. Found: C, 62.96; H, 7.22; N, 4.31.

2.4.2.21. Reaction of $Na_2(\mu-\eta^6,\eta^6\text{-naphthalene})[U(NC[^tBu]Mes)_3]_2$ ($Na_2\text{-}3_2\text{-}\mu\text{-naphthalene}$) with PhSSPh

Solutions of $Na_2\text{-}3_2\text{-}\mu\text{-naphthalene}$ (0.232 g, 0.12 mmol) and PhSSPh (0.054 g, 0.25 mmol, 2 equiv) in diethyl ether (6 mL each) were frozen. To the thawing $Na_2\text{-}3_2\text{-}\mu\text{-naphthalene}$ solution was added dropwise the PhSSPh solution and the reaction mixture was stirred for 1 h at room temperature. After that time, the solvent was removed and the solid extracted in pentane (10 mL). The solution was concentrated and then placed in a refrigerator for several days. $Na\text{-}3_2\text{-}(\mu\text{-SPh})_3$ was obtained as a dark brown microcrystalline solid (0.225 g, 0.10 mmol, 83% yield). Similarly, $K\text{-}3_2\text{-}(\mu\text{-SPh})_3$ was obtained from $K_2\text{-}3_2\text{-}\mu\text{-naphthalene}$.

^{1}H NMR (500 MHz, C$_6$D$_6$, 60 °C): δ = 8.80 (s, 2H, *o* or *m*-PhS); 8.62 (s, 2H, *o* or *m*-PhS); 7.80 (s, 4H, *m-Ar*); 6.65 (s, 1H, *p*-PhS); 3.97 (s, 6H, *p-Me*); 0.34 (s, 18H, *'Bu*); -1.51 (s, 12H, *o-Me*). Anal. calcd. for C$_{102}$H$_{135}$N$_6$U$_2$NaS$_3$: C, 60.06; H, 6.62; N, 4.12. Found: C, 60.65; H, 6.80; N, 4.01. Anal. calcd. for C$_{102}$H$_{135}$N$_6$U$_2$KS$_3$: C, 59.65; H, 6.57; N, 4.09. Found: C, 59.24; H, 6.25; N, 3.91.

2.4.2.22.a. Reaction of $K_2I(\mu-\eta^6,\eta^6\text{-toluene})[U(NC[^tBu]Mes)_3]_2$ ($K_2I\text{-}3_2\text{-}\mu\text{-toluene}$) with PhNNPh

Solutions of $K_2I\text{-}3_2\text{-}\mu\text{-toluene}$ (0.300 g, 0.15 mmol) and PhNNPh (0.055 g, 0.30 mmol, 2 equiv) in diethyl ether (6 mL each) were frozen. To the thawing $K_2I\text{-}3_2\text{-}\mu\text{-toluene}$ solution was added dropwise the PhNNPh solution and the reaction mixture was stirred for 1 h at room temperature. After that time, the solvent was removed and the solid extracted in pentane (10 mL). The solution was concentrated and then placed in a refrigerator for several days. $3_2\text{-}(\mu\text{-NPh})_2$ was obtained as a dark brown microcrystalline solid (0.178 g, 0.09 mmol, 63% yield).

^{1}H NMR (500 MHz, C$_6$D$_6$, 60 °C): δ = 8.34 (m, 2H, *o* or *m*-PhN); 6.80 (s, 6H, *m-Ar*); 2.52 (s, 6H, *o-Me*); 2.27 (s, 9H, *o-Me*); 0.64 (s, 27H, *'Bu*); 0.57 (m, 1H, *p*-PhN); -5.22 (m, 2H, *o* or *m*-PhN).

Anal. calcd. for $C_{96}H_{130}N_8U_2$: C, 61.62; H, 6.95; N, 5.99. Found: C, 61.92; H, 7.36; N, 6.31.

2.4.2.22.b. Reaction of $K_2I(\mu\text{-}\eta^6,\eta^6\text{-toluene})[U(NC[^tBu]Mes)_3]_2$ ($K_2I\text{-}3_2\text{-}\mu\text{-toluene}$) with PhNNPh-$d_{10}$

The experimental procedure is similar to the one that leads to $3_2\text{-}(\mu\text{-NPh})_2$, PhNNPh-$d_{10}$ being used instead of PhNNPh.

^2H NMR (76 MHz, Et_2O, 22 °C): $\delta = 8.20$ (s, 2D), 0.15 (s, 1D); -5.52 (s, 2D).

2.4.3. X-ray crystal structures

2.4.3.1. General considerations

The X-ray data collections were carried out on a Siemens Platform three-circle goniometer with a CCD detector using Mo-K_α radiation ($\lambda = 0.71073$ Å). The data were processed utilizing the program SAINT supplied by Siemens Industrial Automation, Inc. The structures were solved by direct methods (SHELXTL v5.03, Sheldrick, G. M., and Siemens Industrial Automation, Inc., 1995) in conjunction with standard difference Fourier techniques.

2.4.3.2. X-ray crystal structure of $IU(DME)(NC[^tBu]Mes)_3$ (3-I-DME)

Inside the glove box, crystals of **3-I-DME,** obtained from a saturated diethyl ether solution at – 35 °C were coated with Paratone N oil (an Exxon product) on a microscope slide. A dark green block of approximate dimensions $0.26 \times 0.25 \times 0.20$ mm^3 was selected and mounted with wax on a glass fiber. A total of 10956 reflections ($-6 \le h \le 9$, $-28 \le k \le 28$, $-13 \le l \le 12$) were

collected at 183(2) K in the θ range of 2.35 to 23.27 °, of which 7323 were unique (R_{int} = 0.0664). The structure was solved by direct methods (SHELXTL V5.10, G. M. Sheldrick and Siemens Industrial Automation, Inc., 1997) in conjunction with standard difference Fourier techniques. The ^{t}Bu group on C28 contains disordered atoms. C29 and C210 were modeled with occupancies over two sites (C29A and C29B, and, respectively, C21A and C21B). All non-hydrogen atoms were refined anisotropically, except for C21B wich was refined only isotropically. Hydrogen atoms were placed in calculated (d_{C-H} = 0.96 Å) positions, except for C29A, C29B, C21A and C21B for which no hydrogen atoms have been generated. The residual peak and hole electron density were 2.856 and –1.100 e·$Å^{-3}$, respectively and these values are in the normal range due to the large scattering effect of uranium centers. A semi-empirical absorption correction was applied based on pseudo-psi-scans with maximum and minimum transmission equal to 0.3441 and 0.1982, respectively. The least squares refinement converged normally with residuals of R_1 = 0.0580, wR_2 = 0.1673 based upon I > 2σ(I), and GOF = 1.084 (based on F^2). No extinction coefficient was applied to the refinement.

Crystal and refinement data: formula $C_{46}H_{61}N_3O_2IU$, space group $P2_1$, a = 8.957(3) Å, b = 26.048(8) Å, c = 11.715(4) Å, α = 90.0 °, β = 97.026(5) °, γ = 90.0 °, V = 2712.6(14) $Å^3$, Z = 2, μ = 3.592 mm^{-1}, D_{calc} = 1.289 g·cm^{-3}, $F(000)$ = 1038, R_1 (based on F) = 0.0612, and wR_2 (based on F^2) = 0.1705.

2.4.3.3. X-ray crystal structure of $K_2(\mu\text{-}\eta^6,\eta^6\text{-}C_{10}H_8)[U(NC[^tBu]Mes)_3]_2$ ($K_2\text{-}3_2\text{-}\mu\text{-}C_{10}H_8$)

Inside the glove box, crystals of $K_2\text{-}3_2\text{-}\mu\text{-}C_{10}H_8$, obtained from a saturated diethyl ether solution at –35 °C were coated with Paratone N oil (an Exxon product) on a microscope slide. A dark brown plate of approximate dimensions 0.25 × 0.08 × 0.07 mm^3 was selected and mounted with wax on a glass fiber. A total of 18164 reflections (-14 ≤ h ≤ 14, -32 ≤ k ≤ 6, -18 ≤ l ≤ 22) were collected at 183(2) K in the θ range of 2.12 to 23.29 °, of which 11181 were unique (R_{int} = 0.0608). The structure was solved by using the Patterson method (SHELXTL V5.10, G. M.

Sheldrick and Siemens Industrial Automation, Inc., 1997) in conjunction with standard difference Fourier techniques. The unit cell contains one molecule of diethyl ether as crystallization solvent. The carbon atoms of the solvent are disordered, but this disordered has not been modeled. Two dinuclear complexes form an association dimer due to the interaction between one of the potassium centers and C551. All non-hydrogen atoms were refined anisotropically, except for C2 which was refined only isotropically. Some hydrogen atoms were found in the electronic density map, but most of the hydrogen atoms were placed in calculated (d_{C-H} = 0.96 Å) positions. The residual peak and hole electron density were 1.248 and -1.175 e·Å^{-3}, respectively and these values are in the normal range due to the large scattering effect of uranium centers. A semi-empirical absorption correction was applied based on pseudo-psi-scans with maximum and minimum transmission equal to 0.7909 and 0.4735, respectively. The least squares refinement converged normally with residuals of R_1 = 0.0437, wR_2 = 0.1068 based upon I > 2σ(I), and GOF = 1.052 (based on F^2). No extinction coefficient was applied to the refinement.

Crystal and refinement data: formula $C_{98}H_{138}N_6K_2OU$, space group P2$_1$/n, a = 12.820(3) Å, b = 29.511(7) Å, c = 25.647(6) Å, α = 90.0 °, β = 99.737(4) °, γ = 90.0 °, V = 9564(4) Å^3, Z = 4, μ = 3.516 mm^{-1}, D_{calc} = 1.368 g·cm^{-3}, F(000) = 3992, R_1 (based on F) = 0.0648, and wR_2 (based on F^2) = 0.1211.

2.4.3.4. X-ray crystal structure of Na$_2$(Et$_2$O)(μ-η^6,η^6-biphenyl)[U(NC[^{t}Bu]Mes)$_3$]$_2$ (Na$_2$(Et$_2$O)-3$_2$-μ-biphenyl)

Inside the glove box, crystals of **Na$_2$(Et$_2$O)-3$_2$-μ-biphenyl**, obtained from a saturated diethyl ether solution, at -35 °C, were coated with Paratone N oil (an Exxon product) on a microscope slide. A dark reddish brown block of approximate dimensions 0.16 × 0.14 × 0.12 mm^3 was selected and mounted with wax on a glass fiber. A total of 19877 reflections ($-10 \le h \le 16$, $-17 \le k \le 18$, $-23 \le l \le 23$) were collected at 183(2) K in the θ range of 2.09 to 23.29 °, of which

13832 were unique (R_{int} = 0.0342). The structure was solved by Patterson methods (SHELXTL V5.10, G. M. Sheldrick and Siemens Industrial Automation, Inc., 1997) in conjunction with standard difference Fourier techniques. The unit cell contains one molecule of diethyl ether coordinated to one of the sodium ions and half of a molecule of diethyl ether as crystallization solvent. The distance (2.87 Å) between the other sodium ion and C251 of the crystallographically equivalent dinuclear indicates contact with that atom, fact that makes the structure to appear as a dimer of two dinuclear compounds. C19, C110, and C111 were disordered and the disorder modeled over two sites (50%, 45%, and 45%, respectively, one of each sites). All non-hydrogen atoms were refined anisotropically except for C11A and C11C, which were refined only isotropically. Some hydrogen atoms were found in the electronic density map. The other hydrogen atoms were placed in calculated (d_{C-H} = 0.96 Å) positions, except for the disordered carbon atoms, for which no hydrogen atoms were generated. The residual peak and hole electron density were 0.716 and −1.208 e·Å^{-3} and they are in the normal range to the large scattering effect of the uranium nucleus. A semi-empirical absorption correction was applied based on pseudo-psi-scans with maximum and minimum transmission equal to 0.6896 and 0.6166, respectively. The least squares refinement converged normally with residuals of R_1 = 0.0446, wR_2 = 0.0840 based upon I > 2σ(I), and GOF = 1.057 (based on F^2). No extinction coefficient was applied to the refinement.

Crystal and refinement data: formula $C_{102}H_{134}N_6U_2O_{1.5}Na_2$, space group P-1, a = 14.5096(12) Å, b = 16.5305(14) Å, c = 21.2217(18) Å, α = 77.0470(10) °, β = 88.598(2) °, γ = 82.4380(10) °, V = 4917.3(7) Å^3, Z = 2, μ = 3.346 mm^{-1}, D_{calc} = 1.344 g·cm^{-3}, F(000) = 2012, R_1 (based on F) = 0.0580, and wR_2 (based on F^2) = 0.0883.

2.4.3.5. X-ray crystal structure of $K_2(\mu\text{-}\eta^6,\eta^6\text{-}trans\text{-stilbene})[U(NC[^tBu]Mes)_3]_2$ (K_2-3_2-μ-$trans$-stilbene)

Inside the glove box, crystals of **K_2-3_2-μ-$trans$-stilbene,** obtained from a saturated diethyl ether solution, at −35 °C, were coated with Paratone N oil (an Exxon product) on a microscope slide.

A dark reddish brown block of approximate dimensions $0.30 \times 0.28 \times 0.19$ mm^3 was selected and mounted with wax on a glass fiber. A total of 20704 reflections ($-14 \leq h \leq 13$, $-22 \leq k \leq 21$, $-19 \leq l \leq 23$) were collected at 183(2) K in the θ range of 2.14 to 23.35 °, of which 14464 were unique (R_{int} = 0.0717). The structure was solved by direct methods (SHELXTL V5.10, G. M. Sheldrick and Siemens Industrial Automation, Inc., 1997) in conjunction with standard difference Fourier techniques. The unit cell contains one molecule of diethyl ether as crystallization solvent. The following carbon atoms: C29, C210, C211, C231, C251, C271, C39, C310, C311, C351, C371, C49, C410, and C411 were disordered and the disorder modeled over two sites with 50% occupancy each. All non-hydrogen atoms were refined anisotropically. Hydrogen atoms were placed in calculated (d_{C-H} = 0.96 Å) positions, except for the disordered carbon atoms and the solvent atoms, for which no hydrogen atoms were generated. The residual peak and hole electron density were 1.429 and -1.084 e·Å^{-3} and they are in the normal range to the large scattering effect of the uranium nucleus. A semi-empirical absorption correction was applied based on pseudo-psi-scans with maximum and minimum transmission equal to 0.5746 and 0.4395, respectively. The least squares refinement converged normally with residuals of R_1 = 0.0524, wR_2 = 0.1363 based upon I > 2σ(I), and GOF = 1.041 (based on F^2). No extinction coefficient was applied to the refinement.

Crystal and refinement data: formula $C_{102}H_{93}N_6U_2OK_2$, space group P-1, a = 12.716(2) Å, b = 20.127(3) Å, c = 21.269(4) Å, α = 80.677(3) °, β = 74.006(4) °, γ = 81.011(5) °, V = 5127.8(14) Å^3, Z = 2, μ = 3.279 mm^{-1}, D_{calc} = 1.278 g·cm^{-3}, $F(000)$ = 1954, R_1 (based on F) = 0.0693, and wR_2 (based on F^2) = 0.1471.

2.4.3.6. X-ray crystal structure of $K_2I(\mu\text{-}\eta^6,\eta^6\text{-}C_7H_8)[U(NC[^tBu]Mes)_3]_2$ ($K_2I\text{-}3_2\text{-}\mu\text{-toluene}$)

Inside the glove box, crystals of $K_2I\text{-}3_2\text{-}\mu\text{-toluene}$, obtained from a saturated pentane solution, at -35 °C, were coated with Paratone N oil (an Exxon product) on a microscope slide. A reddish brown block of approximate dimensions $0.39 \times 0.34 \times 0.28$ mm^3 was selected and mounted with

wax on a glass fiber. A total of 20544 reflections ($-15 \leq h \leq 16$, $-14 \leq k \leq 11$, $-26 \leq 1 \leq 29$) were collected at 183(2) K in the θ range of 2.50 to 23.27 °, of which 11151 were unique (R_{int} = 0.0348). The structure was solved by Patterson methods (SHELXTL V5.10, G. M. Sheldrick and Siemens Industrial Automation, Inc., 1997) in conjunction with standard difference Fourier techniques. All non-hydrogen atoms were refined anisotropically and hydrogen atoms were placed in calculated (d_{C-H} = 0.96 Å) positions. The residual peak and hole electron density were 1.309 and -0.906 e·Å^{-3}. A semi-empirical absorption correction was applied based on pseudo-psi-scans with maximum and minimum transmission equal to 0.3043 and 0.2021, respectively. The least squares refinement converged normally with residuals of R_1 = 0.0486, wR_2 = 0.1290 based upon I > 2σ(I), and GOF = 1.051 (based on F^2). No extinction coefficient was applied to the refinement.

Crystal and refinement data: formula $C_{91}H_{128}N_6U_2IK_2$, space group P2$_1$, a = 14.965(4) Å, b = 12.845(3) Å, c = 27.007(7) Å, α = 90.0 °, β = 96.342(4) °, γ = 90.0 °, V = 5160(2) Å^3, Z = 2, μ = 3.553 mm^{-1}, D_{calc} = 1.279 g·cm^{-3}, $F(000)$ = 1982, R_1 (based on F) = 0.0528, and wR_2 (based on F^2) = 0.1342.

2.4.3.7. X-ray crystal structure of K(DME)(μ-η^6,η^6-C$_7$H$_8$)[U(NC[^{t}Bu]Mes)$_3$]$_2$ (K(DME)-3$_2$-μ-toluene)

Inside the glove box, crystals of **K(DME)-3$_2$-μ-toluene,** obtained from a saturated diethyl ether solution, at -35 °C, were coated with Paratone N oil (an Exxon product) on a microscope slide. A dark brown block of approximate dimensions 0.27 × 0.13 × 0.02 mm^3 was selected and mounted with wax on a glass fiber. A total of 38721 reflections ($-19 \leq h \leq 17$, $-23 \leq k \leq 21$, $-16 \leq 1 \leq 29$) were collected at 183(2) K in the θ range of 1.93 to 23.28 °, of which 26710 were unique (R_{int} = 0.0746). The structure was solved by Patterson methods (SHELXTL V5.10, G. M. Sheldrick and Siemens Industrial Automation, Inc., 1997) in conjunction with standard difference Fourier techniques. The unit cell contains two independent molecules. All non-hydrogen atoms were refined anisotropically and hydrogen atoms were placed in calculated (d_{C-H}

= 0.96 Å) positions. Some carbon atoms of *t*-Bu groups and the DME atoms are slightly disordered, but this disorder has not been modeled. The residual peak and hole electron density were 1.825 and –1.580 e·Å^{-3} and they are in the normal range to the large scattering effect of the uranium nucleus. A semi-empirical absorption correction was applied based on pseudo-psi-scans with maximum and minimum transmission equal to 0.9330 and 0.4501, respectively. The least squares refinement converged normally with residuals of R_1 = 0.0522, wR_2 = 0.1249 based upon I > 2σ(I), and GOF = 0.985 (based on F^2). No extinction coefficient was applied to the refinement.

Crystal and refinement data: formula $C_{95}H_{138.5}N_6U_2KO_2$, space group P-1, a = 17.1223(9) Å, b = 21.3687(12) Å, c = 26.0973(14) Å, α = 86.9990(10) °, β = 89.4630(10) °, γ = 81.8410(10) °, V = 9438.9(9) Å^3, Z = 4, μ = 3.518 mm^{-1}, D_{calc} = 1.345 g·cm^{-3}, $F(000)$ = 3878, R_1 (based on F) = 0.0840, and wR_2 (based on F^2) = 0.1414.

2.4.3.8. X-ray crystal structure of $Na(Et_2O)(\eta^8-C_8H_8)[U(NC[^tBu]Mes)_3]$ (Na-3-COT)

Inside the glove box, crystals of **Na-3-COT**, obtained from a saturated diethyl ether solution at – 35 °C were coated with Paratone N oil (an Exxon product) on a microscope slide. A dark brown block of approximate dimensions 0.28 × 0.13 × 0.10 mm^3 was selected and mounted with wax on a glass fiber. A total of 20682 reflections (-8 ≤ h ≤ 12, -23 ≤ k ≤ 26, -20 ≤ l ≤ 21) were collected at 183(2) K in the θ range of 2.14 to 23.29 °, of which 7427 were unique (R_{int} = 0.0535). The structure was solved by direct methods (SHELXTL V5.10, G. M. Sheldrick and Siemens Industrial Automation, Inc., 1997) in conjunction with standard difference Fourier techniques. The unit cell contains one molecule of diethyl ether coordinated to the sodium center. The carbon atoms of the ^tBu group on C28 are disordered, and the occupancies of C29 and C211 have been modeled over two sites (C29A and C29B, and, respectively, C21C and C21D). All non-hydrogen atoms were refined anisotropically. Some hydrogen atoms were found in the electronic density map, but most of the hydrogen atoms were placed in calculated (d_{C-H} = 0.96 Å)

positions, except for C29A, C29B, C210, C21C and C21D. The residual peak and hole electron density were 1.129 and –0.759 e·$Å^{-3}$, respectively and these values are in the normal range due to the large scattering effect of uranium centers. A semi-empirical absorption correction was applied based on pseudo-psi-scans with maximum and minimum transmission equal to 0.7409 and 0.4687, respectively. The least squares refinement converged normally with residuals of R_1 = 0.0352, wR_2 = 0.0878 based upon I > 2σ(I), and GOF = 1.053 (based on F^2). No extinction coefficient was applied to the refinement.

Crystal and refinement data: formula $C_{54}H_{69}N_3NaOU$, space group $P2_1/n$, a = 11.4758(10) Å, b = 23.639(2) Å, c = 19.4963(18) Å, α = 90.0 °, β = 102.527(2) °, γ = 90.0 °, V = 5163.1(8) $Å^3$, Z = 4, μ = 3.190 mm^{-1}, D_{calc} = 1.334 g·cm^{-3}, $F(000)$ = 2100, R_1 (based on F) = 0.0470, and wR_2 (based on F^2) = 0.0927.

2.4.3.9. X-ray crystal structure of (μ-η^8,η^8-C_8H_8)[U(NC[^{t}Bu]Mes)$_3$]$_2$ (3_2-μ-COT)

Inside the glove box, crystals of **3_2-μ-COT,** obtained from a saturated pentane solution, at –35 °C, were coated with Paratone N oil (an Exxon product) on a microscope slide. A dark brown block of approximate dimensions 0.36 × 0.25 × 0.23 mm^3 was selected and mounted with wax on a glass fiber. A total of 17253 reflections (-15 ≤ h ≤ 10, -24 ≤ k ≤ 23, -16 ≤ l ≤ 15) were collected at 183(2) K in the θ range of 2.33 to 23.29 °, of which 6287 were unique (R_{int} = 0.0380). The structure was solved by direct methods (SHELXTL V5.10, G. M. Sheldrick and Siemens Industrial Automation, Inc., 1997) in conjunction with standard difference Fourier techniques. The carbon atoms C2-C4 are slightly disordered, but this disorder has not been modeled. All non-hydrogen atoms were refined anisotropically. Some hydrogen atoms were found in the electronic density map, but most of the hydrogen atoms were placed in calculated (d_{C-H} = 0.96 Å) positions. The residual peak and hole electron density were 0.828 and –0.561 e·$Å^{-3}$. A semi-empirical absorption correction was applied based on pseudo-psi-scans with maximum and minimum transmission equal to 0.4804 and 0.3465, respectively. The least

squares refinement converged normally with residuals of $R_1 = 0.0242$, $wR_2 = 0.0580$ based upon $I > 2\sigma(I)$, and GOF = 1.049 (based on F^2). No extinction coefficient was applied to the refinement.

Crystal and refinement data: formula $C_{46}H_{63}N_3U$, space group $P2_1/n$, $a = 13.8845(10)$ Å, $b = 22.2016(16)$ Å, $c = 14.6531(11)$ Å, $\alpha = 90.0$ °, $\beta = 104.0300(10)$ °, $\gamma = 90.0$ °, $V = 4382.2(6)$ Å^3, $Z = 4$, $\mu = 3.736$ mm^{-1}, $D_{calc} = 1.358$ g·cm^{-3}, $F(000) = 1808$, R_1 (based on F) = 0.0301, and wR_2 (based on F^2) = 0.0608.

2.4.3.10. X-ray crystal structure of (COT)U(NC[^{t}Bu]Mes)$_3$ (3-COT)

Inside the glove box, crystals of **3-COT**, obtained from a saturated diethyl ether solution, at –35 °C, were coated with Paratone N oil (an Exxon product) on a microscope slide. A dark brown plate of approximate dimensions $0.58 \times 0.12 \times 0.04$ mm^3 was selected and mounted with wax on a glass fiber. A total of 18671 reflections (-9 $\leq$ h $\leq$ 12, -16 $\leq$ k $\leq$ 13, -31 $\leq$ l $\leq$ 29) were collected at 183(2) K in the θ range of 2.40 to 23.26 °, of which 6638 were unique ($R_{int} = 0.0774$). The structure was solved by direct methods (SHELXTL V5.10, G. M. Sheldrick and Siemens Industrial Automation, Inc., 1997) in conjunction with standard difference Fourier techniques. All non-hydrogen atoms were refined anisotropically and hydrogen atoms were placed in calculated ($d_{C-H} = 0.96$ Å) positions. The residual peak and hole electron density were 1.870 and –0.950 e·Å^{-3} and they are in the normal range to the large scattering effect of the uranium nucleus. A semi-empirical absorption correction was applied based on pseudo-psi-scans with maximum and minimum transmission equal to 0.8716 and 0.2338, respectively. The least squares refinement converged normally with residuals of $R_1 = 0.0451$, $wR_2 = 0.1113$ based upon $I > 2\sigma(I)$, and GOF = 1.042 (based on F^2). No extinction coefficient was applied to the refinement.

Crystal and refinement data: formula $C_{50}H_{68}N_3U$, space group P2(1)2(1)2(1), $a = 11.2787(9)$ Å, $b = 14.5337(12)$ Å, $c = 28.312(2)$ Å, $\alpha = 90$ °, $\beta = 90$ °, $\gamma = 90$ °, $V = 4640.9(7)$ Å^3, $Z = 4$, $\mu =$

3.532 mm^{-1}, D_{calc} = 1.358 g·cm^{-3}, $F(000)$ = 1924, R_1 (based on F) = 0.0465, and wR_2 (based on F^2) = 0.1124.

2.4.3.11. X-ray crystal structure of Na(μ-SPh)$_3$[U(NC[^{t}Bu]Mes)$_3$]$_2$ (Na-3$_2$-(μ-SPh)$_3$)

Inside the glove box, crystals of **Na-3$_2$-(μ-SPh)$_3$**, obtained from a saturated pentane solution, at –35 °C, were coated with Paratone N oil (an Exxon product) on a microscope slide. A dark green plate of approximate dimensions 0.19 × 0.15 × 0.10 mm^3 was selected and mounted with wax on a glass fiber. A total of 21075 reflections (-15 ≤ h ≤ 15, -14 ≤ k ≤ 17, -27 ≤ 1 ≤ 29) were collected at 183(2) K in the θ range of 2.02 to 23.27 °, of which 14557 were unique (R_{int} = 0.0462). The structure was solved by Patterson methods (SHELXTL V5.10, G. M. Sheldrick and Siemens Industrial Automation, Inc., 1997) in conjunction with standard difference Fourier techniques. All non-hydrogen atoms were refined anisotropically and hydrogen atoms were placed in calculated (d_{C-H} = 0.96 Å) positions. The residual peak and hole electron density were 2.041 and –0.784 e·Å^{-3} and they are in the normal range to the large scattering effect of the uranium nucleus. A semi-empirical absorption correction was applied based on pseudo-psi-scans with maximum and minimum transmission equal to 0.7366 and 0.5767, respectively. The least squares refinement converged normally with residuals of R_1 = 0.0498, wR_2 = 0.1363 based upon I > 2σ(I), and GOF = 0.980 (based on F^2). No extinction coefficient was applied to the refinement.

Crystal and refinement data: formula C$_{102}$H$_{136}$N$_6$U$_2$NaS$_3$, space group P-1, a = 14.1784(10) Å, b = 15.5376(10) Å, c = 26.3282(18) Å, α = 96.588(1) °, β = 98.093(1) °, γ = 114.213(1) °, V = 5140.7(6) Å^3, Z = 2, μ = 3.256 mm^{-1}, D_{calc} = 1.319 g·cm^{-3}, $F(000)$ = 2066, R_1 (based on F) = 0.0900, and wR_2 (based on F^2) = 0.1503.

2.4.3.12. X-ray crystal structure of (μ-NPh)$_2$[U(NC[^{t}Bu]Mes)$_3$]$_2$ (3$_2$-(μ-NPh)$_2$)

Inside the glove box, crystals of **3$_2$-(μ-NPh)$_2$**, obtained from a saturated pentane solution, at –35 °C, were coated with Paratone N oil (an Exxon product) on a microscope slide. A dark green plate of approximate dimensions 0.21 × 0.14 × 0.05 mm^3 was selected and mounted with wax on a glass fiber. A total of 19212 reflections (-14 ≤ h ≤ 10, -17 ≤ k ≤ 17, -24 ≤ l ≤ 27) were collected at 183(2) K in the θ range of 2.00 to 23.34 °, of which 13264 were unique (R_{int} = 0.1160). The structure was solved by Patterson methods (SHELXTL V5.10, G. M. Sheldrick and Siemens Industrial Automation, Inc., 1997) in conjunction with standard difference Fourier techniques. The unit cell contains two crystallographically independent halves of each dimer. Some carbon atoms were disordered and the disorder modeled over two sites (C49A and C49B, C41A and C41B, C41C and C41D, C19A and C19B, C11A and C11B, C29A and C29B, C21A and C21B, C59A and C59B, C31A and C31B, C61A and C61B). All non-hydrogen atoms were refined anisotropically except for C11B and C19A, which were refined only isotropically. Hydrogen atoms were placed in calculated (d_{C-H} = 0.96 Å) positions, except for the disordered atoms for which no hydrogen atoms were generated. The residual peak and hole electron density were 1.783 and –1.940 e·Å^{-3} and they are in the normal range to the large scattering effect of the uranium nucleus. A semi-empirical absorption correction was applied based on pseudo-psi-scans with maximum and minimum transmission equal to 0.8446 and 0.5273, respectively. The least squares refinement converged normally with residuals of R_1 = 0.0498, wR_2 = 0.1274 based upon I > 2σ(I), and GOF = 1.048 (based on F^2). No extinction coefficient was applied to the refinement.

Crystal and refinement data: formula C$_{96}$H$_{100}$N$_8$U$_2$, space group P-1, a = 13.332(9) Å, b = 15.976(10) Å, c = 24.367(16) Å, α = 75.067(10) °, β = 77.380(12) °, γ = 70.936(11) °, V = 4688(5) Å^3, Z = 2, μ = 3.4956 mm^{-1}, D_{calc} = 1.305 g·cm^{-3}, F(000) = 1832, R_1 (based on F) = 0.0828, and wR_2 (based on F^2) = 0.1473.

2.4.4. Susceptibility measurements

Magnetic susceptibility measurements were recorded using a SQUID magnetometer at 5000 G. The samples were prepared in the glove box (50 – 100 mg) loaded in a gelatin capsule that was positioned inside a plastic straw and carried to the magnetometer in a tube under N_2. The sample was quickly inserted into the instrument, centered and data obtained from 5 to 300 K. The contribution from the sample holders was not accounted for. The diamagnetic contributions were calculated and subtracted from χ_{mol}. Effective magnetic moments were calculated either by linear regression from plots of $1/\chi_{mol}$ versus T (K) for Curie-Weiss behavior or by using the formula 2.828*sqrt(T* χ_{mol}) for non-Curie-Weiss behavior. Samples used were multiply times recrystallized. Measurements for the same compound were carried out on different recrystallized samples.

2.4.5. Computational details

The Amsterdam Density Functional package (version *ADF2000.02*)[30] was used to do a full geometry optimization on cartesian coordinates of the model compounds specified in the text. Full electronic configuration was used for all atoms. Basis set Zora(V) was used as implemented in the ADF suite. Relativistic effects were included by virtue of the zero order regular approximation (ZORA). The local density approximation (LDA) by Vosko, Wilk and Nusair (VWN) was used together with the exchange and correlation corrections specified in each input file. The calculations were performed spin unrestricted, with the number of spin-α orbitals in excess of spin-β orbitals specified in the input files. Tables with a list of selected MOs with the most significant SFO gross populations (>3%) and input files are given in Appendix 2.

[1] Diaconescu, P. L.; Arnold, P. L.; Baker, T. A.; Mindiola, D. J.; Cummins, C. C. *J. Am. Chem. Soc.* **2000**, *122*, 6108.

[2] Odom, A. L.; Arnold, P. L.; Cummins, C. C. *J. Am. Chem. Soc.* **1998**, *120*, 5836.

[3] Schwindt, M.; Lejon, T.; Hegedus, L. *Organometallics* **1990**, *9*, 2814.

[4] Zhang, S.; Piers, W. E.; Gao, X.; Parvez, M. *J. Am. Chem. Soc.* **2000**, *122*, 5499.

[5] Clark, D. L.; Sattelberger, A. P. *Inorg. Synth.* **1997**, *31*, 307.

[6] Diaconescu, P. L.; Cummins, C. C. *J. Am. Chem. Soc.* **2002**, *124*, 7660.

[7] Bush, B. J.; Lynch, V. M.; Lagowski, J. J. *Organometallics* **1987**, *6*, 1267; Elschenbroich, C.; Heck, J. *J. Am. Chem. Soc.* **1979**, *101*, 6773.

[8] Cotton, F. A. *Chemical Applications of Group Theory*, Wiley-Interscience, New York, 1990.

[9] (a) Moore, M.; Gambarotta, S.; Bensimon, C. *Organometallics* **1997**, *16*, 1086. (b) Caselli, A.; Solari, E.; Scopelliti, R.; Floriani, C.; Re, N.; Rizzoli, C.; Chiesi-Vila, A. *J. Am. Chem. Soc.* **2000**, *122*, 3652.

[10] Martin, T. P. *Angew. Chem. Int. Ed. Engl.* **1986**, *25*, 197.

[11] Due to the fact that there are two molecules in the unit cell and each molecule contains a huge number of atoms, in solving the crystal structure, the command BLOC was used (this command does not allow for the calculation of esds).

[12] Meerholz, K.; Heinze, J. *J. Am. Chem. Soc.* **1989**, *111*, 2325.

[13] Lethe, E. van; Baerends, E. J.; Snijders, J. G. *J. Chem. Phys.* **1993**, *99*, 4597; Lethe, E. van; Baerends, E. J.; Snijders, J. G. *J. Chem. Phys.* **1994**, *101*, 9783; Lethe, E. van; Baerends, E. J.; Snijders, J. G. *J. Chem. Phys.* **1999**, *110*, 8943.

[14] Snijders, J. G.; Baerends, E. J.; Ros, P. *Mol. Phys.* **1979**, *38*, 1909; Boerrigter, P. M.; Baerends, E. J.; Snijders, J. G. *Chem. Phys.* **1988**, *122*, 357; Ziegler, T.; Tschinke, V.; Baerends, E. J.; Snijders, J. G.; Ravenek, W. *J. Chem. Phys.* **1989**, *93*, 3050.

[15] Carlin, R. L.; van Duyneveldt, A. J. *Magnetic Properties of Transition Metal Compounds*, Springer Verlag, New York, 1977.

[16] Kanellakopulos, B. in *Organometallics of the f-Elements*, Marks, T. J.; Fischer, R. D. Eds., Reidel, Dordrecht, 1979,1.

[17] Avens, L. R.; Bott, S. G.; Clark, D. L.; Sattelberger, A. P.; Watkin, J. G.; Zwick, B. D. *Inorg. Chem.* **1994**, *33*, 2248.

[18] Evans, W. J.; Clark, R. D.; Ansari, M. A.; Ziller, J. W. *J. Am. Chem. Soc.* **1998**, *120*, 9555; Evans, W. J.; Johnston, M. A.; Greci, M. A.; Ziller, J. W. *Organometallics* **1999**, *18*, 1460.

[19] Streitwieser, A.; Müller-Westerhoff, U. *J. Am. Chem. Soc.* **1968**, *90*, 7364.

[20] Zalkin, A.; Raymond, K. N. *J. Am. Chem. Soc.* **1969**, *91*, 5667; Avdeef, A.; Raymond, K. N.; Hodgson, K. O.; Zalkin, A. *Inorg. Chem.* **1972**, *11*, 1083.

[21] Streitwieser, A., Jr.; Müller-Westerhoff, U.; Sonnichsen, G.; Mares, F.; Morrell, D. G.; Hodgson, K. O.; Harmon, C. A. *J. Am. Chem. Soc.* **1973**, *95*, 8644.

[22] Elschenbroich, C.; Salzer, A. *Organometallics*, 2nd ed., VCH, Weinheim, 1992, p. 363.

[23] Berthet, J.-C.; Ephritikhine, M. *J. Chem. Soc., Chem. Commun.* **1993**, *20*, 1566; Boisson, C.; Berthet, J.-C.; Lance, M.; Vigner, J.; Nierlich, M.; Ephritikhine, M. *J. Chem. Soc., Dalton Trans.* **1996**, 947.

[24] Evans, A. G.; Evans, J. C.; Emes, P. J.; James, C. L.; Pomery, P. J. *J. Chem. Soc. B: Phys. Org.* **1971**, *7*, 1484.

[25] Rosen, R. K.; Andersen, R. A.; Edelstein, N. M. *J. Am. Chem. Soc.* **1990**, *112*, 4588.

[26] Fryzuk, M. D.; Jafarpour, L.; Kerton, F. M.; Love, J. B.; Patrick, B. O.; Rettig, S. J. *Organometallics* **2001**, *20*, 1387.

[27] Pangborn, A. B.; Giardello, M. A.; Grubbs, R. H.; Rosen, R. K.; Timmers, F. J. *Organometallics* **1996**, *15*, 1518.

[28] Schlosser, M.; Hartmann, J. *Angew. Chem.* **1973**, *85*, 544.

[29] Miura, Y.; Oka, H.; Yamano, E.; Morita, M. *J. Org. Chem.* **1997**, *62*, 1188.

[30] Baerends, E. J.; Ellis, D. E.; Ros, P. *Chem. Phys.* **1973**, *2*, 41; Versluis, L.; Ziegler, T. *J. Chem. Phys.* **1988**, *88*, 322; te Velde, G.; Baerends, E. J. *J. Comput. Phys.* **1992**, *99*, 84.

Uranium 2,2'-Bipyridyl Complexes
Supported by Amide and Ketimide Ligands

3.1. Introduction

Most metals are known to form complexes with 2,2'-bipyridine (bipy) and for a given metal center multiple oxidation states may be encountered.[1] For an electron rich metal, the bipy ligand is commonly reduced to its corresponding radical anion,[1,2] with concomitant formal oxidation of the metal center. Complexes of lanthanides with bipy as a radical anion ligand have been reported increasingly in recent years such as $(Me_5C_5)_2Yb(bipy)$,[3] $[Yb(\mu_2-N_2C_{10}H_8)(THF)_2]_3$,[4] $(Me_5C_5)_2Sm(bipy)$,[5] $Eu(bipy)_4$.[6] Similar complexes for uranium have not yet been described, but investigation of the crystallographic parameters for $[Et_4N][U(NCS)_5(bipy)_2]$[7] and $U(bipy)_4$[8] revealed that one of the bipy ligands in the first complex and all bipy ligands in the latter can be considered radical anions (see below). Other reported complexes of uranium and bipy are consistent with coordination of a neutral bipy ligand.[9-13]

In this study the synthesis and characterization of $(bipy)_2U(N[t-Bu]Ar)_2$ (**1b-(bipy)₂**), $(bipy)U(N[^1Ad]Ar)_3$ (**2a-bipy**), $(bipy)_2U(NC[t-Bu]Mes)_3$ (**3-(bipy)₂**), and $IU(bipy)(NC[t-Bu]Mes)_3$ (**3-I-bipy**) are reported. The geometric and electronic structures of these complexes are investigated both in the solid state (X-ray crystallography, magnetic susceptibility measurements) and in solution (NMR and UV-vis spectroscopies) in order to assess whether the bipy ligands are best viewed as neutral or radical anionic in character.

The complexes discussed here range in *formal* oxidation state at uranium center from +2 to +4 if bipy is assumed to be neutral. As in the case of transition metal and lanthanide compounds,[1] the bipy radical anion is encountered for low oxidation states and neutral bipy for the higher

oxidation states. The existence of complexes of bipy as a radical anion ligand is thus dependent upon the reducing ability of the uranium fragments.

Metrical parameters from X-ray crystal structures can be used to assign the oxidation state of the bipyridyl ligand, since such parameters can be associated with donation of electron density into the LUMO of bipy.[3,14] Since the LUMO of bipy shows a π bond (A in Figure 1) between the carbon atoms connecting the aromatic rings, shortening of the bond between these atoms and coplanarity of the two rings are signatures of a bipy ligand coordinated as a radical anion.

3.2. Results and discussion

3.2.1. Syntheses

Compound (μ-toluene)[U(N[*t*-Bu]Ar)$_2$]$_2$ (**1b$_2$-μ-toluene**)[15] reacts with 4 equiv of bipy to give **1b-(bipy)$_2$** (Scheme 1) as a dark brown microcrystalline solid in 71% isolated yield. In the present study, isolation of **1b-(bipy)$_2$** and the fact that no *mono*-bipy complexes were observed as intermediates in the reaction can be interpreted as a consequence of an open coordination environment since there are only two *t*-butyl-anilide ligands per uranium center.

However, when three *N-tert*-hydrocarbylanilide ligands are coordinated to uranium, only the *mono*-bipy complex is formed (Scheme 2). The synthesis of **2a-bipy** is straightforward and can be accomplished by the reaction of **2a-THF** with one equiv bipy (73% yield, dark brown solid).

As discussed in Chapter 2, the supporting ketimide ligand NC[*t*-Bu]Mes has the steric bulk moved one atom further from the uranium center than an anilide ligand. The iodide *tris*-ketimide IU(DME)(NC[*t*-Bu]Mes)$_3$ (**3-I-DME**)[16] coordinates to a molecule of DME, while iodide uranium

tris-anilide complexes do not coordinate Lewis bases.[15] Replacement of DME from **3-I-DME** with bipy leads to **3-I-bipy** isolated as a green microcrystalline solid in 90% yield (Scheme 3).
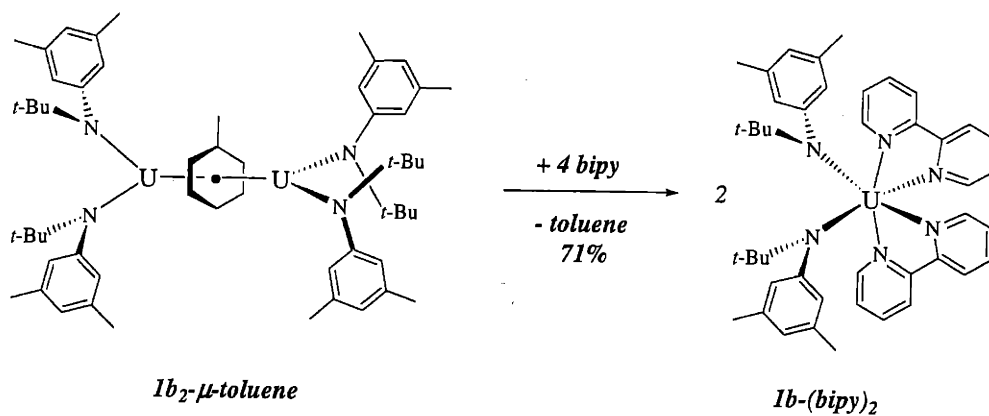
Scheme 1

Scheme 2

Scheme 3

References begin on page 182
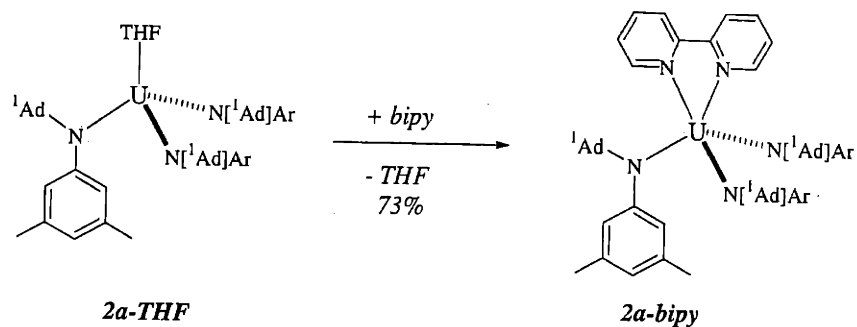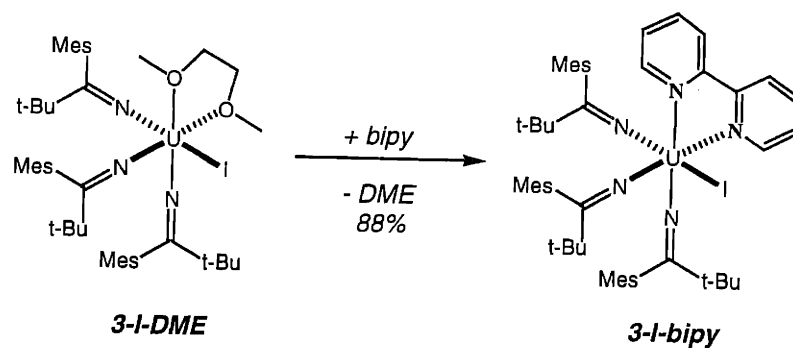
Complex **3-(bipy)₂** was prepared from and Na₂(μ-biphenyl)U₂(NC[*t*-Bu]Mes)₆ (**Na₂-3₂-μ-biphenyl**) and bipy as shown in Scheme 4. The characterization of compound **Na₂-3₂-μ-biphenyl**, which is similar to Na₂(μ-naphthalene)U₂(NC[*t*-Bu]Mes)₆,[12] will be reported elsewhere. The reaction of the bridging arene ketimide diuranium complex **Na₂-3₂-μ-biphenyl** with bipy is more complicated than in the case of the arene-bridged amide complex, **1a₂-μ-toluene**. Minor byproducts arise when the alkali metal cation is lost during the reaction, and additional redox processes occur. The stoichiometry employed, 4 equiv bipy for one arene-bridged dinuclear complex, led to the highest yield of **3-(bipy)₂**. If the only other product of the reaction were Mbipy (M = Na, K), 6 equiv of bipy would be necessary in the reaction. From investigation of the ¹H NMR spectrum of the crude reaction mixture it is apparent that some uranium complexes are formed as byproducts, which have not been identified. Nonetheless, extraction and crystallization from pentane leads to **3-(bipy)₂** isolated as a dark-brown solid in 40% yield.

Na₂-3₂-μ-biphenyl   **3-(bipy)₂**
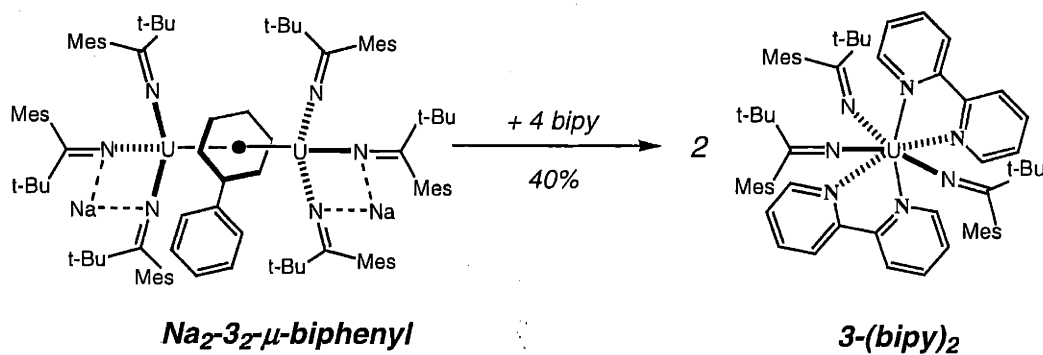
Scheme 4

3.2.2. X-ray crystallography results

X-ray crystal structures have been determined for all four complexes (Figures 2–5) at low temperatures (-90 °C). Tables 1 and 2 present some important bond lengths and angles. Acceptance of an electron into the LUMO of bipy would cause the bonds (Figure 1) A, C, and E to shorten and the bonds B, D, F, and G to lengthen.[3] As mentioned earlier, in $[Et_4N][U(NCS)_5(bipy)_2]^7$ one of the bipy ligands has crystallographic parameters consistent with its assignment as a radical anion (A distance is 1.39(2) Å). In $U(bipy)_4$,[8] A distances are 1.38(4), 1.42(3), 1.43(4), and 1.43(4) Å.

Figure 1. LUMO and bond labeling of bipy.

Table 1. Comparison of bond lengths (Å) in bipy and in complexes.

Bond	bipy[6]	1b-(bipy)₂	2a-bipy	3-(bipy)₂	3-I-bipy
A	1.490(3)	1.429(7); 1.426(7)	1.415(13)	1.471(10); 1.418(10)	1.484(10)
B	1.394(2)	1.409(10); 1.411(10)	1.415(18)	1.396(15); 1.418(13)	1.386(14)
C	1.385(2)	1.368(11); 1.358(11)	1.350(20)	1.353(18); 1.357(17)	1.377(16)
D	1.383(3)	1.395(11); 1.400(11)	1.401(21)	1.374(17); 1.412(18)	1.356(17)
E	1.384(2)	1.353(10); 1.357(10)	1.364(20)	1.381(15); 1.365(16)	1.370(15)
F	1.341(2)	1.353(8); 1.361(8)	1.393(16)	1.324(13); 1.358(13)	1.340(12)
G	1.346(2)	1.388(8); 1.375(8)	1.353(17)	1.352(12); 1.375(11)	1.348(13)
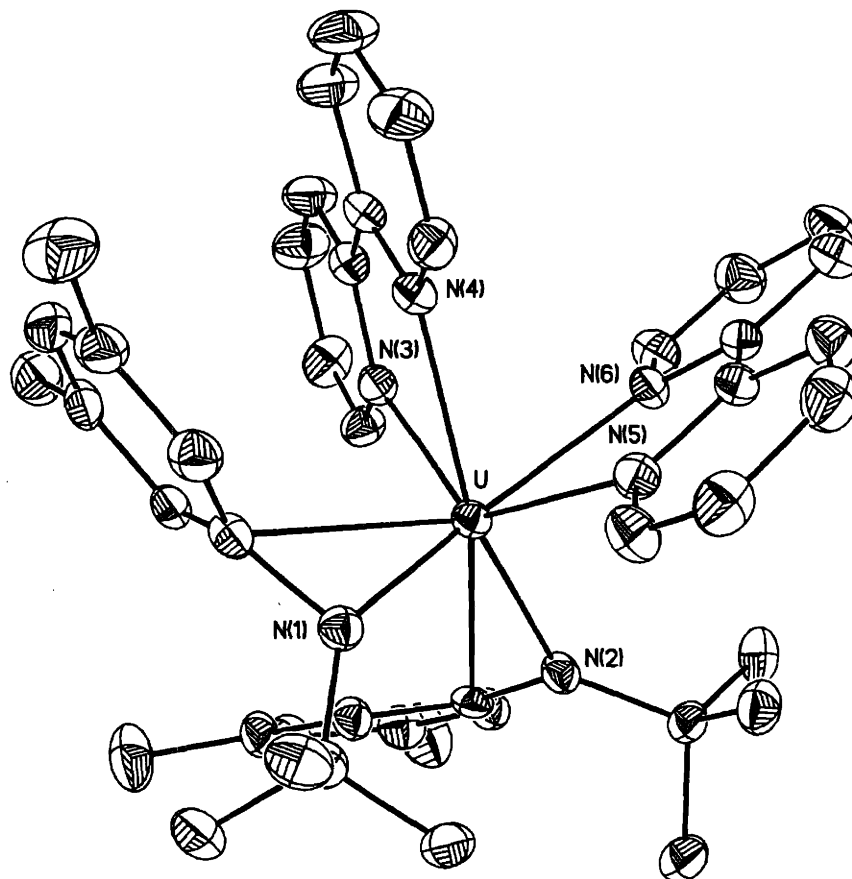
Figure 2. Structural drawing of complex **1b-(bipy)₂** with thermal ellipsoids at the 35% probability level.

Table 2. Selected bond distances (Å) and torsion angles (°) in discussed complexes.

Parameter (avg.)	1b-(bipy)₂	2a-bipy	3-(bipy)₂	3-I-bipy
U-N$_{ligand}$	2.302(6)	2.275(13)	2.263(10)	2.213(9)
U-N$_{bipy}$	2.488(6); 2.454(6)	2.483(10)	2.609(7); 2.528(7)	2.581(7)
N-C-C-N[a]	3.2(6); 1.9(6)	3(1)	2.2(9); 2.4(0.9)	0.9(8)
C-C-C-C[a]	5.8(8); 1.9(6)	2(1)	3(1); 5(1)	3(1)

a: torsion angle
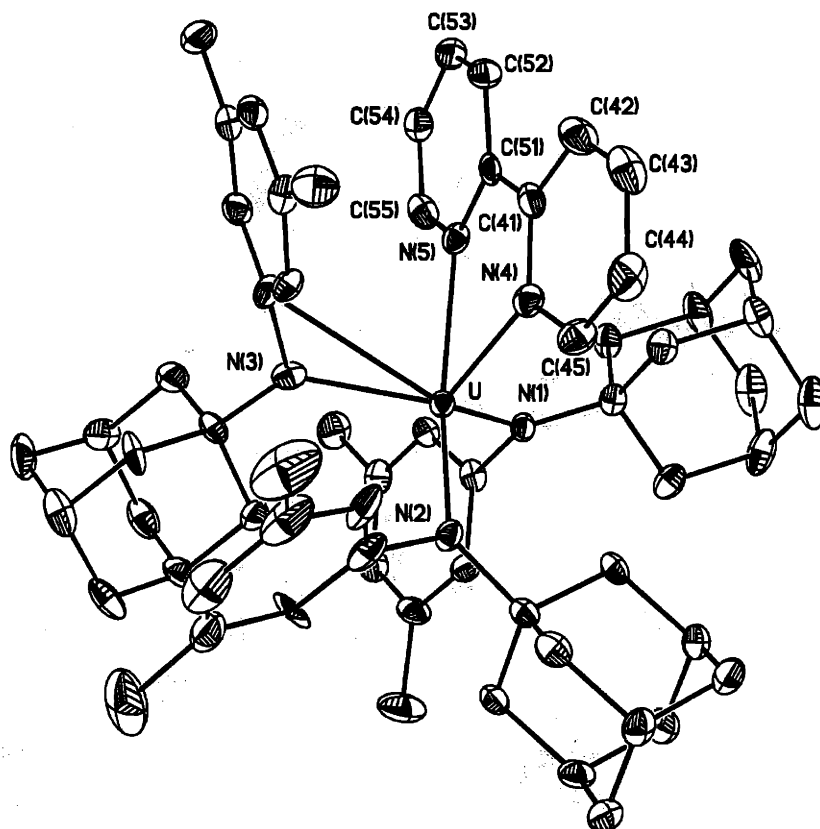
Figure 3. Structural drawing of complex **2a-bipy** with thermal ellipsoids at the 35% probability level.

For **1b-(bipy)₂** the metrical parameters indicate that both bipy ligands should be considered as radical anions; also, the values of the bond lengths for the two inequivalent bipy ligands are similar. Analogously, the bipy ligand in **2a-bipy** is best viewed as a coordinated radical anion. However, the two bipy ligands in **3-(bipy)₂** have different sets of parameters, one of them consistent with assignment as a radical anion, the other one consistent with a neutral bipy ligand. Finally, in **3-I-bipy** the bond lengths suggest a neutral bipy ligand. In **3-I-bipy** there is π-π stacking[17] of bipy with the aromatic rings of two ketimide ligands and, interestingly, similar π-π stacking occurs between the neutral bipy ligand in **3-(bipy)₂** and the aromatic rings of two ketimide ligands. In all complexes then, uranium can be assigned to its +4 formal oxidation state, in agreement with the fact that this oxidation state is encountered most frequently in the organometallic chemistry of uranium.[18]

References begin on page 182
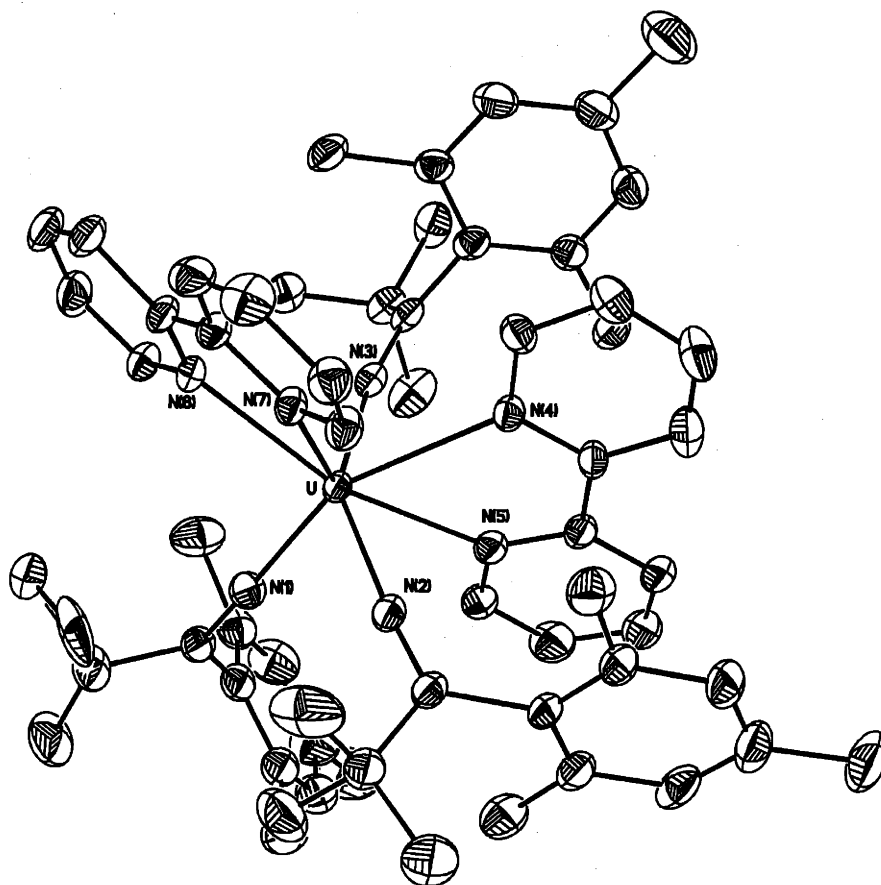
Figure 4. Structural drawing of complex **3-(bipy)₂** with thermal ellipsoids at the 35% probability level.

Another parameter that probes the electronic density present at the uranium center is the distance between uranium and the nitrogen of the supporting ligand (Table 2), since it can be compared with corresponding values in non-bipy complexes for which the oxidation state was experimentally estimated by X-ray absorption near-edge structure (XANES) spectroscopy.[19] The average U-N_{amide} distances for **1b-(bipy)₂** (2.302(6) Å) and **2a-bipy** (2.275(13) Å) are intermediate between U-N_{amide} in **2a-THF** (2.346(9) Å, +3 oxidation state) and the one in IU(N[^{t}Ad]Ar)₃ (**2a-I**, 2.204(9) Å, +4 oxidation state). For **3-(bipy)₂** and **3-I-bipy** the average U-$N_{ketimide}$ distances (2.263(10) and 2.213(9) Å) are similar to the average found in **3-I-DME** (2.189(21) Å). These observations are consistent with the presence of uranium(IV) centers.
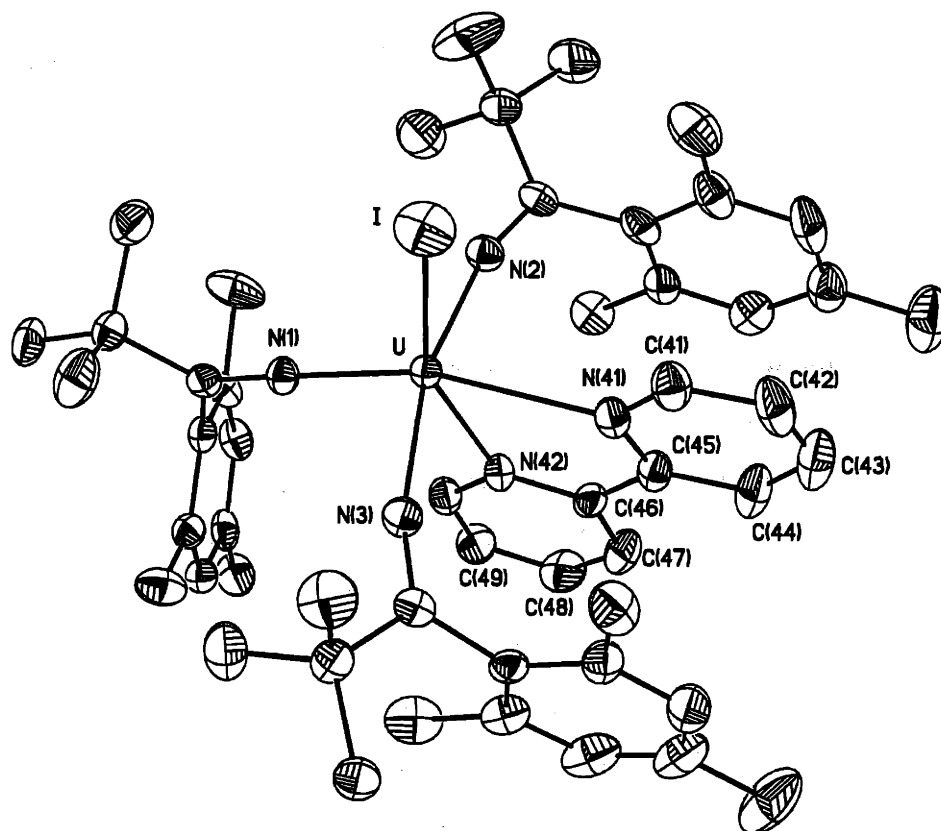
Figure 5. Structural drawing of complex **3-I-bipy** with thermal ellipsoids at the 35% probability level.

Another parameter that could offer some insight into the electronic structure of bipy complexes is the U-N$_{bipy}$ distance (Table 2). This distance (varying from 2.454(6) to 2.609(7) Å), for all complexes listed in Table 2, is shorter than the corresponding one in UI$_3$(bipy)$_2$(py) (2.65(4) Å).[9] This is consistent with the fact that shorter ionic radii are expected for uranium(IV) than for uranium(III) centers. Another uranium(III) complex, (dmb)U(C$_5$Me$_5$)(C$_8$H$_8$), shows metrical parameters for dmb consistent with its assignment as a neutral ligand.[10] Unexpectedly, the U-N$_{dmb}$ distance of 2.426(16) Å is shorter than the U-N$_{bipy}$ distance in complexes listed in Table 2.

The two torsion angles presented in Table 2 have also been used as an indication of the radical anion character of the coordinated bipy ligand. For example, their values are 3° and 3° for (Me$_5$C$_5$)$_2$Yb(bipy), in which bipy is considered a radical anion ligand,[3] and 9.94° and 11.80° for

UI$_3$(bipy)$_2$(py), in which bipy is considered a neutral ligand.[7] In all complexes listed in Table 2 the observed values indicate an almost planar bipy molecule, but for **3-I-bipy** and the neutral bipy ligand of **3-(bipy)$_2$** this could be a consequence of the π - π stacking present in the molecules (Figure 4 and 5).

3.2.3. Solid state magnetic susceptibility measurements

For transition metal complexes, solid-state magnetic properties have been used to propose models for the interaction of different spin carriers.[20] However, theoretical models for quantum mechanical electron exchange coupling are not available for f-element complexes.[21] In the present work, plots of μ_{eff} versus T (Figures 6-8) show that the value of μ_{eff} for **1b-(bipy)$_2$**, **3-(bipy)$_2$**, and **3-I-bipy** varies from ca. 0.5 μ_B at low temperatures to ca. 2.75 μ_B for the *bis*-bipy complexes and to 3.50 μ_B for **3-I-bipy** at 300 K. In all cases, the increase in the value of μ_{eff} as a function of temperature can be attributed to population of low lying excited states, a phenomenon well known and often encountered in the chemistry of f element complexes.[22]
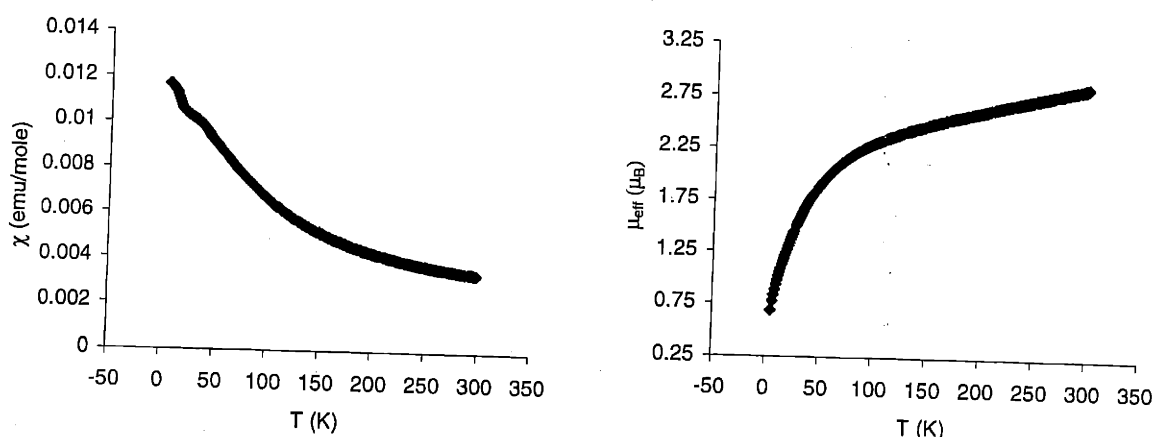
Figure 6. Plots of χ (left) and μ_{eff} (right) versus T for **1b-(bipy)$_2$**.

The very low value for μ_{eff} at low temperatures can be due to antiferromagnetic coupling if the magnetic susceptibility passes through a maximum as the temperature is lowered. The maximum in the magnetic susceptibility displayed in Figure 6 (ca. 20 K) for **1b-(bipy)₂** is not well defined, making difficult its assignment to an antiferromagnetic transition.
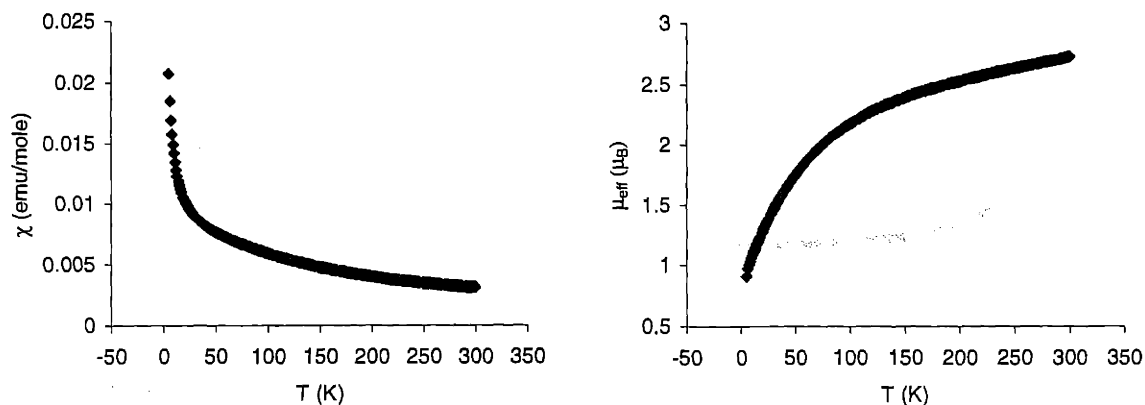
Figure 7. Plots of χ (left) and μ_{eff} (right) versus T for **3-(bipy)₂**.
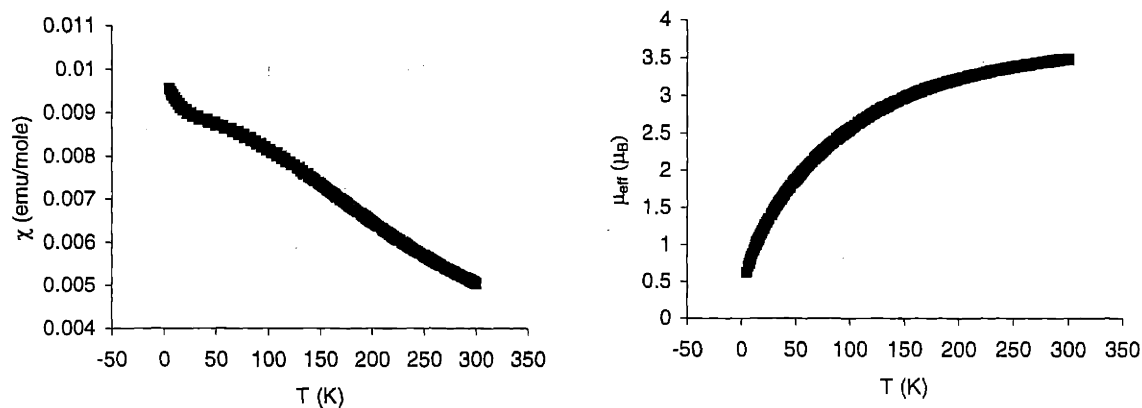
Figure 8. Plots of χ (left) and μ_{eff} (right) versus T for **3-I-bipy**.

One notable exception is **2a-bipy**, which, according to the linear $1/\chi$ versus T plot displayed in Figure 9b, shows Curie-Weiss behavior. The value of μ_{eff} (3.38 μ_B) is similar to values for the

uranium iodide *tris*-amide complexes IU(N[*t*-Bu]Ar)$_3$ (**1a-I**, 3.18 μ_B) and **2a-I** (3.52 μ_B), both compounds considered uranium(IV) species.[16]
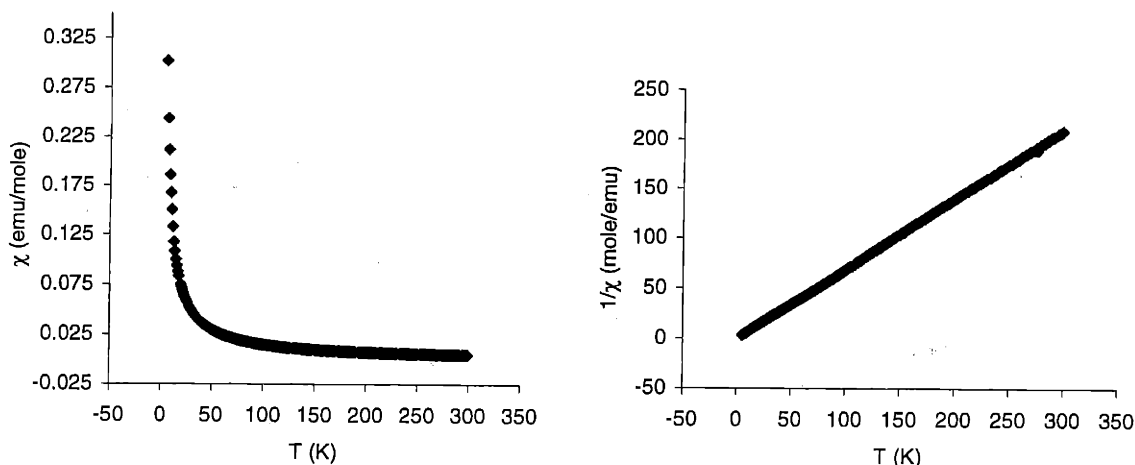
Figure 9. Plots of χ (left) and 1/χ (right) versus T for **2a-bipy**.

The magnetic susceptibility studies were undertaken in order to determine if there is a striking difference in the magnetic properties of complexes that contain bipy as a radical anion (**1b-(bipy)$_2$, 2a-bipy**) versus those containing bipy as a neutral ligand (**3-I-bipy**). This difference could have been translated into antiferromagnetic coupling of the electron localized on bipy and the unpaired electrons on uranium. As described above, the magnetic susceptibilities offer little information to support this comparison, except in the case of **1b-(bipy)$_2$**, for which a weak antiferromagnetic transition can be invoked. However, the study of the magnetic susceptibilities does not ostensibly contradict findings from crystallography.

3.2.4. NMR spectroscopy studies

All compounds treated here are paramagnetic, regardless whether bipy is coordinated to the uranium center as a radical anion or as a neutral ligand. Only **1b-(bipy)$_2$** and **2a-bipy** have peaks

in their ^{1}H NMR spectra that allow variable temperature (VT) studies (Figure 10). The linear δ versus 1/T plots for **1b-(bipy)₂** (Figure 10a, -50 to 100 °C) and **2a-bipy** (Figure 10b, 20-100 °C) indicates that Curie-Weiss behavior is evident for both species. Accurate determination of δ values below the minimum temperatures indicated was inhibited by excessive peak broadening. Linear δ versus 1/T plots indicate that no temperature dependent processes occur in solution.[23]
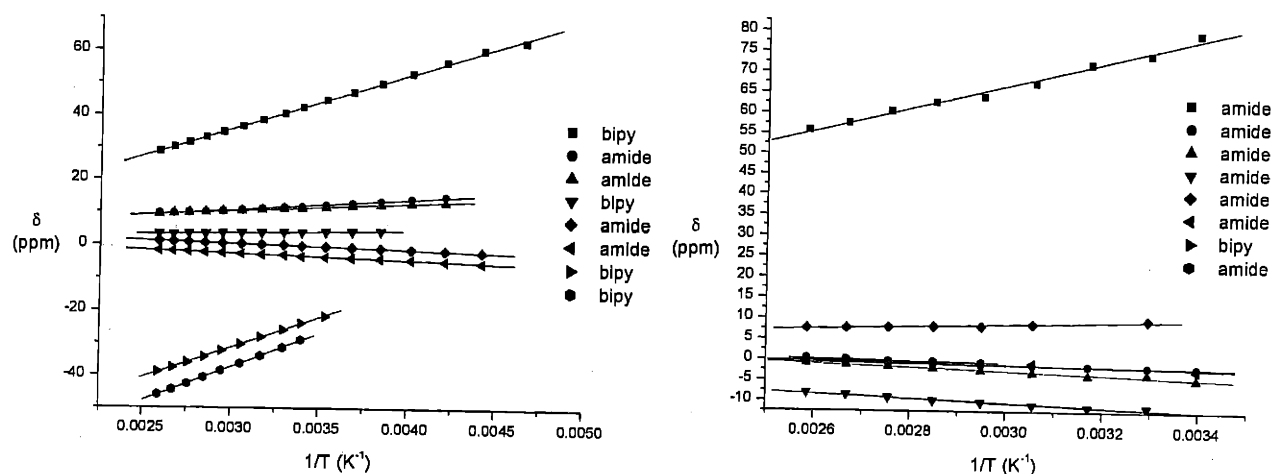
Figure 10. Plots of δ versus 1/T for **1b-(bipy)₂** (left) and **2a-bipy** (right).

Due, most likely, to steric factors that inhibit rotation of the ancillary ligands in solution, the bipy-ketimide compounds do not have straightforward ^{1}H NMR spectra. The peaks are broad and some could not be identified. For example, when recording the VT spectra for **3-I-bipy** from 20 to 100 °C, the peaks broaden and most of them are indistinguishable from the baseline around 40 °C. The compound is not very soluble in aromatic solvents and precipitates out at temperatures below room temperature. Investigation of ^{1}H NMR spectra of **3-(bipy)₂** as a function of temperature revealed complicated behavior. At room temperature, due to the number of peaks identifiable (more than 8, 4 for ketimide protons and 4 for bipy protons), it is possible that the two ketimide and / or bipy ligands are not equivalent on the NMR time scale due to slow rotation. Some peaks broaden into the baseline as temperature is increased, but up to 100 °C, a straightforward spectrum is not obtained. When a spectrum is recorded back at room

temperature, new peaks are observed, but the decomposition product has not been identified.

For a series of ytterbocene bipy compounds it was found that a reduced bipy ligand exchanges more slowly with 4,4'-dimethyl-2,2'-bipyridine (dmb) than does a neutral one.[3] Such studies could not be conducted for **3-I-bipy** because of its low solubility in aromatic solvents at room temperature.

^{1}H NMR spectra of solutions of **1b-(bipy)₂** and free bipy or dmb, taken immediately after mixing the two compounds, appear as the sum of spectra of **1b-(bipy)₂** and bipy or dmb indicating that there is no exchange between the coordinated bipy molecules and free bipy or dmb on the NMR time scale. After three hours, peaks corresponding to **1b-(dmb)₂**, independently synthesized and characterized, are visible. Although most of the chemical shifts are not sharp and different enough to allow for identification of more than two uranium compounds, based on the peaks corresponding to some bipy / dmb protons, a third species was identified in solution. Since this species shows two sets of peaks for each identifiable proton it is assumed to be the mixed **1b-(bipy)(dmb)** compound. The equilibrium between the three species is reached within 5 days and the molar ratio **1b-(bipy)₂** : **1b-(bipy)(dmb)** : **1b-(dmb)₂** is approximately 1 : 2 : 1 based on integration of the peaks mentioned above (see Experimental section for details).

^{1}H NMR spectra of solutions of **2a-bipy** and free bipy or dmb also appear as a sum of the independent spectra of **2a-bipy** and free bipy or dmb, when taken shortly after mixing of the compounds. For a solution of **2a-bipy** and dmb, although peaks for a new compound cannot be observed due to the broadness of signals for **2a-bipy**, the appearance of free bipy was not observed after one day at room temperature, but it was noticed after an additional day of heating the solution at 80 °C.

Unlike in the case of **1b-(bipy)₂** / **2a-bipy** and bipy or dmb solutions, investigation by ^{1}H NMR spectroscopy of solutions of **3-(bipy)₂** and free bipy or dmb indicated that spectra taken within

minutes after mixing **3-(bipy)₂** with bipy or dmb in C_6D_6 were different than the sum of the spectra of the two compounds. Complete assignments of the chemical shifts in the ^1H NMR spectra of these mixtures is not possible due to the broadness of the peaks, but the observations made are consistent with exchange of a bipy ligand with free bipy or dmb.

In similar experiments conducted with the ytterbocenes and $(Me_5C_5)_2Ca(bipy)$ it was reported that a neutral bipy ligand exchanges with dmb upon mixing.[3] On one hand, the slow exchange between bipy and dmb suggests that the bipy ligands in **1a-(bipy)₂** and **2b-bipy** are indeed radical anionic. On the other hand, the fast exchange observed between **3-(bipy)₂** and bipy or dmb indicates the presence of bipy as a neutral ligand. These results corroborate the X-ray data discussed above.

3.2.5. Absorption spectra

The bipyridyl anion has a diagnostic optical spectrum with three intense ($\varepsilon \approx 10^3$ M^{-1} cm^{-1}) absorption bands in the 700-1000 nm.[3] Absorption spectra of **1b-(bipy)₂** and **2a-bipy** toluene solutions at 25 °C are presented in Figure 11, showing high intensity bands ($\varepsilon \approx 10^3$ M^{-1} cm^{-1}) in the 500-1000 nm region. A comparison with spectra of classical uranium compounds is useful in determining the nature of these bands. Although the absorption spectra of **2a-I** or **2a-THF** have bands in the 500-1000 nm region,[15] they are not as intense as expected for the bipy radical anion. In accord with other data presented, the high intensity bands observed in the spectra of **1b-(bipy)₂** and **2a-bipy** are attributed to transitions of the bipy radical anion (Table 3). Consistent with the presence of bipy coordinated as a neutral ligand in **3-I-bipy**, its UV-vis spectrum lacks the characteristics intense bands in the 700-1000 nm region (Table 3). Such bands are also absent from the UV-vis spectrum of **3-(bipy)₂**, for which X-ray crystallography indicated the presence of one bipy coordinated as a radical anion and one bipy coordinated as a neutral ligand. This finding suggests that in the conditions of the UV-vis experiment the two bipy ligands are

equivalent. Similarly, no bands were reported in the region 700-1000 nm from the UV-vis spectrum of $LaI_2(bipy)_2(DME)$, for which X-ray crystallography parameters indicate two equivalent bipy ligands with intermediate character between radical anions and neutral ligands.[24]

Table 3. Optical spectra of bipyridyl complexes (in toluene unless otherwise specified).

Complex	λ_{max} in nm ($\varepsilon \times 10^{-3}$ in M^{-1} cm^{-1})
1b-(bipy)₂	790 (3.2); 470 (5.1); 415 (7.2); 370 (15.1); 285 (38.8)
2a-bipy	891 (3.6); 777 (4.2); 447 (7.1); 370 (17.4); 285 (35.8)
3-(bipy)₂	476 (2.8); 423 (4.1); 376 (6.4); 285 (34.4)
3-I-bipy	685 (0.6); 413 (2.7); 307 (12.4)
Na(bipy) in THF³	952 (1.3); 833 (1.5); 752 (1.1); 562 (6.5); 532 (6.2); 386 (29.5)
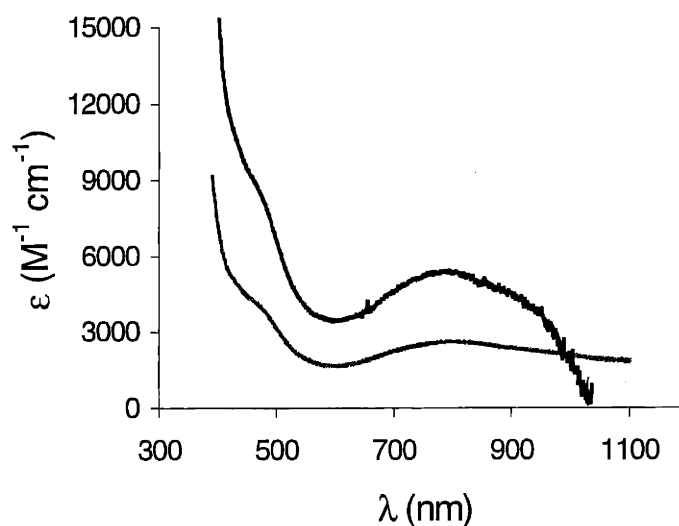
Figure 11. UV-vis absorption spectra of **1b-(bipy)₂** (---) and **2a-bipy** (—)toluene solutions at 25 °C.

3.2.6. Conclusions

The bipyridyl compounds discussed in this chapter include *bis-* and *tris*-amidouranium complexes, such as **1b-(bipy)₂** and **2a-bipy**, and *tris*-ketimidouranium complexes, such as **3-(bipy)₂** and **3-I-bipy**. Their X-ray crystal structures indicate the presence of bipy coordinated as a radical anion in **1b-(bipy)₂** and **2a-bipy** leading to uranium(IV) centers, and as a neutral ligand in **3-I-bipy**, where uranium already possesses the +4 oxidation state. In **3-(bipy)₂**, the crystallographic parameters indicate that one bipy is coordinated as a radical anion, while the other is coordinated as a neutral ligand. These findings are not surprising since the +4 oxidation state is often encountered in the organometallic chemistry of uranium. The radical anion character is corroborated by exchange studies, monitored by ^{1}H NMR spectroscopy, and by absorption spectroscopy (for **1b-(bipy)₂** and **2a-bipy**). The investigation of solid-state magnetic properties did not offer straightforward conclusions due to the difficulty in modeling or interpreting these properties. The fact that bipy coordinates as a radical anion in **2a-bipy**, but dmb coordinates as a neutral ligand in (dmb)U(C₅Me₅)(C₈H₈) indicates that the *tris*-amido uranium fragment is more reducing than the U(C₅Me₅)(C₈H₈) with respect to their effect on the coordination of bipy.

3.3. Experimental

3.3.1. General considerations

Unless stated otherwise, all operations were performed in a Vacuum Atmospheres drybox under an atmosphere of purified nitrogen or using Schlenk techniques under an argon atmosphere. Anhydrous diethyl ether was purchased from Mallinckrodt; pentane, *n*-hexane and tetrahydrofuran were purchased from EM Science. Diethyl ether, toluene, benzene, pentane and *n*-hexane were dried and deoxygenated by the method of Grubbs.[25] THF was distilled under nitrogen from purple sodium benzophenone ketyl. Distilled solvents were transferred under

vacuum into bombs before being pumped into a Vacuum Atmospheres dry box. C_6D_6 and toluene-d_8 were purchased from Cambridge Isotopes and were degassed and dried over 4 Å sieves. 4 Å sieves, alumina and Celite were dried *in vacuo* overnight at a temperature just above 200 °C. 2,2'-Bipyridine and 4,4'-dimethyl-2,2'-bipyridine were dissolved into diethyl ether and THF, respectively, and their solutions passed through alumina. The crystalline solids obtained from the concentrated solutions at –35 °C were extensively dried under vacuum (6-12 h) before use. Other chemicals were used as received. ^1H and ^2H NMR spectra were recorded on Varian XL-300 or Varian INOVA-501 spectrometers at room temperature unless otherwise specified. Chemical shifts are reported with respect to internal or external solvent, 7.16 ppm (C_6D_6). UV-vis spectra were recorded on a HP spectrophotometer from 200 to 1100 nm using matched 1 cm quartz cells; NIR spectra were recorded on an Aviv 14DS spectrophotometer from 800 to 1500 nm using matched 1 cm quartz cells; all spectra were obtained using a solvent reference blank. Numerical modeling of all data was done using the program Origin 6.0. CHN analyses were performed by H. Kolbe Mikroanalytisches Laboratorium (Mülheim an der Ruhr, Germany).

3.3.2.1.a. Synthesis of 1b-(bipy)₂

1b₂-μ-toluene (0.253 g, 0.199 mmol) and bipy (0.124 g, 0.794 mmol, 4 equiv) were dissolved each in 5 mL of toluene and the two solutions were frozen. The thawing bipy solution was added dropwise to the stirring thawing solution of **1b₂-μ-toluene**. After 35 min, volatiles were removed under vacuum, the product mixture was extracted with 20 mL of pentane and the solution filtered through Celite. The solvent was removed again and the extraction in pentane repeated. After filtration through Celite and concentration to 10 mL, 0.211 g (0.234 mmol) of the desired product, **1b-(bipy)₂**, (59% yield) was obtained as dark brown crystals from cooling the above solution to -35 °C (after three days). A second crop was obtained after ca. two weeks from concentrating the solution decanted from the crystals and cooling it to -35 °C (0.044 g, 0.049 mmol, total yield of 71%).

^{1}H NMR (300 MHz, C_6D_6, 22 °C): δ = 41.76 (s, 2H, *bipy*);* 11.43 (s, 1H, *p*-Ar); 11.27 (s, 9H, *t*-*Bu*); 3.80 (s, 2H, *o*-Ar); -0.35 (s, 1H, *bipy*);* -3.42 (s, 6H, *Me*-Ar); -23.22 (s, 2H, 4,4'-*bipy*); -28.57 (s, 2H, *bipy*).

UV-vis (toluene, 22 °C): λ_{max} (nm, ε × 10^{-2} M^{-1}, cm^{-1}) = 285 (387.9 ± 13.5); 370 (150.7 ± 12.3); 415 (71.8 ± 5.3); 470 (51.1 ± 3.7); 790 (32.3 ± 2.4).

Anal. calcd. for $C_{44}H_{52}N_6U$: C, 58.47; H, 5.76; N, 9.30. Found: C, 58.55; H, 5.92; N, 9.36.

3.3.2.1.b. Synthesis of 1b-(dmb)₂

Similar procedure as for **1b-(bipy)₂**, using 4,4'-dimethyl-2,2'-bipyridyl (dmb) instead of bipy. Yield: 53%.

^{1}H NMR (300 MHz, C_6D_6, 22 °C): δ = 39.10 (s, 2H, *bipy*);* 28.33 (s, 6H, C*H₃*-bipy); 11.45 (s, 9H, *t-Bu*); 11.26 (s, 1H, *p*-Ar); -0.60 (s, 2H, *bipy*);* -2.11 (s, 2H, *o*-Ar); -3.39 (s, 6H, *Me*-Ar); -38.17 (s, 2H, *bipy*).

Anal. calcd. for $C_{48}H_{60}N_6U$: C, 60.06; H, 6.26; N, 8.76. Found: C, 59.85; H, 6.25; N, 8.70.

3.3.2.2. Synthesis of 2a-bipy

2a-THF (0.136 g, 0.12 mmol) and bipy (0.019 g, 0.12 mmol, 1 equiv) were dissolved each in 3 mL of diethyl ether and the two solutions were frozen. The thawing bipy solution was added dropwise to the stirring thawing solution of **2a-THF**. After 1 h, volatiles were removed under vacuum, the product mixture was extracted with 10 mL of pentane and the solution filtered through Celite. The solvent was removed again and the extraction in pentane repeated. After filtration through Celite and concentration to 3 mL, 0.103 g (0.09 mmol) of the desired product, **2a-bipy**, (73% yield) was obtained as dark brown crystals from cooling the above solution to -35 °C (after five days).

^{1}H NMR (500 MHz, C$_7$D$_8$, 80 °C): δ = 60.39 (s, 1H, *p*-Ar); 7.82 (s, 2H, *o*-Ar); -0.31 (s, 3H, Ad distal CH_2); -0.74 (s, 3H, Ad distal CH_2); -0.94 (s, 6H, Ad proximal CH_2); -1.65 (s, 3H, Ad CH); -9.13 (s, 6H, *Me*-Ar).

UV-vis (toluene, 22 °C): λ$_{max}$ (nm, ε × 10^{-2} M^{-1}, cm^{-1}) = 285 (304.3 ± 25.9); 388 (107.7 ± 13.7); 426 (48.7 ± 9.2); 482 (33.0 ± 7.7); 850 (17.8 ± 5.7).

Anal. calcd. for C$_{64}$H$_{80}$N$_5$U: C, 66.41; H, 6.97; N, 6.05. Found: C, 66.33; H, 6.76; N, 6.45.

3.3.2.3. Synthesis of 3-(bipy)$_2$

Na$_2$-3$_2$-μ-biphenyl (0.115 g, 0.06 mmol) and bipy (0.038 g, 0.24 mmol, 4 equiv) were dissolved each in 3 mL of pentane and the two solutions were frozen. The thawing bipy solution was added dropwise to the stirring thawing solution of **Na$_2$-3$_2$-μ-biphenyl**. After 0.5 h, volatiles were removed under vacuum, the product mixture was extracted with 10 mL of pentane and the solution filtered through Celite. The solvent was removed again and the extraction in pentane repeated. After filtration through Celite and concentration to 3 mL, 0.043 g (0.09 mmol) of the desired product, **3-(bipy)$_2$**, (31% yield) was obtained as dark brown crystals from cooling the above solution to -35 °C (after six days).

^{1}H NMR (500 MHz, C$_7$D$_8$, 80 °C): δ = 19.86 (s), 11.82 (s), 8.68 (s), 8.23 (s), 7.45 (s), 6.71 (s), 6.22 (s), 1.87 (s), -3.14 (s), -3.36 (s).

UV-vis (toluene, 22 °C): λ$_{max}$ (nm, ε × 10^{-2} M^{-1}, cm^{-1}) = 476 (2.8); 423 (4.1); 376 (6.4); 285 (34.4).

Anal. calcd. for C$_{62}$H$_{76}$N$_7$U: C, 64.37; H, 6.57; N, 8.48. Found: C, 64.36; H, 6.75; N, 7.63.

3.3.2.4. Synthesis of 3-I-bipy

Diethyl ether solutions of IU(DME)(NC[*t*-Bu]Mes)$_3$ (1.220 g, 1.149 mmol, 40 mL) and of bipy (0.179 g, 1.149 mmol, 1 equiv, 12 mL) were frozen. The thawing bipy solution was added

dropwise to the thawing and stirring uranium solutin and the reaction mixture let to warm to room temperature. After 2 h the volatiles were removed, 10 mL of pentane added to the solid obtained and the slurry filtered. The solid was dried under reduced pressure and it amounted to 1.140 g of **3-I-bipy** (1.011 mmol, 88% yield).

^{1}H NMR (300 MHz, C_6D_6, 80 °C): δ = 44.60 (s), 20.50 (s), 15.34 (s), 7.50 (s), -3.21 (s), -16.80 (s), -19.25 (s).

UV-vis (toluene, 22 °C): λ_{max} (nm, ε × 10^{-2} M^{-1}, cm^{-1}) = 307 (123.8 ± 14.9); 413 (26.8 ± 1.1); 685 (5.9 ± 0.1).

Anal. calcd. for $C_{52}H_{68}N_5IU$: C, 55.37; H, 6.08; N, 6.21. Found: C, 55.18; H, 5.54; N, 5.74.

3.3.2.5. Exchange of coordinated bipy with free bipy or dmb

Solutions in C_6D_6 of uranium compounds and free bipy (not exact amounts) were loaded into an NMR tube and their ^{1}H NMR spectra recorded. For the exchange with dmb, ca. 0.01 mmol of uranium compound and stoichiometric amounts of dmb (1 or 2 equiv, depending on the number of coordinated bipy molecules) were dissolved in C_6D_6 or toluene-d_8, and the solutions transferred to an air-free NMR tube. Spectra of these solutions were recorded periodically, as specified in the text of the paper. The peaks that were monitored in the case of **1a-(bipy)$_2$** and **1a-(dmb)$_2$** are indicated in the description of their ^{1}H NMR spectra by *.

3.3.3. X-ray crystal structures

3.3.3.1. General considerations

The X-ray data collections were carried out on a Siemens Platform three-circle goniometer with a CCD detector using Mo-K_α radiation (λ = 0.71073 Å). The data were processed utilizing the

program SAINT supplied by Siemens Industrial Automation, Inc. The structures were solved by direct methods (SHELXTL v5.03, Sheldrick, G. M., and Siemens Industrial Automation, Inc., 1995) in conjunction with standard difference Fourier techniques.

3.3.3.2. X-ray crystal structure of 1b-(bipy)₂

Crystals of **1b-(bipy)₂** grown from a concentrated diethyl ether solution at -35 °C were coated with Paratone N oil (an Exxon product) on a microscope slide. A dark green plate of approximate dimensions 0.28 x 0.23 x 0.11 mm³ was selected and mounted with wax on a glass fiber. A total of 16300 reflections ($-11 \leq h \leq 11$, $-12 \leq k \leq 12$, $-21 \leq l \leq 12$) were collected at 173(2) K in the θ range of 2.41 to 23.26 °, of which 5904 were unique (R_{int} = 0.0314). The structure was solved by Patterson methods (SHELXTL V5.0, G. M. Sheldrick and Siemens Industrial Automation, Inc., 1995) in conjunction with standard difference Fourier techniques. All non-hydrogen atoms were refined anisotropically and hydrogen atoms were placed in calculated (d_{CH} = 0.96 Å) positions except for the solvent atoms. The unit cell contains half of a molecule of diethyl ether as crystallization solvent. C1S of the solvent molecule has been modeled into C1S and C1S' each with ½ occupancies. The residual peak and hole electron density were 1.045 and -1.486 e · Å⁻³, in the typical range due to the scattering effect of the large uranium nucleus. A semi-empirical absorption correction was applied based on pseudo-psi-scans with maximum and minimum transmission equal to 0.6734 and 0.4079, respectively. The least squares refinement converged normally with residuals of (all data) R_1 = 0.0310, wR_2 =0.0727 based on I > 2σ(I), and GOF = 1.086 (based on F^2). No extinction coefficient was applied to the refinement.

Crystal and refinement data: formula $C_{46}H_{52}N_6UO_{0.5}$, space group P-1, a = 10.2945(7) Å, b = 11.0569(7) Å, c = 19.0658(12) Å, α = 76.2790(10) °, β = 85.6930(10) °, γ = 86.8400(10) °, V = 2100.7(2) Å³, Z = 2, D_{calc} = 1.478 g·cm⁻³, $F(000)$ = 932, R_1 (based on F) = 0.0282, and wR_2 (based on F^2) = 0.0714.

3.3.3.3. X-ray crystal structure of 2a-bipy

Inside the glove box, crystals of **2a-bipy** grown from a concentrated pentane solution at -35 °C were coated with Paratone N oil (an Exxon product) on a microscope slide. An orange brown plate of approximate dimensions 0.07 x 0.04 x 0.02 mm^3 was selected and mounted with wax on a glass fiber. A total of 12729 reflections ($-14 \leq h \leq 13$, $-14 \leq k \leq 14$, $-23 \leq l \leq 23$) were collected at 173(2) K in the θ range of 2.07 to 23.30 °, of which 8818 were unique (R_{int} = 0.0703). The structure was solved by Patterson methods (SHELXTL V5.0, G. M. Sheldrick and Siemens Industrial Automation, Inc., 1995) in conjunction with standard difference Fourier techniques. All non-hydrogen atoms were refined anisotropically. The unit cell contains one and a half molecules of pentane as crystallization solvent. C3S lies in the inversion center. Most hydrogen atoms were found in the electronic density map and the remaining ones were placed in calculated (d_{CH} = 0.96 Å) positions, except for C3S. The residual peak and hole electron density were 2.629 and -2.606 e · Å^{-3}, in the typical range due to the scattering effect of the large uranium nucleus. A semi-empirical absorption correction was applied based on pseudo-psi-scans with maximum and minimum transmission equal to 0.9491 and 0.8368, respectively. The least squares refinement converged normally with residuals of (all data) R_1 = 0.0686, wR_2 =0.1526 based on I > 2σ(I), and GOF = 1.086 (based on F^2). No extinction coefficient was applied to the refinement.

Crystal and refinement data: formula $C_{71.5}H_{97}N_5U$, space group P-1, a = 12.7236(15) Å, b = 13.1198(16) Å, c = 21.535(3) Å, α = 96.427(2) °, β = 103.920(2) °, γ = 112.905(2) °, V = 3128.1(7) Å^3, Z = 2, D_{calc} = 1.343 g·cm^{-3}, μ = 2.639 mm^{-1}, $F(000)$ = 1306, R_1 (based on F) = 0.0609, and wR_2 (based on F^2) = 0.1479.

3.3.3.4. X-ray crystal structure of 3-(bipy)₂

Inside the glove box, crystals of **3-(bipy)₂**, obtained from a saturated pentane solution at –35 °C were coated with Paratone N oil (an Exxon product) on a microscope slide. A dark brown prism

of approximate dimensions 0.55 x 0.10 x 0.06 mm^3 was selected and mounted with wax on a glass fiber. A total of 28057 reflections (-17 ≤ h ≤ 16, -13 ≤ k ≤ 19, -28 ≤ l ≤ 28) were collected at 183(2) K in the θ range of 2.50 to 23.32 °, of which 10025 were unique (R_{int} = 0.0499). The structure was solved by direct methods (SHELXTL V5.10, G. M. Sheldrick and Siemens Industrial Automation, Inc., 1997) in conjunction with standard difference Fourier techniques. The unit cell contains a molecule of pentane as crystallization solvent. The carbon atoms of the solvent molecule were disordered and the disorder modeled over two sites for C2S, C4S, and C5S. These atoms were not refined anisotropically and no hydrogen atoms were added to them. All the other non-hydrogen atoms were refined anisotropically. One of the *t*-butyl groups was disordered and the disorder was modeled over two sites: C19A and C19B, C11A and C11B, C11C and C11D. All these atoms were refined anisotropically. Some hydrogen atoms were found in the electronic density map and refined isotropically. The rest of the hydrogen atoms were placed in calculated (d_{C-H} = 0.96 Å) positions. The residual peak and hole electron density were 0.972 and -0.708 e·Å^{-3}, respectively and these values are in the normal range due to the large scattering effect of uranium centers. A semi-empirical absorption correction was applied based on pseudo-psi-scans with maximum and minimum transmission equal to 0.8711 and 0.3561, respectively. The least squares refinement converged normally with residuals of R_1 = 0.0385, wR_2 = 0.1233 based upon I > 2σ(I), and GOF = 1.065 (based on F^2). No extinction coefficient was applied to the refinement.

Crystal and refinement data: formula $C_{67}H_{67}N_7U$, space group P2(1)/n, a = 15.989(2) Å, b = 17.137(2) Å, c = 25.732(4) Å, α = 90.0 °, β = 98.460(2) °, γ = 90.0 °, V = 6973.8(17) Å^3, Z = 4, μ = 2.366 mm^{-1}, D_{calc} = 1.151 g·cm^{-3}, $F(000)$ = 2440, R_1 (based on F) = 0.0538, and wR_2 (based on F^2) = 0.1335.

3.3.3.5. X-ray crystal structure of 3-I-bipy

Inside the glove box, crystals of **3-I-bipy**, obtained from a saturated diethyl ether solution at –35 °C were coated with Paratone N oil (an Exxon product) on a microscope slide. A dark brown

prism of approximate dimensions 0.37 x 0.35 x 0.28 mm^3 was selected and mounted with wax on a glass fiber. A total of 21176 reflections ($-13 \leq h \leq 14$, $-23 \leq k \leq 22$, $-21 \leq 1 \leq 21$) were collected at 183(2) K in the θ range of 2.29 to 23.27 °, of which 7764 were unique (R_{int} = 0.0318). The structure was solved by direct methods (SHELXTL V5.10, G. M. Sheldrick and Siemens Industrial Automation, Inc., 1997) in conjunction with standard difference Fourier techniques. All non-hydrogen atoms were refined anisotropically and hydrogen atoms were placed in calculated (d_{C-H} = 0.96 Å) positions. The residual peak and hole electron density were 2.179 and -0.550 e·Å^{-3}, respectively and these values are in the normal range due to the large scattering effect of uranium centers. A semi-empirical absorption correction was applied based on pseudo-psi-scans with maximum and minimum transmission equal to 0.3528 and 0.2075, respectively. The least squares refinement converged normally with residuals of R_1 = 0.0321, wR_2 = 0.1069 based upon I > 2σ(I), and GOF = 1.062 (based on F^2). No extinction coefficient was applied to the refinement.

Crystal and refinement data: formula $C_{52}H_{68}N_5UI$, space group P2(1)/c, a = 12.987(3) Å, b = 21.245(4) Å, c = 25.732(4) Å, α = 90.0 °, β = 97.038(3) °, γ = 90.0 °, V = 5410.9(18) Å^3, Z = 4, μ = 3.605 mm^{-1}, D_{calc} = 1.385 g·cm^{-3}, $F(000)$ = 2240, R_1 (based on F) = 0.0414, and wR_2 (based on F^2) = 0.1135.

3.3.4. Susceptibility measurements

Magnetic susceptibility measurements were recorded using a SQUID magnetometer at 5000 G. The samples were prepared in the glove box (50 – 100 mg) loaded in a gelatin capsule that was positioned inside a plastic straw and carried to the magnetometer in a tube under N_2. The sample was quickly inserted into the instrument, centered and data obtained from 5 to 300 K. The contribution from the sample holders was not accounted for. The diamagnetic contributions were calculated and subtracted from χ_{mol}. Effective magnetic moments were calculated either by linear regression from plots of $1/\chi_{mol}$ versus T (K) for Curie-Weiss behavior or by using the formula 2.828*sqrt(T* χ_{mol}) for non-Curie-Weiss behavior. Samples used were multiply times recrystallized. Measurements for the same compound were carried out on different recrystallized samples.

[1] McWhinnie, W. R.; Miller, J. D. *Adv. Inorg. Chem. Radiochem.* **1969**, *12*, 135.

[2] Hanazaki, I.; Nagakura, S. *Bull. Chem. Soc. Jpn.* **1971**, *44*, 2312.

[3] Schultz, M.; Boncella, J. M.; Berg, D. J.; Tilley, T. D.; Andersen, R. A. *Organometallics* **2002**, *21*, 460.

[4] Fedushkin, I. L.; Petrovskaya, T. V.; Girgsdies, F.; Köhn, R. D.; Bochkarev, M. N.; Schumann, H. *Angew. Chem., Int. Ed.* **1999**, *38*, 2262.

[5] Evans, W. J.; Drummond, D. K. *J. Am. Chem. Soc.* **1989**, *111*, 3329.

[6] Feistel, G. R.; Mathai, T. P. *J. Am. Chem. Soc.* **1968**, *90*, 2988.

[7] Wiley, R. O.; von Dreele, R. B.; Brown, T. M. *Inorg. Chem.* **1980**, *19*, 3351.

[8] Del Piero, G.; Perego, G.; Zazzetta, A.; Brandi, G. *Cryst. Struct. Comm.* **1975**, *4*, 521.

[9] Rivière, C.; Nierlich, M.; Ephritikhine, M.; Madic, C. *Inorg. Chem.* **2001**, *40*, 4428.

[10] Schake, A. R.; Avens, L. R.; Burns, C. J.; Clark, D. L.; Sattelberger, A. P.; Smith, W. H. *Organometallics* **1993**, *12*, 1497.

[11] Arnaudet, L.; Bougon, R.; Buu, B.; Lance, M.; Nierlich, M.; Vigner, J. *Inorg. Chem.* **1994**, *33*, 4510.

[12] Alcock, N. W.; Flanders, D. J.; Brown, D. *J. Chem. Soc., Dalton Trans.* **1985**, *5*, 1001.

[13] Deacon, G. B.; Mackinnon, P. I.; Taylor, J. C. *Polyhedron* **1985**, *4*, 103.

[14] Chisholm, M. H.; Huffman, J. C.; Rothwell, I. P.; Bradley, P. G.; Kress, N.; Woodruff, W. H. *J. Am. Chem. Soc.* **1981**, *103*, 4945.

[15] Diaconescu, P. L.; Arnold, P. L.; Baker, T. A.; Mindiola, D. J.; Cummins, C. C. *J. Am. Chem. Soc.* **2000**, *122*, 6108.

[16] Diaconescu, P. L.; Cummins, C. C. *J. Am. Chem. Soc.* **2002**, *124*, 7660.

[17] Roesky, H. W.; Andruh, M. *Coordin. Chem. Rev.* **2003**, *236*, 91.

[18] Edelmann, F. T.; Lorenz V. *Coordin. Chem. Rev.* **2000**, *209*, 99.

[19] Diaconescu, P. L.; Lukens, W. W.; Cummins, C. C. *submitted.*

[20] Kahn, O. *Molecular magnetism*; VCH Publishers: New York, 1993.

[21] Edelstein, N. *Electronic structure and optical spectroscopy of f^n ions and compounds*; Marks, T. J.; Fragala, I. L., Eds.; D Reidel Publishing Company: Dordrecht, Netherlands, 1984, 229.

[22] Kanellakopulos, B. in *Organometallics of the f-Elements*, Marks, T. J.; Fischer, R. D. Eds., Reidel, Dordrecht, 1979,1.

[23] Lukens, W. W.; Beshouri, S. M.; Blosch, L. L.; Stuart, A. L.; Andersen, R. A. *Organometallics* **1999**, *18*, 1235.

[24] Bochkarev, M. N.; Fedushkin, I. L.; Nevodchikov, V. I.; Cherkasov, V. K.; Schumann, H.; Hemling, H. Weimann, R. *J. Organomet. Chem.* **1996**, *524*, 125.

[25] Pangborn, A. B.; Giardello, M. A.; Grubbs, R. H.; Rosen, R. K.; Timmers, F. J. *Organometallics* **1996**, *15*, 1518.

Appendix 1: Tables for X-ray Crystal Structures

Chapter 1

A.1.1. X-ray crystal structure of 2a-THF

Atomic coordinates (x 10^4) and equivalent isotropic displacement parameters (Å^2x 10^3) for 2a-THF. U(eq) is defined as one third of the trace of the orthogonalized U^{ij} tensor.

	x	y	z	U(eq)
U(1)	1204(1)	3546(1)	1150(1)	27(1)
N(1)	1174(1)	3638(5)	2079(3)	33(1)
C(29)	1702(2)	1323(6)	2092(3)	35(2)
C(31)	584(1)	3627(6)	27(3)	26(1)
C(37)	682(2)	1499(5)	19(3)	29(2)
C(21)	1729(2)	2982(6)	777(3)	30(2)
N(2)	1657(1)	2555(5)	1237(3)	32(1)
N(3)	761(1)	2638(4)	327(2)	28(1)
C(36)	530(1)	4413(6)	413(3)	30(2)
C(110)	859(2)	1925(6)	1926(3)	34(2)
C(35)	386(2)	5483(6)	202(3)	32(2)
C(22)	1471(2)	3290(6)	179(3)	34(2)
C(32)	476(2)	3990(6)	-610(3)	32(2)
C(25)	2076(2)	3699(6)	368(3)	37(2)
C(351)	335(2)	6274(6)	642(4)	39(2)
C(34)	283(2)	5779(6)	-430(3)	34(2)
C(216)	2052(2)	-406(6)	2459(4)	46(2)
C(210)	2027(2)	855(6)	1581(3)	35(2)
C(27)	1887(2)	1865(6)	1783(3)	30(2)
C(18)	740(2)	3703(6)	2359(3)	33(2)
C(114)	778(2)	2551(6)	3279(3)	41(2)
C(211)	2245(2)	108(7)	2167(4)	45(2)
C(23)	1509(2)	3811(6)	-302(3)	41(2)
C(33)	326(2)	5031(6)	-831(3)	37(2)
C(19)	1228(2)	2565(6)	3040(3)	33(2)
C(214)	2179(2)	1309(7)	3170(3)	48(2)

Appendix 1

C(215)	1910(2)	568(7)	2668(4)	46(2)
C(15)	1845(2)	5576(8)	3149(3)	45(2)
C(28)	2157(2)	2586(6)	2309(3)	35(2)
C(11)	1347(2)	4642(6)	2392(3)	34(2)
C(14)	1703(2)	6640(8)	2937(4)	56(2)
C(113)	552(2)	2961(7)	2601(3)	38(2)
C(16)	1664(2)	4587(7)	2874(3)	38(2)
C(24)	1813(2)	4013(7)	-203(4)	43(2)
C(17)	1007(2)	2976(6)	2350(3)	30(2)
C(151)	2190(2)	5469(10)	3640(4)	71(3)
C(213)	2371(2)	1832(7)	2889(3)	45(2)
C(251)	2406(2)	3869(7)	465(4)	46(2)
C(26)	2036(2)	3196(6)	851(3)	34(2)
C(212)	2513(2)	859(7)	2668(4)	53(2)
C(13)	1388(2)	6752(7)	2465(5)	57(2)
C(331)	207(2)	5358(8)	-1526(4)	58(2)
C(115)	1043(2)	1825(6)	3280(3)	41(2)
C(12)	1211(2)	5741(6)	2201(4)	41(2)
C(231)	1221(2)	4077(9)	-945(4)	66(3)
C(112)	411(2)	1916(7)	2168(4)	47(2)
C(116)	901(2)	765(7)	2840(4)	48(2)
C(111)	672(2)	1181(6)	2171(4)	46(2)
C(315)	675(3)	60(7)	-783(4)	65(3)
C(39)	754(3)	1308(7)	-528(5)	68(3)
C(316)	878(2)	-768(7)	-266(5)	67(3)
C(131)	1232(3)	7935(8)	2209(6)	87(4)
C(314)	342(3)	-186(10)	-1025(6)	122(6)
C(38)	341(2)	1212(9)	-219(7)	109(5)
C(311)	809(5)	-628(9)	278(5)	125(7)
C(310)	886(3)	630(7)	532(4)	108(5)
C(313)	266(3)	-16(12)	-506(12)	157(9)
C(312)	452(7)	-843(12)	21(12)	197(13)
O(1)	1323(1)	5515(4)	911(2)	40(1)
C(444)	1159(2)	6157(6)	325(4)	49(2)
C(441)	1645(2)	5922(8)	1290(4)	56(2)
O(2)	0	2569(11)	-2500	147(6)
C(443)	1419(2)	6716(8)	240(5)	68(3)
C(353)	225(3)	2130(13)	-2562(7)	114(4)
O(3)	1849(3)	9155(12)	-397(7)	192(7)
C(442)	1677(3)	6885(13)	926(6)	122(5)
C(464)	2056(3)	7294(14)	-219(8)	131(5)
C(462)	1820(4)	10335(13)	-260(8)	122(5)

C(463)	2040(5)	8536(18)	-48(12)	188(10)
C(461)	1655(4)	10950(13)	-848(8)	153(7)
C(354)	453(5)	2657(18)	-2624(12)	226(12)

A.1.2. X-ray crystal structure of 2a-I

Atomic coordinates (x 10^4) and equivalent isotropic displacement parameters (Å^2x 10^3) for **2a-I**. U(eq) is defined as one third of the trace of the orthogonalized U^{ij} tensor.

	x	y	z	U(eq)
U(1)	9066(1)	3733(1)	3051(1)	24(1)
N(1)	8554(5)	5565(4)	3200(2)	30(1)
I	7978(1)	3027(1)	4350(1)	39(1)
N(2)	8150(5)	3961(4)	2220(2)	31(1)
N(3)	11190(5)	2592(4)	2778(2)	30(1)
C(11)	9801(6)	5620(5)	3260(3)	30(1)
C(12)	10480(6)	6126(5)	2785(3)	35(1)
C(13)	11722(7)	6122(6)	2834(4)	47(2)
C(14)	12282(7)	5581(7)	3365(4)	52(2)
C(15)	11642(7)	5082(6)	3841(3)	45(2)
C(16)	10397(7)	5099(6)	3784(3)	37(2)
C(17)	7260(6)	6541(5)	3408(3)	27(1)
C(18)	7128(7)	6668(6)	4080(3)	36(2)
C(19)	6115(6)	6221(6)	3324(3)	34(1)
C(21)	7833(6)	2947(5)	2383(3)	30(1)
C(22)	8582(7)	1884(6)	2115(3)	39(2)
C(23)	8376(8)	849(6)	2349(4)	47(2)
C(24)	7438(7)	871(6)	2869(3)	44(2)
C(25)	6696(7)	1888(6)	3143(3)	40(2)
C(26)	6882(6)	2936(6)	2889(3)	34(1)
C(27)	7712(6)	4760(6)	1656(3)	31(1)
C(28)	8342(7)	4126(6)	1079(3)	39(2)
C(29)	8133(6)	5796(6)	1606(3)	35(1)
C(31)	11400(6)	1692(5)	3294(3)	33(1)
C(32)	11906(6)	1777(6)	3791(3)	36(2)
C(33)	11940(7)	997(6)	4319(3)	41(2)
C(34)	11443(7)	136(6)	4344(3)	43(2)

Appendix 1

C(35)	10935(7)	16(6)	3859(3)	43(2)
C(36)	10906(6)	808(6)	3337(3)	36(2)
C(37)	12313(6)	2449(5)	2277(3)	32(1)
C(38)	12798(7)	1250(6)	2028(3)	39(2)
C(39)	13529(7)	2539(7)	2463(3)	42(2)
C(110)	7099(6)	7751(5)	3038(3)	32(1)
C(111)	5722(6)	8698(5)	3250(3)	37(2)
C(112)	5605(7)	8815(6)	3920(3)	41(2)
C(113)	5755(7)	7617(6)	4289(3)	40(2)
C(114)	4624(7)	7282(6)	4195(3)	47(2)
C(115)	4731(7)	7189(6)	3526(3)	41(2)
C(116)	4594(7)	8370(6)	3155(3)	42(2)
C(131)	12449(9)	6668(9)	2319(5)	77(3)
C(151)	12229(9)	4562(8)	4430(4)	67(2)
C(210)	6168(6)	5262(6)	1690(3)	41(2)
C(211)	5696(7)	6144(7)	1129(3)	54(2)
C(212)	6340(8)	5511(8)	563(3)	54(2)
C(213)	7880(7)	5025(7)	512(3)	47(2)
C(214)	8318(7)	6043(7)	488(3)	49(2)
C(215)	7671(7)	6679(6)	1050(3)	42(2)
C(216)	6131(8)	7165(7)	1102(3)	53(2)
C(231)	9172(10)	-284(8)	2057(5)	77(3)
C(251)	5675(8)	1915(8)	3701(4)	58(2)
C(310)	11768(6)	3457(6)	1772(3)	35(1)
C(311)	12866(7)	3368(6)	1224(3)	43(2)
C(312)	13317(8)	2178(7)	983(3)	51(2)
C(313)	13915(7)	1165(7)	1476(3)	49(2)
C(314)	15101(7)	1260(8)	1671(3)	62(2)
C(315)	14630(7)	2445(8)	1911(3)	58(2)
C(316)	14061(8)	3454(8)	1417(3)	55(2)
C(331)	12487(9)	1101(8)	4861(3)	59(2)
C(351)	10409(9)	-932(7)	3894(4)	63(2)
C(1S)	8040(30)	2600(30)	-415(13)	230(11)
C(2S)	7150(20)	-150(20)	-27(10)	188(8)
C(3S)	8050(30)	1350(30)	-421(16)	255(14)
C(4S)	7320(40)	1040(30)	-67(16)	263(15)
C(5S)	9080(30)	2740(20)	-763(13)	222(11)

A.1.3. X-ray crystal structure of 2a-NSiMe₃

Atomic coordinates (x 10^4) and equivalent isotropic displacement parameters ($Å^2$x 10^3) for **2a-NSiMe₃**. U(eq) is defined as one third of the trace of the orthogonalized U^{ij} tensor.

U	-9724(1)	1274(1)	2406(1)	28(1)
Si	-6824(1)	-1251(1)	2597(1)	45(1)
N(2)	-11116(4)	966(3)	3016(2)	31(1)
N(1)	-9104(4)	2906(3)	2626(2)	32(1)
N(3)	-10046(4)	1044(4)	1557(2)	38(1)
N(4)	-8144(4)	-11(4)	2556(2)	39(1)
C(17)	-8290(5)	2992(4)	3081(2)	32(1)
C(22)	-12412(5)	3077(5)	3054(2)	42(1)
C(11)	-9450(5)	3872(4)	2197(2)	32(1)
C(314)	-9051(6)	331(5)	737(2)	40(1)
C(16)	-10693(5)	4117(4)	1977(2)	34(1)
C(111)	-7757(6)	2042(5)	4030(2)	48(1)
C(15)	-11088(5)	4960(5)	1527(2)	41(1)
C(12)	-8620(6)	4534(5)	1952(2)	41(1)
C(37)	-9466(5)	1409(4)	1060(2)	33(1)
C(13)	-9017(6)	5397(5)	1508(2)	45(1)
C(27)	-11276(5)	104(4)	3492(2)	33(1)
C(213)	-11534(6)	731(5)	3988(2)	41(1)
C(32)	-10556(5)	-842(5)	1940(2)	38(1)
C(112)	-8545(6)	2053(6)	3531(2)	44(1)
C(34)	-12435(6)	-1389(6)	1708(2)	50(2)
C(31)	-10858(5)	214(5)	1570(2)	36(1)
C(18)	-6854(5)	2643(6)	2975(2)	42(1)
C(19)	-6064(6)	2646(6)	3478(2)	51(2)
C(212)	-12386(5)	-481(5)	3404(2)	41(1)
C(312)	-8266(6)	1796(6)	1206(2)	41(1)
C(21)	-12208(4)	1970(4)	2847(2)	32(1)
C(311)	-7560(6)	2167(6)	719(2)	53(2)
C(33)	-11333(5)	-1646(5)	2022(2)	44(1)
C(23)	-13382(5)	4111(5)	2854(3)	51(2)
C(36)	-11986(5)	449(6)	1270(2)	43(1)
C(38)	-10344(6)	2507(5)	707(2)	42(1)
C(215)	-11623(5)	-214(6)	4466(2)	47(1)
C(315)	-8369(5)	711(5)	244(2)	45(1)
C(214)	-10367(7)	-1211(7)	4546(2)	56(2)
C(151)	-12433(7)	5214(7)	1310(3)	58(2)

C(110)	-6329(6)	1711(6)	3920(2)	50(2)
C(26)	-12991(5)	1906(5)	2426(2)	41(1)
C(313)	-9264(7)	1799(6)	-101(2)	50(2)
C(35)	-12766(5)	-357(6)	1330(2)	49(1)
C(14)	-10238(6)	5581(5)	1297(2)	48(2)
C(25)	-13969(5)	2923(6)	2215(2)	51(2)
C(211)	-12474(6)	-1429(6)	3885(2)	53(2)
C(28)	-10044(5)	-903(5)	3580(2)	41(1)
C(310)	-8465(7)	3256(6)	376(3)	58(2)
C(216)	-12719(6)	-788(7)	4375(2)	54(2)
C(39)	-9647(6)	2880(5)	212(2)	50(2)
C(29)	-10128(6)	-1852(5)	4059(2)	50(2)
C(210)	-11221(7)	-2433(6)	3967(3)	56(2)
C(113)	-8676(6)	4260(5)	3264(2)	43(1)
C(115)	-7872(7)	4250(6)	3759(2)	56(2)
C(316)	-7171(6)	1072(7)	407(3)	54(2)
C(351)	-13982(6)	-110(7)	992(3)	70(2)
C(24)	-14135(6)	4005(6)	2437(3)	58(2)
C(114)	-6469(7)	3921(6)	3644(3)	61(2)
C(116)	-8146(8)	3307(6)	4204(2)	61(2)
C(251)	-14798(6)	2834(7)	1757(3)	78(2)
C(131)	-8140(9)	6121(9)	1252(3)	70(2)
C(231)	-13541(7)	5310(6)	3076(3)	78(2)
C(43)	-6425(9)	-1723(9)	1929(4)	124(4)
C(331)	-10971(9)	-2784(6)	2426(3)	58(2)
C(42)	-5372(7)	-880(8)	2837(5)	129(4)
C(41)	-7156(9)	-2622(8)	2990(6)	188(8)
C(5S)	-7997(16)	-4476(13)	5356(7)	178(7)
C(1S)	-5893(15)	-1725(16)	4566(7)	192(7)
C(3S)	-6695(19)	-3602(17)	4857(10)	221(10)
C(4S)	-6970(40)	-3740(30)	5335(11)	360(30)
C(2S)	-5750(30)	-2758(16)	4759(11)	312(17)
C(6S)	-15130(50)	5510(90)	220(20)	230(30)
C(7S)	-15410(40)	6290(30)	11(14)	290(20)
C(8S)	-15780(20)	7087(17)	207(9)	229(10)

A.1.4. X-ray crystal structure of Li(OEt₂)Me₃SiNU(N[¹Ad]Ar)₃

Atomic coordinates (x 10^4) and equivalent isotropic displacement parameters (Å^2 x 10^3) for Li(OEt₂)Me₃SiNU(N[¹Ad]Ar)₃. U(eq) is defined as one third of the trace of the orthogonalized U^{ij} tensor.

	x	y	z	U(eq)
U	2563(1)	530(1)	9858(1)	24(1)
Si	1678(1)	-528(1)	10750(1)	34(1)
C(312)	3907(3)	-544(4)	11488(2)	33(1)
N(2)	2235(2)	-907(3)	9013(2)	26(1)
N(1)	2084(2)	2134(3)	9553(2)	25(1)
C(37)	4012(2)	631(3)	11391(2)	25(1)
N(3)	3649(2)	847(3)	10665(2)	24(1)
C(313)	4768(2)	819(4)	11676(2)	30(1)
C(21)	1608(2)	-657(3)	8497(2)	30(1)
C(18)	2368(3)	3701(4)	9051(3)	36(1)
C(23)	748(2)	-528(4)	7341(2)	42(1)
C(316)	5014(3)	-652(4)	12486(3)	40(1)
C(314)	5125(2)	523(4)	12418(2)	36(1)
C(28)	3041(2)	-748(3)	8506(2)	25(1)
C(27)	2757(2)	-1449(3)	8883(2)	27(1)
N(4)	2143(2)	-400(3)	10320(2)	28(1)
C(15)	2338(2)	3600(4)	11095(2)	36(1)
C(251)	21(3)	592(6)	8448(4)	57(2)
C(351)	4384(3)	4529(5)	10483(3)	43(1)
C(11)	1932(2)	2728(3)	10012(2)	27(1)
C(31)	3913(2)	1613(4)	10387(2)	26(1)
C(36)	4060(2)	2667(3)	10597(2)	26(1)
C(35)	4253(2)	3392(4)	10252(2)	29(1)
C(22)	1392(2)	-799(4)	7808(2)	33(1)
C(29)	3635(2)	-1291(4)	8456(2)	30(1)
C(115)	1568(3)	4396(4)	7934(3)	44(1)
C(311)	4269(3)	-859(4)	12226(3)	36(1)
C(16)	2454(2)	3093(4)	10600(2)	33(1)
C(310)	3990(3)	-206(4)	12617(3)	40(1)
C(212)	3332(2)	-1681(4)	9564(2)	30(1)
C(210)	4193(2)	-1525(4)	9144(3)	33(1)
C(12)	1284(3)	2896(4)	9927(3)	37(1)

C(34)	4316(2)	3076(4)	9692(2)	30(1)
C(39)	4107(3)	964(4)	12542(2)	37(1)
C(26)	1136(2)	-193(4)	8676(3)	33(1)
C(14)	1685(3)	3747(4)	10985(3)	38(1)
C(113)	1237(2)	2889(4)	8447(2)	32(1)
C(315)	4849(3)	1181(4)	12801(3)	38(1)
C(151)	2922(3)	3947(6)	11729(3)	51(2)
C(43)	2090(3)	-1349(7)	11521(3)	99(3)
C(33)	4191(2)	2045(4)	9473(2)	28(1)
C(13)	1148(2)	3399(4)	10403(3)	40(1)
C(114)	1175(3)	3368(4)	7788(2)	36(1)
C(213)	2542(2)	-2523(4)	8526(3)	30(1)
C(32)	3997(2)	1333(4)	9826(2)	29(1)
C(25)	499(2)	114(4)	8221(3)	38(1)
C(216)	3682(3)	-3267(4)	9143(3)	43(1)
C(38)	3740(3)	1276(4)	11799(2)	33(1)
C(19)	2302(3)	4180(4)	8398(3)	41(1)
C(116)	1450(3)	2571(5)	7461(3)	43(1)
C(17)	1974(2)	2672(3)	8918(2)	27(1)
C(215)	3382(3)	-2317(4)	8072(3)	39(1)
C(331)	4285(4)	1676(6)	8881(3)	46(2)
C(24)	306(3)	-68(4)	7552(3)	43(1)
C(110)	2587(3)	3410(5)	8063(3)	48(2)
C(111)	2189(3)	2378(4)	7910(2)	40(1)
C(211)	3920(2)	-2232(4)	9519(3)	35(1)
C(231)	528(4)	-768(9)	6616(3)	67(2)
C(131)	442(3)	3523(8)	10314(4)	64(2)
C(214)	3125(3)	-3038(4)	8454(3)	37(1)
C(42)	866(4)	-1230(9)	10248(4)	78(3)
C(112)	2252(3)	1912(4)	8569(3)	33(1)
C(41)	1465(8)	739(7)	11002(8)	107(4)
O(1S)	1790(2)	-3166(3)	9758(2)	67(1)
C(3S)	1145(5)	-3624(7)	9315(6)	88(3)
C(4S)	796(5)	-2940(8)	8742(6)	92(3)
C(2S)	2120(6)	-3799(7)	10330(5)	95(3)
C(1S)	2826(7)	-3415(11)	10721(7)	115(4)
Li	1973(5)	-1659(7)	9697(4)	45(2)

A.1.5. X-ray crystal structure of $1b_2$-$(\mu$-SPh$)_2$(SPh$)_2$

Atomic coordinates (x 10^4) and equivalent isotropic displacement parameters ($\mathring{A}^2$ x 10^3) for $1b_2$-$(\mu$-SPh$)_2$(SPh$)_2$. U(eq) is defined as one third of the trace of the orthogonalized U^{ij} tensor.

	x	y	z	U(eq)
U(1)	6521(1)	4436(1)	155(1)	28(1)
S(1)	5339(4)	6125(6)	285(4)	35(2)
N(1)	6566(13)	3041(16)	895(11)	33(5)
S(2)	6504(4)	3976(6)	-1231(4)	42(2)
N(2)	7694(15)	5489(19)	402(11)	42(6)
C(11)	6949(17)	2114(22)	581(15)	36(7)
C(12)	6494(17)	1612(25)	-17(14)	44(8)
C(13)	6823(19)	748(21)	-373(14)	40(7)
C(14)	7670(20)	413(28)	-93(16)	57(9)
C(15)	8135(20)	865(24)	508(16)	47(8)
C(16)	7808(15)	1747(21)	838(15)	34(7)
C(17)	6297(20)	2951(23)	1585(14)	45(8)
C(18)	6990(23)	2722(35)	2178(17)	82(13)
C(19)	5870(17)	4046(22)	1725(14)	37(7)
C(110)	5617(25)	2039(23)	1543(18)	70(11)
C(21)	8142(16)	5191(22)	1062(15)	36(7)
C(22)	7975(16)	5728(20)	1690(15)	34(7)
C(23)	8401(22)	5435(39)	2343(16)	69(11)
C(24)	9006(26)	4633(31)	2408(18)	66(11)
C(25)	9218(19)	4019(29)	1824(17)	56(10)
C(26)	8790(15)	4355(21)	1175(17)	39(7)
C(27)	8106(16)	6418(20)	16(15)	33(7)
C(28)	7432(17)	6680(23)	-631(15)	44(7)
C(29)	8278(18)	7425(20)	480(14)	39(7)
C(31)	5688(14)	7195(19)	931(16)	32(7)
C(32)	5663(19)	7059(28)	1632(14)	50(9)
C(33)	5953(19)	7925(30)	2090(17)	54(9)
C(34)	6222(20)	8878(32)	1819(21)	62(10)
C(35)	6233(18)	8991(25)	1111(19)	51(8)
C(36)	5966(16)	8154(21)	660(14)	34(7)
C(41)	7624(18)	3807(24)	-1339(15)	40(7)
C(42)	8155(18)	3053(22)	-940(14)	38(7)
C(43)	9052(18)	2931(28)	-1065(18)	56(9)
C(44)	9381(21)	3560(31)	-1576(17)	57(9)
C(45)	8842(22)	4257(24)	-1943(17)	49(8)
C(46)	8008(19)	4407(30)	-1832(16)	57(9)

C(131)	6273(22)	280(31)	-1035(19)	76(12)
C(151)	9045(22)	438(31)	787(22)	94(15)
C(210)	8929(16)	5975(21)	-199(15)	39(7)
C(231)	8230(30)	6005(46)	3025(22)	119(18)
C(251)	9908(19)	3180(32)	1892(20)	86(13)

A.1.6. X-ray crystal structure of 1b$_2$-(μ-NPh)$_2$

Atomic coordinates (x 10^4) and equivalent isotropic displacement parameters (Å^{2}x 10^3) for 1b$_2$-(μ-NPh)$_2$. U(eq) is defined as one third of the trace of the orthogonalized U^{ij} tensor.

	x	y	z	U(eq)
U(1)	9729(1)	6208(1)	196(1)	26(1)
C(1)	10376(6)	5099(5)	1619(4)	29(2)
N(1)	10278(5)	7496(4)	-426(4)	30(1)
N(2)	7996(4)	6331(4)	396(4)	27(1)
C(2)	11081(6)	5848(6)	1920(5)	36(2)
C(3)	11075(8)	6211(7)	2706(5)	53(2)
N(3)	10319(5)	4780(4)	813(3)	26(1)
C(4)	10426(9)	5827(8)	3230(6)	59(3)
C(5)	9745(8)	5103(7)	2957(5)	52(2)
C(6)	9704(7)	4734(6)	2175(5)	43(2)
C(11)	11138(6)	7840(5)	165(4)	26(2)
C(12)	10906(7)	8251(5)	895(5)	37(2)
C(13)	11720(7)	8531(6)	1514(5)	39(2)
C(14)	12779(7)	8411(6)	1374(5)	43(2)
C(15)	13046(7)	7988(6)	660(5)	42(2)
C(16)	12209(6)	7693(5)	77(5)	33(2)
C(17)	9942(6)	8081(6)	-1163(5)	35(2)
C(18)	8975(7)	7590(6)	-1620(5)	47(2)
C(19)	9648(8)	9074(6)	-906(6)	50(2)
C(21)	7971(5)	7209(5)	820(4)	27(2)
C(22)	8363(6)	7262(6)	1663(4)	31(2)
C(23)	8383(6)	8104(6)	2090(5)	38(2)
C(24)	8020(6)	8928(6)	1675(5)	39(2)
C(25)	7624(6)	8905(6)	835(5)	36(2)
C(26)	7616(6)	8044(6)	434(5)	31(2)

C(27)	6984(6)	5777(6)	290(5)	32(2)
C(28)	7257(8)	4796(7)	-1(8)	71(3)
C(29)	6518(8)	5697(7)	1105(5)	51(2)
C(110)	10818(8)	8137(7)	-1741(5)	50(2)
C(131)	11462(9)	8961(7)	2320(5)	61(3)
C(151)	14198(8)	7863(9)	520(8)	76(3)
C(210)	6156(7)	6249(7)	-349(5)	52(2)
C(231)	8770(8)	8134(7)	3010(5)	55(3)
C(251)	7214(8)	9806(6)	389(6)	52(2)

A.1.7. X-ray crystal structure of 1a$_2$-μ-Se

Atomic coordinates (x 10^4) and equivalent isotropic displacement parameters (Å^2 x 10^3 for 1a$_2$-μ-Se. U(eq) is defined as one third of the trace of the orthogonalized U^{ij} tensor.

	x	y	z	U(eq)
U	1503(1)	919(1)	1936(1)	30(1)
N(2)	202(12)	-183(11)	2453(9)	31(3)
N(3)	3443(13)	883(12)	2175(11)	40(3)
C(21)	675(15)	-959(14)	2731(12)	30(4)
C(31)	4208(15)	1592(15)	3207(12)	38(4)
C(11)	1425(18)	3007(15)	2888(13)	45(4)
N(1)	1882(16)	2727(12)	2141(11)	48(4)
C(22)	788(20)	-1729(17)	2039(14)	45(5)
C(17)	2121(22)	3411(16)	1569(14)	48(5)
C(36)	4052(15)	1127(13)	3920(11)	32(3)
C(33)	5457(20)	3350(16)	4346(15)	48(5)
C(331)	6331(22)	4545(18)	4576(20)	78(8)
C(27)	-1162(17)	-309(15)	2363(12)	39(4)
C(24)	1763(19)	-2418(16)	3193(16)	52(5)
C(26)	1147(18)	-1006(16)	3683(14)	49(5)
C(37)	4207(19)	442(17)	1708(13)	46(4)
C(35)	4651(18)	1811(17)	4883(16)	51(5)
C(16)	1888(16)	2695(15)	3701(12)	40(4)
C(34)	5358(19)	2873(17)	5126(18)	67(7)
C(110)	2853(28)	2993(19)	1071(16)	67(7)
C(15)	1420(19)	2777(16)	4432(15)	53(5)
C(14)	522(19)	3259(16)	4347(15)	51(5)

C(12)	573(21)	3523(16)	2893(15)	56(6)
C(210)	-1426(16)	554(16)	2061(13)	41(4)
C(23)	1331(22)	-2457(20)	2259(15)	60(6)
C(13)	140(21)	3642(19)	3595(19)	72(8)
C(25)	1628(19)	-1712(17)	3898(15)	46(5)
C(19)	926(24)	3378(20)	814(15)	63(6)
C(310)	4769(23)	-275(19)	2272(15)	56(5)
C(32)	4938(16)	2679(14)	3484(13)	42(4)
C(151)	1891(25)	2396(21)	5236(14)	61(6)
C(251)	2157(24)	-1754(24)	4934(17)	75(7)
C(39)	3222(24)	-298(24)	719(17)	79(8)
C(18)	3023(30)	4641(18)	2229(17)	78(8)
C(29)	-1291(23)	-262(23)	3319(17)	67(6)
C(28)	-2147(23)	-1391(21)	1577(26)	104(12)
C(38)	5369(27)	1384(27)	1717(23)	89(10)
C(231)	1440(28)	-3249(23)	1537(18)	82(9)
C(131)	-856(32)	4146(33)	3564(31)	168(24)
Se	0	0	0	44(1)
C(351)	4556(23)	1299(20)	5687(14)	61(6)

Chapter 2

A.1.8. X-ray crystal structure of IU(DME)(NC[^{t}Bu]Mes)₃ (3-I-DME)

Atomic coordinates (x 10^4) and equivalent isotropic displacement parameters (Å^2 x 10^3) for **3-I-DME**. U(eq) is defined as one third of the trace of the orthogonalized U^{ij} tensor.

	x	y	z	U(eq)
U	-9475(1)	-1477(1)	-8407(1)	32(1)
I	-12462(1)	-1257(1)	-9890(1)	59(1)
C(4S)	-6180(30)	-1945(14)	-6964(19)	105(10)
N(2)	-9619(14)	-1411(6)	-6572(10)	45(3)
N(3)	-9924(16)	-2306(5)	-8450(12)	44(3)
N(1)	-8837(16)	-667(5)	-8542(13)	49(3)
C(1S)	-8630(20)	-1349(7)	-11313(14)	61(6)
O(1)	-8149(11)	-1616(4)	-10221(9)	47(3)
C(21)	-9727(16)	-1446(10)	-5494(12)	50(3)
C(151)	-9770(30)	57(10)	-11150(20)	80(7)
C(14)	-7542(19)	-84(5)	-9700(16)	48(4)
C(31)	-10285(18)	-2758(6)	-8843(15)	48(4)
C(13)	-5941(19)	-125(6)	-9418(19)	57(5)
C(22)	-8397(17)	-1657(7)	-4648(13)	47(4)
C(15)	-8100(20)	23(6)	-10802(16)	52(4)
C(12)	-5030(20)	-44(7)	-10229(19)	64(5)
C(17)	-5580(30)	71(8)	-11347(19)	70(6)
C(131)	-5250(20)	-259(9)	-8220(20)	76(6)
C(11)	-8530(17)	-201(6)	-8755(16)	48(4)
C(33)	-8040(20)	-3339(7)	-8905(16)	57(5)
C(38)	-11790(20)	-3004(6)	-8635(18)	56(4)
C(18)	-9110(19)	245(7)	-8058(16)	53(4)
C(27)	-8220(20)	-2174(7)	-4445(15)	51(4)
C(32)	-9190(17)	-3045(6)	-9521(14)	43(4)
C(19)	-8660(30)	130(8)	-6802(18)	76(6)
C(34)	-6990(20)	-3583(7)	-9579(19)	60(5)
C(35)	-7050(20)	-3521(7)	-10706(17)	55(4)
C(2S)	-6574(19)	-1653(12)	-10053(17)	88(9)
C(24)	-6007(18)	-1547(9)	-3511(14)	53(4)
O(2)	-6742(11)	-1733(5)	-8045(10)	52(3)
C(23)	-7227(18)	-1326(6)	-4189(13)	45(4)
C(371)	-10360(30)	-2632(9)	-11351(18)	69(6)
C(26)	-6990(20)	-2353(8)	-3761(15)	62(5)

Appendix 1

C(37)	-9232(19)	-2983(6)	-10711(16)	47(4)
C(36)	-8200(19)	-3207(7)	-11238(17)	52(4)
C(25)	-5866(19)	-2036(8)	-3299(14)	54(4)
C(39)	-12510(20)	-2710(8)	-7690(20)	69(5)
C(271)	-9380(20)	-2562(9)	-5020(20)	78(6)
C(3S)	-6170(20)	-1958(9)	-8988(15)	64(5)
C(231)	-7210(30)	-755(10)	-4410(30)	98(9)
C(331)	-7890(30)	-3435(10)	-7630(20)	82(7)
C(111)	-10830(20)	243(10)	-8240(30)	101(9)
C(110)	-8570(30)	777(7)	-8440(20)	76(6)
C(171)	-4540(30)	163(13)	-12310(20)	106(9)
C(16)	-7160(30)	110(8)	-11622(19)	68(5)
C(251)	-4510(30)	-2252(12)	-2573(18)	85(7)
C(351)	-5900(20)	-3789(9)	-11290(20)	80(7)
C(311)	-12840(30)	-2968(14)	-9780(20)	104(10)
C(310)	-11670(30)	-3577(8)	-8350(30)	107(10)
C(28)	-11190(20)	-1260(7)	-5008(16)	54(4)
C(211)	-10890(40)	-1262(11)	-3670(20)	121(11)
C(21A)	-12430(60)	-1700(40)	-5380(70)	170(50)
C(21B)	-11730(70)	-1740(30)	-4260(60)	112(18)
C(29A)	-11800(90)	-820(40)	-5530(70)	230(60)
C(29B)	-12190(80)	-1080(50)	-6300(80)	230(50)

A.1.9. X-ray crystal structure of $K_2(\mu\text{-}\eta^6,\eta^6\text{-}C_{10}H_8)[U(NC[^tBu]Mes)_3]_2$ ($K_2\text{-}3_2\text{-}\mu\text{-}C_{10}H_8$)

Atomic coordinates (x 10^4) and equivalent isotropic displacement parameters (Å^2 x 10^3) for $K_2\text{-}3_2\text{-}\mu\text{-}C_{10}H_8$. U(eq) is defined as one third of the trace of the orthogonalized U^{ij} tensor.

	x	y	z	U(eq)
U(1)	3805(1)	-2163(1)	1128(1)	30(1)
K(1)	5245(2)	-1796(1)	2405(1)	44(1)
N(1)	5425(6)	-1817(3)	1330(3)	39(2)
C(1)	2730(8)	-2839(3)	1488(4)	34(3)
C(1S)	5800(30)	-3123(10)	-184(12)	243(19)
U(2)	3639(1)	-3632(1)	1484(1)	28(1)
K(2)	4771(2)	-3777(1)	2901(1)	43(1)
C(2)	2784(9)	-2922(3)	952(6)	34(3)
N(2)	3154(6)	-1722(2)	1708(3)	32(2)
C(2S)	6630(30)	-3230(20)	-375(16)	340(30)
N(3)	3050(7)	-1830(3)	375(4)	46(3)

C(3)	3823(8)	-3004(3)	813(5)	35(3)
O(1S)	7640(30)	-2964(7)	17(15)	310(20)
N(4)	2773(6)	-3805(2)	2167(3)	32(2)
C(4)	4756(9)	-2944(3)	1188(5)	35(3)
C(4S)	8250(40)	-2980(20)	-180(20)	460(70)
N(5)	3049(6)	-4187(3)	911(3)	36(2)
C(5)	4697(7)	-2877(3)	1730(5)	29(3)
C(5S)	9170(30)	-2759(9)	282(18)	310(30)
N(6)	5184(6)	-3971(2)	1835(3)	32(2)
C(6)	5618(10)	-2869(3)	2158(6)	37(3)
C(7)	5558(13)	-2792(3)	2658(7)	50(4)
C(8)	4541(10)	-2699(3)	2828(5)	45(3)
C(9)	3655(10)	-2705(3)	2437(5)	36(3)
C(10)	3654(8)	-2792(3)	1903(5)	37(3)
C(11)	6361(8)	-1679(3)	1300(4)	38(3)
C(12)	7229(8)	-1720(4)	1769(5)	45(3)
C(13)	7811(9)	-2134(4)	1859(6)	55(4)
C(14)	8529(12)	-2188(6)	2338(8)	75(5)
C(15)	8707(10)	-1850(7)	2705(7)	82(5)
C(16)	8169(10)	-1459(6)	2618(6)	69(4)
C(17)	7440(9)	-1381(4)	2155(6)	57(4)
C(18)	6633(9)	-1474(4)	769(5)	53(3)
C(19)	6281(10)	-1806(5)	319(5)	78(4)
C(21)	2648(8)	-1470(3)	1987(4)	40(3)
C(22)	3308(7)	-1187(3)	2423(4)	26(2)
C(23)	3884(8)	-819(3)	2279(4)	36(3)
C(24)	4562(9)	-600(3)	2688(6)	47(3)
C(25)	4710(8)	-724(3)	3208(5)	39(3)
C(26)	4121(9)	-1081(3)	3339(5)	48(3)
C(27)	3398(8)	-1312(3)	2945(5)	37(3)
C(28)	1444(7)	-1416(3)	1867(5)	43(3)
C(29)	1200(11)	-1135(5)	1365(6)	62(4)
C(31)	2640(10)	-1647(3)	-59(5)	47(3)
C(32)	3303(9)	-1304(3)	-312(4)	45(3)
C(33)	3977(9)	-1442(4)	-654(5)	49(3)
C(34)	4573(10)	-1107(4)	-852(5)	54(3)
C(35)	4583(9)	-665(4)	-715(4)	51(3)
C(36)	3936(8)	-537(4)	-360(5)	44(3)
C(37)	3291(8)	-844(3)	-158(4)	41(3)
C(38)	1521(9)	-1769(4)	-350(5)	54(3)
C(39)	1196(11)	-1506(5)	-861(6)	72(4)
C(41)	2139(8)	-3913(3)	2470(4)	34(3)
C(42)	2529(7)	-4049(3)	3048(5)	35(3)
C(43)	2953(9)	-4492(3)	3136(5)	42(3)

Appendix 1

C(44)	3397(8)	-4612(4)	3651(6)	53(4)
C(45)	3475(9)	-4327(4)	4078(6)	56(3)
C(46)	3023(10)	-3895(4)	3976(5)	54(3)
C(47)	2570(8)	-3755(3)	3477(5)	38(3)
C(48)	910(8)	-3946(3)	2270(5)	44(3)
C(49)	503(10)	-3482(5)	2099(8)	79(5)
C(51)	2641(7)	-4375(3)	486(5)	37(3)
C(52)	2341(7)	-4093(3)	-8(4)	36(3)
C(53)	1391(8)	-3846(3)	-82(4)	39(3)
C(54)	1195(12)	-3557(5)	-501(6)	56(4)
C(55)	1852(11)	-3494(4)	-869(5)	53(3)
C(56)	2760(10)	-3742(4)	-795(5)	54(3)
C(57)	3051(7)	-4032(3)	-361(4)	39(3)
C(58)	2405(8)	-4899(3)	448(4)	43(3)
C(59)	1788(13)	-5038(5)	-88(7)	69(4)
C(61)	6025(7)	-4212(3)	1922(4)	35(3)
C(62)	6278(7)	-4461(3)	2438(4)	35(3)
C(63)	5800(8)	-4886(3)	2491(5)	37(3)
C(64)	5877(9)	-5065(4)	2987(5)	47(4)
C(65)	6433(9)	-4870(3)	3444(5)	46(3)
C(66)	6977(9)	-4465(4)	3377(6)	47(4)
C(67)	6900(8)	-4262(3)	2883(5)	37(3)
C(68)	6750(8)	-4262(3)	1496(4)	42(3)
C(69)	7596(11)	-4628(4)	1647(6)	59(4)
C(110)	6010(11)	-1028(5)	650(7)	67(4)
C(111)	7839(10)	-1378(5)	832(7)	68(4)
C(131)	7701(12)	-2494(5)	1461(7)	72(5)
C(151)	9512(14)	-1935(7)	3225(7)	129(7)
C(171)	6893(10)	-929(7)	2087(9)	72(5)
C(210)	946(11)	-1173(4)	2291(8)	55(4)
C(211)	888(11)	-1876(4)	1757(7)	67(4)
C(231)	3857(12)	-675(4)	1725(6)	56(4)
C(251)	5465(9)	-483(4)	3615(5)	61(4)
C(271)	2834(13)	-1716(4)	3128(7)	54(4)
C(310)	757(12)	-1682(6)	27(7)	71(5)
C(311)	1530(13)	-2282(5)	-461(8)	79(5)
C(331)	4055(13)	-1922(4)	-827(7)	67(4)
C(351)	5261(11)	-319(4)	-936(5)	76(4)
C(371)	2598(12)	-681(5)	223(6)	57(4)
C(410)	741(10)	-4257(5)	1778(6)	63(4)
C(411)	347(9)	-4157(4)	2673(5)	68(4)
C(431)	2941(9)	-4824(3)	2700(5)	58(3)
C(451)	3867(18)	-4478(6)	4638(8)	89(6)
C(471)	2157(9)	-3275(3)	3402(5)	56(3)

C(510)	1829(12)	-5034(4)	888(5)	80(5)
C(511)	3467(10)	-5165(4)	554(5)	72(4)
C(531)	651(9)	-3889(4)	304(5)	60(3)
C(551)	1549(11)	-3202(5)	-1351(5)	79(4)
C(571)	4094(9)	-4283(4)	-306(5)	69(4)
C(610)	7290(9)	-3806(4)	1427(5)	55(3)
C(611)	6016(9)	-4374(4)	960(5)	62(4)
C(631)	5130(9)	-5116(4)	2012(5)	46(3)
C(651)	6475(10)	-5074(4)	3981(5)	66(4)
C(671)	7465(10)	-3824(4)	2843(6)	45(3)

A.1.10. X-ray crystal structure of $Na(Et_2O)(\eta^8\text{-}C_8H_8)[U(NC[^tBu]Mes)_3]$ (Na-3-COT)

Atomic coordinates (x 10^4) and equivalent isotropic displacement parameters (Å^2 x 10^3) for **Na-3-COT**. U(eq) is defined as one third of the trace of the orthogonalized U^{ij} tensor.

	x	y	z	U(eq)
U	7368(1)	1527(1)	7653(1)	30(1)
N(1)	7195(4)	625(2)	7323(2)	37(1)
Na	4818(2)	2046(1)	8151(1)	48(1)
N(3)	6492(4)	1356(2)	8579(2)	38(1)
N(2)	5516(4)	1803(2)	7041(2)	35(1)
C(37)	4014(5)	961(2)	9070(3)	35(1)
C(36)	3021(6)	1051(3)	9363(3)	44(2)
C(1)	9779(6)	1392(3)	7744(5)	53(2)
C(111)	5402(6)	-188(3)	7196(5)	72(2)
C(28)	4491(5)	1669(3)	5801(3)	44(2)
C(21)	4634(5)	1915(2)	6554(3)	33(1)
C(110)	7096(7)	-840(3)	7555(5)	91(3)
C(25)	1894(6)	3051(3)	6955(3)	50(2)
C(32)	5059(5)	1268(2)	9341(3)	38(1)
C(251)	921(9)	3449(5)	7081(6)	77(3)
C(2)	9697(6)	1607(3)	8399(5)	57(2)
C(26)	2928(6)	3257(3)	6775(3)	49(2)
C(18)	6576(5)	-367(2)	7024(4)	51(2)
C(27)	3804(5)	2901(2)	6633(3)	40(1)
C(35)	3028(6)	1415(3)	9907(3)	48(2)
C(351)	1973(7)	1472(3)	10255(4)	68(2)
C(31)	6222(5)	1136(2)	9119(3)	36(1)
C(22)	3663(5)	2313(2)	6684(3)	35(1)

C(5)	7918(6)	2650(3)	7618(5)	60(2)
C(271)	4885(7)	3156(4)	6441(5)	62(2)
C(24)	1772(6)	2473(3)	7005(4)	50(2)
C(231)	2479(7)	1476(3)	6998(6)	64(2)
C(23)	2647(5)	2101(2)	6889(3)	42(2)
C(33)	5045(6)	1685(2)	9856(3)	43(2)
C(38)	7036(6)	698(3)	9593(3)	48(2)
C(34)	4039(6)	1743(3)	10131(3)	49(2)
C(371)	3952(6)	539(2)	8485(3)	44(2)
C(331)	6101(6)	2075(3)	10086(3)	57(2)
C(11)	7453(5)	138(2)	7106(3)	37(1)
C(39)	8309(6)	920(3)	9768(4)	80(2)
C(19)	6381(8)	-615(4)	6301(5)	110(4)
O(1S)	4031(5)	2797(2)	8697(2)	64(1)
C(17)	9658(5)	-98(2)	7474(3)	43(2)
C(8)	9302(6)	1543(3)	7051(4)	56(2)
C(12)	8674(5)	46(2)	6941(3)	38(1)
C(13)	8843(6)	154(3)	6261(4)	51(2)
C(311)	6666(9)	569(4)	10274(4)	59(2)
C(310)	6994(7)	143(3)	9171(4)	68(2)
C(16)	10765(6)	-172(3)	7300(5)	58(2)
C(14)	10002(7)	77(3)	6131(5)	64(2)
C(3)	9090(6)	2054(3)	8632(4)	58(2)
C(7)	8576(7)	1986(4)	6724(4)	61(2)
C(4)	8357(7)	2485(3)	8300(5)	64(2)
C(171)	9565(6)	-147(3)	8228(4)	63(2)
C(6)	8009(6)	2444(3)	6960(5)	64(2)
C(131)	7884(7)	389(4)	5682(4)	77(2)
C(4S)	4357(10)	3357(4)	8657(5)	99(3)
C(1S)	2794(9)	2719(4)	8812(5)	102(3)
C(15)	10947(6)	-93(3)	6647(5)	57(2)
C(151)	12166(7)	-168(3)	6484(5)	91(3)
C(3S)	5504(10)	3398(4)	8519(7)	117(4)
C(2S)	2548(13)	2968(5)	9415(7)	177(6)
C(210)	4498(12)	994(4)	5853(6)	118(4)
C(29A)	5573(11)	1826(6)	5483(6)	75(3)
C(29B)	5540(20)	1339(11)	5751(12)	58(6)
C(21C)	3340(10)	1805(7)	5295(5)	106(5)
C(21D)	4510(40)	2221(11)	5302(13)	80(12)

A.1.11. X-ray crystal structure of $(\mu\text{-}\eta^8,\eta^8\text{-}C_8H_8)[U(NC[^tBu]Mes)_3]_2$ $(3_2\text{-}\mu\text{-COT})$

Atomic coordinates (x 10^4) and equivalent isotropic displacement parameters (Å^2 x 10^3) for $3_2\text{-}\mu\text{-COT}$. U(eq) is defined as one third of the trace of the orthogonalized U^{ij} tensor.

	x	y	z	U(eq)
U	9050(1)	9253(1)	5175(1)	33(1)
N(3)	9484(3)	8324(2)	4982(2)	46(1)
N(1)	7574(3)	9191(2)	4266(3)	45(1)
C(31)	9990(3)	7855(2)	5037(3)	44(1)
N(2)	8678(3)	9098(2)	6514(3)	48(1)
C(22)	8665(3)	9768(2)	7792(3)	47(1)
C(37)	11641(3)	7989(2)	6193(3)	43(1)
C(12)	6831(3)	9446(2)	2644(3)	44(1)
C(11)	6806(3)	9168(2)	3588(3)	44(1)
C(17)	7271(3)	9133(2)	2020(3)	46(1)
C(21)	8491(3)	9160(2)	7317(3)	46(1)
C(111)	5477(5)	9167(3)	4473(4)	64(1)
C(38)	9505(3)	7218(2)	4916(3)	53(1)
C(16)	7268(4)	9385(2)	1161(4)	57(1)
C(311)	8849(5)	7168(3)	5623(5)	72(2)
C(33)	11615(4)	7916(2)	4544(3)	54(1)
C(32)	11102(3)	7907(2)	5259(3)	43(1)
C(27)	9563(4)	9907(2)	8417(3)	53(1)
C(310)	10285(5)	6719(2)	5075(5)	73(2)
C(24)	8117(5)	10782(3)	7938(4)	72(2)
C(36)	12663(4)	8038(2)	6384(4)	52(1)
C(18)	5859(3)	8846(2)	3705(3)	51(1)
C(28)	8071(4)	8631(2)	7790(3)	60(1)
C(23)	7950(4)	10218(2)	7535(3)	61(1)
C(35)	13187(4)	8017(2)	5701(4)	58(1)
C(34)	12645(4)	7971(2)	4788(4)	62(2)
C(4)	10413(7)	9579(3)	4129(6)	98(3)
C(271)	10391(5)	9458(4)	8656(5)	71(2)
C(110)	6162(5)	8203(3)	4042(6)	75(2)
C(26)	9703(5)	10481(3)	8796(3)	69(2)
C(371)	11123(5)	8034(3)	6977(4)	57(1)
C(19)	5050(4)	8826(4)	2790(4)	73(2)
C(13)	6434(3)	10015(2)	2400(3)	53(1)
C(15)	6856(4)	9943(2)	891(4)	66(1)
C(171)	7774(6)	8538(3)	2285(5)	63(2)
C(3)	11021(4)	9490(2)	5095(8)	97(3)

Appendix 1

C(131)	6016(5)	10392(3)	3069(5)	72(2)
C(331)	11072(7)	7886(3)	3528(4)	77(2)
C(39)	8834(6)	7169(3)	3922(4)	79(2)
C(1)	10292(6)	10077(3)	6285(4)	86(2)
C(25)	8996(6)	10924(3)	8578(4)	78(2)
C(14)	6453(4)	10250(3)	1529(4)	69(2)
C(351)	14308(5)	8045(4)	5967(6)	85(2)
C(2)	10946(5)	9745(3)	5984(5)	93(3)
C(231)	7014(6)	10104(5)	6783(7)	96(2)
C(211)	8801(8)	8108(3)	7927(7)	104(3)
C(210)	7116(7)	8424(5)	7102(6)	116(3)
C(251)	9151(12)	11543(4)	9027(7)	123(4)
C(29)	7888(8)	8805(4)	8729(5)	96(3)
C(151)	6814(8)	10204(5)	-75(6)	98(2)

A.1.12. X-ray crystal structure of $K_2I(\mu-\eta^6,\eta^6-C_7H_8)[U(NC[^tBu]Mes)_3]_2$ (K_2I-3_2-μ-toluene)

Atomic coordinates (x 10^4) and equivalent isotropic displacement parameters ($Å^2$ x 10^3) for K_2I-3_2-μ-toluene. U(eq) is defined as one third of the trace of the orthogonalized U^{ij} tensor.

	x	y	z	U(eq)
U(1)	-7851(1)	-5244(1)	-6479(1)	32(1)
U(2)	-9290(1)	-4749(1)	-7985(1)	31(1)
C(38)	-5776(11)	-2724(12)	-6141(6)	46(4)
C(1)	-9430(9)	-5276(15)	-7056(5)	39(3)
C(6)	-9142(9)	-4213(13)	-7032(5)	39(4)
N(2)	-8341(8)	-4873(11)	-5757(4)	42(3)
C(4)	-7745(8)	-4634(14)	-7413(5)	36(3)
C(42)	-12118(9)	-4779(14)	-8674(5)	43(3)
C(44)	-12578(13)	-5180(20)	-9530(7)	79(6)
C(3)	-7999(10)	-5739(14)	-7434(5)	43(4)
C(47)	-12056(9)	-4600(13)	-9175(5)	45(4)
C(21)	-8794(9)	-4520(11)	-5414(5)	40(4)
N(6)	-9167(7)	-6092(9)	-8488(4)	36(3)
C(5)	-8321(10)	-3892(11)	-7212(5)	35(3)
N(5)	-8659(8)	-3559(10)	-8453(4)	42(3)
C(2)	-8844(10)	-6042(11)	-7264(4)	37(3)
C(311)	-4819(11)	-2278(17)	-6022(7)	67(5)
C(7)	-10318(11)	-5638(17)	-6883(6)	63(5)
N(3)	-6523(8)	-4417(9)	-6357(4)	41(3)

C(610)	-9980(13)	-8548(15)	-9157(8)	69(5)
C(31)	-5801(11)	-3913(13)	-6249(5)	47(4)
C(68)	-10017(10)	-7676(13)	-8741(6)	49(4)
C(61)	-9262(10)	-6868(11)	-8773(5)	42(3)
C(32)	-4901(9)	-4499(11)	-6257(5)	40(4)
C(511)	-8147(14)	-1076(14)	-9093(8)	71(5)
C(471)	-11409(12)	-3822(17)	-9343(6)	68(5)
C(12)	-6509(11)	-8418(13)	-6336(7)	55(4)
C(46)	-13157(12)	-6185(17)	-8874(8)	71(6)
C(13)	-6511(13)	-8844(16)	-6787(8)	67(5)
C(51)	-8263(10)	-2860(12)	-8684(5)	40(3)
C(510)	-9673(12)	-1898(18)	-9020(8)	82(7)
N(1)	-7403(9)	-6874(10)	-6315(4)	47(3)
C(18)	-8057(15)	-8374(15)	-5938(7)	71(5)
C(69)	-10936(12)	-7096(17)	-8853(10)	87(7)
C(28)	-8389(10)	-4460(14)	-4854(5)	52(5)
C(211)	-9040(16)	-3980(20)	-4535(8)	112(10)
C(310)	-6298(12)	-2554(16)	-5684(7)	68(5)
C(59)	-8723(17)	-1256(16)	-8247(8)	87(7)
C(131)	-7337(17)	-8881(18)	-7167(8)	89(7)
C(431)	-12689(13)	-5826(18)	-7977(7)	75(6)
C(39)	-6264(13)	-2143(15)	-6598(7)	68(5)
C(17)	-5740(17)	-8400(20)	-5995(12)	113(11)
C(210)	-7568(16)	-3750(30)	-4816(8)	115(11)
N(4)	-10728(6)	-4345(10)	-8164(4)	39(3)
C(11)	-7347(13)	-7810(13)	-6201(5)	55(4)
C(19)	-7838(17)	-9534(15)	-5840(8)	88(7)
C(410)	-13027(12)	-3125(19)	-8211(8)	79(6)
C(37)	-4620(11)	-5129(15)	-5841(5)	54(4)
C(63)	-7812(11)	-7595(12)	-9023(6)	48(4)
C(371)	-5092(13)	-5106(16)	-5376(5)	70(5)
C(48)	-12055(11)	-3173(14)	-8051(6)	55(4)
C(36)	-3888(12)	-5818(14)	-5876(7)	61(5)
C(35)	-3464(13)	-5885(15)	-6292(8)	67(5)
C(41)	-11545(11)	-4115(14)	-8282(5)	48(4)
C(671)	-9601(13)	-5840(16)	-9737(6)	66(5)
C(67)	-8726(11)	-6481(15)	-9605(5)	53(4)
C(631)	-7654(12)	-8177(15)	-8524(7)	63(5)
C(23)	-9855(10)	-3089(13)	-5763(5)	46(4)
C(33)	-4454(10)	-4570(15)	-6677(6)	55(4)
C(34)	-3745(11)	-5274(18)	-6683(7)	68(5)
C(25)	-11463(11)	-3407(15)	-5895(5)	56(4)
C(24)	-10714(11)	-2759(16)	-5918(6)	56(4)
C(231)	-9074(12)	-2413(15)	-5816(6)	60(4)

C(22)	-9741(9)	-4119(12)	-5571(5)	43(3)
C(611)	-9937(15)	-8194(19)	-8249(8)	85(6)
C(27)	-10486(9)	-4748(15)	-5544(5)	46(3)
C(271)	-10378(14)	-5870(17)	-5376(7)	77(6)
C(43)	-12666(10)	-5571(14)	-8517(7)	56(4)
C(26)	-11339(13)	-4395(14)	-5709(6)	58(5)
C(45)	-13127(12)	-6002(18)	-9382(9)	78(7)
C(62)	-8601(10)	-7022(12)	-9159(5)	41(3)
C(49)	-11608(14)	-2179(16)	-8206(8)	75(6)
C(29)	-8150(30)	-5490(20)	-4667(7)	144(14)
K(1)	-7250(2)	-5422(3)	-8633(1)	47(1)
C(56)	-5800(12)	-3442(14)	-8725(7)	59(4)
C(531)	-8220(11)	-3548(15)	-9735(6)	57(4)
C(57)	-6590(10)	-3035(13)	-8573(6)	49(4)
C(55)	-5774(12)	-3865(14)	-9170(8)	63(5)
C(64)	-7144(13)	-7602(17)	-9372(10)	80(7)
C(66)	-8084(15)	-6513(18)	-9910(6)	69(5)
C(65)	-7265(16)	-7060(20)	-9798(8)	85(7)
K(2)	-5655(2)	-6541(3)	-6767(1)	53(1)
C(331)	-4722(14)	-3904(15)	-7141(6)	68(5)
C(251)	-12404(12)	-3005(16)	-6050(7)	68(5)
C(571)	-6555(13)	-2491(16)	-8055(6)	68(5)
C(551)	-4940(13)	-4398(18)	-9315(8)	82(6)
C(53)	-7379(9)	-3501(12)	-9362(5)	40(3)
C(58)	-8688(12)	-1731(13)	-8758(7)	58(4)
C(14)	-5690(20)	-9280(20)	-6902(12)	118(11)
C(110)	-8964(13)	-8260(20)	-6285(8)	90(7)
C(451)	-13719(17)	-6660(30)	-9785(10)	127(12)
C(52)	-7395(9)	-3098(11)	-8884(5)	36(3)
C(171)	-5720(20)	-7900(20)	-5472(12)	135(14)
C(351)	-2734(14)	-6634(19)	-6315(10)	91(7)
C(151)	-4110(20)	-9820(40)	-6710(20)	250(30)
C(15)	-4900(20)	-9230(30)	-6550(17)	118(13)
I	-5450(1)	-6525(1)	-7986(1)	65(1)
C(411)	-11885(14)	-3290(19)	-7481(6)	78(6)
C(111)	-8180(20)	-7813(19)	-5447(8)	110(9)
C(54)	-6576(13)	-3923(14)	-9506(7)	62(5)
C(651)	-6518(19)	-7060(30)	-10138(11)	122(10)
C(16)	-5030(20)	-8820(40)	-6110(20)	190(30)

Appendix 1

A.1.13. X-ray crystal structure of $K(DME)(\mu-\eta^6,\eta^6-C_7H_8)[U(NC[^tBu]Mes)_3]_2$ $(K(DME)-3_2-\mu-toluene)$

Atomic coordinates (x 10^4) and equivalent isotropic displacement parameters (Å^2 x 10^3) for $K(DME)-3_2-\mu-toluene$. U(eq) is defined as one third of the trace of the orthogonalized U^{ij} tensor.

	x	y	z	U(eq)
U(1)	6104	7499	5383	31
K(1)	8211	7389	5807	68
N(1)	6953	8183	5165	46
C(1')	8371	2414	8501	53
C(1)	6260	7571	6364	71
O(1S)	9551	7409	6374	163
C(1S)	10300	7131	6225	197
U(2)	4961	7827	6894	30
K(2)	6367	2624	9045	56
N(2)	5442	7462	4652	43
C(2')	8690	1805	8748	54
C(2)	5834	7051	6307	58
O(2S)	8164	7602	6899	148
C(2S)	9555	7530	6879	178
U(3)	8441	2593	9483	31
N(3)	7051	6663	5362	46
C(3')	9387	1731	9026	54
C(3)	5117	7132	6070	60
O(3S)	6453	2300	8002	120
C(3S)	8764	7919	6967	169
U(4)	9757	2029	8073	32
N(4)	5203	8695	7256	46
C(4')	9834	2252	9052	47
C(4)	4788	7728	5878	57
O(4S)	5082	2363	8570	133
C(4S)	7959	7225	7309	235
N(5)	3661	7952	6966	46
C(5')	9531	2847	8805	51
C(5)	5200	8252	5944	64
C(5S)	6408	2697	7544	140
N(6)	5252	7125	7537	43
C(6)	5915	8170	6182	65
C(6')	8839	2912	8543	45
C(6S)	5965	1912	8004	181

Appendix 1

N(7)	7567	1918	9717	40
C(7')	10051	3371	8818	103
C(7)	4608	6593	6041	152
C(7S)	5131	2087	8106	131
N(8)	9058	2703	10215	43
C(8S)	4322	2537	8730	121
N(9)	7458	3432	9420	42
N(10)	11053	1809	8063	52
C(10C)	12132	3054	7954	61
C(10A)	11816	1242	9272	65
C(10B)	12691	3258	9816	95
C(10D)	13231	1451	7961	159
C(10E)	12232	1350	7343	173
C(10F)	12365	643	8084	185
N(11)	9539	1137	7730	46
C(11')	9420	643	7528	45
C(11)	7289	8644	5002	48
C(11F)	9426	-554	7506	63
C(11E)	10381	-109	8053	67
C(11C)	10575	536	6702	76
C(11A)	7742	880	7280	94
C(11D)	8965	17	8293	87
C(11B)	8418	805	5391	143
N(12)	9671	2743	7431	51
C(12)	8083	8752	5209	44
C(12')	10188	3629	7029	42
C(12C)	9222	4416	7481	84
C(12A)	11176	2805	6620	67
C(12F)	9041	3669	6213	78
C(12E)	8172	3239	6875	116
C(12D)	9102	2515	6403	95
C(12B)	11969	4891	7054	127
C(13)	8782	8485	4983	60
C(14)	9497	8557	5201	91
C(15)	9547	8877	5639	72
C(16)	8852	9124	5859	59
C(17)	8120	9068	5653	47
C(18)	6892	9122	4571	74
C(19)	6706	8736	4112	99
C(21)	4999	7421	4279	42
C(22)	5144	6822	3969	47
C(23)	4762	6302	4103	55
C(24)	4906	5772	3820	70
C(25)	5441	5723	3421	71

C(26)	5823	6229	3290	65
C(27)	5695	6774	3565	52
C(28)	4325	7938	4101	54
C(29)	3558	7674	4052	117
C(31)	7408	6094	5302	46
C(32)	8267	5933	5451	48
C(33)	8467	5704	5959	57
C(34)	9251	5547	6084	67
C(35)	9857	5609	5742	67
C(36)	9647	5867	5261	65
C(37)	8876	6026	5104	55
C(38)	6994	5578	5076	63
C(39)	7435	4916	5170	117
C(41)	5349	9195	7446	39
C(42)	5799	9161	7946	40
C(43)	6622	9102	7938	60
C(44)	7013	9020	8416	77
C(45)	6593	9026	8880	85
C(46)	5816	9072	8860	89
C(47)	5387	9142	8412	54
C(48)	5084	9865	7181	49
C(49)	5475	9896	6660	72
C(51)	2931	8000	6897	39
C(52)	2626	7690	6431	36
C(53)	2473	7073	6475	47
C(54)	2267	6795	6036	60
C(55)	2164	7107	5554	54
C(56)	2331	7727	5535	50
C(57)	2560	8025	5956	43
C(58)	2313	8378	7250	49
C(59)	2335	9074	7135	181
C(61)	5422	6716	7911	35
C(62)	6277	6493	8042	37
C(63)	6672	6819	8381	45
C(64)	7462	6614	8492	57
C(65)	7871	6094	8262	57
C(66)	7470	5798	7912	47
C(67)	6694	5974	7791	36
C(68)	4772	6444	8232	44
C(69)	4235	6998	8474	76
C(71)	7275	1472	9907	45
C(72)	6491	1310	9736	52
C(73)	6445	891	9343	56
C(74)	5732	731	9218	76

Appendix 1

C(75)	5032	976	9445	75
C(76)	5074	1410	9808	75
C(77)	5789	1580	9954	60
C(78)	7685	1022	10344	59
C(79)	7762	1420	10804	96
C(81)	9455	2815	10589	45
C(82)	9307	3459	10818	39
C(83)	9697	3954	10629	51
C(84)	9528	4551	10840	67
C(85)	8966	4683	11212	58
C(86)	8575	4183	11372	67
C(87)	8708	3590	11178	53
C(88)	10098	2312	10861	55
C(89)	10238	1735	10575	236
C(91)	7077	3978	9390	45
C(92)	6275	4082	9138	43
C(93)	5577	4082	9428	58
C(94)	4837	4143	9174	68
C(95)	4794	4208	8646	72
C(96)	5485	4213	8377	58
C(97)	6217	4151	8610	42
C(98)	7410	4565	9591	60
C(99)	6897	5189	9417	73
C(101)	11783	1750	8173	39
C(102)	12036	2141	8599	41
C(103)	12042	1910	9115	52
C(104)	12268	2277	9500	64
C(105)	12450	2873	9401	58
C(106)	12407	3109	8897	52
C(107)	12204	2759	8495	45
C(108)	12410	1297	7889	49
C(110)	6128	9445	4778	114
C(111)	7401	9619	4398	117
C(112)	9150	664	6984	46
C(113)	8348	773	6868	64
C(114)	8109	822	6353	91
C(115)	8636	767	5963	78
C(116)	9460	676	6068	89
C(117)	9702	626	6583	61
C(118)	9552	-9	7835	50
C(121)	9610	3150	7051	44
C(123)	10951	3462	6823	47
C(124)	11492	3872	6831	69
C(125)	11311	4463	7038	74

Appendix 1

C(126)	10611	4608	7242	82
C(127)	10017	4206	7241	53
C(128)	8998	3156	6630	58
C(131)	8784	8119	4492	108
C(151)	10339	8946	5879	121
C(171)	7384	9352	5926	73
C(210)	4515	8264	3600	97
C(211)	4207	8457	4479	109
C(231)	4226	6289	4561	77
C(251)	5613	5102	3127	111
C(271)	6193	7281	3425	72
C(310)	6956	5725	4485	116
C(311)	6156	5633	5267	93
C(331)	7832	5623	6358	81
C(351)	10724	5431	5890	103
C(371)	8706	6330	4575	86
C(410)	4198	9915	7090	70
C(411)	5276	10394	7495	66
C(431)	7073	9083	7449	90
C(451)	7068	8938	9371	138
C(471)	4510	9156	8418	83
C(510)	1498	8219	7180	133
C(511)	2554	8234	7784	147
C(531)	2580	6674	6970	73
C(551)	1890	6821	5096	87
C(571)	2755	8697	5866	58
C(610)	4273	6123	7889	74
C(611)	5111	5964	8659	66
C(631)	6281	7401	8628	68
C(651)	8741	5877	8373	76
C(671)	6295	5620	7414	45
C(710)	8507	745	10178	74
C(711)	7235	480	10518	85
C(731)	7178	631	9063	72
C(751)	4246	748	9316	117
C(771)	5781	2086	10361	80
C(810)	10876	2541	10859	275
C(831)	10314	3868	10193	82
C(851)	8797	5326	11413	97
C(871)	8182	3116	11361	102
C(910)	8244	4562	9376	96
C(911)	7479	4485	10180	101
C(931)	5573	4005	10006	92
C(951)	3977	4311	8391	115

C(971)	6944	4161	8275	57
C(811)	9947	2158	11358	330

A.1.14. X-ray crystal structure of $Na_2(Et_2O)(\mu-\eta^6,\eta^6$-biphenyl)[U(NC[^{t}Bu]Mes)$_3$]$_2$ ($Na_2(Et_2O)$-3_2-μ-biphenyl)

Atomic coordinates (x 10^4) and equivalent isotropic displacement parameters ($\mathring{A}^2$ x 10^3) for $Na_2(Et_2O)$-3_2-μ-biphenyl. U(eq) is defined as one third of the trace of the orthogonalized U^{ij} tensor.

	x	y	z	U(eq)
U(2)	7748(1)	891(1)	7477(1)	28(1)
U(1)	8076(1)	-1733(1)	7318(1)	28(1)
N(4)	7200(4)	1976(4)	6633(3)	36(2)
N(3)	7159(4)	-2631(4)	7982(3)	39(2)
N(5)	6615(4)	1438(4)	8123(3)	41(2)
N(6)	9003(4)	1418(4)	7714(3)	38(2)
N(1)	8025(4)	-2136(4)	6380(3)	36(2)
N(2)	9382(4)	-2600(4)	7798(3)	36(2)
C(74)	7807(5)	-136(4)	6665(4)	36(2)
C(73)	7007(5)	-273(4)	7048(4)	34(2)
C(75)	8701(5)	-271(4)	6967(4)	35(2)
C(76)	8795(6)	-556(5)	7655(4)	36(2)
C(72)	7076(5)	-526(5)	7741(3)	32(2)
C(21)	10210(5)	-2966(5)	7832(4)	36(2)
C(17)	8340(5)	-751(5)	5022(4)	43(2)
C(11)	7914(5)	-2079(5)	5787(4)	37(2)
C(71)	7988(5)	-698(4)	8070(3)	34(2)
C(52)	5374(5)	2239(5)	8584(3)	37(2)
C(41)	7195(5)	2548(4)	6123(4)	35(2)
C(25)	10950(5)	-5047(5)	9443(4)	49(2)
C(51)	6289(5)	1651(5)	8626(4)	38(2)
C(12)	7656(5)	-1229(5)	5325(3)	38(2)
C(31)	6477(6)	-3028(5)	8126(4)	42(2)
C(61)	9802(5)	1521(5)	7864(3)	37(2)
C(32)	6461(5)	-3679(5)	8766(4)	42(2)
C(16)	8081(6)	15(5)	4608(4)	48(2)
C(58)	6765(6)	1390(5)	9300(4)	51(2)
C(631)	10295(6)	408(6)	9147(4)	58(2)
C(27)	10912(5)	-3571(5)	8945(4)	42(2)

C(62)	10627(5)	819(5)	7939(4)	38(2)
C(15)	7154(6)	350(5)	4494(4)	46(2)
C(67)	11139(5)	674(5)	7400(4)	44(2)
C(38)	5637(6)	-2944(5)	7661(4)	50(2)
C(66)	11899(6)	60(6)	7495(5)	54(2)
C(81)	8091(6)	-1107(4)	8751(4)	40(2)
C(13)	6716(5)	-876(5)	5243(4)	43(2)
C(22)	10498(5)	-3699(4)	8392(4)	40(2)
C(33)	5969(6)	-3484(6)	9304(4)	49(2)
C(24)	10562(6)	-5163(5)	8902(5)	50(2)
C(48)	7957(5)	2560(5)	5592(4)	41(2)
C(65)	12162(6)	-430(5)	8096(5)	54(2)
C(53)	5374(6)	3109(5)	8384(4)	51(2)
C(26)	11123(5)	-4255(5)	9473(4)	51(2)
C(68)	10026(6)	2395(5)	7961(4)	48(2)
C(18)	8031(6)	-2863(5)	5483(4)	51(2)
C(47)	6474(7)	3967(5)	6286(4)	60(3)
C(42)	6413(6)	3271(5)	6021(4)	45(2)
C(271)	11153(7)	-2729(5)	8995(5)	64(3)
C(23)	10326(5)	-4509(5)	8369(4)	46(2)
C(57)	4517(6)	1942(5)	8680(4)	46(2)
C(231)	9933(6)	-4681(5)	7771(4)	58(2)
C(251)	11215(7)	-5777(5)	10021(5)	69(3)
C(311)	5994(7)	-3234(6)	7059(4)	69(3)
C(671)	10884(6)	1170(6)	6731(4)	61(3)
C(171)	9351(6)	-1035(6)	5159(5)	64(3)
C(28)	10938(6)	-2717(5)	7302(4)	52(2)
C(131)	5952(6)	-1311(6)	5627(4)	59(2)
C(34)	5967(6)	-4105(7)	9881(4)	67(3)
C(63)	10850(5)	312(5)	8546(4)	45(2)
C(36)	6878(6)	-5083(6)	9389(4)	59(2)
C(571)	4425(7)	1010(6)	8834(5)	71(3)
C(56)	3696(6)	2487(7)	8640(5)	65(3)
C(82)	7310(8)	-1342(6)	9136(4)	70(3)
C(85)	9027(9)	-1783(6)	9708(5)	82(4)
C(14)	6499(6)	-96(5)	4830(4)	51(2)
C(37)	6929(6)	-4486(5)	8815(4)	47(2)
C(310)	4847(7)	-3447(7)	7956(5)	84(4)
C(211)	10601(7)	-2805(7)	6652(5)	86(4)
C(55)	3707(7)	3344(7)	8471(5)	68(3)
C(35)	6407(7)	-4901(7)	9917(5)	70(3)
C(86)	8953(7)	-1345(5)	9048(4)	58(2)
C(43)	5600(7)	3214(7)	5711(4)	68(3)
C(210)	11017(7)	-1781(6)	7239(5)	85(4)

C(351)	6361(8)	-5571(7)	10550(5)	98(4)
C(411)	8096(8)	1716(6)	5407(5)	78(3)
C(151)	6875(6)	1171(5)	4018(4)	63(3)
C(410)	7742(7)	3265(6)	5002(5)	79(3)
C(371)	7514(7)	-4718(6)	8274(5)	69(3)
C(651)	12998(6)	-1089(6)	8174(5)	75(3)
C(331)	5431(7)	-2640(6)	9284(5)	72(3)
C(54)	4560(7)	3639(6)	8341(5)	67(3)
C(471)	7354(8)	4081(6)	6602(5)	84(3)
C(64)	11614(6)	-302(5)	8611(4)	52(2)
C(431)	5498(7)	2483(8)	5425(5)	97(4)
C(611)	11034(7)	2371(6)	8161(6)	84(3)
C(46)	5714(10)	4590(7)	6241(6)	94(4)
C(511)	6908(8)	2175(7)	9562(5)	86(4)
C(39)	5243(6)	-2014(6)	7462(5)	73(3)
C(510)	7717(7)	923(6)	9245(5)	74(3)
C(45)	4941(11)	4545(9)	5939(8)	110(6)
C(610)	9833(9)	3031(6)	7331(5)	101(4)
C(69)	9381(9)	2652(7)	8474(6)	100(4)
C(29)	11886(6)	-3224(7)	7441(5)	83(3)
C(59)	6202(8)	863(8)	9785(5)	95(4)
C(44)	4853(8)	3876(10)	5679(6)	101(5)
C(551)	2801(8)	3950(8)	8439(7)	118(5)
C(531)	6257(7)	3506(6)	8210(5)	75(3)
C(49)	8878(6)	2656(7)	5888(5)	80(3)
C(84)	8251(12)	-1994(7)	10055(5)	97(5)
C(83)	7409(11)	-1767(7)	9771(5)	97(4)
C(451)	4081(10)	5217(9)	5896(8)	185(9)
Na(1)	8407(2)	-2935(2)	8807(2)	55(1)
Na(2)	5682(2)	2278(2)	7184(2)	49(1)
O(1S)	4346(4)	1710(4)	7013(4)	77(2)
C(3S)	3392(8)	2002(9)	6978(8)	95(4)
C(4S)	3248(8)	2919(7)	6880(5)	95(4)
C(2S)	4503(9)	764(8)	7158(6)	101(4)
C(1S)	4438(9)	469(9)	6603(7)	124(5)
O(2S)	10000	-5000	5000	220(20)
C(6S)	10836(19)	-5282(14)	5958(8)	234(19)
C(5S)	10380(20)	-5186(18)	5480(20)	310(30)
C(19A)	9092(19)	-3262(17)	5591(13)	67(7)
C(19B)	8289(16)	-3669(9)	6018(9)	97(7)
C(11A)	7360(20)	-3433(18)	5746(14)	87(8)
C(11B)	7029(16)	-2985(13)	5235(13)	104(9)
C(11C)	8807(17)	-2830(16)	5009(13)	81(7)
C(11D)	7990(30)	-2607(12)	4730(8)	117(11)

A.1.15. X-ray crystal structure of $K_2(\mu\text{-}\eta^6,\eta^6\text{-}trans\text{-stilbene})[U(NC[^tBu]Mes)_3]_2$ ($K_2\text{-}3_2\text{-}\mu\text{-}trans$-stilbene)

Atomic coordinates (x 10^4) and equivalent isotropic displacement parameters (Å^2 x 10^3) for $K_2\text{-}3_2\text{-}\mu\text{-}trans$-stilbene. U(eq) is defined as one third of the trace of the orthogonalized U^{ij} tensor.

	x	y	z	U(eq)
U(1)	8775(1)	8570(1)	8138(1)	47(1)
N(1)	7483(6)	9445(4)	8243(4)	55(2)
C(1)	10240(7)	7978(5)	7171(5)	60(2)
K(1)	10981(2)	7607(1)	8863(1)	75(1)
C(1S)	5580(40)	3420(30)	7690(30)	430(50)
U(2)	9433(1)	7352(1)	6461(1)	45(1)
C(2)	9578(8)	8511(5)	6850(5)	63(3)
N(2)	8513(7)	8061(5)	9187(4)	72(2)
K(2)	11265(2)	5762(1)	6857(1)	58(1)
C(2S)	5830(50)	3050(30)	7210(30)	310(30)
N(3)	10281(6)	8976(4)	8216(4)	64(2)
C(3)	8444(8)	8505(5)	6953(5)	63(3)
C(3S)	5310(30)	2450(20)	7205(19)	225(14)
C(4)	7920(7)	7975(5)	7403(5)	60(3)
N(4)	8740(6)	7672(4)	5593(4)	60(2)
O(1S)	4530(50)	2990(60)	7360(30)	850(120)
C(5)	8535(7)	7434(5)	7730(4)	57(2)
N(5)	11228(5)	7081(4)	5935(3)	51(2)
N(6)	9017(6)	6265(4)	6711(4)	60(2)
C(6)	9740(7)	7432(5)	7606(5)	54(2)
C(7)	10335(10)	6839(6)	7886(5)	80(3)
C(11)	6842(7)	9971(5)	8167(4)	55(2)
C(12)	7245(7)	10651(5)	8045(5)	62(3)
C(13)	7755(8)	10923(5)	7397(5)	67(3)
C(14)	8189(10)	11530(6)	7296(7)	86(3)
C(15)	8152(13)	11887(7)	7808(10)	106(5)
C(16)	7657(11)	11625(7)	8420(9)	101(4)
C(17)	7216(9)	10994(6)	8561(6)	74(3)
C(18)	5609(8)	9942(6)	8181(6)	72(3)
C(19)	5013(8)	10637(6)	8052(7)	89(4)
C(21)	8269(9)	7806(6)	9777(5)	80(3)
C(22)	9063(8)	7315(5)	10064(4)	84(3)
C(23)	9290(11)	6660(5)	9892(5)	116(5)
C(24)	10227(13)	6250(5)	9997(6)	192(14)
C(25)	10938(9)	6494(10)	10274(7)	290(30)

C(26)	10712(10)	7149(11)	10446(6)	260(20)
C(27)	9774(12)	7559(6)	10341(5)	157(8)
C(28)	7070(20)	8013(14)	10244(9)	197(12)
C(29A)	7190(50)	8851(16)	10298(19)	150(20)
C(29B)	6670(60)	8670(50)	10140(30)	300(70)
C(31)	11076(8)	9296(5)	8155(5)	68(3)
C(32)	12082(8)	8911(5)	8334(5)	68(3)
C(33)	12858(9)	8540(8)	7858(11)	116(6)
C(34)	13695(13)	8089(9)	7998(13)	141(8)
C(35)	13741(19)	7972(10)	8618(15)	146(8)
C(36)	13101(15)	8274(10)	9122(9)	120(6)
C(37)	12201(13)	8815(8)	8968(8)	118(5)
C(38)	11030(14)	10069(9)	7922(12)	148(8)
C(39A)	12050(30)	10304(16)	7980(20)	100(13)
C(39B)	12360(40)	10300(30)	7640(30)	200(40)
C(41)	8212(7)	8012(5)	5188(5)	56(2)
C(42)	7461(7)	8646(5)	5381(4)	54(2)
C(43)	6338(8)	8598(5)	5735(5)	63(2)
C(44)	5654(8)	9198(6)	5855(6)	73(3)
C(45)	6000(11)	9838(5)	5703(6)	79(3)
C(46)	7106(11)	9859(5)	5386(6)	83(3)
C(47)	7845(9)	9281(6)	5223(6)	72(3)
C(48)	8312(9)	7781(6)	4514(5)	76(3)
C(49)	8570(40)	8335(15)	3962(12)	112(10)
C(49A)	7590(30)	8340(20)	4106(15)	125(13)
C(410)	7230(20)	7470(20)	4556(15)	109(11)
C(41A)	7910(40)	7154(16)	4564(17)	121(13)
C(411)	9300(20)	7157(14)	4411(12)	83(7)
C(41B)	9500(30)	7800(30)	4083(15)	180(20)
C(51)	12192(6)	7029(4)	5569(4)	44(2)
C(52)	12836(7)	6325(4)	5555(4)	51(2)
C(53)	13514(7)	6082(5)	5965(5)	57(2)
C(54)	13935(8)	5399(6)	6000(6)	83(3)
C(55)	13719(10)	4954(6)	5649(8)	96(4)
C(56)	13089(10)	5203(6)	5225(8)	98(4)
C(57)	12607(8)	5891(5)	5170(5)	69(3)
C(58)	12731(8)	7646(5)	5140(5)	59(2)
C(59)	12728(10)	8161(6)	5589(6)	92(4)
C(61)	8548(7)	5735(5)	6845(5)	60(2)
C(62)	9185(7)	5081(5)	7075(5)	54(2)
C(63)	9103(9)	4903(5)	7746(5)	68(3)
C(64)	9792(11)	4357(6)	7950(7)	91(4)
C(65)	10564(12)	3975(6)	7505(9)	98(4)
C(66)	10626(10)	4162(6)	6829(8)	91(4)

C(67)	9937(9)	4699(6)	6616(6)	74(3)
C(68)	7338(9)	5742(6)	6789(6)	80(3)
C(69)	6984(11)	5014(7)	6990(8)	114(5)
C(71)	11344(10)	6677(6)	7877(6)	86(3)
C(72)	11876(9)	6070(6)	8159(5)	71(3)
C(73)	11426(11)	5471(7)	8413(6)	88(3)
C(74)	12010(14)	4909(8)	8625(8)	127(6)
C(75)	13065(19)	4918(12)	8596(10)	163(9)
C(76)	13595(12)	5491(12)	8359(9)	147(8)
C(77)	12951(11)	6071(8)	8148(6)	102(4)
C(110)	5587(9)	9524(7)	7659(7)	101(4)
C(111)	5014(10)	9612(7)	8851(7)	106(4)
C(131)	7885(10)	10546(6)	6812(6)	86(3)
C(151)	8729(15)	12522(8)	7683(10)	153(7)
C(171)	6707(11)	10718(7)	9259(6)	95(4)
C(210)	6260(40)	7900(40)	9860(50)	180(30)
C(21A)	6340(60)	7540(60)	9840(50)	330(80)
C(211)	7110(50)	7750(30)	10920(20)	150(20)
C(21B)	6850(60)	7450(40)	10980(30)	210(40)
C(231)	8660(60)	6210(30)	9700(30)	140(20)
C(23A)	8280(50)	6480(20)	9620(30)	109(16)
C(271)	9780(40)	8146(17)	10600(19)	118(12)
C(27A)	9150(40)	8420(20)	10560(30)	170(20)
C(310)	9960(40)	10355(19)	8640(30)	119(16)
C(31A)	10170(40)	10540(20)	8220(30)	140(20)
C(311)	10670(40)	10350(30)	7320(40)	180(30)
C(31B)	10880(50)	10040(20)	7120(20)	140(20)
C(331)	12730(50)	8830(30)	7050(20)	130(20)
C(33A)	12920(30)	8520(30)	7230(30)	101(15)
C(351)	14630(80)	7520(30)	9000(70)	400(90)
C(35A)	14800(40)	7390(30)	8650(50)	210(40)
C(371)	11310(30)	9397(17)	9429(16)	101(9)
C(37A)	11550(30)	9064(18)	9559(17)	104(9)
C(431)	5905(10)	7921(6)	5972(8)	106(5)
C(451)	5223(13)	10454(7)	5853(8)	122(5)
C(471)	9042(10)	9346(7)	4914(8)	104(4)
C(510)	12022(11)	7956(7)	4678(7)	100(4)
C(511)	13895(9)	7439(6)	4745(6)	83(3)
C(531)	13800(8)	6541(6)	6379(6)	82(3)
C(551)	14155(13)	4211(6)	5691(9)	146(8)
C(571)	11914(11)	6135(7)	4689(6)	90(4)
C(610)	7360(11)	5982(7)	6074(7)	98(4)
C(611)	6588(9)	6233(7)	7254(7)	97(4)
C(631)	8315(10)	5292(7)	8255(5)	91(4)

C(651)	11293(16)	3401(8)	7747(12)	167(8)
C(671)	10044(10)	4886(7)	5884(6)	88(4)
C(251)	12200(60)	6410(40)	10490(40)	250(40)
C(25A)	12060(40)	5890(30)	10190(30)	180(30)
C(5S)	4010(50)	2170(30)	7120(20)	400(50)

A.1.16. X-ray crystal structure of Na(μ-SPh)₃[U(NC[ᵗBu]Mes)₃]₂ (Na-3₂-(μ-SPh)₃)

Atomic coordinates (x 10^4) and equivalent isotropic displacement parameters ($\mathring{A}^2$ x 10^3) for **Na-3₂-(μ-SPh)₃**. U(eq) is defined as one third of the trace of the orthogonalized U^{ij} tensor.

	x	y	z	U(eq)
U(1)	2589(1)	13443(1)	6707(1)	31(1)
U(2)	5432(1)	16034(1)	7409(1)	33(1)
S(2)	4484(2)	14055(2)	7515(1)	35(1)
C(65)	8645(11)	14786(12)	8821(5)	60(4)
N(3)	2589(7)	12027(7)	6637(4)	43(2)
N(2)	1630(7)	13301(6)	7329(3)	42(2)
N(4)	5237(8)	16265(6)	8249(3)	44(2)
N(6)	6979(7)	16011(6)	7436(3)	40(2)
N(5)	5830(7)	17463(7)	7224(4)	44(2)
N(1)	1530(7)	13208(6)	5956(3)	41(2)
C(57)	7624(9)	19516(9)	7822(5)	49(3)
C(231)	974(10)	14873(9)	8163(5)	55(3)
C(48)	6456(10)	17323(9)	9026(5)	55(3)
C(51)	6182(8)	18296(8)	7113(4)	39(3)
C(45)	2827(10)	16893(9)	9353(5)	55(3)
C(46)	3223(9)	16247(8)	9485(5)	46(3)
C(68)	8496(9)	16111(8)	7046(4)	42(3)
C(471)	4335(10)	15399(8)	9405(5)	54(3)
C(17)	-873(10)	13025(8)	5502(4)	47(3)
C(18)	1325(9)	13227(9)	5018(4)	50(3)
C(15)	-2455(10)	11542(11)	5404(5)	60(4)
C(52)	6600(9)	19178(7)	7535(4)	39(3)
C(26)	1020(9)	12582(10)	8889(5)	57(4)
C(12)	-289(8)	12501(8)	5493(4)	37(3)
C(81)	4549(8)	13763(7)	8148(4)	32(3)
C(61)	7813(9)	15894(7)	7467(4)	41(3)
C(23)	1007(9)	14040(8)	8409(4)	43(3)
C(21)	807(9)	13067(7)	7527(4)	36(3)

C(34)	1411(11)	9647(9)	7559(6)	65(4)
C(85)	3789(10)	12855(9)	8782(5)	55(3)
C(41)	5367(9)	16724(8)	8694(4)	41(3)
C(47)	4002(9)	16159(8)	9267(4)	42(3)
C(37)	3409(9)	10994(8)	7503(5)	48(3)
C(63)	8804(9)	16128(10)	8394(5)	51(3)
C(42)	4445(9)	16754(8)	8909(4)	40(3)
C(32)	2530(9)	10735(8)	7086(4)	42(3)
C(62)	8155(8)	15507(8)	7929(4)	41(3)
C(67)	7770(8)	14505(8)	7901(5)	43(3)
C(22)	920(8)	13180(8)	8105(4)	41(3)
C(43)	4028(10)	17395(8)	8769(4)	45(3)
C(13)	-748(9)	11523(9)	5456(4)	46(3)
C(11)	905(9)	13003(8)	5530(4)	41(3)
C(271)	842(10)	11511(9)	8044(5)	58(4)
C(571)	8346(9)	19071(8)	7727(5)	54(3)
C(14)	-1857(10)	11044(10)	5411(5)	62(4)
C(53)	5946(10)	19612(8)	7641(5)	51(3)
C(171)	-365(10)	14135(9)	5582(5)	60(4)
C(27)	932(9)	12444(8)	8349(4)	43(3)
C(611)	8961(12)	17176(9)	7039(5)	72(4)
C(24)	1084(9)	14112(9)	8946(5)	54(3)
C(451)	1933(11)	16997(10)	9596(6)	79(5)
C(38)	2897(11)	10730(9)	6135(5)	59(4)
C(28)	-285(9)	12693(8)	7184(4)	42(3)
C(31)	2664(9)	11237(8)	6623(5)	46(3)
C(56)	8014(11)	20305(9)	8232(5)	60(4)
C(55)	7372(13)	20778(10)	8351(5)	67(4)
C(86)	3683(9)	13115(8)	8292(5)	48(3)
C(54)	6330(12)	20401(9)	8064(5)	62(4)
C(33)	1515(9)	10089(8)	7122(5)	48(3)
C(66)	8033(10)	14174(10)	8354(6)	62(4)
C(82)	5524(8)	14151(8)	8489(4)	42(3)
C(83)	5626(10)	13877(10)	8970(5)	56(3)
C(25)	1100(11)	13367(11)	9200(5)	61(4)
C(44)	3251(10)	17448(9)	8982(5)	54(3)
C(84)	4742(11)	13230(9)	9118(5)	57(4)
C(371)	4510(9)	11717(8)	7508(5)	58(4)
C(210)	-336(11)	13440(10)	6868(5)	65(4)
C(671)	7061(10)	13824(9)	7429(5)	60(4)
C(131)	-132(9)	10939(8)	5459(5)	59(4)
C(64)	9027(10)	15765(12)	8820(5)	62(4)
C(36)	3263(11)	10534(9)	7926(5)	60(4)
C(35)	2250(13)	9863(10)	7962(6)	68(4)

C(16)	-1939(10)	12550(10)	5464(5)	58(4)
C(331)	548(10)	9865(9)	6728(6)	71(4)
C(551)	7841(13)	21675(11)	8790(6)	92(5)
C(29)	-1144(9)	12431(11)	7515(5)	71(4)
C(310)	2880(11)	11273(9)	5681(5)	63(4)
C(651)	8811(12)	14369(12)	9294(5)	82(5)
C(431)	4478(11)	18034(9)	8403(5)	65(4)
C(58)	6225(11)	18394(9)	6537(5)	60(4)
C(39)	2006(18)	9672(10)	5967(7)	149(10)
C(510)	6598(17)	19436(12)	6486(6)	129(8)
C(151)	-3666(9)	11013(10)	5351(6)	81(5)
C(631)	9308(10)	17219(9)	8453(5)	68(4)
C(610)	9410(11)	15829(12)	7144(6)	92(5)
C(69)	7815(12)	15598(11)	6513(5)	87(5)
C(531)	4838(11)	19242(10)	7351(5)	66(4)
C(411)	6480(12)	17761(13)	9592(5)	108(7)
C(111)	1998(14)	12725(12)	4934(6)	101(6)
C(59)	6771(15)	17877(13)	6321(6)	107(6)
C(110)	409(12)	12893(15)	4543(5)	128(8)
C(410)	7095(12)	18118(10)	8750(6)	94(5)
C(251)	1131(14)	13428(12)	9780(5)	97(6)
C(49)	7043(12)	16667(11)	9077(6)	92(5)
C(19)	2027(12)	14316(11)	5094(6)	91(5)
S(3)	4369(2)	14846(2)	6375(1)	38(1)
C(91)	4941(9)	14217(10)	6003(4)	48(3)
C(211)	-469(10)	11766(9)	6804(5)	61(4)
C(96)	5304(10)	13633(10)	6200(6)	65(4)
C(94)	5733(12)	13240(12)	5376(6)	82(5)
C(95)	5688(12)	13127(11)	5868(6)	77(4)
C(511)	5117(14)	17949(13)	6222(6)	103(6)
C(311)	3986(15)	10746(15)	6287(5)	127(8)
C(92)	4962(14)	14358(14)	5496(5)	104(6)
C(93)	5354(16)	13825(17)	5184(6)	129(8)
Na	3205(4)	14814(3)	8111(2)	53(1)
S(1)	3124(2)	15475(2)	7182(1)	40(1)
C(71)	2665(10)	16184(9)	6853(6)	61(4)
C(72)	2531(13)	16076(11)	6333(9)	106(7)
C(76)	2368(11)	16816(11)	7108(9)	113(7)
C(74)	1940(20)	17306(17)	6332(18)	220(30)
C(75)	2094(19)	17457(19)	6846(15)	171(16)
C(73)	2182(16)	16662(16)	6042(10)	162(12)
C(351)	2062(13)	9339(12)	8416(7)	104(6)

A.1.17. X-ray crystal structure of (μ-NPh)₂[U(NC[ᵗBu]Mes)₃]₂ (3₂-(μ-NPh)₂)

Atomic coordinates (x 10^4) and equivalent isotropic displacement parameters ($Å^2$ x 10^3) for 3₂-(μ-NPh)₂. U(eq) is defined as one third of the trace of the orthogonalized U^{ij} tensor.

	x	y	z	U(eq)
U(1)	9893(1)	8863(1)	5241(1)	31(1)
N(1)	9684(7)	8442(6)	4502(3)	43(2)
U(2)	5743(1)	4259(1)	9513(1)	36(1)
N(2)	8553(7)	8480(5)	5818(4)	42(2)
N(3)	10993(6)	7835(6)	5792(3)	45(2)
N(4)	5448(8)	4347(6)	8656(4)	53(2)
N(5)	5374(7)	2958(6)	9873(4)	50(2)
N(6)	7429(7)	4217(7)	9174(4)	53(2)
N(7)	9026(6)	10349(5)	5247(3)	36(2)
N(8)	5714(6)	4581(6)	10339(3)	41(2)
C(11)	9534(9)	8108(7)	4117(4)	45(3)
C(11A)	10060(30)	6509(15)	4674(9)	94(13)
C(11B)	9190(50)	6580(40)	4580(20)	170(20)
C(12)	8812(9)	8708(7)	3678(4)	47(3)
C(13)	7687(10)	8863(9)	3813(5)	58(3)
C(14)	7033(11)	9404(10)	3417(6)	77(4)
C(15)	7414(11)	9805(9)	2882(6)	64(3)
C(16)	8493(11)	9662(8)	2757(5)	64(4)
C(17)	9238(10)	9105(9)	3130(5)	58(3)
C(18)	10036(12)	7067(8)	4102(6)	69(4)
C(19A)	11200(40)	6820(40)	4172(19)	103(17)
C(19B)	11350(30)	6920(20)	3852(19)	108(14)
C(21)	7938(8)	8098(7)	6187(5)	42(3)
C(21A)	8370(60)	8860(30)	6845(16)	120(20)
C(21B)	8560(30)	7910(50)	7141(16)	170(30)
C(22)	7494(9)	7440(7)	6046(4)	44(3)
C(23)	8144(9)	6541(7)	6057(4)	48(3)
C(24)	7776(11)	5937(8)	5890(5)	58(3)
C(25)	6810(12)	6199(10)	5702(5)	64(3)
C(26)	6174(11)	7081(10)	5678(5)	69(4)
C(27)	6507(9)	7696(8)	5844(5)	52(3)
C(28)	7611(9)	8298(7)	6806(4)	46(3)
C(29A)	7850(30)	7430(30)	7220(16)	58(11)
C(29B)	7060(40)	7640(30)	7216(11)	145(17)
C(31)	11687(8)	7446(7)	6130(4)	45(3)
C(31A)	12610(50)	7380(40)	6970(30)	140(20)
C(31B)	11838(17)	7714(14)	7067(8)	57(5)

Appendix 1

C(32)	12225(8)	6436(7)	6190(4)	45(3)
C(33)	11916(10)	5806(8)	6657(4)	53(3)
C(34)	12428(12)	4877(8)	6669(6)	67(4)
C(35)	13201(13)	4566(9)	6244(6)	77(4)
C(36)	13484(11)	5229(8)	5799(5)	67(4)
C(37)	13019(9)	6135(7)	5742(4)	47(3)
C(38)	12061(9)	7993(8)	6445(5)	49(3)
C(39)	13217(13)	7933(14)	6211(9)	130(8)
C(41)	5385(9)	4371(8)	8150(5)	53(3)
C(41A)	5170(30)	5120(20)	7084(10)	57(8)
C(41B)	4460(40)	5430(40)	7290(30)	230(40)
C(41C)	6520(30)	5370(20)	7501(15)	66(10)
C(41D)	6320(70)	4960(40)	7260(30)	290(60)
C(42)	5343(11)	3541(10)	7985(5)	65(4)
C(43)	6302(16)	2858(11)	7871(6)	91(5)
C(44)	6189(19)	2089(12)	7725(7)	117(7)
C(45)	5200(20)	1978(14)	7718(6)	110(7)
C(46)	4315(17)	2630(12)	7852(5)	96(6)
C(47)	4333(14)	3423(11)	7976(5)	75(4)
C(48)	5383(11)	5216(9)	7647(5)	63(3)
C(49A)	5460(50)	5970(40)	7960(20)	138(18)
C(49B)	4560(20)	6105(13)	7831(10)	67(6)
C(51)	5260(10)	2169(8)	10003(5)	56(3)
C(52)	4276(10)	1978(7)	10359(5)	51(3)
C(53)	3359(12)	2150(9)	10105(5)	65(4)
C(54)	2429(12)	1953(10)	10457(6)	76(4)
C(55)	2381(11)	1582(10)	11029(5)	71(4)
C(56)	3310(12)	1420(9)	11267(5)	73(4)
C(57)	4211(11)	1623(9)	10952(5)	68(4)
C(58)	6113(13)	1393(9)	9761(7)	90(5)
C(59A)	7270(30)	1600(30)	9646(18)	100(13)
C(59B)	7030(20)	1732(19)	9323(12)	85(8)
C(61)	8332(9)	4369(8)	9011(4)	49(3)
C(61A)	7380(30)	5910(20)	9225(16)	81(10)
C(61B)	7290(40)	6010(30)	8941(19)	124(15)
C(62)	9327(9)	3639(9)	8859(5)	58(3)
C(63)	9725(11)	3557(11)	8285(6)	72(4)
C(64)	10632(14)	2855(13)	8162(7)	93(5)
C(65)	11146(12)	2212(13)	8587(8)	92(5)
C(66)	10731(12)	2284(11)	9159(7)	87(4)
C(67)	9821(10)	2980(9)	9296(5)	65(3)
C(68)	8451(10)	5308(9)	9001(5)	63(3)
C(69)	9039(19)	5191(13)	9491(7)	134(8)
C(71)	7952(7)	10740(6)	5472(4)	36(2)

C(72)	7092(8)	10597(7)	5300(5)	45(3)
C(73)	6078(9)	10984(9)	5521(6)	66(4)
C(74)	5839(10)	11506(9)	5923(6)	73(4)
C(75)	6658(11)	11661(8)	6099(5)	67(4)
C(76)	7705(10)	11283(7)	5887(4)	53(3)
C(81)	6542(8)	4085(8)	10670(4)	46(3)
C(82)	6741(10)	3152(9)	10865(5)	70(4)
C(83)	7500(16)	2649(13)	11190(7)	109(6)
C(84)	8150(16)	3088(17)	11332(7)	125(9)
C(85)	7999(11)	3993(15)	11143(6)	95(6)
C(86)	7192(9)	4504(10)	10811(5)	61(3)
C(111)	9860(30)	6834(13)	3596(9)	193(14)
C(131)	7171(12)	8463(13)	4402(6)	103(6)
C(151)	6702(13)	10429(12)	2468(7)	109(6)
C(171)	10418(10)	9041(10)	2977(5)	73(4)
C(211)	6740(30)	9050(20)	6843(9)	290(30)
C(231)	9211(10)	6216(8)	6240(5)	64(3)
C(251)	6427(14)	5519(11)	5517(7)	97(5)
C(271)	5768(9)	8683(9)	5778(6)	68(4)
C(311)	11630(20)	8948(11)	6218(8)	152(10)
C(331)	11045(10)	6060(10)	7135(5)	73(4)
C(351)	13752(17)	3582(10)	6303(7)	125(7)
C(371)	13314(10)	6767(10)	5203(5)	73(4)
C(431)	7403(12)	2942(12)	7883(8)	108(6)
C(451)	5110(20)	1108(13)	7593(8)	164(11)
C(471)	3296(12)	4086(11)	8126(6)	83(4)
C(510)	6366(17)	538(11)	10173(9)	146(9)
C(511)	5610(20)	1225(15)	9287(10)	181(11)
C(531)	3286(13)	2627(13)	9491(6)	105(6)
C(551)	1389(13)	1348(14)	11376(7)	116(7)
C(571)	5113(13)	1506(12)	11271(6)	104(6)
C(611)	9117(17)	5662(13)	8459(7)	134(8)
C(631)	9213(14)	4178(12)	7785(6)	94(5)
C(651)	12157(14)	1424(11)	8442(9)	131(8)
C(671)	9399(11)	3006(10)	9918(5)	78(4)

Appendix 1

A.1.18. X-ray crystal structure of (COT)U(NC[^{t}Bu]Mes)₃ (3-COT)

Atomic coordinates (x 10^4) and equivalent isotropic displacement parameters (Å^2 x 10^3) for **3-COT**. U(eq) is defined as one third of the trace of the orthogonalized U^{ij} tensor.

	x	y	z	U(eq)
U	2438(1)	-4402(1)	4288(1)	25(1)
N(1)	4144(6)	-5086(5)	4362(3)	30(2)
N(2)	1819(7)	-5352(5)	3748(3)	33(2)
C(22)	1384(7)	-5601(7)	2931(3)	33(2)
N(3)	3074(7)	-3432(5)	3768(3)	32(2)
C(21)	1470(8)	-5908(7)	3440(3)	35(2)
C(11)	5097(7)	-5520(7)	4412(3)	30(2)
C(28)	1113(10)	-6916(7)	3560(4)	44(3)
C(12)	5177(7)	-6497(6)	4228(3)	32(2)
C(13)	5668(9)	-6661(8)	3785(4)	39(3)
C(14)	5683(11)	-7550(8)	3612(4)	53(3)
C(15)	5216(12)	-8290(8)	3860(4)	60(3)
C(16)	4745(9)	-8107(7)	4304(4)	50(3)
C(17)	4715(9)	-7239(7)	4485(4)	40(3)
C(18)	6189(8)	-5111(6)	4668(3)	34(2)
C(19)	6571(10)	-4236(8)	4410(4)	58(3)
C(31)	3501(8)	-2854(6)	3474(3)	29(2)
C(32)	4825(8)	-2748(6)	3440(3)	29(2)
C(33)	5460(8)	-3202(7)	3098(3)	33(2)
C(34)	6692(9)	-3100(8)	3079(4)	45(3)
C(35)	7293(9)	-2540(7)	3391(4)	46(3)
C(38)	2673(9)	-2259(6)	3165(3)	37(2)
C(110)	7233(9)	-5787(8)	4695(4)	59(3)
C(131)	6150(11)	-5879(9)	3486(4)	58(3)
C(151)	5218(16)	-9265(9)	3660(5)	93(5)
C(171)	4158(10)	-7069(8)	4976(4)	51(3)
C(351)	8628(9)	-2410(9)	3377(5)	66(4)
C(23)	2372(10)	-5707(6)	2638(3)	45(2)
C(5)	2496(14)	-4676(10)	5240(3)	61(3)
C(7)	2397(18)	-3037(10)	4949(5)	81(5)
C(24)	2268(12)	-5378(7)	2183(4)	58(3)
C(27)	358(9)	-5181(7)	2755(4)	46(3)
C(37)	5410(9)	-2172(7)	3770(3)	35(2)
C(4)	1571(12)	-5205(9)	5086(5)	60(4)
C(6)	2814(13)	-3775(13)	5179(4)	77(5)
C(36)	6626(9)	-2087(7)	3735(3)	38(3)
C(2)	126(10)	-4311(13)	4543(4)	70(4)

C(25)	1274(15)	-5002(8)	1991(4)	64(4)
C(26)	333(13)	-4904(8)	2287(4)	61(4)
C(331)	4870(10)	-3847(8)	2749(4)	53(3)
C(371)	4763(10)	-1710(8)	4164(4)	49(3)
C(111)	5838(11)	-4843(10)	5176(4)	63(3)
C(231)	3515(10)	-6129(9)	2803(5)	60(3)
C(1)	493(14)	-3374(12)	4494(4)	73(5)
C(3)	580(12)	-5065(10)	4789(5)	64(4)
C(271)	-711(12)	-5001(9)	3071(5)	74(4)
C(8)	1448(18)	-2872(9)	4657(6)	78(5)
C(251)	1220(20)	-4705(12)	1479(5)	129(9)
C(211)	1901(16)	-7266(10)	3942(6)	108(7)
C(210)	-155(13)	-6894(13)	3748(7)	110(7)
C(29)	1054(19)	-7522(9)	3128(5)	112(7)
C(39)	3362(10)	-1602(8)	2850(4)	57(3)
C(310)	1839(11)	-1697(9)	3489(4)	59(3)
C(311)	1876(12)	-2888(10)	2866(5)	69(4)

Appendix 1

Chapter 3

A.1.19. X-ray crystal structure of 1b-(bipy)₂

Atomic coordinates (x 10^4) and equivalent isotropic displacement parameters (Å^2 x 10^3) for **1b-(bipy)₂**. U(eq) is defined as one third of the trace of the orthogonalized U^{ij} tensor.

	x	y	z	U(eq)
U	2827(1)	3845(1)	2372(1)	27(1)
O	0	0	0	87(2)
N(1)	4217(4)	5444(3)	2200(2)	31(1)
C(1S)	-1141(15)	-398(13)	403(8)	73(4)
C(1SA)	-177(14)	-235(13)	715(8)	70(4)
N(2)	3986(4)	2321(3)	1905(2)	30(1)
C(2S)	-1289(12)	-744(11)	1096(7)	126(4)
N(3)	2127(4)	2753(3)	3608(2)	31(1)
N(4)	988(4)	4907(3)	2979(2)	32(1)
N(5)	1591(4)	5010(3)	1372(2)	33(1)
N(6)	832(4)	2850(3)	2180(2)	32(1)
C(10)	5593(5)	5298(5)	1133(3)	42(1)
C(11)	3858(4)	5883(4)	2840(3)	32(1)
C(12)	3190(5)	7019(4)	2837(3)	39(1)
C(13)	2682(5)	7317(5)	3466(3)	45(1)
C(14)	2834(5)	6441(5)	4125(3)	45(1)
C(15)	3478(5)	5311(5)	4156(3)	39(1)
C(16)	4009(4)	5054(4)	3503(3)	34(1)
C(17)	5372(5)	5997(4)	1739(3)	38(1)
C(18)	6585(5)	5811(5)	2170(3)	46(1)
C(19)	5175(5)	7404(5)	1415(3)	48(1)
C(21)	4811(4)	1697(4)	2440(2)	29(1)
C(22)	5478(4)	2439(4)	2796(3)	33(1)
C(23)	6219(5)	1934(5)	3383(3)	39(1)
C(24)	6346(5)	647(5)	3614(3)	41(1)
C(25)	5744(5)	-119(5)	3262(3)	39(1)
C(26)	4989(5)	397(4)	2695(3)	35(1)
C(27)	3872(5)	1816(4)	1254(2)	33(1)
C(28)	5228(5)	1479(6)	944(3)	52(1)
C(29)	3251(5)	2863(5)	695(3)	43(1)
C(31)	1080(5)	3181(4)	3992(3)	35(1)
C(32)	644(5)	2458(5)	4675(3)	45(1)

C(33)	1225(6)	1335(5)	4966(3)	51(1)
C(34)	2287(6)	907(5)	4579(3)	46(1)
C(35)	2691(5)	1635(4)	3924(3)	38(1)
C(41)	493(4)	4359(4)	3659(3)	34(1)
C(42)	-509(5)	4971(5)	4004(3)	49(1)
C(43)	-1026(6)	6095(6)	3665(3)	58(2)
C(44)	-538(5)	6645(5)	2960(3)	48(1)
C(45)	438(5)	6032(5)	2659(3)	38(1)
C(51)	361(4)	4670(4)	1260(3)	35(1)
C(52)	-394(5)	5458(5)	737(3)	45(1)
C(53)	78(6)	6537(5)	318(3)	50(1)
C(54)	1341(6)	6850(5)	416(3)	49(1)
C(55)	2020(5)	6090(5)	933(3)	42(1)
C(61)	-42(4)	3495(5)	1688(2)	35(1)
C(62)	-1230(5)	2967(5)	1627(3)	45(1)
C(63)	-1524(5)	1807(5)	2043(3)	50(1)
C(64)	-634(5)	1168(5)	2527(3)	47(1)
C(65)	492(5)	1723(5)	2578(3)	40(1)
C(131)	1932(7)	8547(5)	3442(4)	64(2)
C(151)	3594(6)	4347(6)	4852(3)	52(1)
C(210)	2990(6)	690(5)	1378(3)	47(1)
C(231)	6964(6)	2749(6)	3726(4)	62(2)
C(251)	5942(7)	-1525(5)	3513(4)	68(2)

A.1.20. X-ray crystal structure of 2a-bipy

Atomic coordinates (x 10^4) and equivalent isotropic displacement parameters (Å^2 x 10^3) for **2a-bipy**. U(eq) is defined as one third of the trace of the orthogonalized U^{ij} tensor.

	x	y	z	U(eq)
U	4147(1)	2626(1)	2355(1)	20(1)
N(1)	2384(6)	1411(6)	2440(3)	24(2)
C(1S)	-377(19)	6531(18)	230(20)	280(30)
C(2S)	-330(20)	5890(50)	-152(11)	280(30)
N(2)	5186(6)	1686(6)	2016(4)	25(2)
C(3S)	-510(30)	5016(19)	-256(19)	63(9)
N(3)	5474(7)	3934(6)	3278(3)	27(2)
N(4)	3901(6)	3304(6)	1328(4)	28(2)
N(5)	3207(6)	3977(6)	2315(3)	26(2)

Appendix 1

C(5S)	10370(20)	6880(20)	3008(14)	163(11)
C(6S)	9910(20)	7250(20)	3528(13)	135(9)
C(7S)	9658(13)	8306(13)	3451(7)	76(4)
C(8S)	9302(16)	8758(19)	3957(9)	103(6)
C(9S)	9014(16)	9718(17)	3849(9)	106(6)
C(11)	2525(7)	1090(7)	3061(4)	23(2)
C(12)	2366(8)	1663(8)	3600(4)	27(2)
C(13)	2574(8)	1386(8)	4208(5)	33(2)
C(14)	2975(9)	544(9)	4281(5)	35(2)
C(15)	3162(9)	-17(8)	3774(5)	35(2)
C(16)	2926(8)	244(8)	3164(5)	31(2)
C(17)	1119(8)	908(7)	1998(4)	26(2)
C(18)	299(8)	1257(9)	2306(5)	32(2)
C(19)	563(8)	-408(8)	1829(5)	34(2)
C(21)	6483(9)	2306(8)	2197(5)	35(2)
C(22)	7000(10)	2987(8)	1809(6)	44(3)
C(23)	8212(11)	3577(10)	1917(8)	62(4)
C(24)	8945(11)	3458(11)	2476(8)	65(4)
C(25)	8486(10)	2793(10)	2909(7)	58(3)
C(26)	7229(9)	2229(11)	2724(5)	45(3)
C(27)	4708(7)	485(7)	1640(4)	25(2)
C(28)	4849(9)	-308(8)	2086(5)	26(2)
C(29)	4851(10)	-1666(9)	1167(5)	35(2)
C(31)	5835(8)	5004(7)	3091(4)	29(2)
C(32)	6281(8)	5125(8)	2560(4)	27(2)
C(33)	6458(8)	6067(8)	2278(4)	32(2)
C(34)	6239(8)	6931(8)	2562(4)	32(2)
C(35)	5819(8)	6856(8)	3121(4)	29(2)
C(36)	5622(9)	5911(8)	3367(5)	30(2)
C(37)	6099(8)	3878(8)	3944(4)	27(2)
C(38)	5649(9)	2631(8)	3975(5)	32(2)
C(39)	5848(11)	4483(10)	4507(5)	37(2)
C(41)	3516(8)	4161(8)	1273(4)	30(2)
C(42)	3481(9)	4592(10)	699(5)	40(2)
C(43)	3741(9)	4165(9)	191(5)	43(3)
C(44)	4076(11)	3271(10)	237(5)	46(3)
C(45)	4155(9)	2879(8)	797(5)	36(2)
C(51)	3179(7)	4536(7)	1803(4)	27(2)
C(52)	2796(9)	5416(8)	1840(5)	34(2)
C(53)	2424(9)	5689(9)	2348(5)	38(2)
C(54)	2460(8)	5119(8)	2860(5)	33(2)
C(55)	2856(8)	4290(9)	2807(5)	34(2)
C(110)	1116(9)	1329(9)	1360(5)	32(2)
C(111)	-984(9)	767(11)	1823(5)	44(3)

C(112)	-714(9)	-901(10)	1345(5)	46(3)
C(113)	-181(9)	830(10)	874(5)	39(2)
C(114)	-1520(10)	-518(12)	1646(6)	53(3)
C(115)	-699(10)	-489(11)	713(5)	50(3)
C(116)	-969(15)	1189(19)	1200(7)	54(4)
C(131)	2379(11)	2009(10)	4771(5)	49(3)
C(151)	3669(13)	-878(11)	3884(6)	61(3)
C(210)	5308(9)	360(8)	1107(5)	32(2)
C(211)	4245(9)	-1560(8)	1688(5)	34(2)
C(212)	3359(8)	98(8)	1291(5)	26(2)
C(213)	2782(10)	-1137(9)	891(5)	37(2)
C(214)	4732(9)	-869(8)	710(5)	32(2)
C(215)	2911(9)	-1921(8)	1347(5)	36(2)
C(216)	3384(9)	-1225(9)	376(5)	37(2)
C(231)	8740(13)	4257(11)	1469(9)	87(5)
C(251)	9297(11)	2642(16)	3491(7)	90(6)
C(310)	7474(8)	4394(10)	4067(5)	39(2)
C(311)	6313(10)	2488(10)	4633(5)	44(3)
C(312)	6491(10)	4354(9)	5176(5)	40(2)
C(313)	8109(10)	4259(11)	4745(6)	51(3)
C(314)	6052(10)	3110(10)	5187(5)	42(3)
C(315)	7647(10)	2994(11)	4730(6)	50(3)
C(316)	7854(11)	4886(11)	5284(6)	51(3)
C(331)	6860(10)	6120(9)	1680(5)	46(3)
C(351)	5572(10)	7809(8)	3415(5)	42(2)

A.1.21. X-ray crystal structure of 3-(bipy)$_2$

Atomic coordinates (x 10^4) and equivalent isotropic displacement parameters (Å^2 x 10^3) for 3-(bipy)$_2$. U(eq) is defined as one third of the trace of the orthogonalized U^{ij} tensor.

	x	y	z	U(eq)
U	1821(1)	1326(1)	2495(1)	27(1)
I	946(1)	1731(1)	3811(1)	67(1)
N(1)	2552(4)	386(2)	2592(3)	34(1)
N(3)	3304(4)	1839(3)	2713(3)	40(1)
C(31)	4036(5)	2232(3)	2704(3)	36(2)
N(42)	2117(4)	1397(2)	1236(3)	34(1)
C(12)	3403(5)	-415(3)	2026(3)	34(1)

N(41)	1238(4)	2355(2)	1850(3)	39(1)
C(15)	4050(5)	-780(3)	770(3)	43(2)
C(410)	2550(5)	909(3)	948(3)	41(2)
C(23)	-1509(6)	1992(4)	1412(4)	53(2)
C(27)	-758(5)	1414(3)	517(4)	41(2)
C(36)	3434(7)	3638(4)	1531(5)	64(3)
C(37)	3530(5)	3269(3)	2124(4)	45(2)
C(13)	4390(5)	-245(3)	1865(3)	37(2)
C(46)	1848(5)	1908(3)	853(3)	39(2)
C(32)	4013(5)	2677(3)	2101(3)	37(2)
C(47)	2027(6)	1933(4)	173(4)	52(2)
C(41)	795(6)	2819(3)	2173(4)	50(2)
C(48)	2469(7)	1415(4)	-108(4)	59(2)
C(231)	-1733(7)	2069(5)	2131(5)	72(3)
C(42)	441(7)	3360(4)	1849(5)	64(2)
C(17)	2757(5)	-787(3)	1565(3)	41(2)
C(310)	5801(6)	2716(4)	3138(4)	53(2)
C(38)	4954(5)	2260(3)	3291(3)	43(2)
C(26)	-1035(6)	1904(4)	74(4)	54(2)
C(39)	5402(7)	1597(4)	3395(5)	71(3)
C(16)	3084(5)	-955(3)	942(3)	44(2)
C(44)	996(6)	2973(4)	842(4)	58(2)
C(45)	1355(5)	2436(3)	1185(3)	39(2)
C(34)	4259(7)	2866(5)	938(4)	65(2)
C(18)	3119(5)	-504(3)	3335(3)	39(2)
C(371)	3133(7)	3512(4)	2752(5)	60(2)
C(24)	-1797(6)	2466(4)	941(5)	65(2)
C(11)	2992(5)	-139(3)	2650(3)	33(1)
C(111)	3812(7)	-120(4)	3858(4)	68(2)
C(271)	-240(6)	848(4)	255(4)	53(2)
C(171)	1709(6)	-1005(5)	1722(4)	71(3)
C(49)	2727(6)	896(4)	276(3)	49(2)
C(33)	4391(6)	2476(4)	1507(3)	46(2)
C(151)	4377(6)	-986(4)	106(4)	59(2)
C(14)	4691(5)	-427(3)	1240(4)	42(2)
C(251)	-1856(9)	2980(5)	-224(6)	98(4)
C(43)	535(7)	3438(4)	1178(5)	69(3)
C(110)	3611(7)	-1146(4)	3272(4)	56(2)
C(25)	-1546(6)	2440(4)	266(5)	61(2)
C(131)	5109(6)	142(4)	2359(4)	57(2)
C(19)	2046(7)	-580(4)	3566(4)	63(2)
N(2)	278(4)	987(3)	2030(3)	38(1)
C(22)	-990(5)	1453(3)	1189(4)	44(2)
C(21)	-622(5)	948(3)	1703(3)	38(2)

C(28)	-1349(5)	384(4)	1806(4)	51(2)
C(311)	4533(7)	2456(5)	3938(4)	69(2)
C(331)	4914(7)	1857(4)	1472(4)	65(2)
C(35)	3802(8)	3440(5)	929(4)	70(3)
C(211)	-2358(6)	422(5)	1334(5)	78(3)
C(210)	-796(7)	-229(4)	1653(7)	94(4)
C(351)	3683(11)	3845(6)	300(5)	112(5)
C(29)	-1596(9)	400(6)	2545(5)	103(4)

A.1.22. X-ray crystal structure of 3-I-bipy

Atomic coordinates (x 10^4) and equivalent isotropic displacement parameters (Å^2 x 10^3) for **3-I-bipy**. U (eq) is defined as one third of the trace of the orthogonalized U^{ij} tensor.

	x	y	z	U(eq)
U	9867(1)	6579(1)	1538(1)	36(1)
N(1)	8585(4)	6307(3)	1757(2)	54(2)
N(2)	9303(3)	7529(3)	980(2)	46(1)
N(3)	10703(4)	6222(3)	2291(2)	47(1)
N(4)	11201(3)	7474(3)	1540(2)	44(1)
N(5)	9995(3)	7813(3)	2127(2)	47(1)
N(6)	10067(3)	5128(3)	1418(2)	47(1)
N(7)	10425(3)	6136(3)	718(2)	44(1)
C(11)	7880(4)	6137(4)	1883(3)	51(2)
C(12)	7608(5)	6485(4)	2373(3)	59(2)
C(13)	7137(5)	7171(5)	2342(4)	70(2)
C(14)	6930(6)	7496(6)	2799(5)	91(3)
C(15)	7172(7)	7187(7)	3271(5)	100(3)
C(16)	7652(7)	6489(7)	3305(5)	100(4)
C(17)	7876(5)	6143(5)	2859(4)	71(2)
C(18)	7279(5)	5539(5)	1559(4)	73(2)
C(21)	9003(4)	8127(4)	728(3)	47(2)
C(22)	9327(4)	8948(4)	893(3)	50(2)
C(23)	8928(5)	9375(4)	1247(3)	59(2)
C(24)	9237(7)	10115(5)	1393(4)	75(3)
C(25)	9916(7)	10437(5)	1226(4)	79(3)
C(26)	10311(6)	9998(5)	883(4)	77(3)
C(27)	10026(5)	9253(4)	702(3)	58(2)
C(28)	8300(5)	8063(5)	245(3)	60(2)

C(29)	8027(7)	8848(6)	10(4)	99(3)
C(31)	11334(5)	6146(4)	2645(3)	46(2)
C(32)	12199(4)	6348(4)	2526(3)	49(2)
C(33)	12623(5)	5829(4)	2235(3)	55(2)
C(34)	13390(5)	6035(5)	2099(3)	67(2)
C(35)	13758(5)	6761(6)	2221(4)	73(2)
C(36)	13332(5)	7259(6)	2510(4)	70(2)
C(37)	12569(5)	7069(4)	2669(3)	55(2)
C(38)	11243(5)	5821(4)	3197(3)	60(2)
C(39)	10624(8)	6350(6)	3438(4)	92(3)
C(41)	11207(4)	8208(4)	1737(3)	47(2)
C(42)	11835(6)	8734(5)	1651(3)	69(2)
C(43)	12461(6)	8520(5)	1378(4)	76(3)
C(44)	12486(5)	7769(5)	1213(3)	69(2)
C(45)	11845(4)	7268(5)	1297(3)	52(2)
C(51)	10553(5)	8384(4)	2067(3)	49(2)
C(52)	10539(6)	9090(5)	2340(4)	67(2)
C(53)	9973(6)	9195(6)	2676(4)	79(3)
C(54)	9417(6)	8594(6)	2749(4)	84(3)
C(55)	9446(5)	7920(5)	2456(3)	58(2)
C(61)	10457(4)	4826(4)	1028(3)	49(2)
C(62)	10680(5)	4019(4)	1024(3)	65(2)
C(63)	10481(6)	3539(4)	1400(4)	71(2)
C(64)	10052(6)	3844(5)	1802(4)	73(2)
C(65)	9861(5)	4624(4)	1788(3)	55(2)
C(71)	10639(4)	5362(4)	639(3)	50(2)
C(72)	10998(5)	5168(5)	189(3)	67(2)
C(73)	11131(6)	5719(6)	-176(3)	74(2)
C(74)	10915(5)	6498(5)	-96(3)	62(2)
C(75)	10569(5)	6656(5)	345(3)	53(2)
C(131)	6830(6)	7567(6)	1839(4)	95(3)
C(151)	6934(9)	7538(9)	3769(5)	165(6)
C(171)	8425(9)	5426(8)	2910(6)	99(4)
C(210)	8591(7)	7543(8)	-163(4)	132(5)
C(211)	7516(6)	7680(7)	438(4)	107(4)
C(231)	8175(6)	9071(5)	1468(4)	78(3)
C(251)	10275(8)	11231(6)	1399(5)	121(4)
C(271)	10490(5)	8828(5)	323(3)	72(2)
C(310)	12083(7)	5749(6)	3558(4)	75(3)
C(311)	10851(5)	5000(5)	3131(3)	67(2)
C(331)	12253(5)	5053(4)	2057(3)	67(2)
C(351)	14587(6)	7007(8)	2053(5)	117(4)
C(371)	12153(7)	7658(6)	2985(4)	66(3)
C(11A)	7670(20)	5430(20)	1050(12)	121(13)

C(11B)	7057(15)	5770(16)	954(7)	117(9)
C(11C)	6411(8)	5473(10)	1768(8)	129(6)
C(11D)	6460(30)	6020(40)	1380(30)	70(20)
C(19A)	7681(10)	4706(9)	1572(9)	101(5)
C(19B)	7290(40)	4790(30)	1910(12)	200(30)
C(3S)	14000(40)	8840(40)	260(20)	440(40)
C(1S)	15490(20)	8740(30)	848(17)	370(20)
C(2SA)	15180(50)	8980(40)	340(30)	260(30)
C(2SB)	15020(60)	8140(50)	190(30)	300(30)
C(4SB)	14470(70)	9070(50)	120(40)	590(60)
C(5SA)	13520(40)	9300(40)	-210(30)	170(20)
C(5SB)	12700(20)	9080(18)	-142(12)	196(11)

Appendix 2: DFT Computational Details

Chapter 1

A.2.1. Computational details for $H_3SiNU(NH_2)_3$

Input file:[1]

```
$ADFBIN/dirac   < $ADFRESOURCES/Dirac/U.5d
rm -f FILE* logfile

$ADFBIN/dirac   < $ADFRESOURCES/Dirac/N
rm -f FILE* logfile

$ADFBIN/dirac   < $ADFRESOURCES/Dirac/H
rm -f FILE* logfile

$ADFBIN/dirac   < $ADFRESOURCES/Dirac/Si.2p
rm -f FILE* logfile

mv TAPE12 t12.rel

$ADFBIN/adf   <<eor
Create   U  File=$ADFRESOURCES/ZORA/TZ2P/U.5d
XC
GGA   Becke Perdew
End
Relativistic   ZORA
CorePotentials t12.rel &
 U 1
End
End Input
eor
mv TAPE21   t21.U

$ADFBIN/adf   <<eor
Create   N  File=$ADFRESOURCES/ZORA/TZ2P/N
XC
GGA   Becke Perdew
End
Relativistic    ZORA
CorePotentials t12.rel &
 N 2
End
End Input
```

---

[1] The input files for the calculations with the other density functionals are similar, except for indicating what type of gradient exchange correlation was used.

```
eor
mv TAPE21   t21.N

$ADFBIN/adf  <<eor
Create   H   File=$ADFRESOURCES/ZORA/TZ2P/H
XC
GGA   Becke Perdew
End
Relativistic  ZORA
CorePotentials t12.rel &
 H 3
End
End Input
eor
mv TAPE21   t21.H

$ADFBIN/adf  <<eor
Create   Si  File=$ADFRESOURCES/ZORA/TZ2P/Si.2p
XC
GGA   Becke Perdew
End
Relativistic  ZORA
CorePotentials t12.rel &
 Si 4
End
End Input
eor
mv TAPE21   t21.Si

$ADFBIN/adf << eor > output
Title H3SiNU(NH2)3

Atoms
     1.U          0.017515     0.000051     0.000030
     2.N          1.957215    -0.000257    -0.000148
     3.N         -0.706993     2.117330    -0.000328
     4.N         -0.707665    -1.058782    -1.833210
     5.N         -0.707329    -1.058048     1.833825
     6.Si         3.691689    -0.000532    -0.000306
     7.H          4.237424     1.400449    -0.001401
     8.H          4.237202    -0.700248     1.213526
     9.H          4.236979    -0.702058    -1.213194
    10.H         -0.037869     2.884100    -0.000543
    11.H         -1.705597     2.313424    -0.000276
    12.H         -0.872639    -2.062711    -1.809237
    13.H         -0.872477    -0.536374    -2.690875
    14.H         -0.282433    -0.859863     2.737069
    15.H         -1.461859    -1.737420     1.764527
End
symmetry=nosym
Geometry
Optim
converge grad=3e-2, rad=3e-2, angle=2
Iterations 200
```

```
End

XC
GGA Becke Perdew
End

SCF
   Iterations 100
End

unrestricted
charge 0 1

Maxmemoryusage 40

Fragments
U  t21.U
N  t21.N
H  t21.H
Si t21.Si
End

Relativistic  ZORA
CorePotentials  t12.rel  &
  U  1
  N  2
  H  3
Si  4
End

End Input
eor
```

A.2.2. Computational details for [$H_3SiNU(NH_2)_3$]$^-$

Table 1. Optimized variables (distances in Å and angles in °) for [$H_3SiNU(NH_2)_3$]$^-$ and experimental values for Li(OEt$_2$)Me$_3$SiNU(N[^{1}Ad]Ar)$_3$.

Variable	Calcd.	Exp.
U-Nligand	2.278; 2.282; 2.304	2.255(3); 2.323(3); 2.492(3)
U-Nimide	2.006	2.050(3)
N-Si	1.687	1.709(4)
UNSi	165.5	150.2(2)

Input file:

```
$ADFBIN/dirac  < $ADFRESOURCES/Dirac/U.5d
```

```
rm -f FILE* logfile

$ADFBIN/dirac  < $ADFRESOURCES/Dirac/N
rm -f FILE* logfile

$ADFBIN/dirac  < $ADFRESOURCES/Dirac/H
rm -f FILE* logfile

$ADFBIN/dirac  < $ADFRESOURCES/Dirac/Si.2p
rm -f FILE* logfile

mv TAPE12 t12.rel

$ADFBIN/adf  <<eor
Create  U  File=$ADFRESOURCES/ZORA/TZ2P/U.5d
XC
GGA   Becke Perdew
End
Relativistic  ZORA
CorePotentials t12.rel &
 U 1
End
End Input
eor
mv TAPE21  t21.U

$ADFBIN/adf  <<eor
Create  N  File=$ADFRESOURCES/ZORA/TZ2P/N
XC
GGA   Becke Perdew
End
Relativistic    ZORA
CorePotentials t12.rel &
 N 2
End
End Input
eor
mv TAPE21  t21.N

$ADFBIN/adf  <<eor
Create  H  File=$ADFRESOURCES/ZORA/TZ2P/H
XC
GGA   Becke Perdew
End
Relativistic  ZORA
CorePotentials t12.rel &
 H 3
End
End Input
eor
mv TAPE21  t21.H

$ADFBIN/adf  <<eor
Create  Si  File=$ADFRESOURCES/ZORA/TZ2P/Si.2p
```

```
XC
GGA   Becke Perdew
End
Relativistic   ZORA
CorePotentials t12.rel &
  Si 4
End
End Input
eor
mv TAPE21   t21.Si

$ADFBIN/adf << eor > output
Title H3SiNU(NH2)3 anion

Atoms
  U      0.000000      0.000000      0.000000
  N      0.000000      0.000000      2.050000
  N      2.056831      0.000000     -0.924376
  H      2.771509     -0.612513     -0.563645
  H      2.235287      0.539722     -1.756793
  N     -1.244120      2.149563      0.203980
  H     -0.744271      3.024740      0.187271
  H     -2.160726      2.242158     -0.205073
  N     -0.953785     -2.032375     -0.596720
  H     -0.949692     -2.327370     -1.560580
  H     -1.137576     -2.729141      0.108122
Si     0.793658     -0.302434      3.533011
  H     1.681559     -0.766667      3.422632
  H     0.969494      0.548566      4.043838
  H     0.252748     -0.856678      4.178219
End

symmetry=nosym

Geometry
Optim
converge grad=3e-2, rad=3e-2, angle=2
Iterations 200
End

XC
GGA Becke Perdew
End

SCF
   Iterations 100
End

unrestricted
charge -1 2

Maxmemoryusage 40

Fragments
```

```
U  t21.U
N  t21.N
H  t21.H
Si t21.Si
End

Relativistic  ZORA
CorePotentials  t12.rel  &
  U  1
  N  2
  H  3
Si  4
End

End Input
eor
```

A.2.3. Computational details for IU(NH$_2$)$_3$

Input file:[2]

```
$ADFBIN/adf  -n1<<eor
Create  U  $ADFRESOURCES/TZP/U.5d
End Input
eor
mv TAPE21  t21.U

$ADFBIN/adf  -n1<<eor
Create  N  $ADFRESOURCES/TZP/N
End Input
eor
mv TAPE21  t21.N

$ADFBIN/adf  -n1<<eor
Create  H  $ADFRESOURCES/TZP/H
End Input
eor
mv TAPE21  t21.H

$ADFBIN/adf  -n1<<eor
Create  I  $ADFRESOURCES/TZP/I.4d
End Input
eor
mv TAPE21  t21.I
```

---

[2] The input files for the calculations with the other density functionals are similar, except for indicating what type of gradient exchange correlation was used.

```
$ADFBIN/adf << eor > output
Title iodide amide

Atoms
     1.U          0.010907    -0.000047     0.000046
     2.I          2.965933     0.000121    -0.000119
     3.N         -0.701252     2.068189     0.000627
     4.N         -0.701176    -1.033756    -1.791364
     5.N         -0.700976    -1.034693     1.790994
     6.H         -1.053997     2.484485    -0.856965
     7.H         -0.679438     2.612975     0.858489
     8.H         -1.412633    -1.755447    -1.712698
     9.H         -0.320616    -0.792417    -2.702476
    10.H         -0.042120    -1.310902     2.514053
    11.H         -1.690635    -1.239272     1.900167
End

symmetry=nosym

Geometry
Optim
converge grad=3e-2, rad=3e-2, angle=2
Iterations 200
End

XC
GGA Becke Perdew
End

SCF
   Iterations 100
End

unrestricted
charge 0 2

Maxmemoryusage 40

Fragments
U   t21.U
N   t21.N
H   t21.H
I   t21.I
End

End Input
eor
```

A.2.4. Computational details for $(Me_2O)U(NH_2)_3$

Input file:[3]

```
$ADFBIN/dirac  < $ADFRESOURCES/Dirac/U.5d
rm -f FILE* logfile

$ADFBIN/dirac  < $ADFRESOURCES/Dirac/N
rm -f FILE* logfile

$ADFBIN/dirac  < $ADFRESOURCES/Dirac/H
rm -f FILE* logfile

$ADFBIN/dirac  < $ADFRESOURCES/Dirac/O
rm -f FILE* logfile

$ADFBIN/dirac  < $ADFRESOURCES/Dirac/C
rm -f FILE* logfile

mv TAPE12 t12.rel

$ADFBIN/adf  <<eor
Create  U  File=$ADFRESOURCES/ZORA/TZ2P/U.5d
XC
GGA  Becke Perdew
End
Relativistic  ZORA
CorePotentials t12.rel &
 U 1
End
End Input
eor
mv TAPE21  t21.U

$ADFBIN/adf  <<eor
Create  N  File=$ADFRESOURCES/ZORA/TZ2P/N
XC
GGA  Becke Perdew
End
Relativistic  ZORA
CorePotentials t12.rel &
 N 2
End
End Input
eor
mv TAPE21  t21.N

$ADFBIN/adf  <<eor
```

---

[3] The input files for the calculations with the other density functionals are similar, except for indicating what type of gradient exchange correlation was used.

```
Create  H  File=$ADFRESOURCES/ZORA/TZ2P/H
XC
GGA  Becke Perdew
End
Relativistic  ZORA
CorePotentials t12.rel &
 H 3
End
End Input
eor
mv TAPE21  t21.H

$ADFBIN/adf  <<eor
Create  O  File=$ADFRESOURCES/ZORA/TZ2P/O
XC
GGA  Becke Perdew
End
Relativistic  ZORA
CorePotentials t12.rel &
 O 4
End
End Input
eor
mv TAPE21  t21.O

$ADFBIN/adf  <<eor
Create  C  File=$ADFRESOURCES/ZORA/TZ2P/C
XC
GGA  Becke Perdew
End
Relativistic  ZORA
CorePotentials t12.rel &
 C 5
End
End Input
eor
mv TAPE21  t21.C
$ADFBIN/adf << eor > output

Title Me2OU(NH2)3

Atoms
     1.U         0.078293     0.000000     0.000000
     2.O         2.654575     0.000000     0.000000
     3.N        -0.874349     1.990793     0.210450
     4.N        -0.874349    -0.813141    -1.829303
     5.N        -0.874349    -1.177652     1.618852
     6.H        -0.404171     2.726956     0.731041
     7.H        -1.781474     2.167745    -0.213613
     8.H        -0.404171    -0.730378    -2.727134
     9.H        -1.781474    -1.268867    -1.770515
    10.H        -0.404171    -1.996578     1.996092
    11.H        -1.781474    -0.898878     1.984129
    12.C         3.448818     1.064359    -0.539890
```

```
    13.C           3.448818    -1.064359     0.539890
    14.H           2.796908     1.854197    -0.940531
    15.H           4.087343     1.493159     0.246087
    16.H           4.087343     0.683467    -1.350169
    17.H           2.796908    -1.854197     0.940531
    18.H           4.087343    -1.493159    -0.246087
    19.H           4.087343    -0.683467     1.350169
End

symmetry NOSYM

Geometry
Optim
converge grad=3e-2, rad=3e-2, angle=2
Iterations 200
End

XC
GGA Becke Perdew
End

SCF
   Iterations 200
End

unrestricted
charge 0 3

Maxmemoryusage 40

Fragments
U   t21.U
N   t21.N
H   t21.H
O   t21.O
C   t21.C
End

Relativistic  ZORA
CorePotentials  t12.rel  &
 U  1
 N  2
 H  3
 O  4
 C  5
End

End Input
eor
```

A.2.5. Computational details for (μ-C_6H_6)U_2(NH_2)$_4$

Input file:[4]

```
$ADFBIN/dirac  < $ADFRESOURCES/Dirac/U.5d
rm -f FILE* logfile

$ADFBIN/dirac  < $ADFRESOURCES/Dirac/N
rm -f FILE* logfile

$ADFBIN/dirac  < $ADFRESOURCES/Dirac/H
rm -f FILE* logfile

$ADFBIN/dirac  < $ADFRESOURCES/Dirac/C
rm -f FILE* logfile

mv TAPE12 t12.rel

$ADFBIN/adf  <<eor
Create  U  File=$ADFRESOURCES/ZORA/TZ2P/U.5d
XC
GGA  Becke Perdew
End
Relativistic  ZORA
CorePotentials t12.rel &
 U 1
End
End Input
eor
mv TAPE21  t21.U

$ADFBIN/adf  <<eor
Create  N  File=$ADFRESOURCES/ZORA/TZ2P/N
XC
GGA  Becke Perdew
End
Relativistic   ZORA
CorePotentials t12.rel &
 N 2
End
End Input
eor
mv TAPE21  t21.N

$ADFBIN/adf  <<eor
Create  H  File=$ADFRESOURCES/ZORA/TZ2P/H
XC
GGA  Becke Perdew
```

---

[4] The input files for the calculations with the other density functionals are similar, except for indicating what type of gradient exchange correlation was used.

```
End
Relativistic  ZORA
CorePotentials t12.rel &
 H 3
End
End Input
eor
mv TAPE21  t21.H

$ADFBIN/adf  <<eor
Create  C  File=$ADFRESOURCES/ZORA/TZ2P/C
XC
GGA  Becke Perdew
End
Relativistic  ZORA
CorePotentials t12.rel &
 C 4
End
End Input
eor
mv TAPE21  t21.C

$ADFBIN/adf << eor > outfile
title mu-benzene amide BP86

atoms
 1.XX      0               0               0
 2.C       1.463326        0               0
 3.C       0.731663        1.267277        0
 4.C      -0.731663        1.267277        0
 5.C      -1.463326        0               0
 6.C      -0.731663       -1.267277        0
 7.C       0.731663       -1.267277        0
 8.H       2.551105        0               0
 9.H       1.275552        2.209322        0
10.H      -1.275552        2.209322        0
11.H      -2.551105        0               0
12.H      -1.275552       -2.209322        0
13.H       1.275552       -2.209322        0
14.U       0               0              -2.113737
15.U       0               0               2.113737
16.N       1.295532        1.295532        3.458488
17.N      -1.295532       -1.295532        3.458488
18.N       1.295532       -1.295532       -3.458488
19.N      -1.295532        1.295532       -3.458488
20.H       0.871679        2.048961        4.005383
21.H       2.048961        0.871679        4.005383
22.H      -0.871679       -2.048961        4.005383
23.H      -2.048961       -0.871679        4.005383
24.H       0.871679       -2.048961       -4.005383
25.H       2.048961       -0.871679       -4.005383
26.H      -0.871679        2.048961       -4.005383
27.H      -2.048961        0.871679       -4.005383
end
```

```
Symmetry=D(2)

fragments
U t21.U
C t21.C
H t21.H
N t21.N
end

Relativistic  ZORA
CorePotentials  t12.rel  &
 U  1
 N  2
 H  3
 C  4
End

XC
GGA Becke Perdew
END

unrestricted
charge 0 4

scf
ITERATIONS 300
MIXING 0.05
end

geometry
optim
converge grad=3e-2, rad=3e-2, angle=2
end

end input
```

A.2.6. Computational details for $(C_6H_6)U_2(NH_2)_4$

Input file for the calculation with two electrons of spin α in excess of spin β:

```
$ADFBIN/dirac  < $ADFRESOURCES/Dirac/U.5d
rm -f FILE* logfile

$ADFBIN/dirac  < $ADFRESOURCES/Dirac/N
rm -f FILE* logfile

$ADFBIN/dirac  < $ADFRESOURCES/Dirac/H
rm -f FILE* logfile
```

```
$ADFBIN/dirac  < $ADFRESOURCES/Dirac/C
rm -f FILE* logfile

mv TAPE12 t12.rel

$ADFBIN/adf  <<eor
Create  U  File=$ADFRESOURCES/ZORA/TZ2P/U.5d
XC
GGA  pw91
End
Relativistic  ZORA
CorePotentials t12.rel &
 U 1
End
End Input
eor
mv TAPE21  t21.U

$ADFBIN/adf  <<eor
Create  N  File=$ADFRESOURCES/ZORA/TZ2P/N
XC
GGA  pw91
End
Relativistic   ZORA
CorePotentials t12.rel &
 N 2
End
End Input
eor
mv TAPE21  t21.N

$ADFBIN/adf  <<eor
Create  H  File=$ADFRESOURCES/ZORA/TZ2P/H
XC
GGA  pw91
End
Relativistic  ZORA
CorePotentials t12.rel &
 H 3
End
End Input
eor
mv TAPE21  t21.H

$ADFBIN/adf  <<eor
Create  C  File=$ADFRESOURCES/ZORA/TZ2P/C
XC
GGA  pw91
End
Relativistic  ZORA
CorePotentials t12.rel &
 C 4
End
End Input
```

```
eor
mv TAPE21   t21.C

$ADFBIN/adf << eor > outfile

title mono u benzene amide 2- cartesian

atoms
     1.XX         0.000000     0.000000     0.199791
     2.C          1.422213     0.000000     0.199791
     3.C          0.711107     1.231673     0.199791
     4.C         -0.711107     1.231673     0.199791
     5.C         -1.422213     0.000000     0.199791
     6.C         -0.711107    -1.231673     0.199791
     7.C          0.711107    -1.231673     0.199791
     8.H          2.508780     0.000000     0.199791
     9.H          1.254390     2.172667     0.199791
    10.H         -1.254390     2.172667     0.199791
    11.H         -2.508780     0.000000     0.199791
    12.H         -1.254390    -2.172667     0.199791
    13.H          1.254390    -2.172667     0.199791
    14.U          0.000000     0.000000    -2.049299
    15.N          1.259333    -1.259333    -3.429802
    16.N         -1.259333     1.259333    -3.429802
    17.H          0.826301    -2.000809    -3.981320
    18.H          2.000809    -0.826301    -3.981320
    19.H         -0.826301     2.000809    -3.981320
    20.H         -2.000809     0.826301    -3.981320
end

Symmetry=C(2)

fragments
U t21.U
C t21.C
H t21.H
N t21.N
end

Relativistic   ZORA
CorePotentials   t12.rel   &
 U   1
 N   2
 H   3
 C   4
End

XC
GGA pw91
END

unrestricted
charge 0 2
```

```
scf
ITERATIONS 300
MIXING 0.05
end

geometry
optim
converge grad=3e-2, rad=3e-2, angle=2
end

end input
```

Input file for the calculation with no electrons of spin α in excess of spin β:

```
$ADFBIN/dirac   < $ADFRESOURCES/Dirac/U.5d
rm -f FILE* logfile

$ADFBIN/dirac   < $ADFRESOURCES/Dirac/N
rm -f FILE* logfile

$ADFBIN/dirac   < $ADFRESOURCES/Dirac/H
rm -f FILE* logfile

$ADFBIN/dirac   < $ADFRESOURCES/Dirac/C
rm -f FILE* logfile

mv TAPE12 t12.rel

$ADFBIN/adf   <<eor
Create   U  File=$ADFRESOURCES/ZORA/TZ2P/U.5d
XC
GGA   pw91
End
Relativistic  ZORA
CorePotentials t12.rel &
 U 1
End
End Input
eor
mv TAPE21   t21.U

$ADFBIN/adf   <<eor
Create   N  File=$ADFRESOURCES/ZORA/TZ2P/N
XC
GGA   pw91
End
Relativistic   ZORA
CorePotentials t12.rel &
 N 2
End
End Input
```

```
eor
mv TAPE21   t21.N

$ADFBIN/adf   <<eor
Create   H   File=$ADFRESOURCES/ZORA/TZ2P/H
XC
GGA   pw91
End
Relativistic   ZORA
CorePotentials t12.rel &
 H 3
End
End Input
eor
mv TAPE21   t21.H

$ADFBIN/adf   <<eor
Create   C   File=$ADFRESOURCES/ZORA/TZ2P/C
XC
GGA   pw91
End
Relativistic   ZORA
CorePotentials t12.rel &
 C 4
End
End Input
eor
mv TAPE21   t21.C

$ADFBIN/adf << eor > outfile
title mono-benzene amide cartesian

atoms
     1.XX        0.000000     0.000000     0.086357
     2.C         1.428035     0.000000     0.086357
     3.C         0.714018     1.236715     0.086357
     4.C        -0.714018     1.236715     0.086357
     5.C        -1.428035     0.000000     0.086357
     6.C        -0.714018    -1.236715     0.086357
     7.C         0.714018    -1.236715     0.086357
     8.H         2.515271     0.000000     0.086357
     9.H         1.257635     2.178289     0.086357
    10.H        -1.257635     2.178289     0.086357
    11.H        -2.515271     0.000000     0.086357
    12.H        -1.257635    -2.178289     0.086357
    13.H         1.257635    -2.178289     0.086357
    14.U         0.000000     0.000000    -2.006214
    15.N         1.221539    -1.221539    -3.472411
    16.N        -1.221539     1.221539    -3.472411
    17.H         0.770624    -1.946277    -4.033604
    18.H         1.946277    -0.770624    -4.033604
    19.H        -0.770624     1.946277    -4.033604
    20.H        -1.946277     0.770624    -4.033604
end
```

```
Symmetry=C(2)

fragments
U t21.U
C t21.C
H t21.H
N t21.N
end

Relativistic  ZORA
CorePotentials  t12.rel  &
 U  1
 N  2
 H  3
 C  4
End

XC
GGA pw91
END

scf
ITERATIONS 300
MIXING 0.05
end

geometry
optim
converge grad=3e-2, rad=3e-2, angle=2
end

end input
```

A.2.7. Computational details for $(C_8H_8)U(NH_2)_2$

Input file:

```
$ADFBIN/dirac  < $ADFRESOURCES/Dirac/U.5d
rm -f FILE* logfile

$ADFBIN/dirac  < $ADFRESOURCES/Dirac/N
rm -f FILE* logfile

$ADFBIN/dirac  < $ADFRESOURCES/Dirac/H
rm -f FILE* logfile

$ADFBIN/dirac  < $ADFRESOURCES/Dirac/C
rm -f FILE* logfile
```

```
mv TAPE12 t12.rel

$ADFBIN/adf  <<eor
Create  U  File=$ADFRESOURCES/ZORA/TZ2P/U.5d
XC
GGA  Becke Perdew
End
Relativistic  ZORA
CorePotentials t12.rel &
 U 1
End
End Input
eor
mv TAPE21  t21.U

$ADFBIN/adf  <<eor
Create  N  File=$ADFRESOURCES/ZORA/TZ2P/N
XC
GGA  Becke Perdew
End
Relativistic  ZORA
CorePotentials t12.rel &
 N 2
End
End Input
eor
mv TAPE21  t21.N

$ADFBIN/adf  <<eor
Create  H  File=$ADFRESOURCES/ZORA/TZ2P/H
XC
GGA  Becke Perdew
End
Relativistic  ZORA
CorePotentials t12.rel &
 H 3
End
End Input
eor
mv TAPE21  t21.H

$ADFBIN/adf  <<eor
Create  C  File=$ADFRESOURCES/ZORA/TZ2P/C
XC
GGA  Becke Perdew
End
Relativistic  ZORA
CorePotentials t12.rel &
 C 4
End
End Input
eor
mv TAPE21  t21.C
```

```
$ADFBIN/adf << eor > outfile
title mono u COT amide

atoms
    1.XX          0.000000      0.000000     -0.013591
    2.C           1.848043      0.000000     -0.013591
    3.C           1.306764      1.306764     -0.013591
    4.C           0.000000      1.848043     -0.013591
    5.C          -1.306764      1.306764     -0.013591
    6.C          -1.848043      0.000000     -0.013591
    7.C          -1.306764     -1.306764     -0.013591
    8.C           0.000000     -1.848043     -0.013591
    9.C           1.306764     -1.306764     -0.013591
   10.H           2.937971      0.000000     -0.013591
   11.H           2.077459      2.077459     -0.013591
   12.H           0.000000      2.937971     -0.013591
   13.H          -2.077459      2.077459     -0.013591
   14.H          -2.937971      0.000000     -0.013591
   15.H          -2.077459     -2.077459     -0.013591
   16.H           0.000000     -2.937971     -0.013591
   17.H           2.077459     -2.077459     -0.013591
   18.U           0.000000      0.000000     -1.971675
   19.N           1.155852     -1.155852     -3.473548
   20.N          -1.155852      1.155852     -3.473548
   21.H           0.688911     -1.865349     -4.042302
   22.H           1.865349     -0.688911     -4.042302
   23.H          -0.688911      1.865349     -4.042302
   24.H          -1.865349      0.688911     -4.042302
end

Symmetry=nosym

fragments
U t21.U
C t21.C
H t21.H
N t21.N
end

Relativistic  ZORA
CorePotentials  t12.rel  &
  U  1
  N  2
  H  3
  C  4
End

XC
GGA Becke Perdew
END

unrestricted
charge 0 2
```

```
scf
ITERATIONS 300
MIXING 0.05
end

geometry
optim
converge grad=3e-2, rad=3e-2, angle=2
end
end input
```

Chapter 2

A.2.8. Computational details for $(\mu\text{-}\eta^6,\eta^6\text{-}C_{10}H_8)[U(NCH_2)_3]_2^{2-}$

Table 2. List of selected MOs with the most significant SFO gross populations (>3%).

Orbital	Energy (eV)	Symmetry	Spin	Occupancy	%, SFO (first member; core orbitals not included in numbering), fragment
SOMO-4	2.644	A2	α	1	36.41%, 2Fxyz, 1U
					17.82%, 1Py, 9C
					8.31%, 1Py, 11C
					8.02%, 1Py, 20C
					7.45%, 1Py, 17C
					6.33%, 4Dxz, 1U
					4.22%, 1Py, 15C
					3.43%, 2Fx, 1U
	2.886	A2	β	1	32.59%, 2Fxyz, 1U
					22.67%, 1Py, 9C
					11.86%, 1Py, 11C
					9.33%, 1Py, 17C
					6.25%, 1Py, 20C
					5.71%, 4Dxz, 1U
					3.99%, 1Py, 15C
SOMO-5	2.595	B2	α	1	27.07%, 1Py, 10C
					20.70%, 2Fy, 1U
					15.35%, 2Fz2y, 1U
					4.99%, 2Fz3, 1U
					4.37%, 1Py, 9C
					3.95%, 1Py, 11C
					3.53%, 1Py, 17C

	2.763	B2	β	1	3.44%, 1Pz, 4N 32.81%, 1Py, 10C 13.84%, 2Fz2y, 1U 12.32%, 2Fy, 1U 5.87%, 1Py, 9C 4.76%, 1Py, 17C 4.60%, 1Py, 11C 4.08%, 2Fz3, 1U 3.89%, 1Pz, 4N 3.33%, 1Py, 15C
SOMO[5]	3.330	A1	α	1	31.20%, 2Fy, 1U 26.36%, 2Fz, 1U 15.07%, 1Py, 20C 8.85%, 2Fz2y, 1U 6.00%, 1Py, 4N
	4.056	A1	β	0	29.89%, 1Py, 20C 19.87%, 2Fz, 1U 13.78%, 1Py, 4N 10.41%, 2Fy, 1U 3.94%, 6Py, 1U
SOMO-1	3.328	A2	α	1	28.19%, 1Px, 19C 24.50%, 2Fz2x, 1U 13.54%, 1Px, 3N 12.90%, 2Fxyz, 1U 6.22%, 2Fx, 1U
	3.855	A2	β	0	35.33%, 2Fz2x, 1U 28.23%, 1Px, 19C 11.76%, 1Px, 3N 5.49%, 2Fx, 1U 3.39%, 2Fxyz, 1U 3.10%, 4Dxz, 1U
SOMO-2	3.283	B2	α	1	32.48%, 2Fz, 1U 19.89%, 2Fy, 1U 17.21%, 1Py, 20C 8.74%, 2Fz2y, 1U 5.66%, 1Py, 4N 4.64%, 4Dx2-y2, 1U
	3.974	B2	β	0	25.43%, 1Py, 20C 14.21%, 2Fz, 1U 12.32%, 2Fy, 1U 11.95%, 2Fz3, 1U 9.61%, 4Dx2-y2, 1U 9.23%, 1Py, 4N

[5] Highest Single Occupied Molecular Orbital.

SOMO-3	3.249	B1	α	1	5.30%, 1Py, 15C 38.03%, 2Fx, 1U 19.67%, 1Py, 20C 9.82%, 1Px, 19C 7.16%, 1Py, 4N 6.11%, 4Dxy,1U 4.47%, 1Px, 3N 3.11%, 4Dxz, 1U
	3.794	B1	β	0	30.00%, 2Fx, 1U 27.35%, 1Py, 20C 15.20%, 2Fxyz, 1U 10.69%, 1Py, 4N 3.51%, 2Fz2x, 1U

Input file:

```
$ADFBIN/dirac  < $ADFRESOURCES/Dirac/U
rm -f FILE* logfile

$ADFBIN/dirac  < $ADFRESOURCES/Dirac/N
rm -f FILE* logfile

$ADFBIN/dirac  < $ADFRESOURCES/Dirac/H
rm -f FILE* logfile

$ADFBIN/dirac  < $ADFRESOURCES/Dirac/C
rm -f FILE* logfile

mv TAPE12 t12.rel

$ADFBIN/adf  <<eor
Create  U   File=$ADFRESOURCES/ZORA/V/U
XC
GGA  Becke Perdew
End
Relativistic  ZORA
CorePotentials t12.rel &
  U  1
End
End Input
eor
mv TAPE21  t21.U

$ADFBIN/adf  <<eor
Create  N  File=$ADFRESOURCES/ZORA/V/N
XC
GGA  Becke Perdew
End
```

```
Relativistic   ZORA
CorePotentials t12.rel &
 N 2
End
End Input
eor
mv TAPE21   t21.N

$ADFBIN/adf  <<eor
Create   H  File=$ADFRESOURCES/ZORA/V/H
XC
GGA   Becke Perdew
End
Relativistic  ZORA
CorePotentials t12.rel &
 H 3
End
End Input
eor
mv TAPE21   t21.H

$ADFBIN/adf  <<eor
Create   C  File=$ADFRESOURCES/ZORA/V/C
XC
GGA   Becke Perdew
End
Relativistic  ZORA
CorePotentials t12.rel &
 C 4
End
End Input
eor
mv TAPE21   t21.C

$ADFBIN/adf << eor > geometry.out
Title

Atoms  Z-matrix
XX            0     0     0     0.000000      0.000000      0.000000
XX            1     0     0     aaaaaaaa      0.000000      0.000000
 U            1     2     0     2.200000     90.000000      0.000000
 N            3     1     2     ffffffff    110.000000    180.000000
 N            3     1     2     ffffffff    110.000000     60.000000
 N            3     1     2     ffffffff    110.000000    300.000000
 U            1     2     3     2.200000     90.000000    180.000000
 N            7     1     2     ffffffff    110.000000    180.000000
 N            7     1     2     ffffffff    110.000000     60.000000
 N            7     1     2     ffffffff    110.000000    300.000000
 C            2     1     3     bbbbbbbb     30.000000     90.000000
 C            2     1     3     bbbbbbbb     90.000000     90.000000
 C            2     1     3     bbbbbbbb    150.000000     90.000000
 C            2     1     7     bbbbbbbb     30.000000     90.000000
 C            2     1     7     bbbbbbbb     90.000000     90.000000
 C            2     1     7     bbbbbbbb    150.000000     90.000000
```

Appendix 2

```
C        13   12   11   cccccccc   120.000000   180.000000
C        16   15   14   cccccccc   120.000000   180.000000
C        17   13   12   dddddddd   120.000000   180.000000
C        18   16   15   dddddddd   120.000000   180.000000
H        11   12   13   1.089000   120.000000   180.000000
H        14   15   16   1.089000   120.000000   180.000000
H        12   11   14   1.089000   120.000000   180.000000
H        15   14   11   1.089000   120.000000   180.000000
H        17   19   20   1.089000   120.000000   180.000000
H        18   16   13   1.089000   120.000000   180.000000
H        19   17   13   1.089000   120.000000   180.000000
H        20   18   16   1.089000   120.000000   180.000000
C         3    1    2   gggggggg   110.000000   180.000000
C         3    1    2   gggggggg   110.000000    60.000000
C         3    1    2   gggggggg   110.000000   300.000000
C         7    1    2   gggggggg   110.000000   180.000000
C         7    1    2   gggggggg   110.000000    60.000000
C         7    1    2   gggggggg   110.000000   300.000000
H        31    3    1   1.089000   120.000000    90.000000
H        31    3   35   1.089000   120.000000   180.000000
H        30    3    1   1.089000   120.000000    90.000000
H        30    3   37   1.089000   120.000000   180.000000
H        29    3    1   1.089000   120.000000     0.000000
H        29    3   39   1.089000   120.000000   180.000000
H        34    7    1   1.089000   120.000000    90.000000
H        34    7   41   1.089000   120.000000   180.000000
H        33    7    1   1.089000   120.000000    90.000000
H        33    7   43   1.089000   120.000000   180.000000
H        32    7    1   1.089000   120.000000     0.000000
H        32    7   45   1.089000   120.000000   180.000000
End

symmetry C(2v)

Geovar
aaaaaaaa 0.225670
bbbbbbbb 1.450922
cccccccc 1.414820
dddddddd 1.396759
ffffffff 2.190954
gggggggg 3.482310
End

Integration 7.0

geometry
optim internal selected
End

XC
GGA Becke Perdew
End

SCF
```

```
   Iterations 10000
End

unrestricted

Charge -2 4

Maxmemoryusage 400

Fragments
U t21.U
N t21.N
H t21.H
C t21.C
End

Relativistic  ZORA
CorePotentials  t12.rel  &
 U 1
 N 2
 H 3
 C 4
End

End Input
Eor
$adfrom TAPE21
```

A.2.9. Computational details for $(\mu\text{-}\eta^6,\eta^6\text{-}C_6H_6)[U(NCH_2)_3]_2^-$

Table 3. List of selected MOs with the most significant SFO gross populations (>3%).

Orbital	Energy (eV)	Symmetry	Spin	Occupancy	%, SFO (first member; core orbitals not included in numbering), fragment
SOMO	0.264	8A1.g	α	1	90.10%, 1Fz3, 1U 8.01%, 1S, 1U
	0.722	10E1.u:1	β	0	35.30%, 1Py, 9C 17.08%, 1Py, 15N 14.15%, 1Fxyz, 1U 7.81%, 1Dxy, 1U 5.41%, 1Dxz, 1U 3.11%, 1Px, 9C
SOMO-1	0.168	3A1.u	α	1	74.02%, 1Fx, 1U 17.57%, 1Px, 9C 6.42%, 1Px, 15N
	0.721	10E1.g:2	β	0	32.44%, 1Fxyz, 1U

					17.65%, 1Px, 9C
					15.81%, 1Px, 9C
					9.41%, 1Px, 15N
					7.10%, 1Px, 15N
					3.23%, 1Dxz, 1U
SOMO-2	0.147	2A2.g	α	1	74.39%, 1Fx, 1U
					17.45%, 1Px, 9C
					6.21%, 1Px, 15N
	0.721	10E1.g:2	β	0	32.44%, 1Fz, 1U
					17.65%, 1Px, 9C
					15.81%, 1Py, 9C
					9.41%, 1Px, 15N
					7.10%, 1Py, 15N
					3.23%, 1Dyz, 1U
SOMO-3	-0.442	9E1.u:2	α	1	46.13%, 1Fz, 1U
					34.91%, 1Pz, 3C
					6.93%, 1Dx2-y2, 1U
					4.72%, 1Fz2y, 1U
					3.37%, 1Pz, 15N
	-0.242	9E1.u:2	β	1	46.01%, 1Pz, 3C
					34.36%, 1Fxyz, 1U
					8.23%, 1Dx2-y2, 1U
					4.30%, 1Pz, 15N
SOMO-4	-0.442	9E1.u:1	α	1	46.13%, 1Fz, 1U
					34.91%, 1Pz, 3C
					6.93%, 1Dxy, 1U
					4.72%, 1Fz2x, 1U
					3.37%, 1Pz, 15N
	-0.242	9E1.u:1	β	1	46.01%, 1Pz, 3C
					34.36%, 1Fxyz, 1U
					8.23%, 1Dxy, 1U
					4.30%, 1Pz, 15N

Input file:

```
title u2(benzene)(NCH2)6 anion in D3d - zora relativistic - spin unrestricted

atoms Z-matrix
1 XX 0 0 0 0 0 0
2 XX 1 0 0 1.26 0 0
3 U 1 2 0 m 90 0
4 C 1 3 2 d 90 0
5 C 1 3 2 d 90 60
6 C 1 3 2 d 90 120
7 C 1 3 2 d 90 180
```

```
8 C 1 3 2 d 90 240
9 C 1 3 2 d 90 300
10 U 1 2 3 m 90 180
11 N 3 1 2 a aa 0
12 N 3 1 2 a aa 120
13 N 3 1 2 a aa 240
14 C 11 3 1 b bb 0
15 C 12 3 1 b bb 0
16 C 13 3 1 b bb 0
17 H 14 11 1 1.1 120 0
18 H 15 12 1 1.1 120 0
19 H 16 13 1 1.1 120 0
20 H 14 11 1 1.1 120 180
21 H 15 12 1 1.1 120 180
22 H 16 13 1 1.1 120 180
23 N 10 1 2 a aa 180
24 N 10 1 2 a aa 300
25 N 10 1 2 a aa 60
26 C 23 10 1 b bb 0
27 C 24 10 1 b bb 0
28 C 25 10 1 b bb 0
29 H 26 23 1 1.1 120 0
30 H 27 24 1 1.1 120 0
31 H 28 25 1 1.1 120 0
32 H 26 23 1 1.1 120 180
33 H 27 24 1 1.1 120 180
34 H 28 25 1 1.1 120 180
35 H 1 3 2 e 90 0
36 H 1 3 2 e 90 60
37 H 1 3 2 e 90 120
38 H 1 3 2 e 90 180
39 H 1 3 2 e 90 240
40 H 1 3 2 e 90 300
end

geovar
b 1.27
bb 170
m 2.25
e 2.94
d 1.85
a 2.25
aa 120
end

Symmetry=D(3d)

fragments
U t21.U
N t21.N
H t21.H
C t21.C
end
```

```
corepotentials TAPE12 &
U 1
N 2
H 3
C 4
end

xc
LDA VWN
GRADIENTS BECKE PERDEW
end

relativistic zora

unrestricted

charge -1 3

scf
ITERATIONS 150
MIXING 0.025
end

geometry
optim internal selected
end

end input
```

A.2.10. Computational details for $(\mu-\eta^8,\eta^8-C_8H_8)[U(NCH_2)_3]_2$

Table 4. List of selected MOs with the most significant SFO[*] gross populations (>3%).

Orbital	Energy (eV)	Symmetry	Spin	%, SFO (first member; core orbitals not included in numbering), fragment
SOMO-10	-5.809	Au	α	59.60%, 1Py, 4C
				11.04%, 1Fxyz, 1U
				8.18%, 1Dxz, 1U
				6.61%, 1Py, 18N
	-5.721	Au	β	61.93%, 1Py, 4C
				8.17%, 1Py, 18N
				7.02%, 1Fxyz, 1U
				6.63%, 1Dxz, 1U
				3.02%, 1Pz, 18N
SOMO-11	-5.799	Bu	α	30.39%, 1Py, 3C

[*] Symmetrized Fragment Orbitals

			30.33%, 1Py, 5C
			6.92%, 1Fz2y, 1U
			6.33%, 1Dz2, 1U
			4.05%, 1Fy, 1U
			3.64%, 1Py, 17N
-5.723	Bu	β	31.32%, 1Py, 3C
			31.29%, 1Py, 5C
			5.36%, 1Dz2, 1U
			4.64%, 1Fz2y, 1U
			4.41%, 1Py, 17N
			3.09%, 1Py, 18N

Input file:

```
Parallel Execution: Process Information
=========================================

 Actual Number of Tasks running:      1
 The Master (kid 0) runs on host localhost
(INPUT FILE)
title u2(COT)(NCH2)6 in C2h - zora relativistic - spin unrestricted

atoms Z-matrix
1 XX 0 0 0 0 0 0
2 XX 1 0 0 1.26 0 0
3 U 1 2 0 m 90 0
4 C 1 3 2 d 90 0
5 C 1 3 2 d 90 45
6 C 1 3 2 d 90 90
7 C 1 3 2 d 90 135
8 C 1 3 2 d 90 180
9 C 1 3 2 d 90 225
10 U 1 2 3 m 90 180
11 N 3 1 2 a aa 0
12 N 3 1 2 a aa 120
13 N 3 1 2 a aa 240
14 C 11 3 1 b bb 0
15 C 12 3 1 b bb 0
16 C 13 3 1 b bb 0
17 H 14 11 1 1.1 120 0
18 H 15 12 1 1.1 120 0
19 H 16 13 1 1.1 120 0
20 H 14 11 1 1.1 120 180
21 H 15 12 1 1.1 120 180
22 H 16 13 1 1.1 120 180
23 N 10 1 2 a aa 180
24 N 10 1 2 a aa 300
25 N 10 1 2 a aa 60
26 C 23 10 1 b bb 0
```

```
27 C 24 10 1 b bb 0
28 C 25 10 1 b bb 0
29 H 26 23 1 1.1 120 0
30 H 27 24 1 1.1 120 0
31 H 28 25 1 1.1 120 0
32 H 26 23 1 1.1 120 180
33 H 27 24 1 1.1 120 180
34 H 28 25 1 1.1 120 180
35 C 1 3 2 d 90 270
36 C 1 3 2 d 90 315
37 H 1 3 2 e 90 0
38 H 1 3 2 e 90 45
39 H 1 3 2 e 90 90
40 H 1 3 2 e 90 135
41 H 1 3 2 e 90 180
42 H 1 3 2 e 90 225
43 H 1 3 2 e 90 270
44 H 1 3 2 e 90 315
end
geovar
b 1.27
bb 169
m 2.28
e 2.94
d 1.85
a 2.15
aa 119
end

Symmetry=C(2h)

fragments
U t21.U
N t21.N
H t21.H
C t21.C
end

corepotentials TAPE12 &
U 1
N 2
H 3
C 4
end

xc
LDA VWN
GRADIENTS BECKE PERDEW
end

relativistic zora

unrestricted
```

```
charge 0 4

scf
ITERATIONS 100
MIXING 0.025
end

geometry
optim internal selected
end

end input
```

EDUCATION

Doctor of Philosophy, Chemistry   *June 2003*
       Massachusetts Institute of Technology, Cambridge, MA, USA
       Advisor: Professor Christopher C. Cummins
       Thesis: "Arene bridged diuranium compounds supported by amide and ketimide ligands"

Bachelor of Science, Chemistry   *July 1998*
       University of Bucharest, Romania
       Advisor: Professor Marius Andruh
       Thesis: "Solid state reaction of complex cation – complex anion type compounds involving tetrabromometallates"

RESEARCH EXPERIENCE

Massachusetts Institute of Technology   *January 1999 - March 2003*
Advisor: Professor Christopher C. Cummins

    Synthesis and characterization of organometallic uranium compounds supported by amide and ketimide ligands. Study of a series of arene bridged inverted sandwiches of diuranium compounds where the arene can be benzene, toluene, naphthalene, biphenyl, *trans*-stilbene, *p*-terphenyl, styrene, cyclooctatetraene. DFT calculations on models for representative complexes. Other projects include isolation and characterization of a uranium silyl compound.

University "Politehnica" of Bucharest   *January 1996 - August 1998*
Advisor: Professor Cornelia Guran

    Study of coordination complexes of various transition and lanthanide ions with heterocyclic ligands of cyclotriphosphazene type. Synthesis and characterization of biologically relevant complexes that involve phenothiazine ligands.

University of Bucharest   *July 1996 - July 1998*
Advisor: Professor Marius Andruh

    Synthesis and characterization of a series of complex cation – complex anion type compounds $[M(AA)_3][MBr_4]$ (AA = phenantroline or bipyridyl). Investigation by absorption spectroscopy of thermal migration of AA from the cation to the anion coordination sphere.

TEACHING EXPERIENCE

Massachusetts Institute of Technology

September – December 2001

Professors Christopher C. Cummins and Alan Davison
    Teaching assistant for Chemistry 5.04, Advanced Inorganic Chemistry.

February – May 1999

Professors Christopher C. Cummins and Daniel G. Nocera
    Teaching assistant for Chemistry 5.03, Inorganic Chemistry.

September – December 1998

    Teaching assistant for Chemistry 5.110, Introductory Laboratory Course.

HONORS AND PROFESSIONAL AFFILIATIONS

P & G Fellowship	*1997 - 1998*
University of Bucharest Scholarship	*1994 - 1998*

American Chemical Society, Member

Acknowledgments

I think that most students, by the time they get to write this part, feel that their thesis is a huge personal accomplishment and I do not differ in that opinion. Like others, I also realize that it would not have been possible to get to this point without the help and / or the influence of some people I encountered during my graduate career.

It is probably an understatement that my advisor, Prof. Christopher Cummins, is the person who played the most important role during these last years with respect to my obtaining a PhD degree. Usually, during talks, I failed rather miserably to acknowledge him properly, so I hope I will do a better job now when I do not need to be spontaneous. I remember now that in the beginning I was very impressed about the insight he had into my project and I realize that it still impresses me. Throughout my entire time here I was overwhelmed by the fact that he always knew how to challenge me and help me move forward. Another thing that left a mark on me was the clarity with which he communicates his scientific thoughts. Besides the chance I had to witness that in the context of scientific research, I was also very impressed by his pedagogical style while teaching the 5.04 class. And the more I think about it, the more I realize that he is a peculiar type of teacher, one that uses non-traditional methods to prepare a student for the present and the future. In that respect, I appreciate that I had the liberty to make mistakes and learn from them. Another thing that belongs to the category of his teaching methods is the specific relationship he has with every student. I remember that when I talked to prospective graduate students I would be asked about what type of relationship Kit has with his students. I had to say that whatever I tell them would be uninformative since every relationship is different and personalized. Although I have tried to write down some things that I consider very important in my case, I am not so sure anymore that I have done a much better job than in the situations that required me to be spontaneous. I look back at all the years spent in his group and I am grateful for all the events that marked me, the apparent failures maybe more than the seeming accomplishments, because in all cases I learned something.

Moving to the other acknowledgments, I will try to order them chronologically. Before I started my research work, I met Theo Agapie and his enthusiasm about the group helped me make my own decision. He is one of the few friends I managed to make since I have been in this country and my only bridge partner. Dan Mindiola initiated me in the secrets of the group and before he had time to take advantage of his authority we became friends. He remained the person whom I sought for advice for the time we spent together in the group, but now I am glad that our relationship extends outside the lab. I think my friendship with Misha Barybin, although it probably developed gradually, is due to the fact that he always willingly helped me when I asked him something. I always appreciated his methodical knowledge of chemistry and I enjoyed our conversations outside it. On the list of people in the group who knew more than me at a specific time I want to add James Blackwell. Although I did not think I was entitled to it, he spent a lot of time helping me organize my thoughts about my work, in general, and my thesis, in particular. Past members of the group that I like to remember include James Tsai because I always appreciated him for his techniques in the lab and his laconic humor during group meetings and John-Paul Cherry for being the individual he was. The present members include Josh Figueroa

(the only one who likes to declare that I taught him something about life in the group), Arjun Mendiratta (who probably enjoys arguing as much as I do), Fran Stephens, and the new additions Emma Sceats and Chris Clough to whom I wish good luck. My best wishes also go to Erin Daida and Han Sen Soo who are currently senior undergraduate students in the group.

In the end of this section I want to thank several people who, directly or indirectly, helped me in my personal life during the time I was in graduate school. My first thoughts go to my mother, Elena Diaconescu, and to my brother, Dragoș Diaconescu, who unconditionally supported me throughout my entire life. My mother was the first person to teach me to go beyond the appearance of events and to always want more than what the present offers. And, not being inclined towards it, she also made sure that I understood the importance of hard work in achieving something, regardless of visible results. I have a deep sympathy for my brother for all the times when I fooled him into doing something and all the respect for the times when he willingly helped me through college. The best friend that I have ever had (and most likely will have in the future) is Vlad Iluc. And what else can I say about somebody who is cynical and practices sarcasm as a great virtue without fearing that it will hang over my head for the rest of my life? (After all, *verba volent, scripta manent*.) That we went through a lot of crises together and he had to support all my hysterical inclinations? I am glad I found somebody who likes to play the game of life by the rules I follow. I will always remember Parisa Mehrkhodavandi as the friend who helped me the most to adjust when I came here and who went through the same ordeals of graduate school as I did. Thinking about my professional development, I owe to my high-school chemistry teacher, Maria Munteanu, my determination to pursue chemistry and to my college advisor, Cornelia Guran, my early achievements that helped me get to this point in my career.